Winning Silver

Jorge Daniel Moncada de la Rosa

Dissertation submitted to the faculty of the Virginia Polytechnic Institute and State University in partial fulfillment of the requirements for the degree of

Doctor of Philosophy
In
Geosciences

Robert J. Bodnar, Committee Chair
J. Donald Rimstidt
Neil E. Johnson
James B. Campbell

April 26, 2013
Blacksburg, Virgnia

Keywords: epithermal precious metals deposits, mineral exploration, boiling textures, flashing, fluid inclusions, Guanajuato mining district

Winning Silver

Daniel Moncada

ABSTRACT

The search for mineral deposits is a time consuming, risky and very expensive process. Applying new models and methods provides a competitive advantage in the search for mineral deposits because an explorationist can quickly evaluate potential targets and eliminate areas without good potential for mineralization.

This dissertation presents a practical technique for prediction to finding precious metal mineralization at Guanajauato mining district (GMD) base on theoretical and experimental studies of fluids properties, mineral phase equilibrium, physical and chemical mechanisms. Making the technique highly transportable so that it can be applied in the field during an exploration program base on petrographic characteristics of mineral textures produced during boiling events in quartz, calcite and adularia, and fluid inclusions contained in these phases. While this work was conducted in GMD, the results should be applicable in exploration for epithermal deposits worldwide.

The GMD is one of the largest silver producing districts in the world. Ore shoots are localized along three major northwest trending vein systems, the La Luz, Veta Madre and Vetas de la Sierra. More than 1200 samples were collected from surface outcrops, underground mine and historical and recent drill core. Traverses perpendicular to veins in all system were also conducted. Most of the samples (approximately 90%) were also assayed for Au, Ag, Cu, Pb, Zn, As, Sb.

Samples from the GMD show a wide range in silica textures are indicative of rapid precipitation, such as occurs when fluids boil. Other mineral phases, including illite, rhombic adularia and bladed calcite are also indicative of rapid growth in a hydrothermal system and are characteristic of boiling systems. Because boiling is an effective mechanism for precipitating gold and silver from hydrothermal fluids, the presence of mineral textures indicative of boiling is a desirable feature in exploration. In many samples, textural evidence for boiling is supported by coexisting liquid-rich and vapor-rich fluid inclusions, or Fluid Inclusion Assemblages consisting of only vapor-rich inclusions, suggesting “flashing” of the hydrothermal fluids. Textural and fluid inclusion evidence for boiling has been observed in the deepest levels of the GMD, suggesting that additional precious metal resources may occur beneath these levels.

Acknowledgements

I would like to take the time first and foremost to thank my family for supporting me during all these years. I want to thank my mother Martha Agueda de la Rosa Espinosa for all her love and her sacrifice. My advisor, Dr. Robert J. Bodnar for his unselfish help, and I am very grateful for his support and for the experience and knowledge I have gained through last five years.

Staff from Great Panther Silver Limited, especially Robert Archer and Robert Brown, and Staff from Endeavour Silver Corp, specially Barry Devlin and Luis Castro are thanked for providing financial support and access to samples and information.

I thank CONACyT, Virginia Tech Graduate School, Society of Economic Geology, National Science Foundation, and Geochemical Society for providing funding during this dissertation.

I thank the office staff, especially Mary McMurray who helped with travel issues and Connie Lowe for advice and other work that she is doing all the time to help me.

My committee members, Dr. J. Donald Rimstidt, Dr. Neil E. Johnson, and Dr. James B. Campbell are thanked for their support and for discussions that improved the quality of my research.

I am very grateful to my wife, Elva being always there for me, especially in the difficult moments. Thanks for all your patience, support, and love that helped me to accomplish this thesis.

My fellow graduate students and members of the Fluids Research Laboratory, Charles Farley provided help with Raman analysis, all helped during difficult times and Felicia for those wonderful espressos.

In memory of my grandparents, they can see me from heaven Elisa Espinosa and Jorge de la Rosa.

Table of contents

List of Figures

List of Tables

Preface

This dissertation is presented in the form of three manuscripts. Chaper 1 was published in the Journal of *Geochemical Exploration in 2012*. Chaper 2 was published in the *Central European Journal of Geosciences* in 2012. Chapter 3 is in presentation to be summited for publication.

Chapter 1 Mineral Textures and Fluid Inclusion Petrography of the Epithermal Ag-Au Deposits at Guanajuato, Mexico: Application to Exploration

Abstract: Fluid inclusion petrography and vein mineral textures indicative of boiling have been characterized in 855 samples from epithermal precious metals deposits along the Veta Madre at Guanajuato, Mexico. Mineral textures and fluid inclusions characteristic of fluid immiscibility or boiling, including colloform quartz, plumose/feathery/flamboyant quartz, lattice-bladed calcite and lattice-bladed calcite replaced by quartz, as well as coexisting liquid-rich and vapor-rich fluid inclusions and assemblages of vapor-rich only inclusions, have been identified in mineralized samples from the Veta Madre. Most samples studied were assayed for Au, Ag, Cu, Pb, Zn, As and Sb, and were divided into ore grade and sub-economic samples based on the gold and silver concentrations. For silver, samples containing >100 ppm were classified as ore grade, and ore grade gold samples contained >1 ppm Au. The feature that is most closely associated with ore grades of both gold and silver is colloform quartz that was originally precipitated as amorphous silica, and this feature also shows the largest difference in average grade between samples that show colloform texture (178.8 ppm Ag and 1.1 ppm Au) and those that do not exhibit this texture (17.2 ppm Ag and 0.2 ppm Au). Statistical analysis of the data confirmed the petrographic observations that indicated that colloform quartz is the feature that has the greatest predictive power for distinguishing between ore grade and sub-economic samples. For both Ag and Au, there is no significant difference in average grade of samples containing coexisting liquid-rich and vapor-rich fluid inclusions or assemblages of vapor-only inclusions and those that do not, suggesting that fluid inclusion evidence for boiling is not correlative with ore grades. This result is consistent with the fact that most forms of silica that are precipitated during boiling do not trap useful fluid inclusions. The results of this study suggest that mineral textures and fluid inclusions provide complementary information that should both be used in exploration for epithermal precious metal deposits.

Metal grades and boiling intensity of samples collected along a traverse perpendicular to the Veta Madre and above known economic mineralization are both low at relatively short distances away from the vein and increase as the vein is approached. This suggests that mineralogical and fluid inclusion evidence for boiling are restricted to the immediate vicinity of, and increase in the direction of, mineralized veins and may be used in exploration to establish vectors towards vein systems that may host precious metal mineralization. Previous studies of epithermal systems show that the Ag and Au mineralization zone is most often located at or above the bottom of the boiling zone. In this regard, the presence of abundant evidence for boiling that is observed in the deepest levels of the Veta Madre that have been sampled suggests that additional precious metal mineralization may be present beneath the deepest levels that have been explored.

1.1 Introduction

Over the past several decades there have been numerous studies of fluids and fluid inclusions in both active terrestrial geothermal systems and their fossil equivalents, the epithermal precious metal deposits (Kamilli and Ohoto 1977; Roedder, 1984; Bodnar et al., 1985; Vikre, 1985; Hedenquist et al., 2000; Albinson et al., 2001; Simmons et al., 2005; Camprubí and Albinson, 2007). There is now a large database of fluid characteristics in these systems that documents the close association between boiling and mineral deposition in the epithermal environment (c.f., Brown, 1986). In this paper we use the term "boiling" to indicate the presence of two immiscible fluids, even though we recognize that "boiling" refers *sensu stricto* to one-component systems in which the compositions of the liquid and vapor phases are identical, and that "effervescence" or "immiscibility" are more appropriate for multi-component systems in which the compositions of the liquid and vapor phases are different. Once boiling begins at depth, the fluid will usually continue to boil all the way to the surface (Fig. 1.1) if the system is composed of interconnected open fractures that are open to the surface (Fournier, 1985; Henley and Brown, 1985; Vikre, 1985; Cline et al., 1992). Above the boiling horizon low to moderate salinity liquid and a low-density vapor coexist. Fluid inclusion

assemblages trapped from the boiling horizon to the surface are characterized by coexisting liquid-rich and vapor-rich inclusions that generally homogenize at ≤300°C near the base of the boiling zone (Bodnar et al., 1985; Simmons and Christenson, 1994), to <220°C near the top of the system (Albinson et al., 2001), and provide a valuable tool in exploration for epithermal deposits (Roedder and Bodnar, 1997). At depths beneath the boiling horizon, fluid inclusion assemblages consist of a mono-modal assemblage of liquid-rich inclusions with consistent liquid to vapor ratios (Bodnar et al., 1985) (Fig. 1.1). Note, however, that hydrothermal systems associated with the formation of epithermal deposits are dynamic systems, and the bottom of the boiling zone likely shifts upward and downward over time as the fluid temperature, flow rate, fracture apertures, etc., vary through time. As a result, at a given depth “boiling assemblages” and “non-boiling assemblages” may alternate through time as the hydrothermal system evolves.

The "intensity" of boiling may also vary in time and space within the hydrothermal system as the fluid PTX characteristics of the system vary. Figure 1.1 shows schematically two end-member scenarios, one in which a small portion of the original liquid is converted to vapor during boiling (path $B_0 \rightarrow B_1 \rightarrow B_2$), and another in which 100% of the liquid is converted to vapor (path $F_0 \rightarrow F_1 \rightarrow F_2$). The exact proportion of the liquid that will vaporize depends on the P-T conditions of the system as well as on the ability of the fluid to extract "excess heat" from the surrounding wallrock (Henley and Hughes, 2000). In some cases, especially in an open hydrothermal system in which the fluid pressure is controlled by the weight of the overlying hydrothermal fluid column that extends from depth to the surface, a one-phase liquid may migrate upwards and intersect the liquid-vapor curve and remain on the liquid-vapor curve all the way to the surface (Fig. 1.1). In such cases, a relatively small portion of the original liquid mass may be transferred to the vapor phase – in this paper we refer to this as "gentle boiling", for lack of a better term, and to distinguish between this style of boiling and more intense boiling described below. In other cases, the liquid hydrothermal fluid at depth may be present in numerous poorly connected and/or highly cemented fractures, resulting in fluid pressures that exceed hydrostatic and may approach lithostatic (Fig. 1.1). If the rock fractures, perhaps as a result of seismic activity or increased fluid

pressure, a pressure decrease to less than hydrostatic pressure might occur instantaneously, resulting in conversion of essentially 100% of the original liquid into a low density vapor phase. This type of boiling is referred to as "flashing", and has been observed to occur in active geothermal systems as the high temperature geothermal fluids (liquids) pass through a pressure plate into a low pressure environment and all of the liquid is instantaneously converted to steam (Brown, 1986). As discussed in more detail below, euhedral quartz with coexisting liquid-rich and vapor-rich inclusions will be precipitated during less intense boiling. Conversely, flashing is likely to deposit amorphous silica with a colloform texture and does not result in trapping of primary fluid inclusions, although secondary fluid inclusion assemblages containing vapor-only (or vapor-rich) inclusions may be trapped in earlier-formed minerals in the vein (Fig. 1.1).

The presence or absence of boiling determines the fluid inclusion types that are trapped at a given location in then system, and may also control ore metal distribution in the system. Beneath the boiling horizon many systems are characterized by higher base metal and lower (or absent) precious metal grades, whereas above the boiling horizon precious metals are more common. The highest gold grades are often found immediately above the boiling horizon (Buchanan, 1981; Cline et al., 1992; Hedenquist et al., 2000). In systems in which flashing occurs, a high grade (bonanza) zone is more likely at the base of the boiling zone (Fig. 1.1), whereas in systems characterized by more gentle boiling precious metal grades may be lower and distributed over a greater vertical distance above the bottom of the boiling zone, and the highest grades may occur at some distance above the bottom of the boiling zone (Simmons and Browne, 2000). Albinson et al. (2001) note that ore zones in boiling epithermal systems often show an economic bottom that is characterized by a dramatic change from high-grade ore to barren rock over a depth range of a few tens of meters to about a hundred meters (see Fig. 1.1), whereas in the less common non-boiling (or gently boiling?) epithermal deposits the economic bottom of the deposit occurs due to a gradual decrease in ore grade with depth and/or increased mining costs that make the deeper mineralization uneconomic to mine.

The spatial relationship between boiling, fluid inclusion and gangue mineral characteristics and precious metal mineralization provides a potentially valuable tool in

exploration for epithermal precious metals deposits. Thus, the presence of fluid inclusions or mineral textures indicative of boiling (or flashing) in surface outcrops suggests that the base of the boiling zone is below, and that deeper levels in the hydrothermal system may contain precious metal mineralization. Moreover, the presence of modest precious metals grades that decrease gradually with depth in the vein system without evidence of boiling suggests that boiling was not the cause of metal deposition and that a high-grade bonanza-type deposit is unlikely at depth.

1.1.1 *Previous fluid inclusion studies in the Guanajuato Mining District*

During the past half-century numerous fluid inclusion studies have been conducted in the Guanajuato Mining District (GMD) (Table 1.1). One of the earliest studies, by Wilson et al. (1950), focused on the Rayas and Cata mines in the central part of GMD (Fig. 1.2). Thirty samples containing quartz crystals from these deposits showed homogenization temperatures ranging from 215 to 299 ºC, with an average of 254 ºC. These workers did not comment on whether the samples contained boiling assemblages with both liquid-rich and vapor-rich inclusions.

Gross (1975) reported fluid inclusion homogenization temperatures from several samples collected along the Veta Madre and adjacent Sierra vein systems (Fig. 1.2). Homogenization temperatures ranged from about 260 to 330°C and showed a systematic increase with depth. For example, the homogenization temperature at an elevation of 1700 m above sea level was 320°C and dropped to 260°C at 2400 m elevation along the Veta Madre. As with the earlier work by Wilson et al. (1950), Gross (1975) did not comment on whether the samples contained both liquid-rich and vapor-rich inclusions.

The most detailed fluid inclusion study in the GMD, and one of the first to relate boiling and precipitation of precious metals in the district, was conducted by Buchanan (1979), whose research focused on the Las Torres mine and the deepest levels of the Rayas mine (1705 meter level) (Fig. 1.2). In both mines, coexisting liquid-rich and vapor-rich inclusions indicated that boiling occurred during precious metal mineralization. In the Las Torres mine, a correlation was observed between silver

sulfide deposition, high abundance of fluid inclusions with homogenization temperatures ranging from 231 to over 360 ºC, and deposition of adularia and sericite. In addition, a sample from the Rayas mine collected at an elevation of 1705 m showed evidence of boiling and homogenization temperatures from 290 to 385 ºC. Twelve other samples from the Rayas mine contained vapor-rich inclusions but these were interpreted to have formed by necking down (Buchanan, 1979). Two boiling horizons were observed in the Las Torres Mine. The shallow horizon was interpreted to represent “normal” hydrostatic boiling, whereas the deeper horizon was thought to represent flashing of the hydrothermal fluids when the impermeable seal fractured. The boundary between the boiling zone (above) and the non-boiling zone (below) was located at an elevation of about 1800 m (Buchanan, 1979).

In contrast to the observations of Buchanan (1979; 1980), Mango (1988) and Mango et al. (1991) found no evidence of boiling in fluid inclusions in quartz, calcite, and sphalerite from the Rayas Mine, and stable isotope analyses indicated that the precious and base-metals were deposited from meteoric water (Mango, 1988). Homogenization temperatures of fluid inclusions ranged from 230 to 305 ºC and salinity ranged from 0.5 to 3.3 wt. % NaCl equivalent. Results from gas analysis showed 0.3 to 2.1 mole % CO_2, 0.06 to 0.8 mole % H_2S, and less than 1 mole % CH_4, H_2 and CO in the inclusions (Mango et al., 1991). Mango et al. (1991) reported that boiling did not occur at any of the levels studied at Rayas, and suggested that if boiling of the hydrothermal fluids did occur it was at higher stratigraphic levels which have since been eroded. These workers also report that up to 850 m of erosion may have occurred above the Rayas ore body. This result disagrees with Buchanan (1981), who indicated that boiling only occurred to a depth of 650 m below the paleosurface during mineralization. It should be noted that Rayas contains more base metal sulfides than most other mines in the GMD (i.e., Las Torres), and less gold than others (i.e., El Cubo).

In this study, the relationship between fluid inclusion and mineral textural evidence for boiling and precious metal grades in the classic epithermal Ag-Au deposits at Guanajuato, Mexico, have been investigated to test for systematic correlations that may be used in exploration for similar deposits. Eight hundred and fifty-five (855) samples were collected from surface outcrops, underground workings, and recent drill core over

a strike length of 4 km and to depths of 750 m beneath the surface in four active mines and one closed mine along the Veta Madre. Each sample was assayed for Au, Ag, Cu, Pb, Zn, As, Sb. The goal of this study was to develop a method to target and prioritize areas for future exploration based only on data obtained during petrographic examination of thin sections. The method does not involve microthermometry or microanalysis of the inclusions.

1.2 Geological Setting

The Guanajuato Mining District (GMD) is located at the southern end of the Sierra Madre Occidental Eocene-Oligocene volcanic province and between the Sierra Madre Oriental and the Trans-Mexican volcanic belt (Clark et al., 1982). The GMD is part of a large northwest trending belt of silver-lead-zinc deposits that parallels the eastern flanks of the Sierra Madre Occidental (Randall et al., 1994). Aranda-Gómez et al. (2003) divide the rocks in this area into a “basal complex” and “cover rocks”. The basal complex consists of metamorphosed marine sediments of Mesozoic to early Tertiary age, while the Cenozoic cover rocks are composed of continental sediments and subaerial volcanic rocks. The Cenozoic volcanism has been divided into seven pulses (Aranda-Gómez et al., 2003), ranging in age from about 51 Ma to 8 Ma. Felsic to intermediate volcanism that occurred from 37 to 27 Ma produced the rock units and structures that host the mineral deposits at Guanajuato (Godchaux et al., 2003).

The regional geology in the GMD has been studied in detail by Edwards (1955), Echegoyen-Sanchez (1964), Taylor (1971), Gross (1975), Buchanan (1979) and Randall et al. (1994). The lowermost unit present in the area is the Esperanza Formation composed of carbonaceous and calcareous mudstones, shales, limestones and andesitic to basaltic flows that have all been metamorphosed to phyllite, slate and marble (Wandke and Martinez, 1928; Randall et al., 1994; Stewart, 2006). The thickness of this unit exceeds 600 m in the GMD and it has been assigned a Cretaceous age based on radiolaria (Dávila and Martínez-Reyes, 1987).

The next youngest unit in the GMD is the La Luz andesite (Randall et al., 1994), but this unit is absent in the vicinity of the city of Guanajuato and along the portion of the

Veta Madre that is the focus of this study (Buchanan, 1979). In this area, the Guanajuato Formation lies unconformably on the Esperanza Formation. The Guanajuato Fm. is composed of red, poor- to well-sorted conglomerate, sandstone and shale (Buchanan, 1979). The Guanajuato Fm. ranges from 1500 – 2000 m in thickness and is Eocene to early Oligocene in age based on vertebrate fossils (Edwards, 1955).

The Guanajuato Fm. is conformably overlain by the Loseros Fm., which is a 10 to 52 m thick, green andesitic volcaniclastic sandstone (Echegoyen-Sanchez, 1964; Buchanan, 1979). While no ages have been determined for the Loseros Fm., it is assumed to be early Oligocene based on its conformable location between the underlying Guanajuato Fm. and overlying Oligocene Bufa Fm.

The Bufa Formation conformably overlies the Loseros Fm. The Bufa Fm. represents a 350 m thick distal volcano-sedimentary unit with white, yellow and pink rhyolitic lapilli air-fall ash that has been dated at 37 +/- 3.0 Ma using K-Ar (Gross, 1975). The Bufa Fm. is separated from the overlying Calderones Fm. by a disconformity (Buchanan, 1979). The Calderones Formation consists of chloritized, crystal-rich andesitic tuff, except at the base. Here, andesitic volcanoclastic shale and sandstone lie unconformably on the Bufa Fm. The Calderones Fm. is 200-250 m thick (Gross, 1975; Stewart, 2006) and has been assigned a late Oligocene age based on cross-cutting relationships (Gross, 1975).

Overlying the Calderones Fm. is the Cedros Fm., which consists of grey to black andesitic flows interbedded with grey to green andesitic tuffs (Buchanan, 1979). The thickness of this unit is highly variable and ranges from 100 – 240 m in the district (Gross, 1975; Stewart, 2006).

The Chichindaro Fm. is the youngest formation in the area and has been dated at 32 +/- 1 Ma by K- Ar (Gross, 1975; Randall et al., 1994). It unconformably overlies the Cedros Formation and is composed of felsic ash and flow breccias (Taylor, 1971). Buchanan (1979) reports that the Chichindaro Fm. is pre-mineralization.

Mineralization in the GMD is associated with three parallel, northwest trending fault systems. The La Luz system is to the north and west of the city of Guanajuato, the Sierra system is to the east and south of the city of Guanajuato, and the intermediate Veta Madre system passes through the city of Guanajuato (Fig. 1.2). All samples

studied here were collected from the Veta Madre and along a traverse perpendicular to the vein.

In the study area the Veta Madre dips 35-55° to the SW and varies from hairline to several tens of meters in thickness (Buchanan, 1979). The Esperanza Fm., composed of dull-black carbonaceous and calcareous mudstones, shales, limestones and andesitic to basaltic flows that have all been metamorphosed to phyllite, slate and marble, serves as the footwall of the Veta Madre (Guiza, 1949; Edwards 1955; Cornelius, 1964). The Guanajuato Fm., composed of red, poor- to well-sorted conglomerate, sandstone and shale, forms the hanging wall of the Veta Madre (Edwards, 1955).

The Veta Madre mineralization consists mostly of quartz with various textures and less abundant calcite, fluorite, barite and adularia. The Veta Madre shows multiple generations of silica and carbonate deposition and brecciation to produce a complex system of veins and stockworks (Stewart, 2006) that are dominated by banded quartz (Wandke and Martinez, 1928). The banding structures in the veins are closely associated with mineralization and were an indication to early miners of high grades of ore (Wandke and Martinez, 1928). The stockworks are present in the hanging wall of the main vein and can have stope dimensions of more than 200 m x 100 m (Wandke and Martinez, 1928).

Camprubí and Albinson (2007) summarized data for epithermal deposits in Mexico and classified the deposits at Guanajuato as Type “B” deposits that show characteristics of both intermediate-sulfidation and low-sulfidation end members. According to these workers, the deposits become richer in base metals with depth and formed during multiple hydrothermal events. They also report that fluids responsible for the formation of low sulfidation mineralization are generally < 240°C with salinities of 3.5 - 7.5 wt. % NaCl. On the other hand, the intermediate sulfidation mineralization fluids vary from 230-300°C and show higher salinities of 7.5 - 23 wt. % NaCl. These values are consistent with results of previous fluid inclusion studies in the district summarized above.

1.3 Methodology

1.3.1 *Sample Collection and Preparation*

In collaboration with the staff of Great Panther Silver, 855 samples were collected along a 4 km strike length of the Veta Madre from both surface outcrops (Fig. 1.3, top) and underground locations, including drill core (Fig 1.3, bottom). The accessibility of underground workings in the San Vicente, Cata, Valenciana, Rayas and Guanajuatito Mines offered good three-dimensional geological controls. The northern part of the Valenciana Mine was not accessible because this area was flooded and access was prohibited. Collection of samples from surface outcrops and underground and drill cores focused on samples that contained transparent minerals that could be examined for fluid inclusions, especially quartz and calcite.

Surface samples were collected at each location where veins were encountered outcropping on the surface (Fig. 1.3, top), including along a 400 m traverse perpendicular to the Veta Madre in the vicinity of the San Vicente Mine. In the underground mines, samples were collected at regular intervals along drifts. Sample locations were determined using mine maps and survey marks. Samples were collected from the hanging wall and footwall of the vein where access permitted. Underground areas sampled included the following mines and levels: Rayas Mine (345 and 390 levels), Cata Mine (390 and 414 levels), south Valenciana Mine (320 level), Guanajuatito Mine and San Vicente Mine (190, 220, 270, 275 and 345 levels) (Fig. 1.3, bottom). Levels for all mines indicate depth beneath the surface in meters, relative to the elevation at the top of the Rayas shaft, which is at an elevation of 1,999 m above sea level. Drill core samples were obtained from the underground and surface drilling program and historical drilling (Fig. 1.3, bottom). At each location one sample representing the dominant style of mineralization and/or vein texture at that location was collected, although it should be noted that recognizable heterogeneity often occurred over short distances along each level. In some cases, two or more samples were collected at a given location to better capture the diversity of mineralization styles.

The hand samples were cut perpendicular to the vein to produce a section that extended from the vein wall towards the center of the vein. Then, a thin section-sized billet approximately 13/16 inches x 1 inch (21 mm x 35 mm) was cut from the larger slab and a “thick” section approximately 75 μm thick was prepared. If the vein thickness was greater than twice the long dimension of the billet, the billet was cut to include one of the vein walls. The logic of this approach is that the material closest to the vein wall is the oldest material in the vein, because these are open-space filling veins and not crack-seal type veins that often re-fracture at the wallrock-vein contact and make determination of mineral and fluid inclusion paragenesis problematic (see Becker et al., 2010). Our logic for using this sample preparation protocol was that even if mineralization at that location occurred later than the time represented by the sample, the sample is still likely to contain secondary fluid inclusions containing fluids responsible for precipitating later material. This approach increases the likelihood of sampling all fluid events associated with vein formation while at the same time minimizing the size and/or number of thick sections needed.

Thick section preparation was done by an outside vendor and at Virginia Tech. This study involved only petrographic examination of the samples, thus doubly polished sections were not required. “Quick plates” were prepared (Goldstein and Reynolds, 1994) by grinding the cut surface with 320 micron grit to eliminate the macroscopic imperfections produced by cutting the sample. Next, the sample was mounted to a glass slide with epoxy adhesive. The final process consisted of cutting and grinding the sections to 75-100 micron thickness (Van den Kerkhof and Hein, 2001) in order to study the fluid inclusions and mineral textures.

In addition to preparing thick sections from the samples, one half of each cut sample was assayed for gold (Au), silver (Ag), copper (Cu), lead (Pb), zinc (Zn), arsenic (As) and antimony (Sb).

1.4 Petrography

Goldstein and Reynolds (1994) describe the technique for observing unpolished thick sections (“quick sections”) under the microscope that involves covering the surface with immersion oil to improve the optical properties of the sample for viewing fluid

inclusions. The immersion oil with an index of refraction close to that of the mineral fills all cracks and imperfections. Because our samples consisted mostly of quartz we used oil with an index of refraction of 1.515.

Samples were examined using a petrographic microscope, starting at low magnification and proceeding to higher magnification. The first task for each sample was to identify the mineral phases and to classify the textures of quartz and calcite if present (every sample contained quartz and about one-quarter also contained calcite). Next, the sample was examined systematically to identify fluid inclusion assemblages (FIAs) and the types of fluid inclusions in each FIA were noted. An FIA represents a group of fluid inclusions that were all trapped at the same time (Goldstein and Reynolds, 1994; Bodnar, 2003a) and thus represent the physical and chemical conditions in the system at the time of trapping (assuming that the inclusions have not reequilibrated; Bodnar, 2003b). FIAs may be composed of primary inclusions trapped during precipitation of the host phase, or may contain secondary inclusions that are trapped along fractures in the host phase at some time after the mineral has formed. FIAs in samples from the Veta Madre were further classified as containing either only liquid-rich inclusions with consistent liquid-to-vapor ratios, or containing coexisting liquid-rich and vapor-rich inclusions with a broad range in liquid to vapor ratios, or only vapor-rich inclusions (Fig. 1.4).

Fluid inclusions in the Veta Madre, and in most epithermal deposits, must be interpreted with caution because much of the host material may have been deposited as an amorphous silica phase or chalcedony and has since (re-) crystallized to produce coarse-grained quartz. Primary appearing inclusions in such samples are unlikely to record the original formation conditions (Bodnar et al., 1985; Sander and Black, 1988). In this study, only secondary inclusions that clearly crosscut quartz crystal boundaries, and therefore were trapped after the quartz (re-) crystallized, were studied in quartz that showed textures indicative of original precipitation as an amorphous or fine-grained phase, as described below. Similar arguments apply to fluid inclusions in replacement minerals, such as quartz replacing lattice-bladed calcite.

1.4.1 *Quartz and calcite textures:*

Previous workers have shown that silica and carbonate phases in the epithermal environment often show highly variable and sometimes diagnostic textures (Figs. 1.5 and 1.6) that identify the physical conditions associated with mineralization (Adams, 1920; Bodnar et al., 1985; Sander and Black, 1988; Simmons and Christenson, 1994; Dong et al., 1995; Henley and Hughes, 2000; Camprubí and Albinson, 2007). These various textures can be divided into those that are produced during the original deposition of the phase, those that represent recrystallization textures, and those that represent replacement of originally precipitated material. Further, some of these textures are readily apparent in hand samples, others require microscopic observation, and some textures are only revealed under crossed-polars. Finally, some of these phases contain fluid inclusions that may be used to infer the paleo-environment in the hydrothermal system, whereas others rarely contain useful fluid inclusions (Bodnar et al., 1985). In this study, we have characterized the mineralogy and mineral textures observable in hand samples and under the microscope, and these are summarized below.

The most common mineral texture observed in 752 out of 855 samples (Fig. 1.7) from the Veta Madre is mosaic or jigsaw-textured quartz (Figs. 1.5 and 1.6A, B). Camprubí and Albinson (2007) report that this texture is the one most commonly associated with ore minerals in the Mexican epithermal deposits. This texture is characterized by aggregates of microcrystalline to crystalline quartz crystals with interpenetrating grain boundaries (Dong et al., 1995), and is only recognizable when observed under crossed polars (Figs. 1.6A, B). The texture is interpreted to result from the recrystallization of massive chalcedony or amorphous silica (Dong et al., 1995; Camprubí and Albinson, 2007). Fournier (1985; see also Saunders, 1994) reports that the presence of jigsaw texture quartz indicates a recrystallization temperature >180°C, which is approximately the upper stability limit for chalcedony. In some cases the original colloform texture is readily apparent in plain polarized light. As noted by Sander and Black (1988), primary fluid inclusions in this type of quartz do not record the original depositional conditions. However, in this study we observed many trails of secondary

fluid inclusions in jigsaw quartz that record fluid conditions in the Veta Madre after recrystallization of the original chalcedony or amorphous silica. As such, these fluid inclusions are useful monitors of the fluid conditions during the later stages of the hydrothermal history of the system, including later stages of Ag-Au mineralization.

The next most abundant texture (549 samples; Fig. 1.7) is plumose quartz texture (Sander and Black, 1988) that shows variable extinction positions when observed under crossed polars (Figs. 1.6C, D). This quartz texture has also been referred to as “feathery” (Fig. 1.5B) or “flamboyant” (Fig. 1.5C) by Adams (1920) and Dong et al. (1995), respectively. This recrystallization texture is thought to develop from aggregates of fibrous chalcedony with rounded external surfaces, and originated as silica gel (Dong et al., 1995). The silica gel is precipitated when supersaturation occurs in response to rapid pressure decrease associated with fracturing and the concomitant temperature decrease, leading to precipitation of amorphous silica (Henley and Hughes, 2000). Depending on the initial temperature and pressure (and enthalpy) of the fluid before fracturing, the fluid may flash with 100% of the liquid converted to vapor (see Brown, 1986), or P-T conditions may remain on the liquid-vapor curve as the fluid continues to boil along its upward flow path. Camprubí and Albinson (2007) report that this type of silica is a transitional phase in the silica precipitation cycle that precipitates after the amorphous silica phase and before the later crystalline quartz phase. As with the jigsaw texture described earlier, primary fluid inclusions in this type of quartz do not record the original depositional conditions, but secondary inclusions may provide useful information concerning later conditions.

Rhombic or massive calcite (Fig. 1.5N) is observed in 190 out 855 samples from the Veta Madre (Fig. 1.7). While bladed calcite is thought to be characteristic of deposition from a boiling solution (see below), an association between rhombic calcite and boiling is less clear. Camprubí and Albinson (2007) report that this type of “blocky” calcite is not associated with mineralization in the Mexican epithermal deposits but, rather, represents the collapse of shallow steam-heated carbonate waters late in a given hydrothermal cycle. Dong and Zhou (1996) also note that massive calcite is late and not associated with mineralization in the Cracow epithermal vein system in Australia.

Quartz with colloform texture is observed in 193 out of 855 samples from the Veta Madre (Fig. 1.7). Rogers (1918) introduced the term “colloform” to describe quartz with a rounded or botryoidal form that occurs in continuous bands (Fig. 1.6I, J). When observed under crossed-polars, the colloform texture sometimes shows an evolution from fine-grained to more coarse-grained quartz with a plumose texture (Fig. 1.5G) along a traverse from the vein wall to the center of the vein. Similarly, colloform texture sometimes shows a jigsaw texture characterized by banding of fine-grained quartz near the wallrock contact, with the grain size increasing towards the vein center, and is most easily recognized when the sample is viewed under crossed polars (Fig. 1.5H). This type of quartz contains no useful primary fluid inclusions (Bodnar et al., 1985). Colloform texture is a primary depositional texture that has been interpreted to indicate rapid deposition of chalcedonic quartz in open space in shallow epithermal systems to produce the rhythmic banding (Roedder, 1984; Bodnar et al., 1985; Fournier, 1985). Henley and Hughes (2000) suggest that this texture is generated during rapid opening of a fracture that produces a pressure drop and rapid cooling associated with boiling or flashing (Fig. 1.1). Saunders (1990) notes that electrum at the Sleeper deposit in Nevada is associated with alternating colloform bands of fine-grained quartz and opaline silica. He suggests that the gold and silica in the opaline bands originally precipitated as colloidal particles in the deeper parts of the system and were then remobilized and transported upwards by later fluids.

Lattice bladed calcite, including lattice bladed calcite replaced by quartz, is observed in 120 out of 855 samples from the Veta Madre (Fig. 1.7). This classification includes bladed calcite that is still compositionally calcite today (Fig. 1.5F, 1.6E, F), as well as bladed calcite that has been replaced by quartz (Fig. 1.5K, 6G, H), and calcite with an acicular texture that has been replaced by quartz (Fig. 1.5L). Albinson (personal communication, 2011) notes that acicular textures similar to those shown in Figure 1.5L may be produced when quartz replaces barite, zeolites or laumontite. Barite and zeolites do occur in the Veta Madre, and the possibility that some of the pseudo-acicular replacement textures interpreted to be pseudomorphs after calcite may in fact be replacements of these other phases.

Simmons and Christenson (1994) described the close association between bladed (platy) calcite and boiling in geothermal systems and attribute this morphology to the rapid growth of calcite as carbon dioxide is lost to the vapor phase during boiling. Camprubí and Albinson (2007) note that bladed calcite is common in Mexican low-sulfidation deposits but is usually not closely associated with ore minerals. The presence of coexisting liquid-rich and vapor-rich inclusions in the calcite often confirms that the fluids were boiling during bladed calcite formation (Simmons and Christenson, 1994; Simmons et al., 2005). Often quartz completely replaces the bladed calcite and this type of replacement texture contains no useful primary fluid inclusions, but secondary inclusions may provide information concerning later conditions. The pseudo-acicular replacement texture (Fig. 1.5L) is produced when bladed calcite is replaced by quartz, but has also been observed in bands of chalcedony (Albinson, personal communication, 2011). An aggregate of fine-grained quartz phases with anhedral to rectangular shape replace the calcite to produce an acicular morphology (Adams, 1920; Dong et al., 1995). This type of replacement texture contains no useful fluid inclusions. The next most abundant texture observed in 52 samples from the Veta Madre is massive quartz (Fig. 1.5O). This term refers to quartz veins that have a homogeneous texture, show no banding or deformation features (Dong et al., 1995). The massive texture represents an original growth feature and can form during slow precipitation in open space, and is generally not associated with boiling.

The remaining mineral textures are observed in less than five percent of the samples. The zonal quartz texture was observed in 23 samples. This primary depositional texture is similar to comb texture, but with euhedral quartz crystals that show growth zoning and which are oriented perpendicular to the vein wall (Fig. 1.5P, R). The growth zones often contain primary fluid inclusions that record the original depositional conditions. The crustiform texture is a primary depositional texture that has been described by Adams (1920), Lindgren (1933), Bodnar et al., (1985) and Dong et al. (1995). The banding is often symmetrically distributed with respect to both walls (Fig. 1.5M) and is formed as a result of rapid, episodic fluctuations in temperature, pressure or fluid conditions during boiling. The original quartz and chalcedony banding is sometimes partially destroyed by recrystallization (Adams, 1920). This type of quartz

can contain useful primary and secondary fluid inclusions. Cockade texture is a primary depositional feature that is confined to breccia zones, where rock fragments are surrounded by concentric crusts of quartz (Fig. 1.5Q) (Adams, 1920; Dong et al., 1995). This occurrence of quartz, which is uncommon in the Veta Madre, can contain useful primary and secondary fluid inclusions. Comb texture quartz (Fig. 1.5R) is a primary depositional texture that was observed in a few samples. This texture is characterized by coarse, imperfect, euhedral crystals growing into open space perpendicular to the vein walls (Adams, 1920). This type of quartz often contains numerous microfractures that contain secondary fluid inclusions (Bodnar et al., 1985). The ghost-sphere and moss textures are deposited from colloidal amorphous silica. Under crossed polars these types of quartz show a jigsaw texture resulting from crystallization (Fig. 1.5I). Ghost-sphere and moss texture quartz contain no useful primary fluid inclusions.

While the goal of this study was not to develop a mineral paragenesis, some generalities concerning the paragenesis of the vein minerals and textures can be summarized. Within a given sequence, colloform quartz is earliest, followed by jigsaw or plumose texture, and finally by coarse euhedral quartz, some of which is amethyst. This sequence may be repeated several times at a given location. Bladed calcite may appear along with any of the quartz textures that are indicative of boiling, but rhombic calcite is always late.

As noted previously, boiling has been linked to metal deposition in precious metal systems (Buchanan, 1979; Roedder, 1984; Bodnar et al., 1985; Brown, 1986; Simmons and Christenson, 1994; Andre-Mayer et al., 2002; Etoh et al., 2002), and many of the textures described above are thought to be produced as a result of boiling (or, at least, rapid temperature and/or pressure drop that leads to over-saturation and rapid precipitation). Shallow hydrothermal systems such as those associated with epithermal deposits often experience repeated episodes of sealing and fracturing during the lifetime of the system, as evidenced by abundant brecciation and broken crystals in epithermal systems. Hydraulic fracturing and the concomitant pressure drop may cause the fluid to boil (or “flash” to steam) (Fig. 1.1). When this occurs the temperature decreases owing to the large heat of vaporization of water. At temperatures ≤340°C, the solubility of quartz decreases with both decreasing pressure and decreasing

temperature (Fournier, 1985). As a result, the fluid that was originally in equilibrium with quartz may achieve a high degree of supersaturation, leading to the precipitation of amorphous silica with a colloform texture. With time, the amorphous silica may recrystallize to chalcedony and/or quartz (Fournier, 1985). This interpretation is consistent with the general quartz paragenesis observed in Mexican epithermal deposits, which includes early amorphous silica, followed by chalcedony and plumose quartz, and finally by coarse crystalline quartz (Camprubí and Albinson, 2007). We note that this sequence relates to a single episode of fracturing, and that this process repeats itself many times during the history of the system. Thus, at any one location up to several tens of fracturing and boiling episodes may be observed.

Those textures observed here that are thought to be produced directly by precipitation from supersaturated solutions, or by crystallization of chalcedony or quartz from original amorphous silica, include jigsaw (Fig. 1.5A), feathery (Fig. 1.5B), flamboyant (Fig. 1.5C), plumose (Fig. 1.5D), colloform (Fig. 1.5E), colloform banded plumose (Fig. 1.5G), colloform banded jigsaw (Fig. 1.5H), crustiform quartz (Fig. 1.5M), moss (Fig. 1.5J) and ghost-sphere (Fig. 1.5I). Similarly, lattice bladed calcite (Fig. 1.5F), lattice-bladed calcite replaced by quartz (Fig. 1.5K) and pseudo-acicular quartz after calcite (Fig. 1.5L) are also textures associated with boiling fluids. In each sample, the presence of these textures has been noted and used to infer whether boiling occurred at the sample location at some time during or after deposition of the original material. The number of samples containing each of the textures described above is summarized in Figure 1.7.

1.4.2 Fluid inclusions

Petrographic examination of Fluid Inclusion Assemblages (FIAs; Goldstein and Reynolds, 1994) can provide evidence concerning the chemical and physical environment of formation of epithermal precious metals deposits (Bodnar et al., 1985). As noted by previous workers (Bodnar et al., 1985; Sander and Black, 1988; Dong et al., 1995), some types of quartz (either originally precipitated or recrystallized amorphous silica) from the epithermal environment contain no useful fluid inclusions.

Thus, primary-appearing fluid inclusions in colloform banded plumose, colloform banded jigsaw, jigsaw and plumose texture quartz do not record the conditions of formation because these phases were originally precipitated as amorphous silica or chalcedony and have subsequently recrystallized. On the other hand, secondary fluid inclusions trapped along healed fractures in quartz that has recrystallized from amorphous silica or fine-grained chalcedony do record the conditions of this later fracture-healing event. In each sample containing these textures, secondary FIAs were monitored to determine if the inclusions showed evidence of boiling. While these secondary fluid inclusions do not record boiling during precipitation of the material immediately surrounding the inclusions, they are thought to reflect boiling conditions nearby in the vein at some later time in the evolution of the system (Fig. 1.1).

When fluid inclusions are trapped in a single-phase fluid system, all of the inclusions will show the same phase behavior when observed under the microscope at room temperature. However, if the inclusions are trapped in a boiling or immiscible fluid system, some inclusions will trap the liquid phase, some will trap the vapor, and some will trap mixtures of the two phases (Bodnar et al., 1985). In each FIA identified as described above, the phase relations of individual inclusions were examined. petrographically to determine if all the inclusions appeared to have the same liquid-to-vapor ratio, or if the inclusions in the FIA showed variable ratios (Fig. 1.4). While variable liquid-to-vapor ratios may be produced by trapping mixtures of liquid and vapor in a boiling system, they may also be produced by necking down of the inclusions *after* a vapor bubble has nucleated in the inclusions. Following Goldstein and Reynolds (1994), we have assumed that if the FIA includes vapor-rich inclusions and liquid-rich inclusions with variable liquid-to-vapor ratios, as well as all-liquid inclusions, that the inclusion phase ratios are the result of necking down or, possibly, recrystallization of amorphous silica or chalcedony (Sander and Black, 1988), and are not the result of boiling

1.5 Results and Interpretation

The goal of this study was to examine possible correlations between precious metal mineralization and mineralogical and fluid inclusion evidence for boiling along the Veta Madre at Guanajuato, Mexico, and to develop a tool that could be used in exploration for epithermal systems. As noted above, many of the textures described for quartz might have formed as a result of rapid precipitation from hydrothermal fluids, likely as a result of boiling. In addition, the presence of coexisting liquid-rich and vapor-rich fluid inclusions in the same FIA (with no single-phase, all-liquid inclusions present, which would suggest necking, rather than boiling) indicates that the inclusions were trapped in a boiling fluid. Importantly, Camprubí and Albinson (2007) report that boiling is the most important depositional mechanism in the Mexican epithermal deposits based on the close temporal and spatial association of mineralogical and fluid inclusion evidence for boiling and ore mineralization. Thus, textural and fluid inclusion evidence can help the explorationist to identify systems that have experienced boiling and may be suitable hosts for precious metal mineralization.

For each of the 855 samples examined, a numerical value was assigned for each mineral texture and fluid inclusion feature described above. A value of 0 (zero) was assigned if a given feature was not observed during petrographic examination of the sample, and a value of 1 (one) was assigned if the feature was observed. The number of observations for each of the boiling features is summarized in Figure 1.7. Jigsaw texture quartz was observed in 88% of the samples (752 of 855). Plumose texture quartz, also referred to as feathery or flamboyant texture quartz in the literature, occurs in 549 samples (64%). Colloform textures, including colloform banded plumose and colloform banded jigsaw textures, were observed in 193 samples (23%), and lattice bladed calcite and/or lattice bladed calcite replaced by quartz and/or acicular calcite replaced by quartz was observed in 120 samples (14%). Fluid inclusion assemblages containing coexisting liquid-rich and vapor-rich fluid inclusions were observed in 193 samples (Fig. 1.7).

For each of the textures described above, the average Au and Ag grade of samples in which the feature is present, and the average Au and Ag grade for samples in which that feature is absent, have been calculated and the results are shown on Figures 1.8 and 9, respectively. The average grade of Au is higher in samples in which the boiling

feature is present, compared to samples for which it is absent, for all features except for cockade texture quartz (Fig. 1.8). Also, the largest difference in grade between samples showing the presence or absence of a feature is for colloform texture quartz (1.1 ppm Au versus 0.2 ppm Au). The average Au grade is lower in samples dominated by non-boiling textures, including massive, zonal and comb texture quartz and rhombic calcite, consistent with the assumption that boiling is the depositional mechanism in these deposits.

The average grade of silver is higher in samples in which a boiling feature is present for all features except for jigsaw texture quartz. This observation is consistent with observations of Camprubí and Albinson (2007), who report that the silica phase that is most closely associated with ore-bearing minerals is colloform-textured jigsaw quartz. Based on these results, we suggest that the jigsaw texture quartz is an indicator of boiling, which may or may not be associated with mineralization, depending on the metal content of the fluid. As noted by Camprubí and Albinson (2007), *"the occurrence of boiling does not necessarily lead to the occurrence of metallic-bearing associations (Camprubi et al., 2001) if the boiling fluids are not endowed with dissolved metals"*.

The average Ag grade is lower in samples that show mineral textures that are indicative of slow crystal growth (non-boiling), including massive, zonal, cockade and comb texture quartz – the lone exception is rhombic calcite, which is not thought to be associated with boiling but may indicate effervescence of CO_2 or descent of steam-heated waters that precipitate calcite as the temperature increases (Simmons et al., 1988; Simpson et al., 2001). Features that show the most dramatic difference in Ag grade when comparing samples that show the presence or absence of that feature are colloform texture quartz (178.8 ppm Ag versus 17.2 ppm Ag) and bladed/platy calcite (128.4 ppm Ag versus 47.5 ppm Ag).

There is no significant difference in average grade of samples containing both liquid-rich and vapor-rich fluid inclusions, compared to those in which fluid inclusion evidence for boiling is absent. The Au grades are essentially identical (≈0.4 ppm Au) in samples containing boiling FIAs and those in which they are absent (Fig. 1.8). The Ag grade is slightly elevated in samples containing coexisting liquid-rich and vapor-rich fluid inclusions, compared to those in which fluid inclusion evidence for boiling is absent

(67.1 ppm Ag versus 49.4 ppm Ag; Fig. 1.9). This lack of correlation likely reflects the fact that the phases being precipitated as a result of boiling (dominantly amorphous silica and chalcedony) are not amenable to the trapping of fluid inclusions that reflect the original trapping conditions, and thus the metal deposition stage and the secondary fluid inclusion trapping events were not concurrent.

Data shown on Figures 1.8 and 1.9 were evaluated using the t-test to assess whether the average grades (means) for samples in which a feature is present are statistically different from those in which the feature is absent. Differences between the presence or absence of a feature indicative for boiling are statistically different at the 95% confidence level ($p<0.05$) for all features except jigsaw texture silica ($p<0.10$) and fluid inclusions ($p<0.25$) for silver, and for fluid inclusions ($p<0.10$) for gold (Fig. 1.10). For comparison, the distribution of grades for samples in which massive quartz (a non-boiling texture) is present and absent are also shown on Figure 1.10.

The textural and fluid inclusion data obtained in this study were analyzed using the binary classifier within the statistical software package SPSS Clementine. The binary classifier builds 10 different statistical models and evaluates the performance of each model. The Au and Ag grades show a log normal distribution based on application of the Shapiro-Wilks test for normality (Fig. 1.11a. b). Our goal was to determine if the statistical models could distinguish between samples with ore grades (≥1 ppm Au or ≥100 ppm Ag) and those that were sub-economic. Each sample was assigned a label that identified whether the concentration was above or below these thresholds. Of the 694 samples for which we had Au and Ag assay data, only about 6% of the samples had concentrations that classified them as ore grade (≥1 ppm Au or ≥100 ppm Ag) for either gold or silver.

In order to build an unbiased statistical model, the number of observations was balanced via random sampling to contain an approximately equal number of ore grade and sub-economic samples. If an equal number of ore grade and sub-economic samples was not selected to develop the model, the model would tend to over-predict the grade with a higher frequency in the sample population. For Au, after balancing, 78 samples were selected to build the models (36 had Au ≤1 ppm and 42>1 ppm).

Similarly, for Ag, 77 samples were selected to build the models, and 38 samples had >100 ppm Ag and 39 <100 ppm Ag.

After balancing the number of ore grade and sub-economic samples, the dataset was split into a training dataset (70% of the observations) and testing dataset (30% of the observations). The software iteratively builds and evaluates the predictive models and ranks the resulting models based on accuracy, i.e., the proportion of correct predictions. The models that showed the highest "profit" or greatest predictive capability for both Au and Ag were the neural network, the C5 decision tree and Quest decision tree models, all of which predicted the correct results in about 70-75% of the tests. For both Ag and Au, most other models showed significantly poorer predictive capability.

The binary classifier model building and testing software also provides information on the relative importance of each of the variables included in the model. For both Au and Ag, the colloform texture was the variable with the greatest importance, i.e., colloform quartz has the greatest predictive power to distinguish between ore grade samples and sub-economic samples (Fig. 1.12). This is consistent with the fact that amorphous silica with colloform texture is precipitated as a result of intense boiling (or flashing), and Camprubí and Albinson (2007) have noted that boiling or fluid immiscibility is temporally and spatially associated with ore mineralization in the Mexican epithermal deposits. For Au, the second most important variable was bladed/platy calcite replaced by quartz (Fig. 1.12a), and for Ag, fluid inclusion evidence for boiling (coexisting liquid-rich and vapor-rich fluid inclusions or FIAs containing only vapor-rich inclusions) showed the second highest importance (Fig. 1.12b). Note that Camprubí and Albinson (2007) report that bladed calcite is usually not associated with ore minerals in the Mexican deposits. The association with bladed calcite may therefore not reflect conditions during deposition of the original calcite but, rather, conditions during replacement of that calcite by quartz.

1.6 Application in Exploration for Epithermal Precious Metal Deposits

The goal of this study was to develop a methodology that could be used in exploration for epithermal precious metal deposits. The method is based on the

assumption that precious metal mineralization and boiling are genetically related and that systems with strong evidence for boiling have greater potential to host ore than those that do not show this evidence. In practice, the method identifies systems in which boiling has occurred, and it must be emphasized that not all hydrothermal fluids in the epithermal environment contain Au and/or Ag. Thus, some systems may show significant evidence of boiling but contain no Au or Ag mineralization, as also emphasized by Camprubí and Albinson (2007).

The feature that is most closely related to higher Au and Ag grades in the Veta Madre is colloform quartz. This texture is often easily recognizable in outcrop and hand sample, as well as during normal petrography. Lattice bladed or platy calcite and plumose texture quartz are also closely associated with higher grade samples in the Veta Madre. While lattice bladed calcite is recognizable in hand sample, it may be necessary to examine samples under crossed polars to recognize plumose texture quartz. Contemporaneous liquid-rich and vapor-rich fluid inclusions show only a poor correlation with higher Au and Ag grades at Guanajuato. This lack of correlation reflects the fact that inclusions are not trapped during precipitation of amorphous silica that later crystallizes to produce colloform quartz, and inclusions that are trapped during precipitation of lattice bladed calcite are often destroyed when the calcite is replaced by quartz. These observations suggest that mineral textures may be better indicators of mineralization in the epithermal precious metal deposits in the Guanajuato Mining District compared to fluid inclusions showing evidence of boiling, but that the two tools are complementary.

Most samples collected from the Veta Madre for this study show some evidence of boiling (>750 out of 855 samples). Most of the samples that do not show evidence of boiling contain only rhombic calcite, and this form of calcite is not thought to be precipitated during boiling but, rather, is precipitated as steam-heated waters descend (Simmons et al., 1988; Simpson et al., 2001).

To test whether the methods developed in this study might be used to establish vectors pointing towards a mineralized vein system that was formed from boiling fluids, four samples were collected along a traverse perpendicular to the Veta Madre. The samples were collected by starting at the Veta Madre outcrop on the surface and

walking perpendicular to the vein, collecting a sample everywhere that a vein oriented approximately parallel to the Veta Madre, or a stockwork outcrop, was encountered. Most of the veins away from the Veta Madre were less than about 10 cm wide.

With distance away from the Veta Madre, the Ag and Au grades quickly drop to subeconomic values (Fig. 1.13 B, C). The only feature indicative of boiling that is recognized in 4 samples collected along a traverse perpendicular to the vein is jigsaw quartz (Fig. 1.13A). The rapid drop-off in boiling intensity indicators (and Ag and Au grades) with distance from the mineralized vein has both advantages and disadvantages for exploration. The disadvantage is that samples collected at a relatively short distance laterally away from a well-mineralized vein may show no evidence of boiling and/or mineralization. Conversely, if a sample collected from a surface outcrop contains good evidence for boiling, it is likely that this represents the surface expression of a vein that has potential to host precious metal mineralization.

As noted earlier, and as observed in modern geothermal systems, once boiling begins at depth it usually continues to the surface. Additionally, the best gold grades would be expected to occur at or above the base of the boiling zone. Therefore, good evidence of boiling in surface samples indicates that the base of the boiling zone where precious metal mineralization is mostly likely to occur is beneath the present surface. Such an area might be given higher priority for drilling to explore the subsurface, even if precious metal grades in the surface samples are poor. At Guanajuato, an angled drill hole from the surface into the Veta Madre showed a systematic increase in boiling intensity indicators as the vein was approached (Fig. 1.13D), even though the metal grades in the drill core were well below economic values. From an exploration perspective, boiling evidence suggests that drilling should be continued, even though metal grades are subeconomic.

Results of this study can also be applied during mining to explore deeper or peripheral parts of a mineralized vein system. For example, at Guanajuato evidence of boiling is present in samples from the surface to the deepest levels of current mining activities (Fig. 1.14), including drill core samples that extend beneath the deepest levels that have been mined at Cata (Fig. 1.3). This suggests that the bottom of the boiling horizon is at some depth greater than that explored by mining, and that additional

precious metal resources might be encountered as deeper levels of the Veta Madre system are explored and developed. This hypothesis was tested and found to be correct when Great Panther Silver explored the deep levels between the Rayas and Cata Mines (Fig. 1.3) and discovered mineralization on the Santa Margarita vein. Mineralization on the Santa Margarita changes from Au-rich (a zone 52 meters long, 3.4 meters wide, with assays averaging 5.06g/t gold and 20g/t silver) to Ag-rich with depth (26 meters long, 3.45 meters wide, with assays averaging 5.23g/t gold and 359g/t silver). The Santa Margarita vein has a total mineralized length of over 300 meters (Great Panther Silver, 2009), and its presence beneath the deepest explored levels at Rayas was suggested in part by the strong evidence for boiling observed in subsurface samples (Moncada and Bodnar, 2012).

1.7 Acknowledgements

The authors thank the staff of Great Panther Silver Ltd., especially Robert Archer, William Vanderwall, Adrian Bray and Robert Brown for providing financial support and access to samples and information used in this study. Consejo Nacional de Ciencia y Tecnología (CONACyT) and the Virginia Tech Graduate School provided partial funding during this study. We also thank Roberto Ontiveros and Juan Jose Martinez Reyes of the Guanajuato School of Mines for providing logistical support during field work in the Guanajuato Mining District. Review comments and suggestions on an earlier version of this manuscript by Tawn Albinson and an anonymous reviewer significantly improved the manuscript.

1.8 References

Abeyta, R. L., 2003. Epithermal gold mineralization of the San Nicholas Vein, El Cubo Mine, Guanajuato, Mexico: Trace element distribution, fluid inclusion microthermometry and gas chemistry. Unpublished Master's thesis, New Mexico Institute of Mining and Technology, Socorro, NM, 129 pp.

Adams, S. F., 1920. A microscopic study of vein quartz. Economic Geology, 15(8): 623-664.

Albinson, T., Norman, D. I., Cole, D., and Chomiak B., 2001. Controls on formation of low-sulfidation epithermal deposits in Mexico: Constraints from fluid inclusion and stable isotope data. Society of Economic Geologists Special Publication 8, 1-32.

Andre-Mayer, A.-S., Leroy, J. L., Bailly, L., Chauvet, A., Marcoux, E., Grancea, L., Llosa, F., and Rosas, J., 2002. Boiling and vertical mineralization zoning; a case study from the Apacheta low-sulfidation epithermal gold-silver deposit, southern Peru. Mineralium Deposita, 37(5): 452-464.

Aranda-Gómez, J. J., Godchaux, M. M., Aguirre-Díaz, G. J., Bonnichsen, B., Martínez-Reyes, J., 2003. Three superimposed volcanic arcs in the southern Cordillera—from the Early Cretaceous to the Miocene, Guanajuato, Mexico. In: Geologic Transects Across Cordilleran Mexico, Guidebook for Field Trips of the 99th Annual Meeting of the Cordilleran Section of the Geological Society of America, Mexico, D. F., April 5–8, 2003. Universidad Nacional Autónoma de México, Instituto de Geología, Publicación Especial 1, Field trip 6, p. 121–168.

Becker, S. P., Eichhubl, P., Laubach, S. E., Reed, R. M., Lander, R. H., Bodnar, R. J., 2010. A 48 m.y. history of fracture opening, temperature and fluid pressure: Cretaceous Travis Peak Formation, East Texas basin. Bulletin of the Geological Society of America, 122, no. 7/8, 1081-1093.

Bodnar, R. J., 2003a. Introduction to fluid inclusions, *in* Samson, I., Anderson, A., and Marshall, D., eds., Fluid Inclusions: Analysis and interpretation: Mineralogical Association of Canada, Short Course 32, p. 1–8.

Bodnar, R. J., 2003b. Reequilibration of fluid inclusions, *in* Samson, I., Anderson, A., and Marshall, D., eds., Fluid inclusions: Analysis and interpretation: Mineralogical Association of Canada, Short Course 32, p. 213–230.

Bodnar, R. J., Reynolds, T. J., and Kuehn, C. A., 1985. Fluid-inclusion systematics in epithermal systems. Reviews in Economic Geology, 2, p. 73-97.

Brown, K. L., 1986. Gold deposition from geothermal discharges in New Zealand. Economic Geology, 81(4): 997-983.

Buchanan, L. J., 1979. The Las Torres Mines, Guanajuato, Mexico: Ore controls of a fossil geothermal system. Unpublished Ph. D. dissertation, Colorado School of Mines, Golden, Colorado, 138 pp.

Buchanan, L. J., 1980. Ore controls of vertically stacked deposits, Guanajuato, Mexico. American Institute of Mining Engineers, Preprint 80-82, 26.

Buchanan, L. J., 1981. Precious metal deposits associated with volcanic environments in the Southwest. Arizona Geological Society Digest 14, p. 237-262.

Camprubí, A., and Albinson, T., 2007. Epithermal deposits in mexico – Update of current knowledge, and an empirical reclassification. Geological Society of America Special Paper 422, p. 377-415.

Camprubí, A., Canals, À., Cardellach, E., Prol-Ledesma, R. M., and Rivera, R., 2001. The La Guitarra Ag-Au low sulfidation epithermal system, Temascaltepec district, Mexico.: Vein structure, mineralogy, and sulfide-sulfosalt chemistry. Society of Economic Geologists Special Publication Series, v. 8, p. 133-158.

Church, J. A., 1907. The Mines of La Luz, Guanajuato, Mexico II. The engineering and mining journal, 105-110.

Clark, K. F., Foster, C. T., and Damon, P. E., 1982. Cenozoic mineral deposits and subduction-related magmatic arcs in Mexico. GSA Bulletin, 93(6): 533-544.

Cline, J. S., Bodnar, R. J., and Rimstidt, J. D., 1992. Numerical simulation of fluid flow and silica transport and deposition in boiling hydrothermal solutions: Application to epithermal gold deposits. Journal of Geophysical Research, 97, B6, 9085-9103.

Cornelius, K. D., 1964. Geology of the footwall formations of the Veta Madre, Guanajuato Mining District, Guanajuato, Mexico. Unpublished Master's thesis, University of Arizona, Tucson, AZ, 42 pp.

Dávila, V. M., and Martínez Reyes, J., 1987. Un edad Cretacica para las rocas basales de la Sierra de Guanajuato. Universidad Nacional Autonoma de Mexico. April 28-30, Resumen, p. 19-20.

Dong, G., Morrison, G., and Jaireth, S., 1995. Quartz textures in epithermal veins, Queensland; classification, origin and implication. Economic Geology, 90(6) 1841-1856.

Dong, G., and Zhou, 1996. Zoning in the Carboniferous-Lower Permian Cracow epithermal vein system, central Queensland, Australia. Mineralium Deposits, 30(1): 210-224.

Echegoyen-Sanchez, J., 1964. Algunos datos sobre la mineralizacion de la Veta Madre de Guanajuato. In I er Seminario sobre Exploracion Geologico-Minera, Mem. p. 134-149.

Edwards , J. D., 1955. Studies of some early Tertiary red conglomerates of central Mexico. U. S. Geological Survey Professional Paper. P0264-H. 185 pp.

Etoh, J., Izawa, E., Watanabe, K., Taguchi, S., and Sekine, R., 2002. Bladed quartz and its relationship to gold mineralization in the Hishikari low-sulfidation epithermal gold deposit, Japan. Economic Geology, 97(8): 1841-1851.

Fournier, R. O., 1985. The behavior of silica in hydrothermal solutions. Reviews in Economic Geology, 2, p. 45-61.

Girnius, R., 1993. Deposition of the upper ore in the El Cubo mine, Guanajuato mining district, Mexico. Unpublished Senior's thesis, Dartmouth College, Hanover, NH, 21 pp.

Godchaux, M. M., Bonnichsen, B., Aguirre Diaz, G. de J., Aranda Gomez, J. J., Rangel Solis, G., and Anonymous., 2003. Volcanological and tectonic evolution of a complex Oligocene caldera system, Guanajuato mining district, central Mexico. Geological Society of America, Abstracts with Programs, 35(4): 8.

Goldstein, R.H., and Reynolds, T.J., 1994. Systematics of fluid inclusions in diagenetic minerals: SEPM Short Course Notes, 31: 213

Great Panther Silver, 2009. http://www.greatpanther.com/s/NewsReleases.asp?ReportID=411437&_Type=News-Releases&_Title=Great-Panther-Discovers-And-Develops-3-New-Zones-At-Guanajuato

Gross, W. H., 1975. New ore discovery and source of silver-gold veins, Guanajuato, Mexico. Economic Geology, 70(7): 1175-1189.

Guiza, R., 1949. Estudio geologico del distrito minero de Guanajuato, Gto. (Zona de la Veta Madre). Mexico Inst. Nac. Inv. Rec. Miner 22 p.

Hedenquist, J. W., Arribas R, A., and Gonzalez-Urien, E., 2000. Exploration for epithermal gold deposits. Reviews in Economic Geology, 13, p. 245-277.

Henley, R. W., 1984. Chapter 4. Gaseous components in geothermal processes, in: Henley, R.W., Truesdall, A.H., Barton, P.B., Jr. (Eds.), Reviews in Economic Geology, Fluid-mineral equilibria in hydrothermal systems. Society of Economic Geologists, Littleton, Colorado, pp. 45-56.

Henley, R. W., and Brown, K. L., 1985. A practical guide to the thermodynamics of geothermal fluids and hydrothermal ore deposits. Reviews in Economic Geology, 2, p. 25-44.

Henley, R. W., and Hughes, G. O., 2000. Underground fumaroles: "Excess heat" effects in vein formation. Economic Geology, 95(3): 453-466.

Kamilli, R. J. and Ohmoto, H., 1977. Paragenesis, zoning, fluid inclusion, and isotopic studies of the Finlandia Vein, Colqui District, central Peru. Economic Geology, 72(6): 950-982.

Lindgren, W., 1933. Mineral deposits, 4th edition, New York, McGraw-Hill, 930 pp.

Mango, H., 1988. A fluid inclusion and isotopic study of the Las Rayas Ag-Au-Pb-Cu mine.Unpublished Master's thesis, Dartmouth College, Hanover, NH, 109 pp.

Mango, H., Zantop, H., and Oreskes. N., 1991. A fluid inclusion and isotope study of the Rayas Ag-Au-Cu-Pb-Zn mine, Guanajuato, Mexico. Economic Geology, 86(7): 1554-1561.

Moncada, D. and Bodnar, R.J., 2012. Mineral textures and fluid inclusion characteristics of the Santa Margarita Vein in the Guanajuato Mining District, Mexico. (in revision Central European Journal of Geosciences),

Randall, J. A., Saldana, E. A., and Clark, K. F., 1994. Exploration in a volcano-plutonic center at Guanajuato, Mexico. Economic Geology, 89(8): 1722-1751.

Roedder, E., 1984. Fluid inclusions. Reviews in Mineralogy, 12,

Roedder, E. and Bodnar, R.J., 1997. Fluid inclusion studies of hydrothermal ore deposits. Geochemistry of hydrothermal ore deposits. John Wiley & Sons, New York, NY, 657-697 pp.

Rogers, A. F., 1918. The occurrence of cristobalite in California. American Journal of Science, 45(267): 222-226.

Sander, M. V. and Black, J. E., 1988. Crystallization and recrystallization of growth-zoned vein quartz crystals from epithermal systems; implications for fluid inclusion studies. Economic Geology, 83(5): 1052-1060.

Saunders, J. A., 1990. Colloidal transport of gold and silica in epithermal precious-metal systems: Evidence from the Sleeper deposit, Nevada. Geology,18(8): 757-760.

Saunders, J. A., 1994. Silica and gold textures in bonanza ores of the Sleeper deposit, Humboldt County, Nevada.: Evidence for colloids and implications for epithermal ore-forming processes. Economic Geology, 89(3): 628-638.

Simmons, S. F. and Browne, P. R. L., 2000. Hydrothermal Minerals and Precious Metals in the Broadlands-Ohaaki Geothermal System: Implications for Understanding Low-Sulfidation Epithermal Environments. Economic Geology, 95(5): 971-999.

Simmons, S.F., Gemmell, J.B., and Sawkins, F.J., 1988. The Santo Nino silver-lead-zinc vein, Fresnillo District, Zacatecas; Part II, Physical and chemical nature of ore-forming solutions. Economic Geology, 83(8): 1619-1641.Simmons, S. F. and Christenson, B. W., 1994. Origins of calcite in a boiling geothermal system. American Journal of Science, 294(3): 361-400.

Simmons, S. F., White, N. C., and John, D. A., 2005. Geological characteristics of epithermal precious and base metal deposits. Economic Geology 100th Anniversary Volume, Economic Geology: One Hundredth Anniversary Volume, 1905-2005, p. 485-522.

Simpson, M.P., Mauk, J.L., and Simmons, S.F., 2001. Hydrothermal Alteration and Hydrologic Evolution of the Golden Cross Epithermal Au-Ag Deposit, New Zealand. Economic Geology, 96(4): 773-796. Stewart, M., 2006. Geology of Guanajuato and La Luz Areas, Mexico. Unpublished geologic map.

Taylor, P. S., 1971. Mineral variations in the silver veins of Guanajuato, Mexico., Unpublished Ph. D. dissertation, Dartmouth College, Hanover, NH, 136 pp.

Van den Kerkhof, A.M. and Hein, U.F., 2001. Fluid inclusion petrography. In: T. Andersen, M.-L. Frezzotti and E.A.J. and Burke (Editors), Lithos. Special volume in

honour of Jacques Touret. Fluid inclusions: Phase relationships- methods- applications. , pp. 27-47.

Vikre, P. G., 1985. Precious metal vein systems in the National District, Humboldt County, Nevada. Economic Geology, 80(2) 360-393.

Wandke, A. and Martinez, J., 1928. The Guanajuato mining district, Guanajuato, Mexico. Economic Geology, 23(1): 1-44.

Wilson, I. F., Milton, C., and Houston, J. R., 1950. A mineralogical study of Guanajuato, Mexico, silver-gold ores, U.S. Geological Survey Report No. IWM-269, U.S. Geological Survey. unpaginated.

1.9 Figure Captions

Figure 1.1 Schematic representation of the relationship between depth and pressure (top) and the types of fluid inclusions, mineral textures and precious metal grades (bottom) for systems undergoing gentle boiling (or effervescence) and those that flash

In the top diagram, the hydrostatic gradient refers to the "cold hydrostatic gradient" (see Henley, 1984; Fig. 4.3) in which the density of the fluid is assumed to be 1 g/cm^3 everywhere. The L-V curve represents the depth-pressure conditions for a fluid whose density is equal to the density of the liquid phase that would be in equilibrium with vapor at that pressure (and temperature). In a gently boiling system, liquid at a pressure slightly greater than the pressure on the liquid-vapor curve migrates upward until the PT path intersects the liquid-vapor curve (path $B_0 \rightarrow B_1$) and boiling or effervescence begins. The fluid continues to follow the liquid-vapor curve as it flows towards the surface (path $B_1 \rightarrow B_2$). Below the depth at which boiling begins, euhedral or massive quartz (or calcite) precipitates in response to gradually decreasing temperature along the flow path and traps FIAs consisting of liquid-rich FI with consistent liquid to vapor ratios. Above the bottom of the boiling horizon euhedral quartz precipitates, trapping coexisting liquid-rich and vapor rich fluid inclusions. Depending on the intensity of boiling , chalcedony or plumose quartz may also precipitate in this region. Depending on the concentration of precious metals in the liquid before boiling occurs, precious metals may deposit at or above the bottom of the boiling zone.

If the fractures are mostly closed at depth, the fluid (liquid) will be at pressures above hydrostatic and perhaps approaching lithostatic. Quartz precipitating from this fluid will be either massive or euhedral and contain FIAs consisting of liquid-rich FI with consistent liquid to vapor ratios. If the fracture opens in response to seismic activity or increased fluid pressure, the pressure may decrease rapidly to less than hydrostatic (path $F_0 \rightarrow F_1$), causing the liquid phase to instantly vaporize, or flash. In this case,

amorphous silica with colloform texture will precipitate and FIAs consisting of all-vapor inclusions may be trapped as secondary inclusions in previously formed quartz. Most or all of the precious metals in the original liquid will precipitate at the bottom of the flashing zone to produce a high-grade (bonanza) ore zone, with little or no precious metals below or above this horizon.

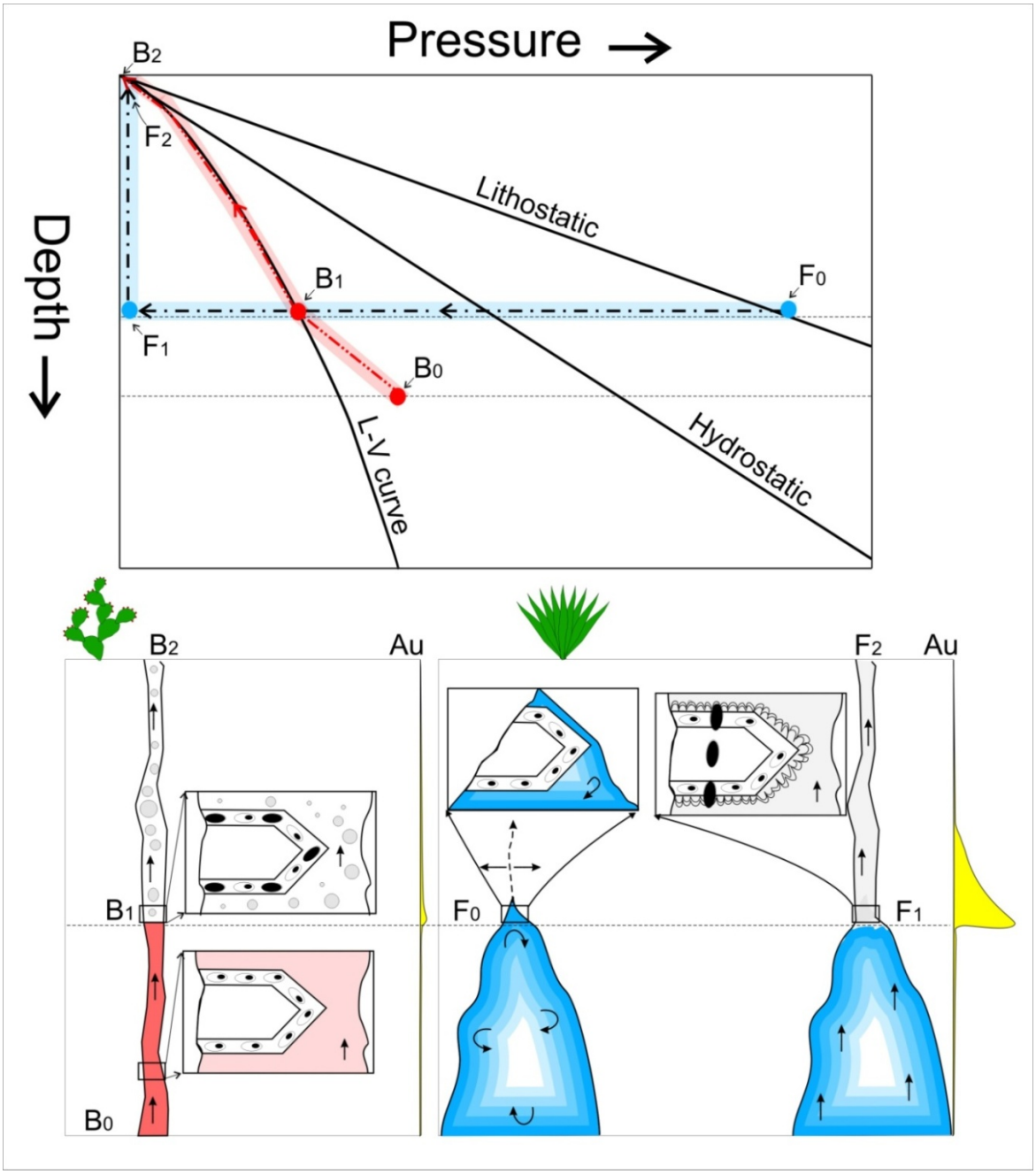

Figure 1.2 Top: Location map of the Guanajuato Mining District.

Showing locations of the three major veins (La Luz, Veta Madre and Sierra) in the district. Bottom: Location of various mines along the central portion of the Veta Madre that were sampled for this study. (modified from Church, 1907 and Taylor, 1971).

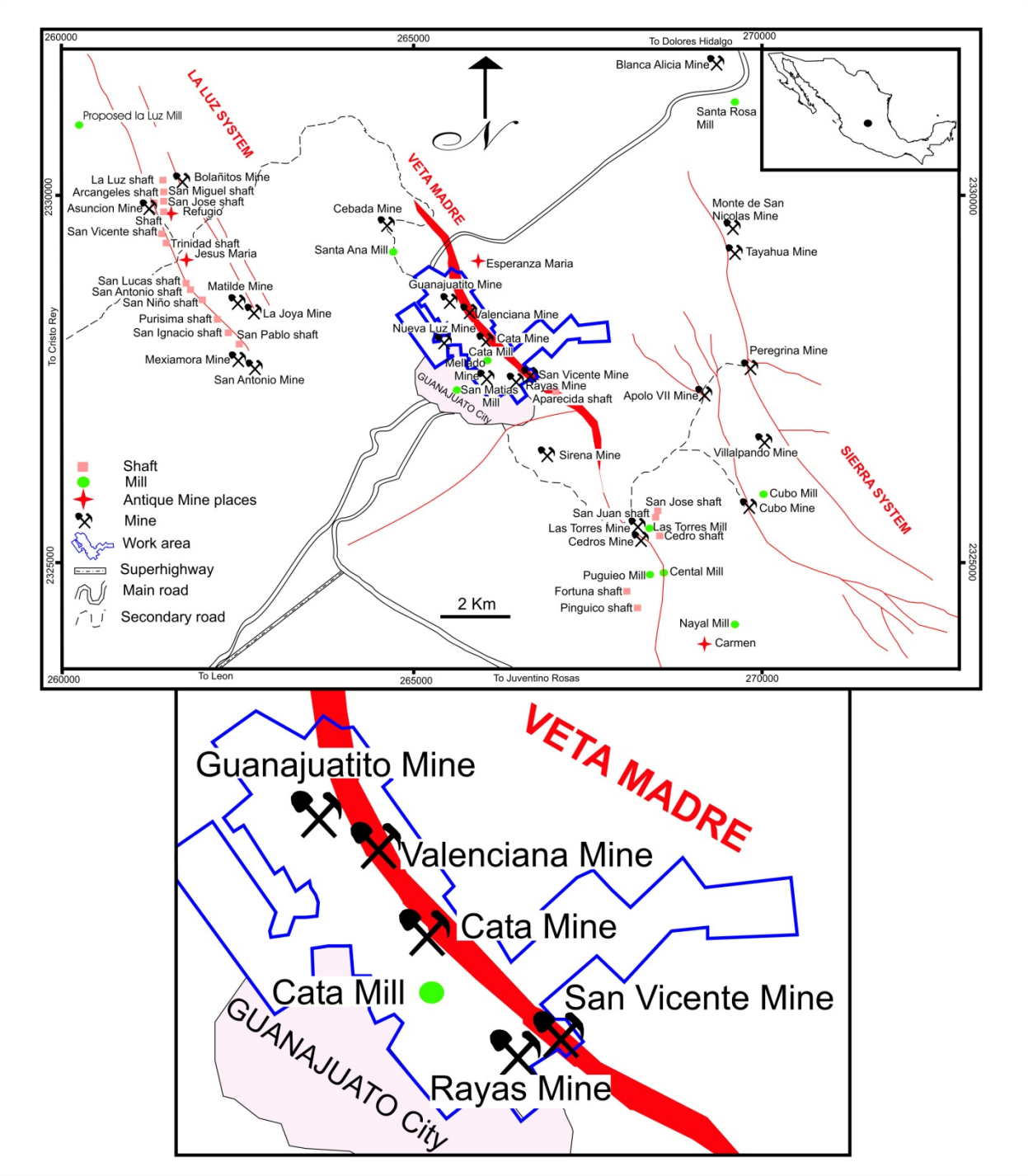

Figure1.3 Plan view and longitudinal section of the Veta Madre

(Top) Plan view of the Veta Madre showing surface sample locations and general geology (modified from Stewart, 2006). Tvbx: Veta Madre vein exposed at surface; *TEanbx*: Tertiary (Eocene) volcanic breccia derived from massive andesite lava flows: *TEanfl*: Tertiary (Eocene) massive andesite lava flows overlain by volcanic breccia; *TEss*: Tertiary (Eocene) monomictic to polymictic conglomerates, breccias, sandstones and ash tuffs; *Kdi:* Cretaceous granodiorite *Kqfp*: Cretaceous rhyolite, quartz porphyry dikes and small plugs; *Ksh*: Cretaceous mudstone, slate, muscovite schist, phyllite, sandstone, quartz arenite, limestone interbeds; *Kanfl*: Cretaceous andesite lava flow. (Bottom) Longitudinal section showing location of all 855 samples, including drill core samples, projected onto a cross-section of the Veta Madre. No vertical exaggeration.

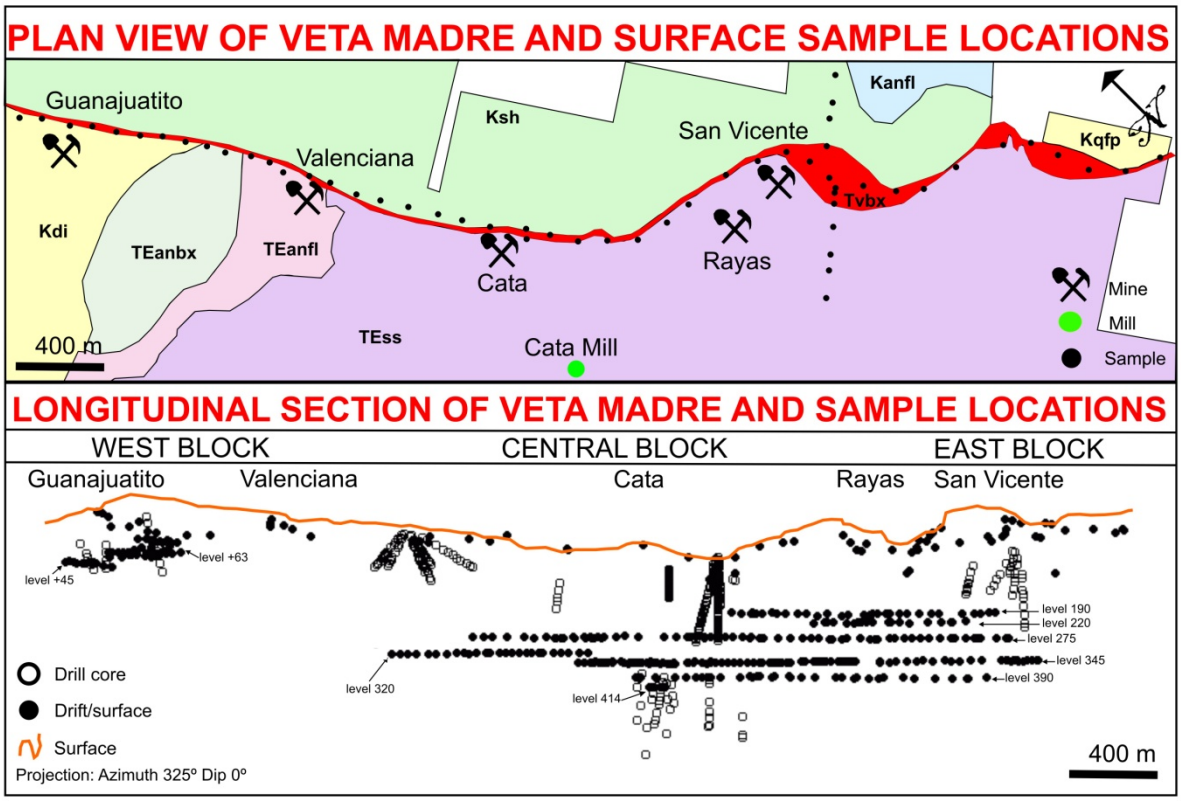

Figure 1.4 Fluid inclusion types observed in samples from the Veta Madre at Guanajuato, Mexico.

The top row shows schematic drawings of the phase ratios of the inclusions, and the bottom row shows photomicrographs of the same inclusion type in samples from the Veta Madre. Fluid inclusion assemblages (FIAs) containing liquid-rich inclusions only with consistent liquid-to-vapor ratios are indicative of non-boiling conditions (left); FIAs consisting of coexisting liquid-rich and vapor-rich inclusions are indicative of boiling conditions (center); and FIAs containing only vapor-rich inclusions indicate flashing of the system (right).

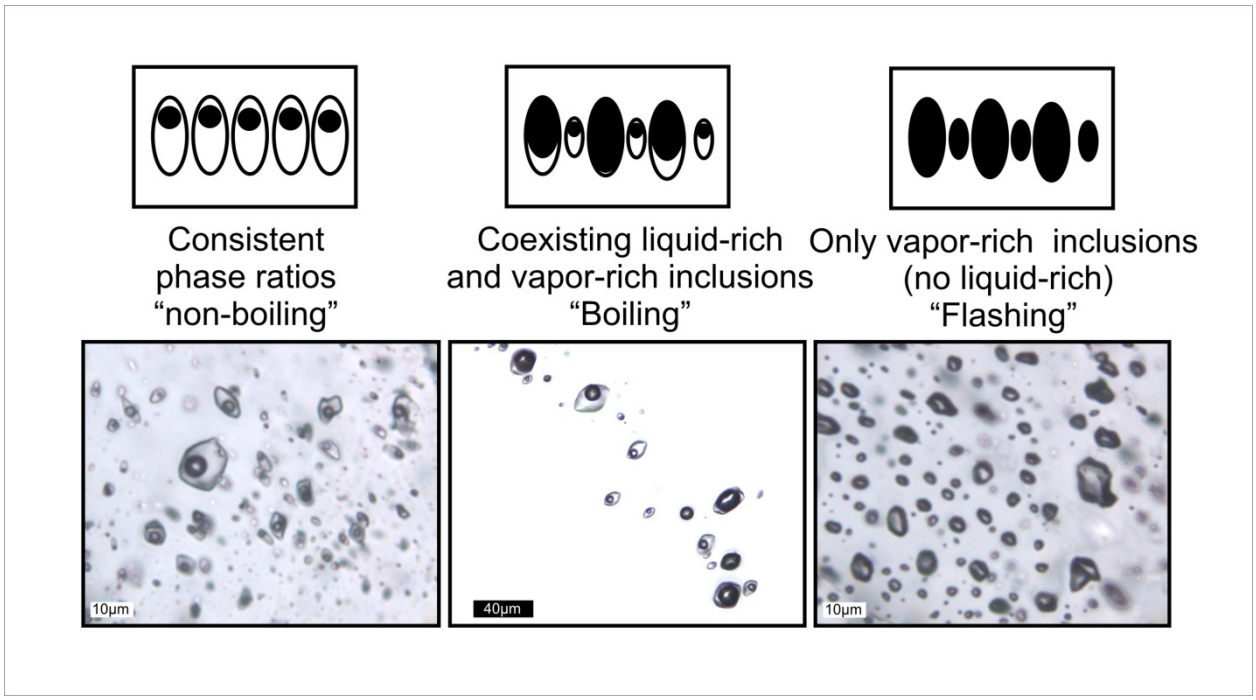

Figure 1.5 Summary of the various silica and calcite textures observed in the epithermal environment

Summary of the various silica and calcite textures observed in the epithermal environment (modified from Bodnar et al., 1985; Sander and Black, 1988; Dong et al., 1995. A) Jigsaw texture quartz; B) Feathery texture quartz; C) Flamboyant texture quartz; D) Plumose quartz; E) Colloform texture quartz; F) Lattice bladed calcite; G) Colloform-banded plumose texture quartz; H) Colloform-banded jigsaw texture quartz; I) Ghost-sphere texture quartz; J) Moss texture quartz; K) Lattice-bladed calcite replaced by quartz; L) Rhombic calcite; M) Massive quartz; N) Zonal quartz; O) Cockade quartz; P) Comb quartz;. (XP = view under crossed polars). Textures A-M are characteristic of rapid deposition, such as might occur during boiling, whereas textures N-R indicate that the fluids precipitating the mineral were not boiling.

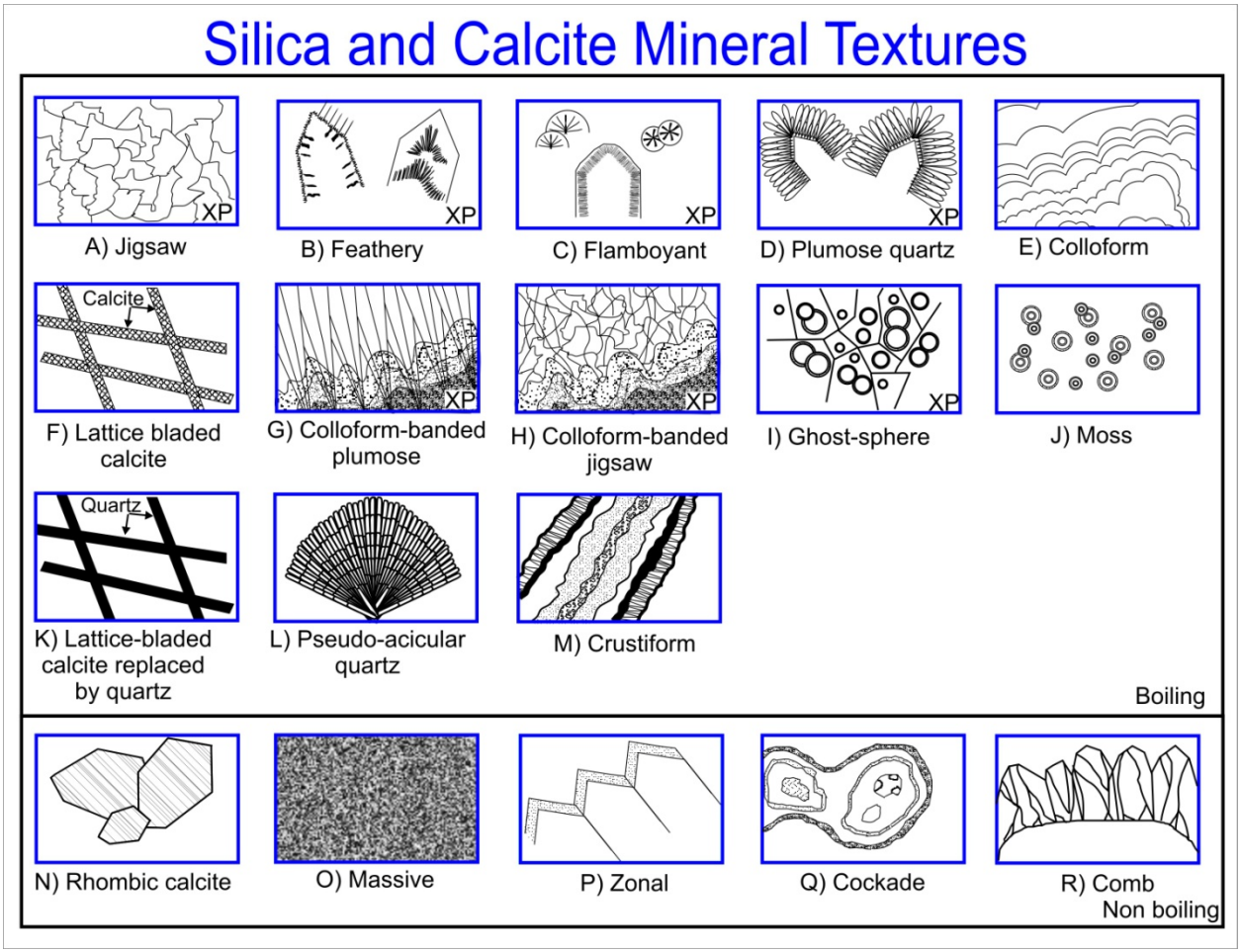

Figure 1.6 Photomicrographs of mineral textures observed in samples from the Veta Madre at Guanajuato.

Jigsaw texture quartz observed in plane-polarized light (A) and under crossed polars (B). Plumose texture quartz in plane polarized light (C) and under crossed polars (D). Lattice bladed calcite in plane polarized light (E) and under crossed polars (F). Lattice bladed calcite replaced by quartz in plane polarized light (G) and under crossed polars (H). Acicular calcite replaced by quartz in plane polarized light (I). Colloform texture silica (now quartz) under crossed polars (J).

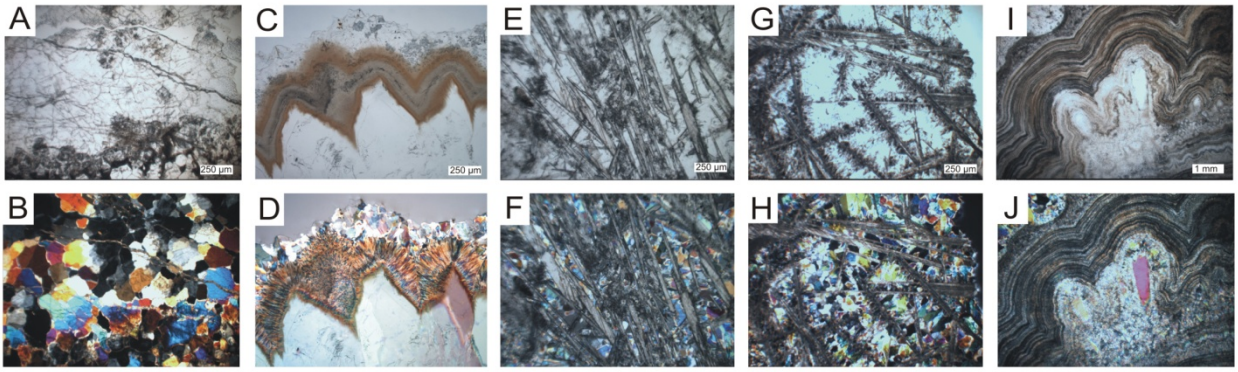

Figure 1.7 Relative abundance of the different mineral textures and fluid inclusion characteristics in samples from the Veta Madre, Guanajuato, Mexico.

The number at the end of each bar represents the number of samples out of the total of 855 samples that contained the feature listed.

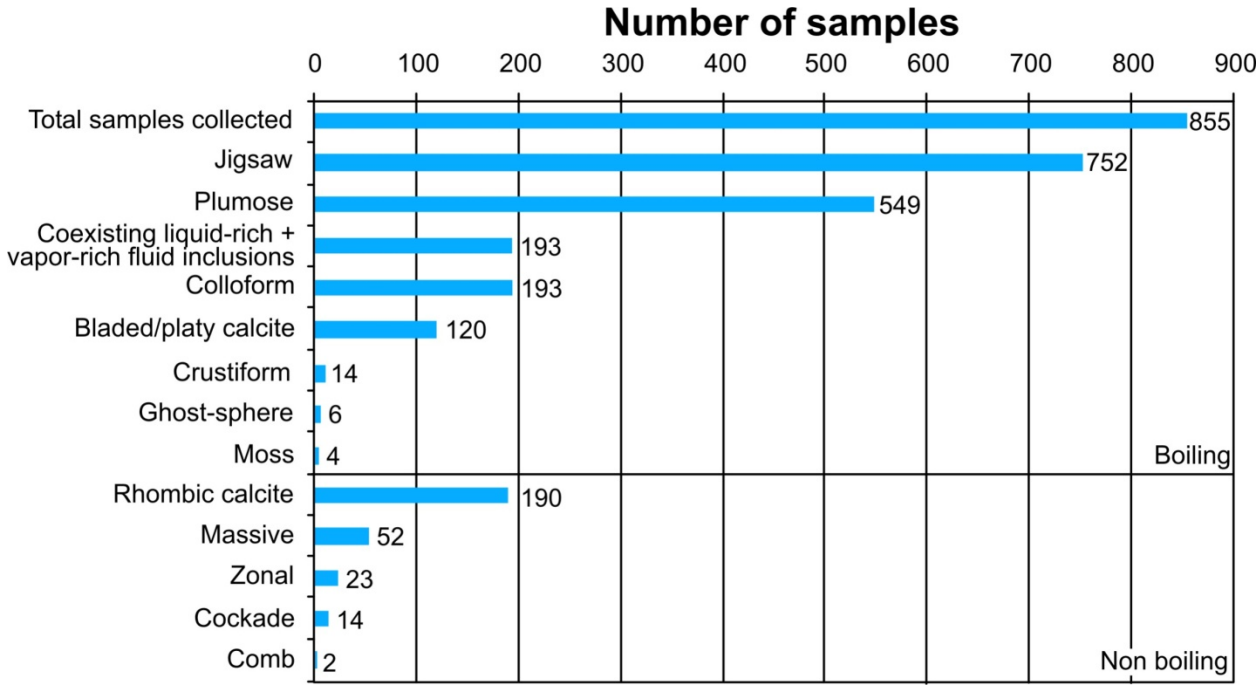

Figure 1.8 Relationship between the average Au grade of samples and the presence or absence of each mineral or fluid inclusion feature in samples from the Veta Madre, Guanajuato, Mexico.

Features listed above the horizontal solid line are those that characterize boiling environments, whereas those below the line are characteristic of non-boiling environments.

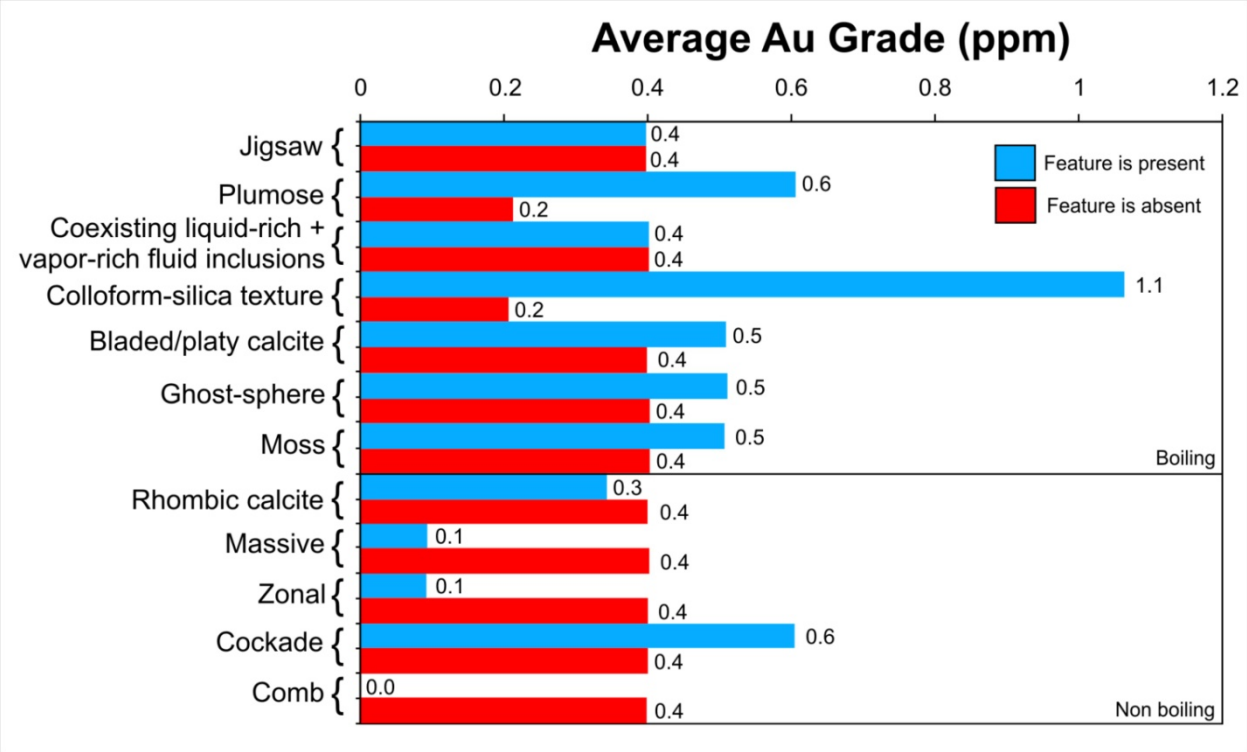

Figure 1.9 Relationship between the average Ag grade of samples and the presence or absence of each mineral or fluid inclusion feature in samples from the Veta Madre, Guanajuato, Mexico.

Features listed above the horizontal solid line are those that characterize boiling environments, whereas those below the line are characteristic of non-boiling environments.

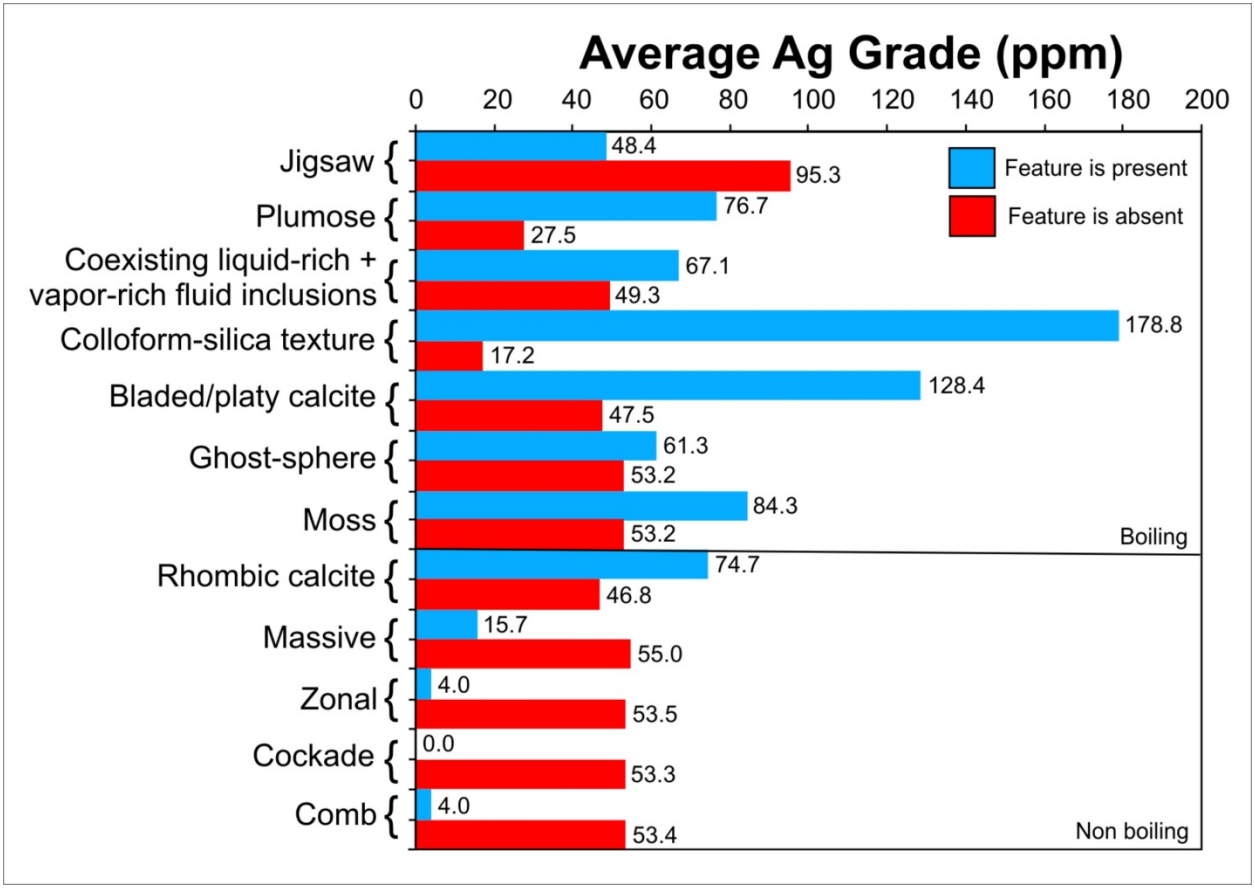

Figure 1.10 Distribution of Au (left) and Ag (right) grades (in log ppm) plotted as a function of whether a particular mineralogical or fluid inclusion feature was present or absent.

Also shown by the vertical line on each histogram is the mean metal grade for samples in which the feature is present (solid) or absent (dashed). A t-test was applied to each pair of data to assess whether the mean values were statistically different and the results are shown as the probability (i.e., P<0.05 indicates that there is less than a 5% chance that the difference is due to chance).

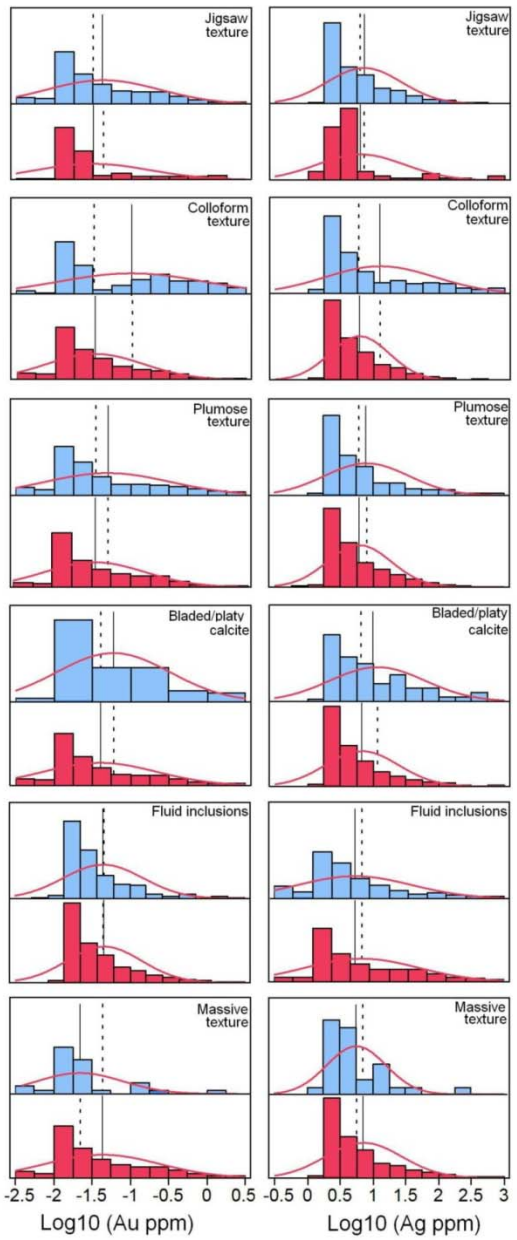

Figure 1.11 Log-normal distribution of Au (top) and Ag (bottom) grades in samples from Guanajuato, Mexico.

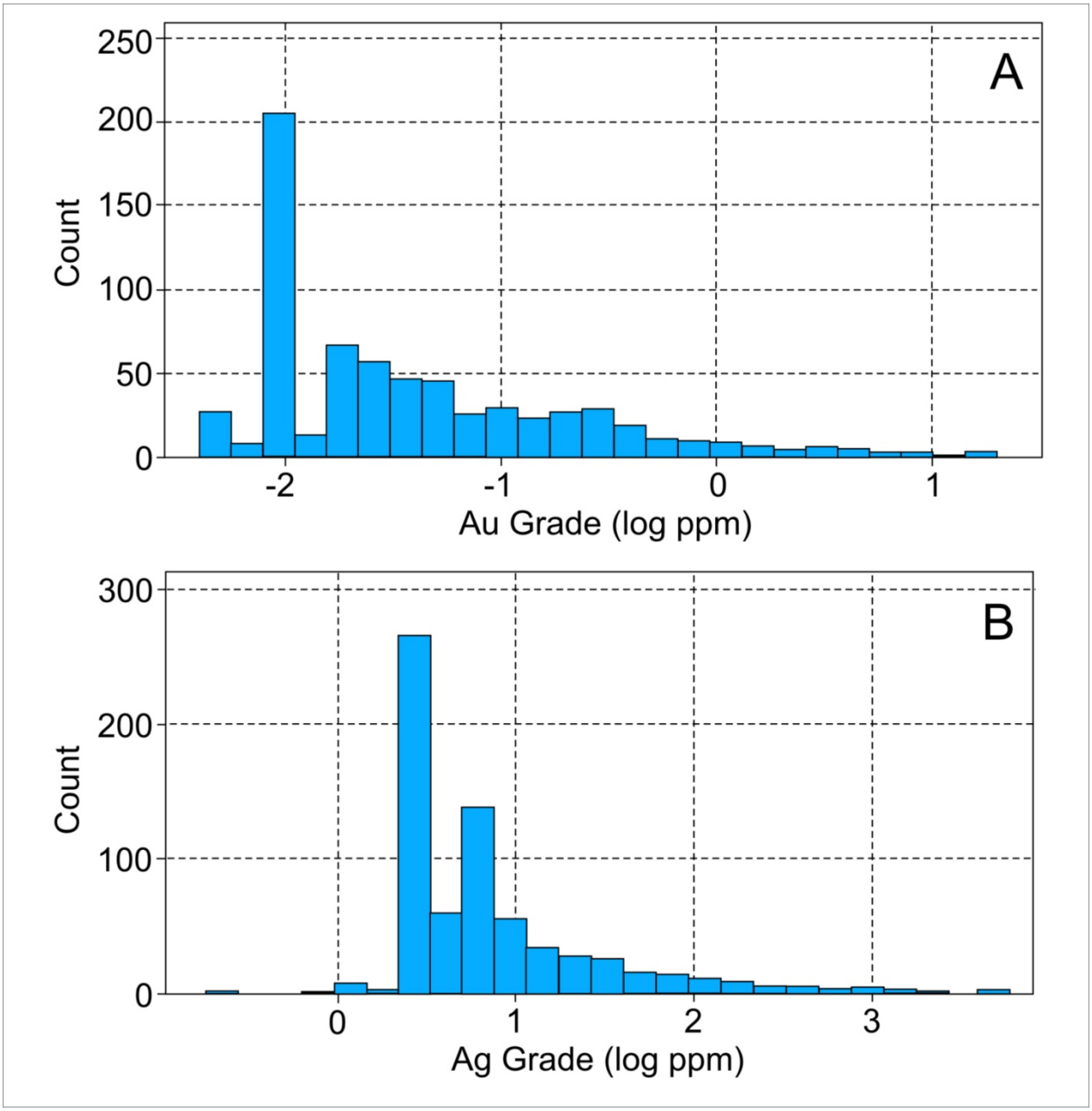

Figure 1.12 Relative importance of variables used to build models to predict Au (top) and Ag (bottom) grades at Guanajuato, Mexico.

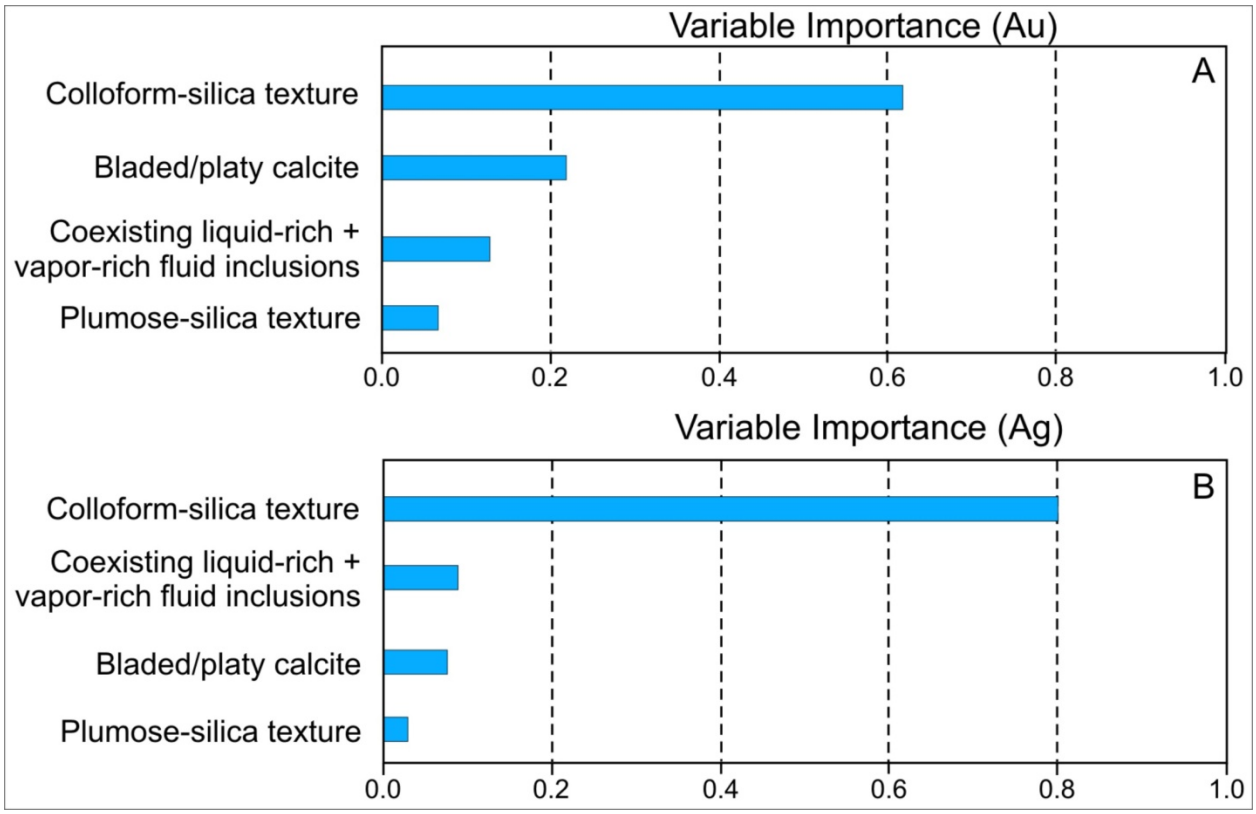

Figure 1.13 Boiling intensity factor (A) and Au (B) and Ag (C) grades of samples collected along a traverse perpendicular to the Veta Madre, and boiling intensity factor for samples from an angled drill core from the surface to the Veta Madre.

Note that along the traverse, boiling intensity factors and gold and silver grades decrease rapidly with distance from the Veta Madre. The boiling intensity factor increases systematically along the drill hole traverse as the Veta Madre is approached. JTS = jigsaw texture silica; CTS = colloform texture silica; PTS = plumose texture silica; FI = fluid inclusions.

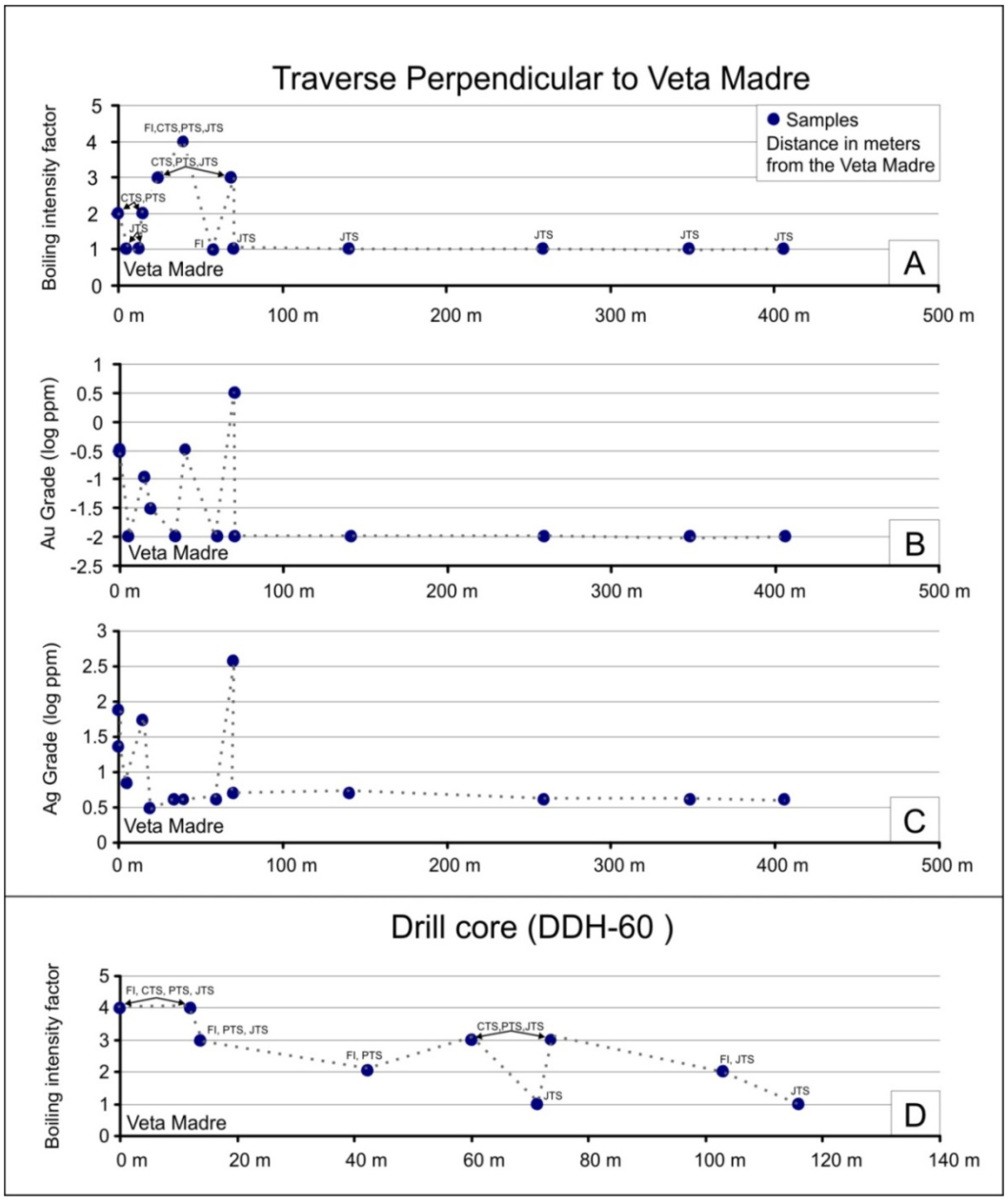

Figure 1.14 Average grades of Au and Ag (top axis) within each 50m depth increment from the surface to depth in the Veta Madre.

Also shown is the percentage of samples (bottom axis) in that same 50m increment that show textural or fluid evidence for boiling.

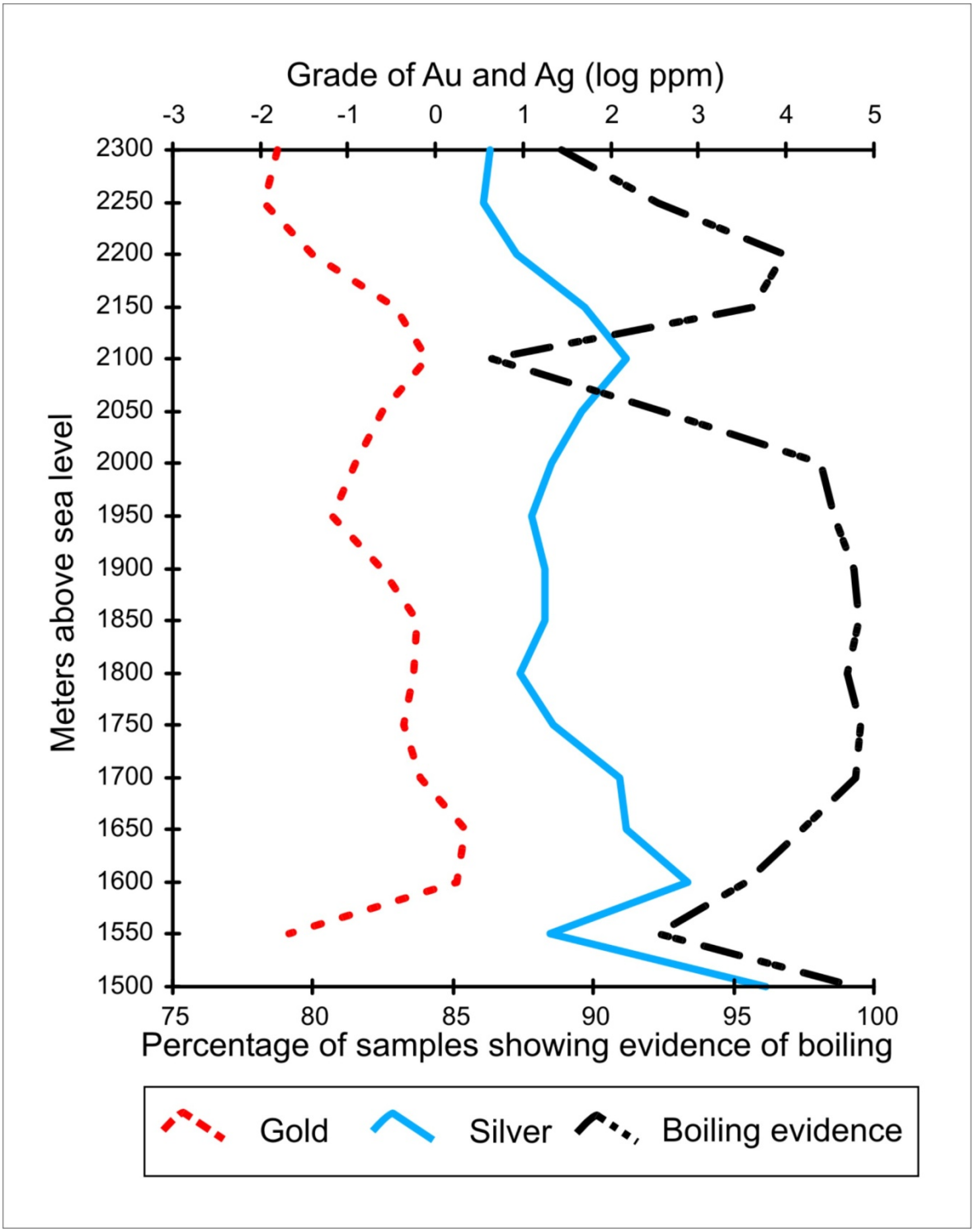

Table 1.1 Summary of previous fluid inclusion studies of the Guanajuato Mining District

Location	Homogenization temperature (Th)	Salinity (% wt. NaCl)	Deeper sample collection, elevation (meters)	Evidence for Boiling Observed?	Reference
Rayas Mine, Cata Mine	215 ºC to 299 ºC	Not reported	1820	Not reported	Wilson, et al., (1950)
Rayas Mine	230 to 305 ºC	0.5 to 3.4	1675	No	Mango, H. (1988) Mango, et al. (1991)
Las Torres, Veta Madre, Rayas Mine	231 ºC to over 360 ºC	Not reported	1705	Yes	Buchanan (1979)
Veta Madre, Sierra System	260 ºC to 320 ºC	Not reported	1700	Not reported	Gross, W. H. (1975)
Cubo Mine	220 ºC to 235 ºC	1.6 to 5	2270	Yes	Girnius, R. (1993)
Cubo Mine (San Nicholas)	172 ºC to 282 ºC	0 to 2.95	2100	Yes	Abeyta, R. L. (2003)

Chapter 2 Gangue mineral textures and fluid inclusion characteristics of the Santa Margarita Vein in the Guanajuato Mining District, Mexico

Abstract: Successful exploration for mineral deposits requires tools that the explorationist can use to distinguish between targets with high potential for mineralization and those with lower economic potential. In this study, we describe a technique based on gangue mineral textures and fluid inclusion characteristics that has been applied to identify an area of high potential for gold-silver mineralization in the epithermal Ag-Au deposits at Guanajuato, Mexico.

The Guanajuato mining district in Mexico is one of the largest silver producing districts in the world with continuous mining activity for nearly 500 years. Previous work conducted on the Veta Madre vein system that is located in the central part of this district identified favorable areas for further exploration in the deepest levels that have been developed and explored. The resulting exploration program discovered one of the richest gold-silver veins ever found in the district. This newly discovered vein that runs parallel to the Veta Madre was named the Santa Margarita vein. Selected mineralized samples from this vein contain up to 249 g/t of Au and up to 2,280 g/t Ag. Fluid inclusions in these samples show homogenization temperatures that range from 184 to 300 °C and salinities ranging from 0 to 5 wt. % NaCl. Barren samples show the same range in homogenization temperature, but salinities range only up to 3 wt. % NaCl. Evidence of boiling was observed in most of the samples based on fluid inclusions and/or quartz and calcite textures. Liquid-rich inclusions with trapped illite are closely associated with high silver grades. The presence of assemblages of vapor-rich-only fluid inclusions, indicative of intense boiling or “flashing”, shows the best correlation with high gold grades.

2.1 Introduction

The Guanajuato Mining District (GMD) in Mexico is one of the largest silver producing districts in the world with continuous mining activity for nearly 500 years. The epithermal deposits in the GMD are hosted by steeply dipping quartz ± carbonate veins that show mineralization over vertical extents of several hundreds of meters. In recent years, there has been much activity in the GMD to explore for additional resources below the known levels of mineralization.

Previous detailed studies of the Veta Madre have documented a strong correlation between boiling and silver and gold deposition (Buchanan 1979, Moncada et al. 2012). In a recently completed study (Moncada et al. 2012) of the Veta Madre vein system, fluid inclusion and gangue mineral textures were examined in 855 samples. Mineral textures and fluid inclusion features characteristic of fluid immiscibility or boiling, including colloform quartz, plumose/feathery/flamboyant quartz, lattice-bladed calcite and lattice-bladed calcite replaced by quartz, as well as coexisting liquid-rich and vapor-rich fluid inclusions and assemblages of vapor-rich only inclusions, were recognized in samples from the Veta Madre. Most samples studied were assayed for Au and Ag, and were divided into ore grade and sub-economic samples based on the gold and silver concentrations. For silver, samples containing >100 ppm were classified as ore grade, and for Au samples containing >1 ppm were considered to be ore grade. The feature that was most closely associated with ore grades of both gold and silver is colloform quartz that was originally precipitated as amorphous silica, and this feature also showed the largest difference in average grade between samples that display colloform texture (178.8 ppm Ag and 1.1 ppm Au) and those that do not exhibit this texture (17.2 ppm Ag and 0.2 ppm Au). Statistical analysis of the data indicated that colloform quartz is the feature that has the greatest predictive power for distinguishing between ore grade and sub-economic samples.

In the study by Moncada et al. 2012, evidence of boiling was present in nearly all samples examined, including those from the deepest levels of exploration and production in the mines. Moreover, samples collected from the surface and from drill

core along a traverse perpendicular to the Veta Madre showed that evidence for boiling becomes more common and pervasive as mineralization is approached. With these results, a new drilling exploration program was undertaken in areas where the evidence for boiling was strongest and one of the richest gold-silver veins ever discovered in the 500+ year mining history of the Guanajuato district was found (Great Panther Silver 2009). This new vein, named the Santa Margarita vein, is the subject of this communication. For this study, gangue mineral textures and fluid inclusion characteristics in samples from the Santa Margarita vein were examined to document evidence for boiling of the hydrothermal fluids during formation of this rich ore zone.

2.2 Evidence for boiling as a depositional mechanism in epithermal precious metals deposits

Fluid inclusion studies of epithermal precious metals deposits and their modern analogs, active continental geothermal systems, document the genetic relationship between boiling and precious metal mineralization (Kamilli and Ohmoto 1977, Buchanan 1980, Roedder 1984, Brown 1986, Clark and Williams-Jones 1990, Hedenquist et al. 2000, Albinson et al. 2001, Etoh et al. 2002, Simmons et al. 2005). One of the earliest studies that described the relationship between fluid properties, silica precipitation and precious metal mineralization was by Weissberg, based on his work in the Taupo volcanic zone, New Zealand (Weissberg 1969). Similarly, Brown 1986 documented the deposition of gold and silver as geothermal fluids passed through a pressure plate and “flashed” in drill hole BR22 at the Broadlands geothermal field, New Zealand. Seward 1989, calculated the effect of boiling on gold-bearing fluids in the Ohaaki-Broadlands geothermal field and found that adiabatic flashing of the geothermal fluid between 290 and 277°C leads to quantitative precipitation of all gold in solution, whereas simple conductive cooling causes only minor gold deposition.

The observed relationship between gold and silver mineralization and boiling in active geothermal systems is consistent with theoretical and experimental studies of gold and silver solubility (Helgeson 1969, Shenberger and Barnes 1989, Stefánsson and Seward 2003, Stefánsson and Seward 2004). The solubility of gold as a bisulfide

complex at 250°C and as a function of fluid pH and oxidation state is shown on Figure 2.1. Also shown on Figure 2.1 are the stability fields for the Fe-bearing phases hematite, pyrite, magnetite and pyrrhotite for a total sulfur activity of 0.01, as well as the H_2S – HS^- and $HSO_4^- - SO_4^{2-}$ equilibrium boundaries. Also shown is neutral pH at 250°C, based on the pK_w of $10^{-11.3}$ from Helgeson 1969. In most epithermal deposits, pyrite or an iron oxide phase, along with adularia and illite, are common gangue minerals (Sillitoe and Hedenquist 2003). We note that illite is found in association with quartz that was precipitated as crystalline quartz as well as with colloform quartz that was originally precipitated as amorphous silica. The illite-adularia equilibrium boundary is shown for equilibrium with both amorphous silica and quartz at 250°C, assuming K^+ concentration of 5 x 10^{-3} m and Mg^{2+} concentration of 4 x 10^{-5} m. Illite-adularia equilibria were calculated using data from Helgeson 1969, combined with the data from Gunnarsson and Arnórsson 2000, for quartz and amorphous silica equilibria. Note that the pH of a fluid in equilibrium with illite and adularia and precipitating quartz will decrease by greater than one pH unit if the fluid begins to precipitate amorphous silica in response to boiling, and will evolve from being slightly basic to slightly acidic (Fig. 2.1). This resulting decrease in pH can lead to a decrease in gold solubility by about 1-2 orders of magnitude and can cause gold to precipitate if the fluid before boiling was at or near gold saturation. This interpretation is consistent with Brown 1989, who found that boiling, mixing with acid sulfate waters (pH decrease) and mixing with oxygenated meteoric waters (increase in oxygen activity) all lead to gold deposition. Within the area bounded by the illite-adularia-amorphous silica and illite-adularia-quartz equilibria, and within the pyrite stability field, gold solubilities shown on figure 2.1 range from about 1 ppb to about 1 ppm, and are consistent with Au concentrations in deep geothermal waters in the Taupo Volcanic Zone (<0.1–23 ppb Au), at Lihir Island, Papua New Guinea (13-26 ppb Au) (Simmons and Brown 2006, Simmons and Brown 2007), and in the La Primavera, Mexico, geothermal system (59 ppb Au) (Prol-Ledesma et al. 1998).

The mechanisms associated with gold and silver transport and deposition in the epithermal environment are well constrained based on recent experimental studies. Stefánsson and Seward 2004, measured the solubility of gold in aqueous sulfide solutions from 100-500°C at 500 bars. These workers found that in the epithermal

temperature range gold (I) sulfide complexes predominate and that boiling of both dilute and saline geothermal fluids leads to quantitative loss of gold from solution. Similarly, Stefánsson and Seward 2003, measured the solubility of silver in aqueous sulfide solutions from 25-400°C and up to 500 bars. Based on their experimental results, these workers concluded that adiabatic boiling results in precipitation of silver sulfide. These experimental studies, combined with observations in active geothermal systems, provide overwhelming evidence that boiling is an effective mechanism to precipitate gold and silver from solution in the epithermal environment. This, combined with other studies that have correlated fluid inclusions (Bodnar et al. 1985) and mineral textures (Fournier 1985, Sander and Black 1988, Simmons and Christenson 1994, Dong et al. 1995) with boiling processes, makes it possible to develop effective exploration models to distinguish between areas that have high probability for precious metal mineralization and those that are less likely to host such mineralization, as described in detail by Moncada et al. 2012.

2.3 Geologic setting

The Santa Margarita vein is a hanging wall structure parallel to the main Veta Madre vein system that has been described in detail by many workers (Taylor 1971, Buchanan 1979, Clark et al. 1982, Randall et al. 1994, Godchaux et al. 2003, Stewart 2006). In cross-section, the Santa Margarita vein occurs at about the same location along the Veta Madre as the Rayas Mine (Figure 2.2). The hanging wall in this area consists of Tertiary monomictic to polymictic conglomerates, breccias, sandstones and ash tuffs (Stewart 2006). The vein is brecciated and cemented by quartz and lesser amounts of calcite. In the upper levels the mineralization consists of acanthite and base metals, whereas electrum is more abundant in the lower levels. We note that this distribution of metals is the opposite of what Buchanan 1979 described at Guanajuato, and the opposite of what is generally observed in epithermal deposits (Buchanan 1981). We interpret the inverted metal distribution in the Santa Margarita vein to represent two different events, one in which the boiling horizon was somewhat above the level of the Sta. Margarita vein (thus, precipitating base metals at the level of the Sta. Margarita

vein) and the other in which the boiling horizon was at or slightly below the level of the Sta. Margarita vein (thus precipitating gold at the level of the vein).

2.4 Methodology

In collaboration with staff of Great Panther Silver Limited, 12 samples were collected from underground working areas, and from exploration drill holes that intersected the Santa Margarita vein "shoot", which is 52 meters long and 3.4 meters wide and about 18 meters high. The Santa Margarita vein is located close to and parallels the hanging wall of the Veta Madre. Samples were collected from the Santa Margarita vein near its footwall, near its hanging wall and from the interior of the vein, which is highly brecciated. The footwall on the Veta Madre has been documented to contain the highest grade gold-silver mineralization (Taylor 1971), and this relationship also holds for the Santa Margarita vein. Later drilling to a depth of 100 meters below where the samples for this study were collected identified mineralization containing up to 44.76 g/t gold and 46 g/t silver over a true width of 1.14 meters in drill hole UGSM11-005 (Great Panther Silver 2011).

One half of each sample collected was assayed for gold (Au), silver (Ag), copper (Cu), lead (Pb), zinc (Zn), arsenic (As) and antimony (Sb), and the other half was used to prepare a polished section to examine mineral textures and fluid inclusions. The samples contain from 0.0017 to 249 g/t Au, and from <3 to 2,280 g/t Ag. Samples that were high in silver contained galena and sphalerite, whereas there was no evidence of base metals, arsenic or antimony for samples that contain electrum. All hand samples were cut perpendicular to the vein to produce a section that extended from the vein wall towards the center of the vein, and a standard doubly-polished thin section was prepared for fluid inclusions petrography.

2.5 Petrography

Polished thin sections were examined using a petrographic microscope to identify the minerals present and to classify the textures of quartz and calcite (every

sample contained quartz and five also contained calcite, and three contained rhombic adularia). The mineral texture classifications that have been observed in the Guanajuato deposits and their interpretations in terms of the physical state of the fluid (boiling vs. non-boiling) have been described in detail elsewhere (Moncada et al. 2012). Next, the sample was examined systematically to identify fluid inclusion assemblages (FIAs) and the types of fluid inclusions in each FIA were noted. An FIA represents a group of fluid inclusions that were all trapped at the same time (Goldstein and Reynolds 1993, Bodnar 2003). FIAs may contain primary inclusions trapped during precipitation of the host phase, or may contain secondary inclusions that were trapped along fractures in the host phase at some time after the mineral formed. It is important to mention that fluid inclusions contained in some quartz and calcite textures do not record original conditions of formation (Bodnar et al. 1985, Sander and Black 1988, Moncada et al. 2012). This applies mostly to quartz that was originally precipitated as amorphous silica and later recrystallized to quartz, and to bladed calcite that was later replaced by quartz.

FIAs in samples from Santa Margarita were further classified as containing (1) only liquid-rich inclusions with consistent liquid-to-vapor ratios, (2) liquid-rich inclusions with consistent liquid-to-vapor ratios and containing a trapped illite crystal, (3) coexisting liquid-rich and vapor-rich inclusions with a broad range in liquid-to-vapor ratios, and (4) assemblages consisting of only vapor-rich inclusions. The illite phase in liquid-rich inclusions was identified based on Raman analysis and is interpreted to represent a trapped solid because its distribution within the inclusions comprising an FIA is not uniform, and the relative size of the illite varies greatly within the FIA (Figure 2.3).

Following detailed petrographic examination of the samples, 58 FIAs were selected for microthermometric analysis. Inclusions were measured using a Linkam THMSG 600 °C heating stage mounted on a standard petrographic microscope. The stage was calibrated using synthetic fluid inclusion standards (Sterner and Bodnar 1984). The precision and accuracy of measured homogenization temperatures are estimated to be ±1.0 °C and the precision and accuracy of ice-melting temperatures are estimated to be ±0.1 °C.

2.6 Data and results

The goal of this study was to document the different gangue mineral textures and fluid inclusion types in samples from the gold- and silver-rich Santa Margarita vein in the Guanajuato Mining District to test the hypothesis that gold and silver deposition was associated with boiling. The Santa Margarita vein represents a bonanza deposit and previous experimental studies and studies of both active and fossil epithermal systems suggest that boiling is commonly the mechanism of deposition in these deposits. Several mineral textures observed in the Santa Margarita samples, including jigsaw texture quartz, plumose texture quartz, colloform texture quartz, lattice bladed calcite, colloform-banded plumose texture, colloform-banded jigsaw texture, and lattice-bladed calcite replaced by quartz (Figure 2.4), are consistent with rapid mineral precipitation as a result of boiling (Fournier 1985, Sander and Black 1988, Simmons and Christenson 1994, Dong et al. 1995). In addition, the presence of coexisting liquid-rich and vapor-rich fluid inclusions in the same FIA indicates that the inclusions were trapped from a boiling fluid.

The homogenization temperatures of fluid inclusions from mineralized samples range from 184 to 300 °C and ice-melting temperatures correspond to salinities between 0 and 5 wt. % NaCl (Bodnar 1993) (Figure 2.5). Barren samples show the same range in homogenization temperature but with a slightly lower maximum salinity of 3 wt. % NaCl (Figure 2.5). There does not appear to be a strong correlation between homogenization temperature and/or salinity and the presence or absence of ore grade mineralization.

Fluid Inclusion Assemblages consisting of coexisting liquid-rich and vapor-rich fluid inclusions show no trend in homogenization temperatures, but salinities of inclusions in these FIAs are always <2 wt. % NaCl. FIAs that consist of fluid inclusions that contain trapped illite homogenize over a relatively narrow range from about 270-300 °C, with salinities between 1-2 wt. % NaCl. One FIA in adularia was identified, and these inclusions had a noticeably lower homogenization temperature (≈185 °C) and

higher salinity (>3 wt. %) compared to most other FIAs in other minerals. FIAs consisting of coexisting liquid-rich and vapor rich inclusions in bladed calcite homogenize from about 240-260 °C, and have low salinities (<1 wt. % NaCl). FIAs consisting of only liquid-rich inclusions in rhombic calcite homogenize at 240-300 °C, with salinities from about 1-3 wt. % NaCl. It should be noted that no FIAs consisting of either coexisting liquid-rich and vapor rich inclusions, or vapor-rich inclusions only, were found in the rhombic calcite, and this is consistent with previous studies that have shown that rhombic calcite is not associated with boiling fluids (Albinson et al. 2001) . Table 2.1 summarizes the microthermometric data for samples from the Santa Margarita vein.

Albinson et al. 2001, documented a clear correlation between fluid salinity and the metal budget of Mexican epithermal deposits. Fluids in gold-rich deposits generally have salinities <3.5 wt. % NaCl, whereas fluid salinities in Ag-rich deposits range up to about 7.5 wt. %, and Ag-base metal epithermal deposits have salinities that extend up to about 23 wt. % NaCl. In this study, all of the fluid inclusions have salinities <5 wt. %. Some Ag-rich samples have salinities > 2 wt. % NaCl, but all of the Au-rich samples have salinities <2 wt. % NaCl (Figure 2.6), consistent with earlier reports by Albinson et al. 2001. The generally low salinity of all fluid inclusions in this study is consistent with previous studies that suggest that gold and silver are not transported as chloride complexes in the epithermal environment, but rather are transported as sulfide and/or hydroxyl complexes (Helgeson 1969, Shenberger and Barnes 1989, Albinson et al. 2001, Stefánsson and Seward 2003, Stefánsson and Seward 2004).

For each of the gangue mineral textures and fluid inclusion characteristics described above for Santa Margarita vein samples, the average silver and gold grades for those samples containing the feature and for those samples not showing that feature were calculated (Figure 2.7). The feature that correlates most closely with high silver grades is the presence of trapped illite crystals in liquid-rich fluid inclusions. The fact that the illite is a trapped phase suggests that illite and a silica phase were co-precipitating in the vein, and that as the silica phase continued to precipitate it engulfed small illite crystals as the fluid inclusions formed. As shown on Figure 2.1, the pH at

which illite and adularia are in equilibrium with quartz differs by about one log unit from the pH at which these minerals are in equilibrium with amorphous silica, and these phase boundaries straddle neutral pH at 250 °C. We also note that in most of the quartz veins in the Veta Madre, there is a trend from colloform texture quartz that gradually changes to coarse grained-quartz towards the vein center, ending in a well-formed euhedral quartz crystal. This textural evolution is repeated several times along a line from the vein wall to the vein center, and is interpreted to represent episodic and cyclic boiling of the hydrothermal fluid, whereby each cycle begins with rapid silica deposition as amorphous silica in response to boiling and, as boiling intensity decreases (or ends), coarser-grained quartz is deposited. Initial boiling deposits amorphous silica with a colloform texture, and as boiling intensity wanes the silica phase being deposited evolves towards chalcedony and finally to coarse quartz when boiling ends. Boiling may be terminated as the vein becomes sealed with silica and other phases, causing the pressure to increase until fracturing occurs with the release of pressure, leading to another phase of amorphous silica-chalcedony-quartz deposition. If illite is precipitating in equilibrium with quartz during a period of non-boiling (at slightly basic pH), and then boiling begins with the precipitation of amorphous silica, the fluid will be driven to slightly acidic pH. Thus, if a fluid is in equilibrium with illite-adularia-quartz and is at or near gold saturation, and the fluid pH rapidly evolves to be in equilibrium with illite-adularia-amorphous silica, gold solubility may be exceeded, leading to gold deposition. This is consistent with the fact that electrum is generally associated with colloform texture quartz and jigsaw texture quartz that are interpreted to have been precipitated from boiling fluids. If we assume that silver solubility relations are topologically similar to gold solubility relations shown on Figure 2.1, then silver may also be deposited as a result of boiling. This interpretation is consistent with experimental studies of gold and silver solubility (Stefánsson and Seward 2003, Stefánsson and Seward 2004).

The feature that correlates most closely with high gold grades is FIAs consisting of only vapor-rich fluid inclusions that are indicative of fluid flashing. Here we use the term flashing to indicate a condition whereby 100% of the liquid is converted to vapor as a result of decompression. We also emphasize that no vapor-rich only FIAs consisting of primary inclusions were observed, and this is consistent with the fact that during

flashing amorphous silica is precipitated, and this phase does not trap (or record) primary inclusions. Buchanan 1979, suggested that fluid flashing was an important mechanism for precious metals deposition in the deposits at Guanajuato, and a numerical modeling study by Cline et al. 1992, showed that isothermal flashing significantly enhances both silica deposition and gold precipitation, compared to the amounts that would be deposited by temperature decrease alone or by less intense boiling accompanied by temperature decrease. We therefore suggest that the presence of FIAs consisting of only vapor-rich inclusions is consistent with flashing as the depositional mechanism for gold in the Santa Margarita vein at Guanajuato. These interpretations are reinforced by theoretical, experimental and field-based studies in active geothermal systems that document the close association of excessive boiling (i.e., “flashing”) and gold and silver deposition (Brown 1989, Seward 1989, Simmons and Browne 2000, Stefánsson and Seward 2003, Stefánsson and Seward 2004).

2.7 Summary

Samples from the Santa Margarita Vein in the deep part of the Rayas Mine in the Guanajuato Mining District, Mexico, show a wide range in gangue mineral textures. Some of these textures, including colloform texture quartz, plumose texture quartz, jigsaw texture quartz and bladed calcite, are indicative of rapid precipitation, such as occurs when fluids boil. Other mineral phases, including illite and rhombic adularia are also characteristic of epithermal systems and are often associated with mineralization. Because boiling is an effective mechanism for precipitating gold and silver from hydrothermal fluids, the presence of mineral textures indicative of boiling is a desirable feature in exploration. In many samples, textural evidence for boiling is supported by coexisting liquid-rich and vapor-rich fluid inclusions, or Fluid Inclusion Assemblages consisting of only vapor-rich inclusions, suggesting “flashing” of the hydrothermal fluids. The Santa Margarita samples show evidence of multiple boiling events based on either gangue mineral textural features observable in a hand sample or by detailed petrographic examination under the microscope. The clear relationship between these various features that are characteristic of boiling and elevated precious metals grades

emphasizes the value of applying this technique in exploration. However, results of this study also show that no single monitor of boiling correlates well with Ag and Au grades, and all of the various boiling indicators should be monitored and assessed in determining whether boiling occurred and the intensity of the boiling event.

2.8 Acknowledgments

The authors thank the staff of Great Panther Silver Ltd, especially Robert Archer and Robert Brown for providing financial support and access to samples and information used in this study. Consejo Nacional de Ciencia y Tecnología (CONACyT) and the Virginia Tech Graduate School also provided partial funding during this study. We also thank Tawn Albinson and two anonymous reviewers of an earlier version of this manuscript for providing many useful suggestions and comments that have significantly improved the presentation.

2.9 Reference

Albinson, T., D. I. Norman, D. Cole and B. Chomiak., 2001. Controls on formation of low-sulfidation epithermal deposits in Mexico; constraints from fluid inclusion and stable isotope data. Special Publication (Society of Economic Geologists (U. S.)) 8: 1-32.

Bodnar, R. J., 1993. Revised equation and table for determining the freezing point depression of H_2O-NaCl solutions. Geochimica et Cosmochimica Acta 57(3): 683-684.

Bodnar, R. J., 2003. Introduction to fluid inclusions. Short Course Series - Mineralogical Association of Canada 32: 1-8.

Bodnar, R. J., T. J. Reynolds and C. A. Kuehn., 1985. Fluid-inclusion systematics in epithermal systems. Reviews in Economic Geology 2: 73-97.

Brown, K. L., 1986. Gold deposition from geothermal discharges in New Zealand. Economic Geology 81(4): 979-983.

Brown, K. L., 1989. Kinetics of gold precipitation from experimental hydrothermal sulfide solutions. Economic Geology Monograph 6: 320-327.

Buchanan, L. J., 1979. The Las Torres Mine, Guanajuato, Mexico; Ore controls of a fossil geothermal system. Doctoral Thesis Colorado School of Mines.

Buchanan, L. J., 1980. Ore controls of vertically stacked deposits, Guanajuato, Mexico. American Institute of Mining Engineers Preprint 80-82: 26.

Buchanan, L. J., 1981. Precious metal deposits associated with volcanic environments in the Southwest. Arizona Geological Society Digest 14: 237-262.

Church, J. A., 1907. The Mines of La Luz, Guanajuato, Mexico II. The engineering and mining journal: 105-110.

Clark, J. R. and A. Williams-Jones E., 1990. Analogues of epithermal gold-silver deposition in geothermal well scales. Nature 346(6285): 644-645.

Clark, K. F., C. T. Foster and Damon P. E., 1982. Cenozoic mineral deposits and subduction-related magmatic arcs in Mexico. GSA Bulletin 93(6): 533-544.

Cline, J. S., Bodnar R. J. and Rimstidt J. D., 1992. Numerical simulation of fluid flow and silica transport and deposition in boiling hydrothermal solutions; application to epithermal gold deposits. Journal of Geophysical Research 97(B6): 9085-9103.

Dong, G., Morrison G. and Jaireth S., 1995. Quartz textures in epithermal veins, Queensland; classification, origin and implication. Economic Geology 90(6): 1841-1856.

Etoh, J., Izawa E., Watanabe K., Taguchi S. and Sekine R. , 2002. Bladed Quartz and Its Relationship to Gold Mineralization in the Hishikari Low-Sulfidation Epithermal Gold Deposit, Japan. Economic Geology 97(8): 1841-1851.

Fournier, R. O., 1985. The behavior of silica in hydrothermal solutions. Reviews in Economic Geology(2): 45-61.

Godchaux, M. M., Bonnichsen B., Aguirre Diaz G. d. J., Aranda Gomez J. J., Rangel Solis G., 2003. Volcanological and tectonic evolution of a complex Oligocene caldera system, Guanajuato mining district, central Mexico. Abstracts with Programs - Geological Society of America 35(4): 8.

Goldstein, R. H. and Reynolds T. J., 1993. Systematics of fluid inclusions in diagenetic minerals. SEPM Short Course Notes 31: 213.

Great Panther Silver., 2009 Great Panther Discovers And Develops 3 New Zones At Guanajuato. News Releases. http://www.greatpanther.com/English/News/News-Details/2009/Great-Panther-Discovers-And-Develops-3-New-Zones-At-Guanajuato/default.aspx

Great Panther Silver., 2011 Great Panther Silver Confirms Continuity of Santa Margarita Gold-Silver Veins and Extends Guanajuatito Mineralized Zone to Depth at Guanajuato. News Releases. http://www.greatpanther.com/English/News/News-Details/2011/Great-Panther-Silver-Confirms-Continuity-of-Santa-Margarita-Gold-Silver-Veins-and-Extends-Guanajuatito-Mineralized-Zone-/default.aspx

Gunnarsson, I. and Arnorsson S., 2000. Amorphous silica solubility and the thermodynamic properties of H4SiO degrees 4 in the range of 0 degrees to 350 degrees C at P sat. Geochimica et Cosmochimica Acta 64(13): 2295-2307.

Hedenquist, J. W., Arribas A. and Gonzalez-Urien E., 2000. Exploration for epithermal gold deposits. Reviews in Economic Geology 13: 245-277.

Helgeson, H. C., 1969. Thermodynamics of hydrothermal systems at elevated temperatures and pressures. American Journal of Science 267(7): 729-804.

Henley, R. W. and Brown K. L., 1985. A practical guide to the thermodynamics of geothermal fluids and hydrothermal ore deposits. Reviews in Economic Geology 2: 25-44.

Kamilli, R. J. and Ohmoto H., 1977. Paragenesis, zoning, fluid inclusion, and isotopic studies of the Finlandia Vein, Colqui District, central Peru. Economic Geology 72(6): 950-982.

Moncada, D., Mutchler S., Nieto A., Reynolds T. J., Rimstidt J. D. and Bodnar R. J., 2012. Mineral textures and fluid inclusion petrography of the epithermal Ag–Au deposits at Guanajuato, Mexico: Application to exploration. Journal of Geochemical Exploration 114: 20-35.

Prol-Ledesma, R. M., Juarez-Sanchez F., Lozano-Santa Cruz R., Alaca-Montiel E., Cruz-Casas V. A., Hernandez-Lombardini S., Canals A. and Cardellach E., 1998. Precious and base metal deposition in an active hydrothermal system, La Primavera, Mexico. Proceedings - International Symposium on Water-Rock Interaction 9: 649-652.

Randall, J. A., Saldana A E. and Clark K. F., 1994. Exploration in a volcano-plutonic center at Guanajuato, Mexico. Economic Geology 89(8): 1722-1751.

Roedder, E., 1984. Fluid inclusions. Reviews in Mineralogy 12: 644.

Sander, M. V. and Black J. E., 1988. Crystallization and recrystallization of growth-zoned vein quartz crystals from epithermal systems; implications for fluid inclusion studies. Economic Geology 83(5): 1052-1060.

Seward, T. M., 1989. The hydrothermal chemistry of gold and its implications for ore formation; boiling and conductive cooling as examples. Economic Geology Monograph 6: 398-404.

Shenberger, D. M. and Barnes H. L., 1989. Solubility of gold in aqueous sulfide solutions from 150 to 350°C. Geochimica et Cosmochimica Acta 53(2): 269-278.

Sillitoe, R. H. and Hedenquist J. W., 2003. Linkages between volcanotectonic settings, ore-fluid compositions, and epithermal precious metal deposits. Special Publication (Society of Economic Geologists (U. S.)) 10: 315-343.

Simmons, S. F. and Brown K. L., 2006. Gold in magmatic hydrothermal solutions and the rapid formation of a giant ore deposit. Science 314(5797): 288-291.

Simmons, S. F. and Brown K. L., 2007. The flux of gold and related metals through a volcanic arc, Taupo Volcanic Zone, New Zealand. Geology 35(12): 1099-1102.

Simmons, S. F. and Browne P. R. L., 2000. Hydrothermal Minerals and Precious Metals in the Broadlands-Ohaaki Geothermal System: Implications for Understanding Low-Sulfidation Epithermal Environments. Economic Geology 95(5): 971-999.

Simmons, S. F. and Christenson B. W., 1994. Origins of calcite in a boiling geothermal system. American Journal of Science 294(3): 361-400.

Simmons, S. F., White N. C. and John D. A., 2005. Geological Characteristics of Epithermal Precious and Base Metal Deposits. Economic Geology 100th Anniversary Volume Economic Geology; One Hundredth Anniversary Volume, 1905-2005: 485-522.

Stefánsson, A. and Seward T. M., 2003. Experimental determination of the stability and stoichiometry of sulphide complexes of silver(I) in hydrothermal solutions to 400°C. Geochimica et Cosmochimica Acta 67(7): 1395-1413.

Stefánsson, A. and Seward T. M., 2004. Gold(I) complexing in aqueous sulphide solutions to 500°C at 500 bar. Geochimica et Cosmochimica Acta 68(20): 4121-4143.

Sterner, S. M. and Bodnar R. J., 1984. Synthetic fluid inclusions in natural quartz; 1, Compositional types synthesized and applications to experimental geochemistry. Geochimica et Cosmochimica Acta 48(12): 2659-2668.

Stewart, M., 2006. Geology of Guanajuato and La Luz Areas, Mexico. Unpublished map.

Taylor, P. S., 1971. Mineral variations in the silver veins of Guanajuato, Mexico. Doctoral Thesis, Dartmouth College

Weissberg, B. G., 1969. Gold-silver ore-grade precipitates from New Zealand thermal waters. Economic Geology 64(1): 95-108.

Wenxin, L., 2001. Modeling description and spectroscopic evidence of surface acid–base properties of natural illites. Water Research 35(17): 4111-4125.

2.10 Figure Captions

Figure 2.1 Solubility of Au as a function of the activity of oxygen and pH.

Solubility of Au as a function of the activity of oxygen and pH maximum Au *solubility is represented by the yellow circle, and gold solubility contours (in ppb) are shown by dashed lines. (modified from Henley and Brown 1985 and Shenberger and Barnes 1989).*

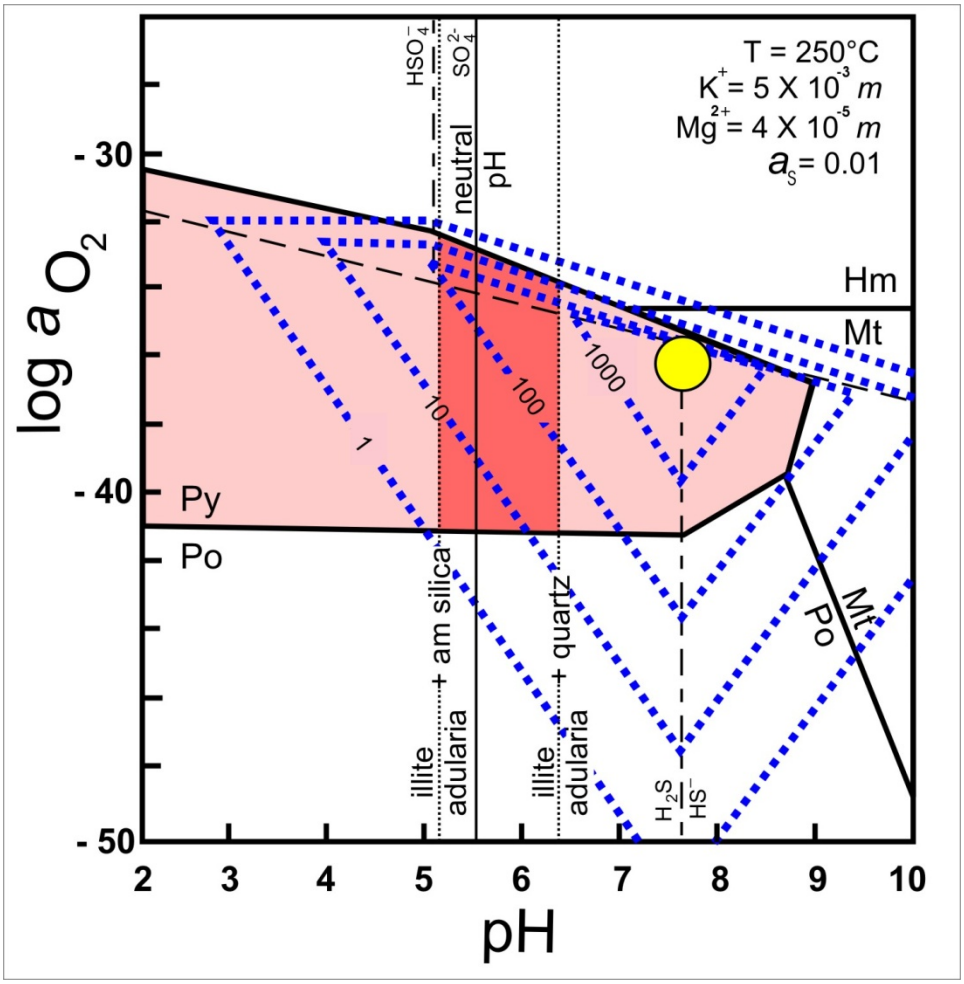

Figure 2.2 Location map of Veta Madre within the Guanajuato Mining District. Showing locations of mines (upper right). Cross section of part of the Veta Madre showing the boiling intensity factor and location of Santa Margarita vein (low). (modified from (Church 1907) and (Taylor 1971)). The boiling intensity factor is defined as the number of textural and fluid inclusion boiling indicators observed in each sample, as described by Moncada et al. 2012.

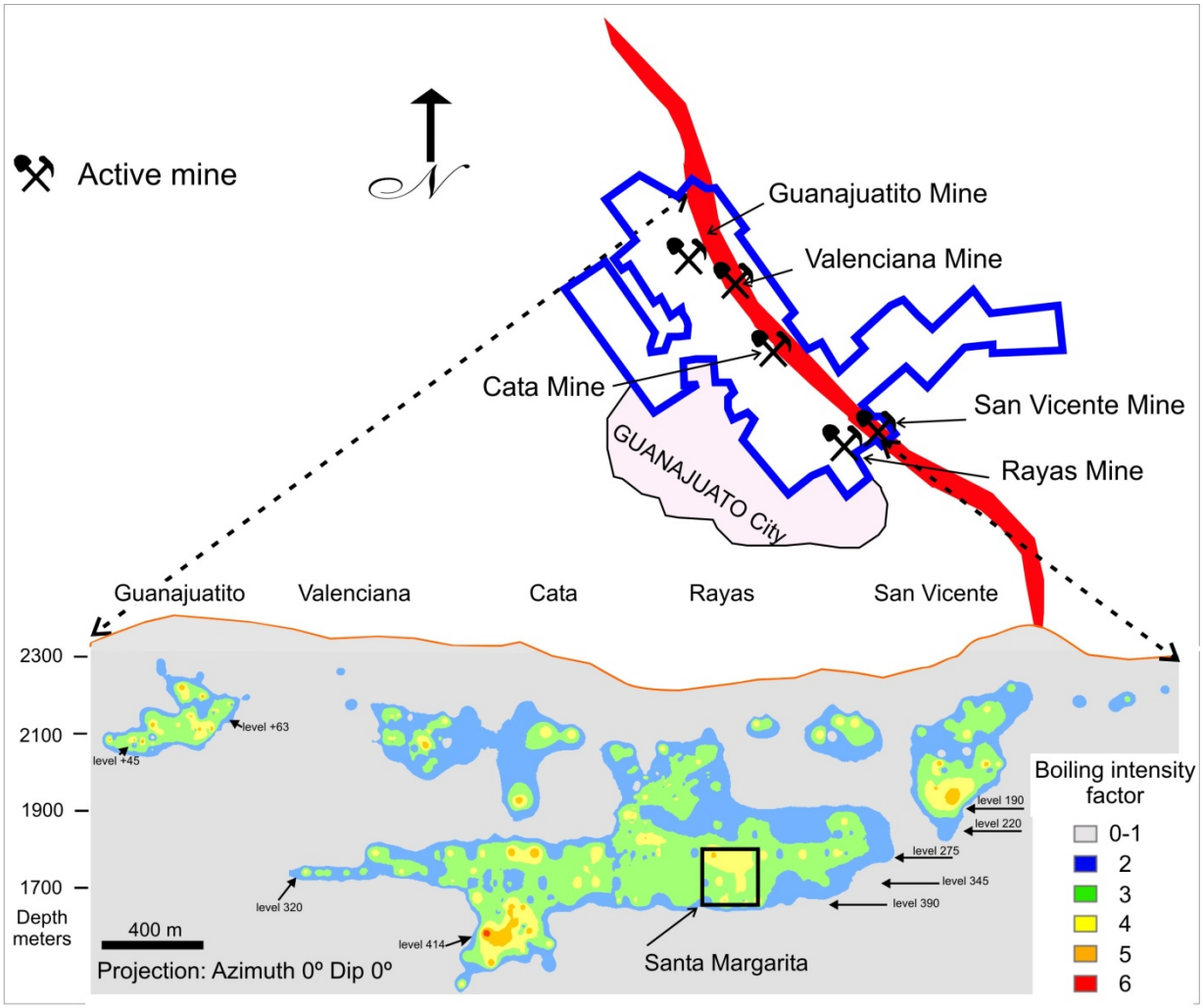

Figure 2.3 Raman spectra of a natural illite

Raman spectra of a natural illite (Wenxin 2001) (top) and a solid phase that occurs in fluid inclusions (bottom) from the Santa Margarita vein at Guanajuato, Mexico. The inset in the bottom spectrum shows three illite-bearing fluid inclusions in quartz.

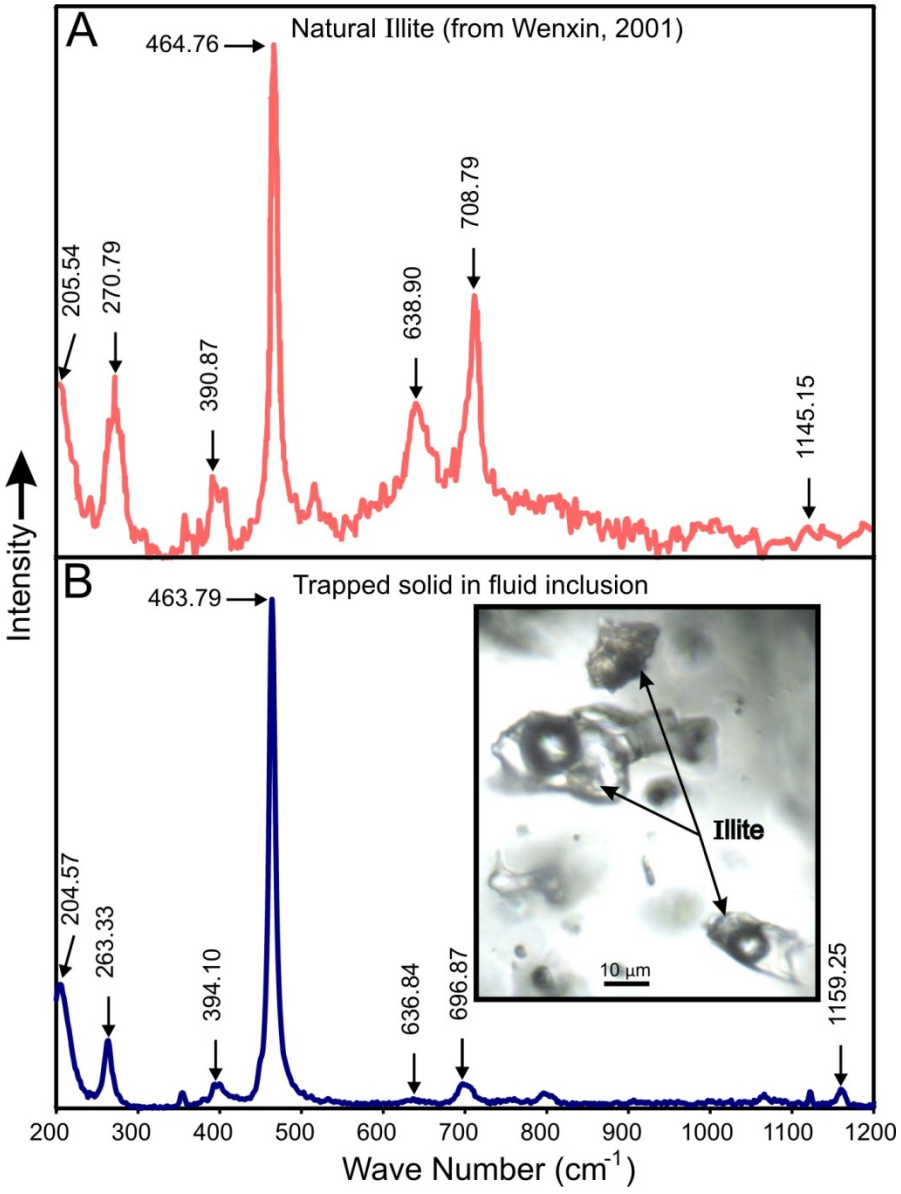

Figure 2.4 Examples of minerals textures observed in samples from the Santa Margarita Vein.

(A) Colloform-banded jigsaw texture quartz; (B) Colloform-banded jigsaw texture quartz using polarize light; (C) Colloform-banded plumose texture quartz; (D) Colloform-banded plumose texture quartz using polarize light; (E) Lattice-bladed calcite replaced by quartz; (F) Lattice-bladed calcite replaced by quartz using polarize light; (G) Illite contained in quartz; (H) Rhombic adularia contained in quartz.

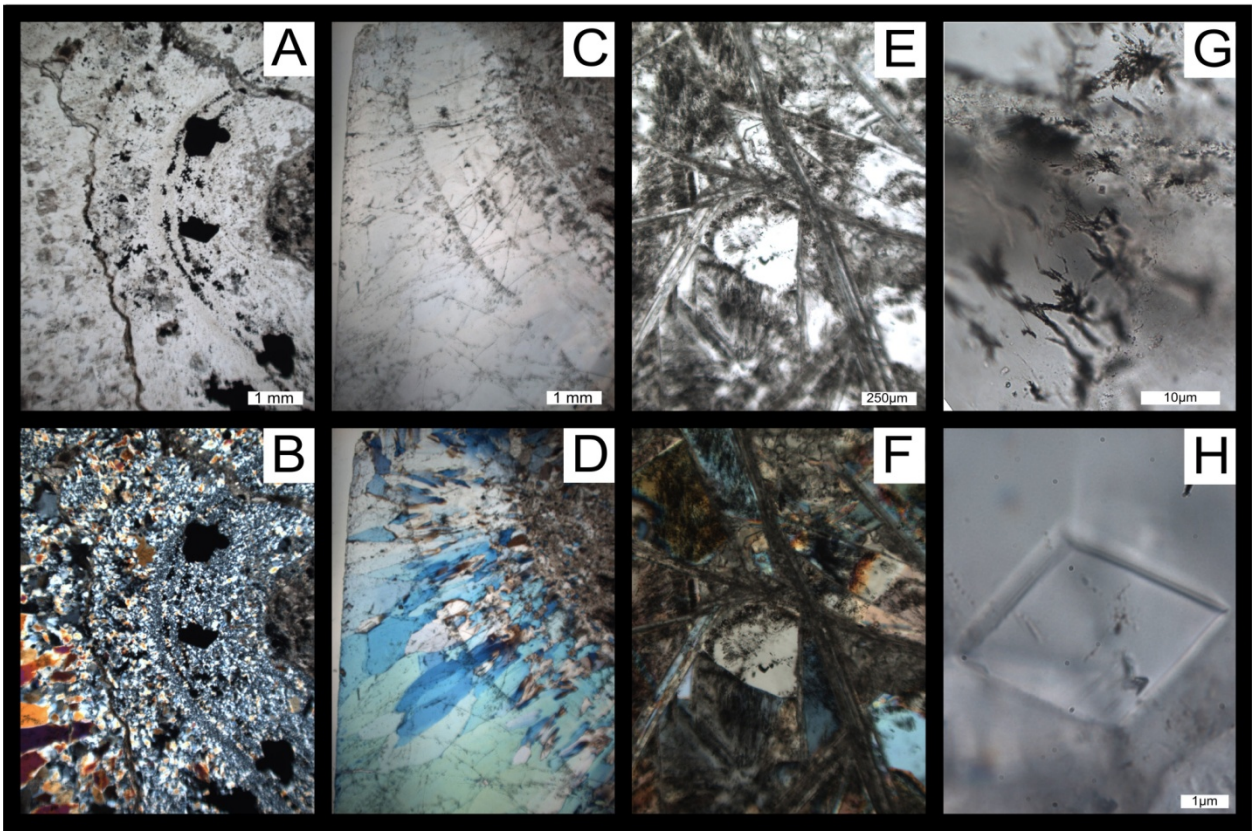

Figure 2.5 Homogenization temperature versus ice-melting temperature from the Santa Margarita Vein.

Homogenization temperature versus ice-melting temperature for 58 Fluid Inclusion Assemblages (FIAs) in mineralized and barren samples from the Santa Margarita Vein. Each FIA consists of two or more fluid inclusions with consistent microthermometric behavior.

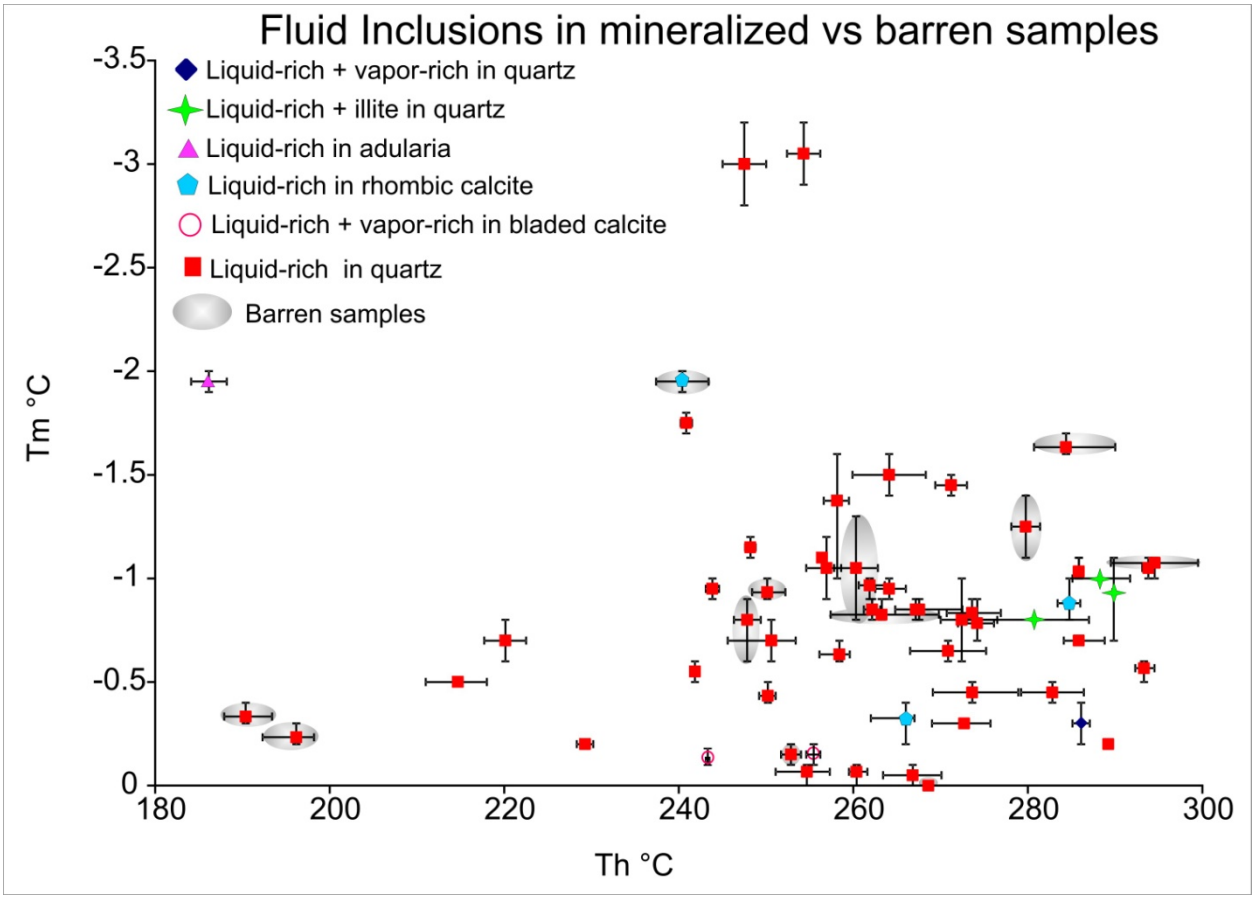

Figure 2.6 Ternary diagram showing Au-Ag-base metal ratios as a function of ice-melting temperature of fluid inclusions from the Santa Margarita Vein.

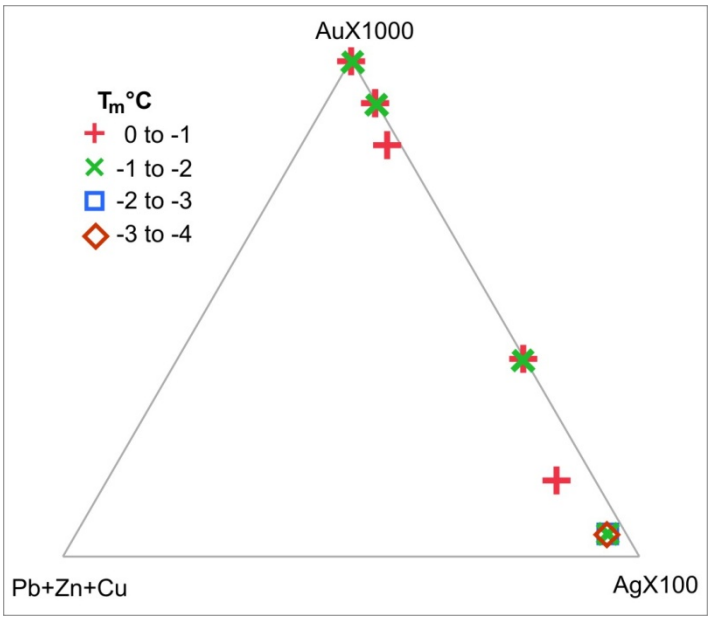

Figure 2.7 Relationship between average Ag and Au grades in samples from the Santa Margarita vein and the presence or absence of various mineral or fluid inclusion textures.

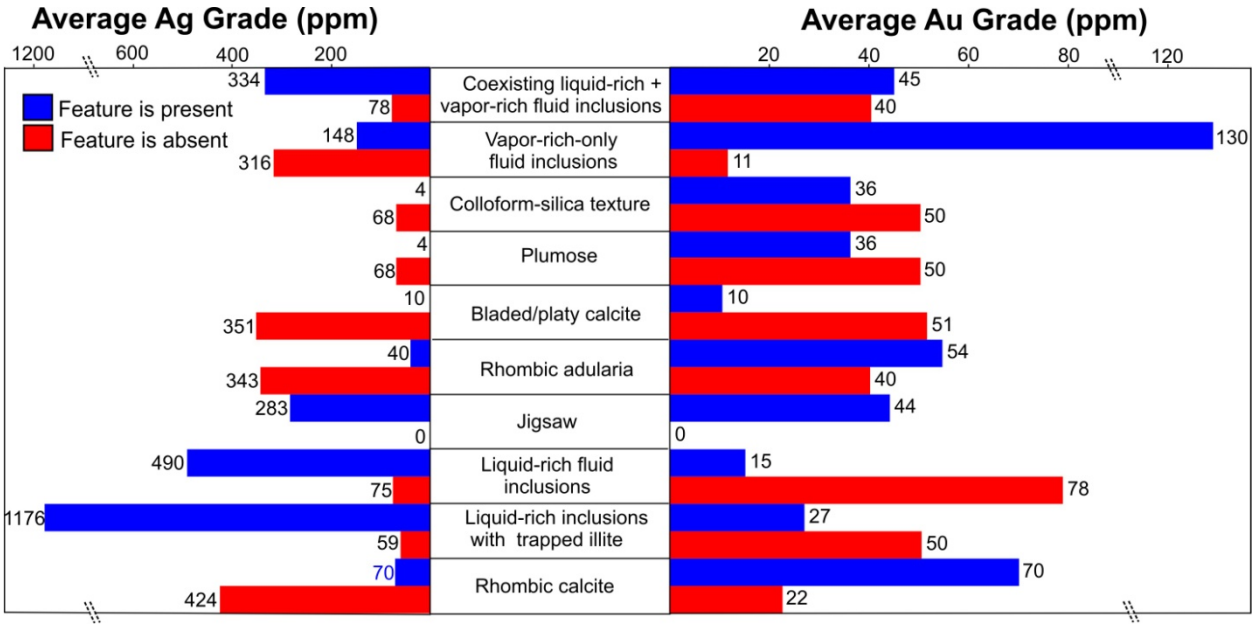

Table 2.1 Microthermometric data for fluid inclusions from the Santa Margarita vein

S= secondary fluid inclusions; P= primary fluid inclusions; T_h= homogenization temperature; T_m= ice melting temperature; n= number of fluid inclusion; [1]Wt. % NaCl equiv from Bodnar (1993)

Sample_ID	Host	Type	n	T_h range (°C)	Ave.	T_m range (°C)	Ave.	wt. % NaCl equiv[1]	Ave.	Notes
2001-123	Quartz	S	3	292.3-294.5	293.3	-0.6 to -0.5	-0.6	0.9-1.1	1.0	Liquid-rich;2001-123B-IV_1FIA
2001-123	Quartz	S	2	267.1-267.2	267.2	-0.9 to -0.8	-0.9	1.4-1.6	1.5	Liquid-rich;2001-123B-IV_2FIA
2001-123	Quartz	S	3	211-218	214.7	-0.5 to -0.5	-0.5	0.9-0.9	0.9	Liquid-rich;2001-123B-IV_3FIA
2001-123	Quartz	S	2	289-289.4	289.2	-0.2 to -0.2	-0.2	0.4-0.4	0.4	Liquid-rich;2001-123B-II_1FIA
2001-123	Quartz	S	4	245.6-253.4	250.6	-0.8 to -0.6	-0.7	1.1-1.4	1.2	Liquid-rich;2001-123B-VII_1FIA
2001-123	Quartz	S	3	256.1-259.6	258.4	-0.7 to -0.6	-0.6	1.1-1.2	1.1	Liquid-rich;2001-123B-VII_2FIA
2001-123	Quartz	S	3	255.9-256.8	256.4	-1.1 to -1.1	-1.1	1.9-1.9	1.9	Liquid-rich;2001-123B-VII_3FIA
2001-123	Quartz	S	3	251.1-257.3	254.7	-0.1 to 0	-0.1	0-0.2	0.1	Liquid-rich;2001-123B-VII_5FIA
2001-123	Quartz	S	3	284.1-288.8	285.8	-0.7 to -0.7	-0.7	1.2-1.2	1.2	Liquid-rich;2001-123B-VII_7FIA
1015917	Quartz	S	4	269.1-278.9	273.6	-0.5 to -0.4	-0.5	0.7-0.9	0.8	Liquid-rich;1015917 IV_1FIA
1015917	Quartz	S	3	269-275.7	272.7	-0.3 to -0.3	-0.3	0.5-0.5	0.5	Liquid-rich;1015917 IV_2FIA
1015917	Quartz	S	3	289.7-289.9	289.8	-1.1 to -0.7	-0.9	1.2-1.9	1.6	Liquid-rich + illite;1015917 I_1FIA_Illite
1015918	Calcite	S	5	283.4-286	284.8	-1 to -0.8	-0.9	1.4-1.7	1.5	Liquid-rich;1015918B_Calcite
1015918	Quartz	S	2	293.1-294.5	293.8	-1.1 to -1	-1.1	1.7-1.9	1.8	Liquid-rich;1015918B_3FIA
1015918	Quartz	S	2	266.5-275.2	270.9	-0.7 to -0.6	-0.7	1.1-1.2	1.1	Liquid-rich;1015918B_4FIA
2001-122	Quartz	S	2	285.1-287.1	286.1	-0.4 to -0.2	-0.3	0.4-1.7	1.1	Liquid-rich + Vapor-rich;2001-122B-II 2FIA LV
2001-122	Quartz	S	3	260.6-263.6	261.9	-1 to -0.9	-1.0	1.6-1.7	1.7	Liquid-rich;2001-122B_1FIA
1015919	Calcite	S	4	262-267	266.0	-0.4 to -0.2	-0.3	0.4-0.7	0.6	Liquid-rich;105919AI_Calcite
105920	Quartz	S	4	262.5-266	264.1	-1 to -0.9	-1.0	1.6-1.7	1.7	Liquid-rich;105920 IV_3FIA
105920	Quartz	S	3	285.4-286.2	285.8	-1.1 to -1	-1.0	1.7-1.9	1.8	Liquid-rich;105920 IV_2FIA
105921	Calcite	S	5	243.1-243.5	243.3	-0.2 to -0.1	-0.1	0.2-0.2	0.2	Liquid-rich + Vapor-rich;105921_III_1FIA_BC
105921	Calcite	S	4	254.6-256.2	255.5	-0.2 to -0.1	-0.2	0.2-0.4	0.3	Liquid-rich + Vapor-rich;105921_III_3FIA_BC
2001-125	Quartz	S	6	254.6-258.6	256.9	-1.2 to -0.9	-1.1	1.6-2.1	1.8	Liquid-rich;2001-125I_4FIA
2001-125	Quartz	S	6	270-276.5	272.4	-1 to -0.6	-0.8	1.1-1.7	1.4	Liquid-rich;2001-125I_3FIA
2001-125	Quartz	P	5	256.6-259.5	258.1	-1.6 to -1	-1.4	1.7-2.7	2.4	Liquid-rich;2001-125I_1FIA
2001-121	Quartz	S	4	263.4-270.1	266.8	-0.1 to 0	-0.1	0-0.2	0.1	Liquid-rich;2001-121I_2FIA
2001-124	Quartz	S	3	259.5-261.6	260.4	-0.1 to 0	-0.1	0-0.2	0.1	Liquid-rich;2001-124III_1FIA
2001-121	Quartz	S	2	228.3-230.2	229.3	-0.2 to -0.2	-0.2	0.4-0.4	0.4	Liquid-rich;2001-121III_3FIA
105919	Quartz	S	2	279.2-286.4	282.8	-0.5 to -0.4	-0.5	0.7-0.9	0.8	Liquid-rich;105919III_4FIA
105919	Quartz	S	3	270.7-276.9	273.6	-0.9 to -0.8	-0.8	1.4-1.6	1.5	Liquid-rich;105919III_5FIA
2001-125	Quartz	S	3	273-287	281.0	-0.8 to -0.8	-0.8	1.4-1.4	1.4	Liquid-rich + illite;2001-125III_6FIA
2001-125	Quartz	S	2	259.9-268.3	264.1	-1.6 to -1.4	-1.5	2.4-2.7	2.6	Liquid-rich;2001-125III_7FIA
2001-125	Quartz	S	2	269.4-273	271.2	-1.5 to -1.4	-1.5	2.4-2.4	2.4	Liquid-rich;2001-125III_7FIA
2001-125	Quartz	S	6	272-276.1	274.2	-0.9 to -0.7	-0.8	1.2-1.6	1.4	Liquid-rich;2001-125II-II
2001-125	Quartz	S	2	252.4-256.2	254.3	-3.2 to -2.9	-3.1	4.8-5.3	5.0	Liquid-rich;2001-125B-IV_2FIA
2001-125	Quartz	S	2	245-250	247.5	-3.2 to -2.8	-3.0	4.6-5.3	5.0	Liquid-rich;2001-125B-IV_3FIA

2001-125	Quartz	S	2	247.6-248.8	248.2	-1.2 to -1.1	-1.2	1.9-2.1	2.0	Liquid-rich;2001-125B-IV_7FIA
2001-125	Quartz	S	2	243.1-244.6	243.9	-1 to -0.9	-1.0	1.6-1.7	1.7	Liquid-rich;2001-125B-IV_9FIA
2001-125	Quartz	S	3	241.5-242.2	241.9	-0.6 to -0.5	-0.6	0.9-1.1	1.0	Liquid-rich;2001-125B-IV_12FIA
2001-125	Quartz	S	2	261.2-263.1	262.2	-0.9 to -0.8	-0.9	1.4-1.6	1.5	Liquid-rich;2001-125B-V_1FIA
2001-125	Quartz	S	4	264.8-272.5	267.6	-0.9 to -0.8	-0.9	1.4-1.6	1.5	Liquid-rich;2001-125A-V_1FIA
2001-125	Quartz	S	2	240.2-241.5	240.9	-1.8 to -1.7	-1.8	2.9-3.1	3.0	Liquid-rich;2001-125B-V_2FIA
2001-125	Quartz	S	4	217.7-222.5	220.1	-0.8 to -0.6	-0.7	1.1-1.4	1.2	Liquid-rich;2001-125A-II_1FIA
2001-125	Adularia	S	2	184.1-188.2	186.2	-2 to -1.9	-2.0	3.2-3.4	3.3	Liquid-rich;2001-125VI_1FIA Adularia
2001-126	Calcite	S	3	237.4-243.4	240.4	-2 to -1.9	-2.0	3.2-3.4	3.3	Liquid-rich;2001-126A_1FIA Calcite
2001-126	Quartz	S	2	268.4-268.8	268.6	0 to 0	0.0	0-0	0.0	Liquid-rich;2001-126A_3FIA
2001-126	Calcite	S	3	280.7-290	284.4	-1.7 to -1.6	-1.6	2.7-2.9	2.8	Liquid-rich;2001-126A_4FIA Calcite
2001-126	Quartz	S	4	289.5-299.5	294.5	-1.1 to -1	-1.1	1.7-1.9	1.9	Liquid-rich;2001-126_B_6FIA
2001-126	Quartz	S	4	257.4-269.8	263.3	-0.9 to -0.8	-0.8	1.4-1.6	1.4	Liquid-rich;2001-126_B_2FIA
2001-126	Quartz	S	3	248.4-252.2	250.1	-1 to -0.9	-0.9	1.6-1.7	1.6	Liquid-rich;2001-126_B_3FIA
2001-126	Quartz	S	3	187.9-193.4	190.4	-0.4 to -0.3	-0.3	0.5-0.7	0.6	Liquid-rich;2001-126_B_1FIA
2001-126	Quartz	S	3	192.3-198.2	196.2	-0.3 to -0.2	-0.2	0.4-0.5	0.4	Liquid-rich;2001-126_B_2FIA
2001-126	Quartz	S	2	251.7-254	252.9	-0.2 to -0.1	-0.2	0.2-0.4	0.3	Liquid-rich;2001-126_C_1FIA
2001-126	Quartz	S	2	257.8-262.8	260.3	-1.3 to -0.8	-1.1	1.4-2.2	1.8	Liquid-rich;2001-126_C_2FIA
2001-126	Quartz	S	3	249.2-251.1	250.2	-0.5 to -0.4	-0.4	0.7-0.9	0.8	Liquid-rich;2001-126_C_3FIA
2001-126	Quartz	S	2	278.1-281.4	279.8	-1.4 to -1.1	-1.3	1.9-2.4	2.2	Liquid-rich;2001-126_C_2FIA
2001-126	Quartz	S	3	246.3-249.4	247.8	-0.9 to -0.6	-0.8	1.1-1.6	1.4	Liquid-rich;2001-126_C_1FIA
2001-125	Quartz	S	3	285.1-291.7	289.2	-1 to -1	-1.0	1.7-1.7	1.7	Liquid-rich + illite;2001-125_III_2FIA_illite

Chapter 3 Structural and fluid controls on epithermal Ag-Au mineralization in the La Luz area, Guanajuato Mining District, México

Abstract: Applying new models and methods provides a competitive advantage in the search for mineral deposits because an explorationist can quickly evaluate potential targets and eliminate areas without good potential for mineralization. In this study, we describe a technique based on gangue mineral textures and fluid inclusion characteristics that has been applied to identify an area of high potential for gold-silver mineralization in different Ag-Au veins at La Luz system in Guanajuato, Mexico.

Structural mapping and detail petrography for more of 200 samples collected in drill holes, historical mine and surface outcrop from the veins Plateros, Melladito, Intermediate, Nombre de Dios, Bolañitos, San José, Lucero, Karina, Daniela, and Belén veins show general strike 315 to 360. Features associated with boiling that have been identified include colloform silica texture, moss silica texture, jigsaw silica texture, plumose silica texture, ghost-sphere silica texture, rhombic adularia, adularia, illite/sericite, lattice-bladed calcite, and lattice-bladed calcite replaced by quartz, coexisting liquid-rich and vapor-rich fluid inclusions, vapor-rich-only inclusions and liquid-rich inclusions with trapped illite. Boiling below the deepest levels explored in the veins is likely, thus increasing the probability of additional resources at depth. In over all the La Luz system show five stages with stage IV the mineralized with acanthine and sulfosalts and many others boiling textures.

Following detailed petrographic examination of the samples, 141 FIAs were selected for microthermometric analysis. The fluid inclusions are hosted by jigsaw silica texture, plumose silica texture, and bladed calcite and rhombic calcite in secondary fluid inclusion assemblages; primary fluid inclusions are present only in euhedral quartz with no evidence of recrystallization. The La Luz area shows homogenization temperatures (T_h) from primary fluid inclusions in quartz from assemblages containing coexisting liquid-rich and vapor-rich inclusions that range from 209-211 °C and salinity from 0.1-0.6 wt. % NaCl. Secondary fluid inclusion assemblages in quartz with coexisting liquid-rich and vapor-rich inclusions show a range in T_h from 180-320 °C and salinity from 0.1-2.1 wt. % NaCl. Primary fluid inclusion assemblages in bladed calcite with coexisting liquid-

rich and vapor-rich inclusions show a range in T_h from 160-188 °C and salinity from 0.6-0.9 wt. % NaCl. Secondary fluid inclusion assemblages in quartz containing only vapor-rich inclusions show a range in T_h from 255-340 °C and salinity from 0.5-1.5 wt. % NaCl. Primary liquid-rich inclusions with trapped illite in quartz show a range in T_h from 251-287 °C and salinity 0.1-0.5 wt. % NaCl. Secondary fluid inclusions in quartz show a range in T_h from 286-289 °C and salinity from 0.9-1.2 wt. % NaCl. In rhombic calcite T_h ranges from 159-197 °C and salinity from 0.4-0.6 wt. % NaCl.

The potential for additional resources in the La Luz area has been documented for veins that extend to the south and north of the main area. Detailed geologic mapping and fluid inclusion petrography of samples from this area might identify additional targets.

3.1 Introduction

The Guanajuato silver district is located in the state of Guanajuato (meaning “hill of frogs” in Tarasco) in central Mexico, approximately 330 km NW of Mexico City. The silver ores occur along three approximately parallel NNW trending vein systems named, from NW to SE the La Luz, Veta Madre and Sierra vein systems (Figure 3.1). The historical development of La Luz area is summarized by Ward (1828), Blake (1902), Percy (1906), Church (1907b), Church (1907a), Botsford (1910). When Hernán Cortéz arrived in Mexico in 1519 the Aztec Empire had mined and refined precious metals for decorating their vases, figures, and jewelry. The Chichimecas Empire (700-1520) that occupied the central and northern parts of Mexico and included the semi-nomadic peoples in Guanajuato who were likely the first humans to extract ore from the outcropping veins in the area (Schmal 2007). According to legend, silver was discovered in La Luz area was in 1548 by mule drivers on their way to find their fortune in the newly discovered bonanza veins in the Mexican state of Zacatecas. They observed that rocks used to confine a bonfire were melting. This discovery took place in the area of the San Bernabe mine, 13 kilometers to the northwest of the present-day Guanajuato city (Figure 3.1). Four years later, in 1552, the Veta Madre was discovered

by Juan de Rayas and one of the mines on the Veta Madre, the La Valenciana mine, for a time during the height of its activity accounted for two-thirds of the world's silver production. Mining activity on the La Luz system has passed through a number of bonanzas and bust cycles. No records remain of work undertaken in the area from 1548 until 1793 (Velazquez 1973). Since 1793 numerous operators have been worked La Luz system, and more details on the history can be found in Velazquez (1973).

Today the La Luz area is the site of much exploration activity by Great Panther Silver Limited and Endeavour Silver Corporation, and several new veins have been discovered. Modern exploration in the La Luz area involves detailed surface and subsurface mapping that combines structural geology, soil sampling and fluid inclusions and mineral textures (Lewis et al. 2011, Moncada and Bodnar 2012a, Moncada and Bodnar 2012b, Waldegger 2012). Over 134 drill holes have produced more than 39,000 m of drill core, and more than 10,000 samples have been collected and analyzed during exploration (Lewis et al. 2011, Waldegger 2012).

It is well known that most successful exploration programs are based on conceptual models that encompass the broad range of structural, tectonic and geochemical factors that are essential for ore-formation (Barton 1986, Hodgson 1989, Carranza and Sadeghi 2012). The application of these models requires that the explorationist be able to effectively identify features that confirm that these essential or necessary conditions were met. Over the past few decades, theoretical and experimental studies, combined with observations from active continental geothermal systems and their fossil equivalents, the epithermal mineral deposits, have documented a close association between boiling and precious metal deposition (Kamilli and Ohmoto 1977, Buchanan 1980, Roedder 1984, Brown 1986, Clark and Williams-Jones 1990, Hedenquist et al. 2000, Albinson et al. 2001, Etoh et al. 2002, Simmons et al. 2005) Thus, the explorationist who can identify quickly and with a high degree of confidence whether boiling occurred in a given prospect will have a competitive advantage in the search for precious metal resources. Here we describe various mineralogical, textural and fluid inclusion features that are produced as a result of boiling hydrothermal fluids, and apply this methodology to identify areas with good potential for epithermal Ag-Au mineralization in the La Luz area, Guanajuato Mining District, Mexico.

3.2 Evidence for boiling in epithermal systems

When a phase is precipitated rapidly from solution, as often happens when a fluid boils, diagnostic textures are often produced that serve to identify phases precipitated as a result of boiling. In other cases, the chemical changes in the fluid that result from boiling or immiscibility often lead to precipitation of specific phases or phase assemblages. Moreover, fluid inclusions trapped from boiling fluids display predictable phase relations at room temperature and during microthermometry.

3.2.1 Silica Phases.

Silica (SiO_2) is a ubiquitous gangue mineral in epithermal deposits and displays various textures depending on whether the silica was precipitated from a boiling or non-boiling fluid (Adams 1920, Sander and Black 1988, Dong et al. 1995, Henley and Hughes 2000). Thus, colloform texture quartz, jigsaw texture quartz and plumose or feathery texture quartz are all thought to represent material that was originally precipitated as amorphous silica as a result of boiling and have subsequently crystallized to quartz. Conversely, euhedral quartz crystals, comb quartz and zonal quartz are thought to be precipitated more slowly from non-boiling solutions.

3.2.2 Calcite

Calcite is a common gangue mineral in epithermal deposits. Rhombic calcite is typical of non-boiling environments, but bladed calcite is precipitated from boiling solutions as a result of the rapid exsolution of carbon dioxide from the solution (Simmons and Christenson 1994). Bladed calcite forms in this environment as a result of rapid crystal growth whereby the (104) face grows faster than the other crystal faces, producing an elongated or bladed crystal morphology (Kaldis 1974). Sometimes bladed calcite can be replaced by quartz if the boiling horizon shifts upward and the bladed calcite is in the presence of a single-phase (non-boiling) fluid containing dissolved silica.

3.2.3 Adularia

Adularia is a low temperature polymorph of potassium feldspar that is a common gangue phase in epithermal deposits. Various morphological forms of adularia, reflecting the structural state in terms of the degree of Al/Si disordering, have been reported from epithermal deposits by Dong and Morrison (1995). The rhombic and tabular forms of adularia show greater Al/Si disorder, suggesting rapid crystallization (Dong and Morrison 1995), and these forms are indicative of precipitation in a boiling system. In support of this conclusion, Browne (1978) suggested that as the fluid becomes more alkaline during boiling adularia would precipitate.

3.2.4 Illite

The presence of illite by itself is not evidence of boiling. However, illite is commonly observed as an alteration phase in epithermal deposits (Vikre 1985) and geothermal system (Prol-Ledesma and Browne 1989), and illite is the predicted K-bearing alteration phase that would be in equilibrium with adularia+amorphous silica and adularia+quartz at epithermal PT conditions (Moncada and Bodnar 2012c).

3.2.5 Fluid Inclusions

The characteristics of fluid inclusions in the epithermal environment have been described by Bodnar et al. (1985) and Bodnar et al. (2013). Fluid inclusion assemblages (FIAs), representing groups of fluid inclusions trapped at the same time, consisting of coexisting liquid-rich and vapor-rich inclusions are produced when FI are trapped in a boiling system. The presence of assemblages consisting of only vapor-rich fluid inclusions is indicative of intense boiling or “flashing” of the fluid.

3.3 Geological setting

The Mesa Central is an elevated plateau of Cenozoic volcanics and volcaniclastics located in the central part of Mexico. The plateau is bounded to the north and east by

the Sierra Madre Oriental, to the west by the Sierra Madre Occidental, and to the south by the Trans-Mexican Volcanic Belt. Cretaceous volcanic rocks underlie the La Luz area and mineralization is thought to have occurred in the Oligocene (Buchanan 1980).

The regional geology in the La Luz area has been studied in detail by Church (1907b), Gómez (1963), Gross (1975), Dávila and Martínez-Reyes (1987), Ortiz et al. (1989), Randall et al. (1994), and Stewart (2006). The following description is based on previous studies and new detailed fieldwork in the area (Figure 3.2). In the La Luz area the rocks have been classified as an undifferentiated volcano-sedimentary complex that includes an unconformity separating sedimentary and low-grade metasediments below (Esperanza Fm.) from igneous rocks above (La Luz Fm.) (Martínez-Reyes and Nieto-Samaniego 1992). The oldest formation in the La Luz area is the Esperanza formation that consists of calcareous and carbonaceous mudstone and slate interbedded with pillow basalts and andesite (Ksh; Fig. 3.2). The thickness of this unit in some areas exceeds 600 m and has been assigned a Cretaceous age based on the presence of radiolaria (Figure 3.3) (Dávila and Martínez-Reyes 1987, Randall et al. 1994).

Overlying the Esperanza Fm. and separated from it by an unconformity is the La Luz Andesite (Randall 1982) that consists of interbedded clastic sediments and pillow lavas (basalt) (Kbas) and andesite lava flows (Kanfl) that have been metamorphosed to greenschist facies. The lavas are chlorite-rich show silica/argillitic alteration, and have been dated by K-Ar at 108.4 ± 6.2 Ma, (Ortiz et al. 1989, Stewart 2006). In some areas the thickness of this unit may exceed 500 m (Figure 3.3) (Randall et al. 1994). A plagioclase-rich ash to lapilli tuff that has been metamorphosed to greenschist facies and is chlorite-rich with weak regional silica and propylitic alteration (Kantf) overlies the La Luz Formation in the central to southern part of the area shown Figure 3.2 (Stewart 2006)

The entire sequence is intruded by aphanitic to finely porphyritic dikes. Generally the diorite intrusions show weak to low grade chlorite alteration (Kdi) and can be transitional to more felsic phases such as granodiorite (Kgd) with rounded, 2-3 mm quartz eyes, and weak clay alteration of feldspars (Stewart 2006). Aquartz-eye rhyolite porphyry shows a wide (meters) argillic alteration halo at the margins consisting mainly of illite,

with kaolinite in more intensely altered locations (Kqfq). In the northern part of the area the Cerro Pelon tonalite (Jtcp) is exposed (Figure 3.3) (Church 1907a).

3.3.1 Ore shots

Mineralized veins are hosted by the Esperanza formation (Ksh) and pillow basalts (Kbas) and andesites of the La Luz Fm. The oldest (historical) stopes on the La Luz vein are located in the northern part of the area (Figure 3.2) and have been reported to be 3 m thick, 30 m long and 18 m high. These older stopes lie 12 to 15 m laterally from the main La Luz vein and were found by following smaller veins (ramaleos or stringers) that extend away from the main structure (Blake 1902, Church 1907b). Some of the stopes are opened to the surface (indicating that mineralization extended to the surface), but in general the mineralization begins ~60 m below the surface (Church 1907b). The recent drilling program has identified new mineralized veins that are up to 600 m long with mineralization over a depth interval of100 m hosted in the La Luz basalts (Kbas) (Figure 3.4). The average silver grades range from 55 to 177 g/t; average gold grades range from 1.2 to 2.5 g/t (Lewis et al. 2011, Waldegger 2012).

3.3.2 Hydrothermal alteration

The area has been mapped intermittently by various companies during the past century, but in general there has been little exploration activity and most effort has been focused on underground production (Gómez 1963, Velazquez 1973). The mineralized veins can be associated with argillic, phyllic, and propylitic alteration and silicification. Most often, mineralization is associated with phyllic alteration (sericite/illite) and silicification, which forms haloes around the mineralized veins. Mineralized veins usually contain adularia and sericite/illite, whereas epidote is found associated with veins that are not mineralized. The surface expression of veins in the area varies greatly. For example, the Boveda vein (Figure 3.1) is two meters wide at the surface, and shows phyllic (sericite) alteration. Some veins pinch to the centimeter scale at the surface, and are associated with weak shear zones and minor argillic alteration suggesting that a structure (vein) may be present beneath the surface.

3.4 Structural setting

The veins that host mineralization in the La Luz area generally strike 315-360°, are steeply dipping and individual veins extend over a strike length of 1-3.5 km. This regional extension is thought to be related to the precious metal mineralization event in the Cenozoic (Buchanan 1980).

One of the earliest descriptions of the structural orientation of the northern part of the La Luz system reported a vein strike of 21SE (339 azimuth), with a vein length of 2,800 m and dipping to the west. In the central part of the La Luz system the Purisima and Plateros veins strike 44SE (316 azimuth) with a length of 1,900 m and dip to the west. In the southern part of the area, the San Antonio vein strikes 69SE (291 azimuth) and has a length of 3,400 m and dips to the west (Church 1907a). Other veins in the La Luz area dip to the east and include Bolañitos, San Pablo, La Joya, Cocinera and Lourdes veins (Church 1907a). The more recent drilling program in 2010-2012 located other veins dipping to the west, including Intermediate, Melladito, Nombre de Dios, Lucero, Karina, Lana and Fernanda veins. The Daniela vein dips to the east. These newly discovered veins extend a few hundred meters in length and trend from NW to SE (Figure 3.4).

Starling (2008) summarized the tectonic and structural history in the La Luz area. Pre-mineralization deformation in the area occurred during the Laramide orogeny (~80-40 Ma) with two main phases; a NE-SW to ENE-WSW compression event followed by a change to NE directed compression. This resulted overthrusting and the development of pre-mineralization folding and thrusting of the Esperanza Fm. in the La Luz area. Early post-Laramide extension (~30 Ma?) was oriented N-S to NNE. Guanajuato is on a NNW trending terrane boundary that was reactivated as a sinistral trans-tensional fault zone during early stage low to intermediate-sulfidation style mineralization in the area. At ~28 Ma, regional extension rotated to the ENE-WSW , resulting in Basin and Range style deformation and faulting that is associated with a second stage of mineralization in the Guanajuato area. Mineralization in the area is thus associated with two stages of extension at ~30-28 Ma. Early mineralization is associated with anticlockwise motion

along the main structures, and second stage mineralization is associated with the Basin and Range style deformation that reactivated earlier structures. This resulted in structural and hydrothermal telescoping, along with pinching of the ore shoots from changes in dip and/or strike as shown on figure 3.4. Starling (2008) suggests that there is potential to find blind, shallow ore bodies as well as extensions to mineralization below barren horizons (Starling 2008).

Five types of veins were described and they define systematic vein paragenesis and textural relationships. Calcite and quartz veins related to early metamorphism or compressional deformation occur early. These are followed by calcite-epidote veins, with epidote possibly related to sub-greenschist facies metamorphism and unrelated to precious metal deposition. Quartz-pyrite ± calcite stockwork veins are the next vein type, and these sometimes contain traces of gold with minor silver. These veins in some cases show that stockwork is present within a breccia fragment, indicating multiple stages of brecciation. The next vein in the paragenesis contains calcite - quartz (colloform texture) – pyrite – sulphosalts and contain the highest silver values. These veins are related to the extensional event. Finally, the paragenesis ends with quartz (amethyst and zonal or comb texture quartz) ± calcite veins this vein representing the final hydrothermal event in the La Luz area. The paragenesis and vein descriptions were used as the basis for collecting samples in the field for petrography and fluid inclusions analysis described below.

3.5 Methodology

In collaboration with staff of Great Panther Silver Limited and Endeavour Silver Corp., a total of 214 samples were collected from surface outcrops, underground workings, and drill core from the La Luz area (Figure 3.1). Below we summarize the results of a petrographic study of samples collected, including a description of the mineral textures and fluid inclusion types observed, and correlate these data with metal contents of the samples, structural orientation, fluid inclusion microthermometry, denudation rate, and paragenetic sequence.

3.5.1 Sample collection

Samples in the La Luz area were collected from underground workings, drill holes and surface outcrops. The samples show a wide variety of silica and calcite textures (Figure 3.5) and fluid inclusion types, many of these features have been associated with boiling hydrothermal fluids. The texture observed most commonly, in 191 samples (Figure 3.5), is jigsaw texture quartz (Figure 3.6 A, B). The gangue mineral calcite (Figure 3.7 E, F) occurs in 135 samples (Figure 3.5). Colloform texture quartz (Figure 3.6 C, D) is found in 117 samples (Figure 3.5) and plumose texture quartz (Figure 3.6 E, F) is observed in 102 samples (Figure 3.5). Adularia is present in 63 samples. Fluid Inclusion Assemblages (FIAs) consisting of coexisting liquid-rich and vapor-rich fluid inclusions were observed in 61 samples (Figures 3.8 & 3.9) and FIAs consisting of only vapor-rich fluid inclusions (i.e., no liquid-rich inclusions were present) were found in 59 samples (Figure 3.10). Bladed calcite was present in 26 samples (Figure 3.6 G, H), and liquid-rich fluid inclusions with trapped illite crystals were present in 16 samples (Figure 11). Comb texture quartz was observed in 11 samples (Figure 3.7 C, D), and zonal texture quartz (Figure 3.7 A, B) and ghost-sphere texture quartz (Figure 3.6 I, J) were each found in only 1 sample.

Underground sampling in several active and inactive historical mines was conducted. From north to south, active mines include Bolañitos, San José, Lucero, Karina and Daniela. Inactive historical mines include Nopal, San Pablo, Sangria, La Boveda, San José, Chayita, San José de abajo, Chuparosa, San Francisco de Asis, and Belén. Drill hole samples were available only from the central part of the La Luz area and include DDH-1, DDH-4, DDH-9, DDH-14, DDH-17 and DDH-21. These drill holes cut the Melladito, Intermediate and Nombre de Dios veins. Two drill holes, DDH-9 and DDH-14, intersect three different veins, the Melladito, Intermediate and Nombre de Dios veins, at approximately the same depth (but at slightly different locations laterally along the vein). In all three veins, samples from DDH-9 have higher grades compared to those from DDH-14, even though both veins show evidence for boiling within the intervals sampled. A detailed description of the metal budget and boiling features in the Melladito vein that was cut by different drill holes provides a vertical description of the

vein. Drill holes LC-03, LC-26, LC-29, LC-31, LC-20, LC-15, DN-1, DN-2, and KA-15 cut the Lucero, Daniela and Karina veins. The Karina and Daniela veins were intersected at different depths by various drill holes, and we have examined metal grades and evidence of boiling at these different depths in section 28600 to characterize the vertical distribution of these features within the vein to better understand the potential for additional resources at depth. Traverses perpendicular to the main veins were conducted on the surface and samples from veins ranging from ≈1 to 20 cm wide were collected. In some cases only the structural expression of the vein was present at the surface and no vein material could be collected.

After sampling, one-half of each sample was analyzed for Au, Ag, Cu, Zn, Pb, Sb, As. A thin section was prepared from the other half of the sample for petrographic study to characterize the silica and calcite textures, identify other minerals that were present, such as adularia, and to examine the fluid inclusions.

3.6 Minerals and Paragenesis

The veins and mines in the La Luz area show a diverse mineralogy. The most common ore minerals reported are acanthite (Ag_2S), miargyrite ($AgSbS_2$), pyrargyrite (Ag_3SbS_3), stephanite (Ag_5SbS_4), prousitite (Ag_3AsS_3) and polybasite [Ag_9CuS_4] [(Ag,Cu)6$(Sb,As)_2S_7$]. Minerals that are les widely distributed in the La Luz deposits are cinnabar (HgS), native silver (Ag), electrum (Au-Ag), silver bromide (AgBr), stibnite (Sb_2S_3), native antimony (Sb), sphalerite (Zn,FeS) and chalcopyrite ($CuFeS_2$) (Blake 1902, Gómez 1963, Vasallo and Reyes-Salas 2007). Note that one of the earliest descriptions of the mineral distribution in the La Luz system was by Gómez (1963), who reported that base metal distribution was random in the veins and did not decrease with depth. The deep vein that was mined in the La Luz area was at the San José de los Muchachos mine (Figure 3.4) and the San Cayetano mine (Figure 3.4), in both mines, mining ceased at a depth of about 2,000 Meter Above Sea Level (MASL). The production stopped for several reasons, the most important being the large of amounts of water in the mines and the lack of equipment to pump the water out. After underground mining stopped, the companies were more interested in reprocessing the

old waste dumps rather than conducting new exploration (Gómez 1963, Velazquez 1973).

Veins in La Luz area are characterized by textures indicating sequential precipitation in open fractures. Intermittently the fractures were sealed as a result of mineralization, leading to overpressure conditions and subsequent fracturing and precipitation of amorphous silica. The different events recorded during compression and extension define a paragenetic sequence that can be divided into five stages (Figure 3.12). Each stage is characterized by a specific set of gangue and ore minerals, boiling textures that include colloform texture quartz, plumose texture quartz, jigsaw texture quartz, ghost-sphere quartz and bladed calcite. Textures produced by precipitation from non-boiling solutions listed include comb texture quartz, zonal texture quartz, amethyst, and rhombic calcite. The ore minerals include acanthite and the sulfosalts pyrargyrite and polybasite. Minor amounts of cinnabar, sphalerite and chalcopyrite also occur.

The sequence in which the gangue and ore minerals were deposited beginning with stage I, is rhombic calcite and zonal to comb quartz in flat veins. Stage II is characterized by zonal and comb quartz followed by rhombic calcite with associated epidote alteration. Stage III contains zonal or comb quartz with small amounts of pyrite and rhombic calcite. In stage III a breccia containing fragments of wall-rock that have been cemented by jigsaw texture quartz contains traces of Au and Ag in the pyrite. Stage IV hosts the ore and is characterized by the presence of argentiferous pyrite within jigsaw texture quartz and by acantite and miargyrite in colloform texture quartz. Minor electrum is observed near the end of stage IV and sulfosalts and adularia occur at the end of stage IV and beginning of stage V. Bladed calcite appears late in stage III and throughout stage IV and, in some samples, continues into stage V. Rounded fragments with calcite and quartz cemented by jigsaw texture quartz were observed in stage IV. Finally, in stage V rhombic calcite appears and amethyst, zonal and comb quartz textures, and ghost-sphere texture quartz are observed (Figure 3.12). The sequence described above involving brecciation and precipitation of phases with textures characteristic of boiling suggests that several episodes of boiling occurred during mineralization.

3.7 Data and Results

Samples in the La Luz area were collected from the main veins, which are oriented 330 azimuth (generally strike 315° to 360°), as well as from veins with a 240 azimuth and oriented perpendicular to the main vein. In some areas, samples were collected from both vein orientations to test if mineralization in this area is structurally controlled, and if vein intersections represent favorable targets.

In veins with a general azimuth of 330, the presence of adularia is associated with the highest gold grades (3.36 ppm) and samples containing liquid-rich inclusions with trapped illite show the second highest average gold grade (2.67 ppm) (Figure 3.13). Adularia is a mineral that is genetically associated with boiling, and although illite has not previously been associated with boiling, its presence is consistent with the equilibrium phase assemblage (amorphous silica/quartz-adularia-illite) predicted for boiling epithermal systems (Moncada and Bodnar 2012c). Illite has been recognized in fractures and pore space in the Broadlands-Ohaaki geothermal system where cooling of the boiling upflow by mixing with the steam-heated waters causes a shift from adularia stability to illite stability (Hedenquist 1990).

Samples containing adularia also show the highest average silver grades (173.9 ppm) and the second highest average Ag grades are found in samples associated with sericite / illite, with 144.6 ppm (Figure 3.13).

Samples that were collected perpendicular to the main veins (i.e., in veins with azimuth 240) all show low (sub-economic) grades, regardless of which feature is present or absent (Figure 3.14).

3.7.1 Distribution of Veins and Petrography

Samples were collected from surface outcrops, underground historical workings, and drill core from various veins within the La Luz area. The description of the veins from west to east is summarized below. The generalized cross section of the veins showing the distribution of mineral textures and alteration from the La Luz area suggests multiple mineralization and boiling events distributed in time and space (vertically) (Figure 3.15).

Most importantly, all samples show some evidence of boiling, indicating that the bottom of the boiling zone has not been reached and offering the potential for additional resources at depth.

3.7.1.1 Plateros vein

A sample was collected from the Plateros Vein in the western part of the La Luz area (Figure 3.15), and additional samples were collected further south along a vein that is interpreted to be the southern extension of the Plateros vein (Figure 3.16). Samples could not be collected in the central region because the area is occupied by dwellings and farm fields. Samples were also collected at the Chayita and Chuparosa historical mine sites that are interpreted to be on the Plateros Vein (Figure 3.16). From the surface to 100 m depth evidence of boiling represented by FIAs with coexisting liquid-rich and vapor-rich fluid inclusions and FIAs containing only vapor-rich fluid inclusions were found. Below this zone is a 40 m vertical interval in which liquid-rich fluid inclusions with trapped illite crystals are present (Figure 3.15). The gangue minerals that were observed include colloform texture quartz, plumose texture quartz, jigsaw texture quartz, bladed calcite or bladed calcite replaced by quartz, adularia and sericite / illite (Figure 3.15).

The feature that correlates with highest gold grades (2.22 ppm) on the Plateros vein is adularia and the feature that correlates with the second highest grades is FIAs consisting of only vapor-rich fluid inclusions that are indicative of intense boiling or flashing (average grade = 2 ppm) (Figure 3.17). For silver, bladed calcite or bladed calcite replaced by quartz correlates with the highest grades (56 ppm) and samples containing adularia show the second highest average grade (42.6 ppm) (Figure 3.17).

All samples collected from the Plateros vein show evidence of boiling except for one surface sample collected at the northern end (Figure 3.18). This indicates that the bottom of the boiling zone has not been reached along the southern part of the vein, indicating the possibility of deeper precious metal mineralization in this area. Samples from the Plateros Vein that show good evidence of boiling also show elevated gold grades (Figure 3.19). The one sample collected at the northern end of the vein that

does not show good evidence of boiling also does not show elevated gold grades. Silver grades are generally below 50 ppm, except for the one sample from the northern part (439 ppm) and one sample from the Chayita mine (89 ppm) (Figure 3.20).

3.7.1.2 Melladito vein

The next vein to the east of the Plateros Vein is the Melladito Vein (Figure 3.21). This vein has good exposure on the surface, and was sampled from drill core (DDH-1, DDH-4, DDH-9, DDH-14, DDH-17 and DDH-21) and from underground historical mines (Nopal, San Pablo, Sangria, La Boveda, San José, San José de Abajo, and San Francisco de Asis), providing good three-dimensional sampling (Figure 3.21). Samples from the surface to the bottom of the explored vein contain FIAs with coexisting liquid-rich and vapor-rich fluid inclusions as well as FIAs consisting of only vapor-rich fluid inclusions. From 2,225 m and 2,375 liquid-rich fluid inclusions with trapped illite crystals were present (Figure 3.15). Gangue minerals present include colloform texture quartz, plumose texture quartz, jigsaw texture quartz, bladed calcite or bladed calcite replaced by quartz, adularia and sericite/illite, all of which can be associated with boiling fluids (Figure 3.15).

The average Au and Ag grades were calculated for each sample and plotted as a function of whether a given feature indicative of boiling was present or absent (Figure 3.22). The mineral adularia is the feature that correlates with the highest grades for both gold and silver, with 4 ppm Au and 239 ppm Ag (Figure 3.22). The feature that correlates with the second highest grades for both gold and silver is sericite/illite, with 2.61 ppm Au and 162.1 ppm Ag (Figure 3.22). Note that both adularia and illite are minerals that are often associated with boiling hydrothermal fluids.

The longitudinal section of the Melladito vein shows that evidence of boiling is erratically distributed along the vein, with some samples showing no or only weak evidence of boiling (Figure 3.23). Areas with good evidence of boiling usually correlated with high gold grades, such as in drill cores and at the San Pablo, Sangria and La Boveda mines (Figure 3.24). Silver grades are also heterogeneously distributed along

the vein, with higher grades (>50 ppm) in drill holes, and at the Nopal, San Pablo, Sangria, La Boveda and San Francisco de Asis mines (Figure 3.25).

Drill hole number 1 from the central part of the La Luz area shows increasing grades of gold and silver as the hole approaches the Melladito vein and evidence of boiling is also observed up to several tens of meters away from the vein (Figure 3.26). This observation can be used in exploration to tell the explorationist that a vein with potential for precious metal mineralization is nearby, before the vein is intersected by the drill hole.

Monitoring the boiling features in samples during drilling can help lead to discovery of new targets or identify veins that deserve more detailed exploration. For example, in drill hole 1 boiling textures and gold and silver grades are increasing with depth in the Melladito and Intermediate veins (Figure 3.27). If the samples show strong evidence of boiling, but good gold and/or silver grades are not present, one should continue drilling because the bottom of the boiling zone (where one might expect to find Au and/or Ag mineralization) has not yet been reached.

A traverse on the surface perpendicular to the Melladito vein was conducted (Figure 3.21). The grades of gold and silver and the boiling intensity increase as the Melladito vein is approached (Figure 3.28). The boiling intensity factor represents the number of boiling indicator observed in each sample and is related to the intensity and/or longevity of boiling at that location.

3.7.1.3 Intermediate vein

The Intermediate vein was sampled only from drill holes because this vein does not outcrop at the surface. Evidence of FIAs containing coexisting liquid-rich and vapor-rich fluid inclusions, FIAs containing only vapor-rich fluid inclusions, and liquid-rich fluid inclusions with trapped illite crystals were present. Gangue minerals include colloform texture quartz, plumose texture quartz, jigsaw texture quartz, adularia and sericite/illite (Figure 3.15).

The average Au and Ag grade for each boiling feature was calculated. FIAs containing only vapor-rich fluid inclusions (indicating flashing of the hydrothermal fluids)

are correlated with both the highest gold grade (2.34 ppm) and the highest Ag grade (709 ppm) (Figure 3.29). The texture that correlates with the second highest grades is plumose quartz, with samples showing this texture containing 1.06 ppm Au and 265 ppm Ag (Figure 3.29).

The longitudinal section of the Intermediate vein shows the location of the samples from the drill holes and the boiling intensity factor (Figure 3.30). Elevated gold grades are associated with evidence of boiling (Figure 3.31). Silver grades only correlate with boiling in one sample (Figure 3.32).

3.7.1.4 Nombre de Dios

The Nombre de Dios vein is located in the west-central part of the La Luz area (Figure 3.15). Samples from this vein were collected from surface outcrops and drill holes (Figure 3.33). Samples from the surface to the bottom of the explored vein contain FIAs consisting of coexisting liquid-rich and vapor-rich fluid inclusions and FIAs of only vapor-rich fluid inclusions. Gangue minerals include colloform texture quartz, plumose texture quartz, jigsaw texture quartz,bladed calcite or bladed calcite replaced by quartz, adularia and sericite/illite (Figure 3.15).

The average Au and Ag grade for each sample was calculated and correlated with the presence or absence of each boiling feature. The feature that correlates with the highest Au grades is FIAs of coexisting liquid-rich and vapor-rich fluid inclusions (2.27 ppm Au) and FIAs consisting of only vapor-rich fluid inclusions is associated with the highest silver grades (45.5 ppm Ag) (Figure 3.34). For gold, the second most important feature is vapor-rich-only FIAs (1.89 ppm Au), and for silver colloform texture quartz correlates with the second highest Ag grades (28.4 ppm) (Figure 3.34).

The longitudinal section of the Nombre de Dios vein shows the boiling intensity factor for samples from drill cores and surface outcrops (Figure 3.35). The areas of boiling overlap areas of elevated gold grades in drill holes and in surface samples (Figure 3.36). Elevated silver (162 to 40 ppm) was only observed in two samples collected from the surface (Figure 3.37).

3.7.1.5 Bolañitos vein

The Bolañitos vein is located in the central part of the La Luz area (Figure 3.15). A longitudinal section of the Bolañitos vein shows locations of samples from level 29606 and from approximately 50 meters below (Figure 3.38). Samples collected from this vein contain FIAs with coexisting liquid-rich and vapor-rich fluid inclusions, FIAs with only vapor-rich inclusions, colloform texture quartz, plumose texture quartz, jigsaw texture quartz, adularia and sericite/illite (Figure 3.15). All of these features are indicative of boiling conditions.

The average Au and Ag grade for each boiling feature was calculated. The highest silver and gold grades (1,213.3 ppm Ag, and 39.5 ppm Au) correlate with the presence of sericite/illite alteration (Figure 39). Samples containing plumose texture quartz correlate with the second highest average grade (902.5 ppm Ag and 39.2 ppm Au) (Figure 3.39).

The longitudinal section of the Bolañitos vein shows the location of the samples from two levels in the mine and the boiling intensity factor (Figure 3.40). The results show that evidence of intense boiling was found in the deepest sample collected (Figure 3.40), suggesting that the bottom of the boiling zone, and the bottom of the mineralized zone, are beneath the deepest levels sampled. The overlap of areas with high boiling intensity factors and elevated grades of gold in the deep part of the system is consistent with a genetic correlation between boiling and gold mineralization (Figure 3.41). High silver grades also overlap with zones of intense boiling in the deep part of the system (Figure 3.42).

3.7.1.6 San José vein

Only one sample was collected underground from the San José vein (Figure 3.15) and this sample contained 5.22 ppm Au and 3,430 ppm Ag. The sample contains FIAs with only vapor-rich inclusions, jigsaw texture quartz, adularia, and sericite/illite, all of which are evidence of boiling.

3.7.1.7 Lucero vein

Samples from the Lucero vein were collected from underground workings and drill holes (Figure 3.43). The samples contain FIAs with only vapor-rich inclusions, and colloform, plumose, and jigsaw texture quartz. From an elevation of 2,200 MASL to the bottom of the sample collection interval, the following features were observed: coexisting liquid-rich and vapor-rich inclusions, assemblages with only vapor-rich inclusions, colloform texture quartz, plumose texture quartz, jigsaw texture quartz, adularia, and sericite/illite (Figure 3.15). In the deepest levels, one sample contains liquid-rich inclusions with trapped illite. The presence of FIAs containing only vapor-rich inclusions correlates with the highest average silver grade (1,095 ppm) and the highest average gold grade (5.1 ppm) (Figure 3.44). The feature that corresponds with the second-highest average silver and gold grades is the presence of sericite/illite alteration (Figure 3.44).

The longitudinal section of the Lucero vein shows the location of the samples from underground workings and drill cores and the boiling intensity factor. The results show evidence for boiling in the deepest samples collected (Figure 3.45). Elevated gold (Figure 3.46) and silver (Figure 3.47) grades correlate with the boiling evidence.

A longitudinal section of the Lucero vein with exploration drill hole intersections shows that samples in the deep part of the system contain evidence of boiling either from fluid inclusions, or from silica, calcite and other mineral textures (Figure 3.48).

3.7.1.8 Karina vein

Samples were collected on the Karina vein from one surface outcrop, underground workings, and drill holes (Figure 3.49). This vein shows the presence of coexisting liquid-rich and vapor-rich inclusions, FIAs with only vapor-rich inclusions, liquid-rich inclusions with trapped illite, colloform texture quartz, plumose texture quartz, jigsaw texture quartz, adularia, and sericite/illite alteration (Figure 3.15). The feature that correlates with the highest silver and gold grades is liquid-rich inclusions with trapped

illite (234 ppm Ag and 0.9 ppm Au). The feature associated with the second highest grades is sericite/illite alteration (156.1 ppm Ag and 0.6 ppm Au) (Figure 3.50)

The longitudinal section of the Karina vein shows the boiling intensity factor for samples from underground workings and drill cores (Figure 3.51). The areas of boiling overlap areas of elevated gold (Figure 52) and silver (Figure 3.53) grades in drill holes and in underground workings.

3.7.1.9 Daniela Vein

The Daniela vein was sampled from surface outcrops, underground workings and drill core (Figure 3.54). Three important observations were made on this vein. From the surface to 2,250 MASL, FIAs with coexisting liquid-rich and vapor-rich fluid inclusions, FIAs with only vapor-rich fluid inclusions, colloform texture quartz, plumose texture quartz, jigsaw texture quartz, bladed calcite replaced by quartz, adularia, and sericite/illite were observed. At 2,200 MASL all of the above-mentioned features were present with the exception of bladed calcite replaced by quartz (Figure 3.15). The deepest samples only contain colloform texture quartz, plumose texture quartz, and jigsaw texture quartz. The average Au and Ag grade for each boiling feature was calculated. The feature that correlates with the highest silver grades (697 ppm Ag) is liquid-rich inclusions with trapped illite and the feature that correlates with the second highest grade is FIAs with only vapor-rich fluid inclusions (540 ppm Ag) (Figure 3.55). The highest average gold grade (15.3 ppm Au) was associated with FIAs containing only vapor-rich inclusions, and the feature that correlated with the second-highest grade was plumose texture quartz (14 ppm Au) (Figure 3.55).

The longitudinal section of the Daniela vein shows the location of samples from drill holes and the boiling intensity factor (Figure 3.56). The boiling intensity and gold (Figure 3.57) and silver (Figure 3.58) grades show good correlation in the north east of the sampled area.

3.7.1.10 Belén vein

Only two samples were collected from the Belén vein, one from a surface outcrop and one from an adit on the vein (Figure 3.15), and they contain an average of 1 ppm Au and 123 ppm Ag. The samples show evidence for boiling in the form of coexisting liquid-rich and vapor-rich inclusions, colloform texture quartz, jigsaw texture quartz and adularia.

3.7.1.11 Veins intersected in drill holes

The Melladito vein was intersected by drill holes DDH-9 and DDH-14 at essentially the same depth (within one meter). The sample from DDH-9 contained 2.96 ppm Au and 35 ppm Ag, whereas the sample from DDH-14 contained 0.18 ppm Au and 35 ppm Ag. The only difference in boiling features is that the sample from DDH-9 contained adularia whereas the one from DDH-14 did not (Table 3.1). No useful fluid inclusions were observed in either sample.

The Intermediate vein was also intersected by drill holes DDH-9 and DDH-14, at similar depths (±1 m). Two samples of the vein were collected from each core, one where the hole first intersected the vein from above and the second approximately 50 cm below, where the hole passed out of the vein. In both drill holes, the metal grades in the upper sample were lower (0.02 ppm Au and 3 ppm Ag in DDH-14 and 0.34 ppm Au and 34 ppm Ag in DDH-9) than those in the lower sample (81 ppm Au and 83 ppm Ag in DDH-14 and 2.34 ppm Au and 709 ppm Ag in DDH-9). Evidence of boiling was present in all samples (Table 3.1).

The Nombre de Dios vein was also cut by DDH-9 and DDH-14 less than meter apart. Samples from the upper part of DDH-14 contain 0.01 ppm Au and 1 ppm Ag, whereas samples from the lower part show Au below detection limits and1 ppm Ag. Samples collected from the upper part of DDH-9 contain 8.26 ppm Au and 10 ppm Ag whereas samples from the lower part contain 3.03 ppm Au and 3 ppm Ag. Evidence of boiling is present in all samples (Table 3.1).

The results above show large variations in metal grades over small distances, even within the same vein. Also, in one vein (Intermediate) the lower part of the vein has higher grades, whereas in another vein (Nombre de Dios) the upper part has higher grades. All samples from both veins show evidence of boiling.

The three veins described above show systematic trends in gangue mineral distribution, starting from the wall rock and moving towards the vein center. The sequence is wall rock, followed by colloform texture quartz, followed by jigsaw or plumose texture quartz (that has sometimes been cut by adularia), bladed calcite or bladed calcite replaced by quartz, and finally rhombic calcite (that is NOT indicative of boiling). Rhombic calcite in some cases is cut by jigsaw texture quartz that presumably represents the next boiling event. This sequence can be repeated many times as the vein is filled with silica and calcite phases.

3.7.1.12 Section 28600

A cross section of the Karina and Daniela veins shows the various boiling indicators that were observed as a function of depth in the two veins (Figure 3.59). The Karina vein shows good evidence of boiling where it is intersected at shallow depths by drill hole KA-15, and also shows good evidence for boiling where it is intersected deeper by drill hole DN-1 (Figure 3.59). The Daniela vein shows evidence of boiling based on fluid inclusions and mineral textures at three depths where it is intersected by drill holes DN-1 (shallow), KA-15 (intermediate depth) and DN-2 (deepest) (Figure 3.59). These results prove that the bottom of the boiling horizon has not yet been intersected by any of the drill holes, and this means that precious metal mineralization might be discovered at greater depths in this area.

The metal budget for the Karina and Daniela veins as a function of depth in section 28600 shows a decrease in metal grades and in the percentage of samples showing evidence of boiling in the Daniela vein, while the number of boiling features increases with depth for the Karina vein. In both veins, features indicating boiling are present at the deepest levels sampled, indicating that the bottom of the boiling horizon has not been reached (Figure 3.60).

3.8 Microthermometry

One of earliest studies that reported homogenization temperatures (T_h) and salinities of fluid inclusions from the La Luz area was by Mango (1992). This work focused on the Bolañitos vein and included 10 samples collected on levels 0, 42 and 84 (meters below current surface). Only two samples were selected for microthermometry, one from level 42 and another from level 32. Homogenization temperatures of FI in calcite from level 42 range from 148 to 196 °C and salinity ranges from 0.7 to 1 wt. % NaCl. The second sample of quartz from level 32 has a reported homogenization temperature of 206 °C and salinity of 0.2 wt. % NaCl. A fluid inclusion study of the Bolañitos vein by Vasallo and Reyes-Salas (2007) reported homogenization temperatures of 230 to 253 °C in quartz associated with polybasite $(Ag,Cu)_{16}Sb_2S_{11}$. Previous studies did not report evidence of boiling from fluid inclusions.

In this study, FIAs in samples from the La Luz system were classified as containing (1) only liquid-rich inclusions with consistent liquid-to-vapor ratios, (2) liquid-rich inclusions with consistent liquid-to-vapor ratios and containing a trapped illite crystal, (3) coexisting liquid-rich and vapor-rich inclusions with a broad range in liquid-to-vapor ratios, and (4) assemblages consisting of only vapor-rich inclusions.

Following detailed petrographic examination of the samples, 141 FIAs were selected for microthermometric analysis. It should be emphasized that only groups of inclusions that were trapped at the same time, i.e., FIAs, were studied here. FIAs were identified based on either the occurrence of FI along a discrete healed fracture, or along a mineral growth zone, or, less often, within an isolated three-dimensional grouping. Microthermometric analysis of vapor-rich inclusions is sometimes problematic owing to the small amount of liquid in the inclusion. However, if the inclusion geometry is somewhat irregular, the small amount of liquid in the vapor-rich inclusion may occur in a reentrant or “arm” and allow the homogenization temperature and/or ice-melting temperature to be measured (Bodnar et al. 1985) Inclusions were measured using a Linkam THMSG 600 heating/cooling stage mounted on a standard petrographic microscope. The stage was calibrated using synthetic fluid inclusion standards (Sterner

and Bodnar 1984). The precision and accuracy of measured homogenization temperatures are estimated to be ±1.0 °C and the precision and accuracy of ice-melting temperatures are estimated to be ±0.1 °C.

The fluid inclusions are hosted by jigsaw texture quartz, plumose texture quartz, and bladed calcite and rhombic calcite in secondary fluid inclusion assemblages; primary fluid inclusions are present in euhedral quartz and in rhombic calcite. The homogenization temperatures of fluid inclusions from the La Luz system is described for each individual vein, from the west to the east including; Plateros, Melladito, Intermediate, Nombre de Dios, Bolañitos, San José, Lucero, Karina, Daniela and Belén.

3.8.1 Plateros vein.

The homogenization temperature (T_h) of FI from the Plateros vein ranges from 187 to 289 °C and ice-melting temperatures correspond to salinities between 0.4 and 1.7 wt. % NaCl (Figure 3.61). Primary Fluid Inclusion Assemblages (FIAs) in rhombic calcite contain liquid-rich fluid inclusions with T_h of 190 to 195 °C and salinity from 1.2 to 1.4 wt. % NaCl. Secondary FIAs in jigsaw texture quartz consist of coexisting liquid-rich and vapor-rich fluid inclusions with T_h that ranges from 260 to 289 °C and salinities of 0.4 to 1.1 wt. % NaCl.

3.8.2 Melladito vein

The Melladito vein homogenization temperatures range from 137 to 290 °C and ice-melting temperatures correspond to salinities between 0 and 6.8 wt. % NaCl (Figure 3.62). Primary liquid-rich FIAs in rhombic calcite show T_h ranges from 180 to 188°C and salinity from 0.2 to 1.1 wt. %. Secondary, liquid-rich FIAs in rhombic calcite show T_h that ranges from 137 to 222 °C and salinity from 0 to 1.4 wt. % NaCl. Secondary FIAs consisting of coexisting liquid-rich and vapor-rich FI hosted in rhombic calcite show T_h ranging from 182 to 187 °C and salinity from 0.5 to 1.1 wt. % NaCl. Secondary FIAs in rhombic calcite consisting of liquid-rich inclusions with trapped illite show T_h ranging from 155 to 184 °C and salinity from 0.4 to 0.5 wt. % NaCl. Secondary FIAs consisting of coexisting liquid-rich and vapor-rich fluid inclusions in bladed calcite show T_h that

ranges from 184 to 192 °C and salinity from 0.5 to 0.7 wt. % NaCl. Secondary, liquid-rich FIAs in bladed calcite show a T_h range from 159 to 192 °C and salinity from 0.7 to 0.9 wt. % NaCl. Secondary, liquid-rich FIAs in adularia show T_h of 289 °C and salinity of 6.9 wt. % NaCl. Primary liquid-rich FIAs in quartz show T_h ranging from 178 to 199 °C and salinities from 0.4 to 1.1 wt. % NaCl. Primary FIAs in quartz consisting of coexisting liquid-rich and vapor-rich fluid inclusions show a T_h range from 205 to 217 °C and salinities from 0.4 to 0.5 wt. % NaCl. Primary liquid-rich FIAs with trapped illite in quartz show a T_h range from 250 to 290 °C and salinity 0 to 0.5 wt. % NaCl. Secondary FIAs in jigsaw texture quartz consist of coexisting liquid-rich and vapor-rich fluid inclusions and show a T_h range from 182 to 279 °C and salinity from 0 to 1.6 wt. % NaCl. Secondary liquid-rich FIAs in jigsaw texture quartz show a T_h range from 163 to 279 °C and salinity from 0.2 to 1.7 wt. % NaCl. Secondary FIAs in jigsaw texture quartz consist of only vapor-rich fluid inclusions and show a T_h range from 252 to 263 °C and salinity from 1.4 to 1.6 wt. % NaCl. Note that, during petrographic examination fragments of rounded rhombic calcite that were surrounded by jigsaw texture quartz with secondary liquid-rich FIAs was observed. The FI show a T_h range from 177 to 222 °C and salinity from 0.4 to 0.7 wt. % NaCl. Fragments of euhedral quartz surrounded by jigsaw texture quartz contained secondary liquid-rich FIAs that show a T_h range of from 163 to 225 °C and salinity from 0.2 to 1.2 wt. % NaCl.

3.8.3 Intermediate

Homogenization temperature of FI from the Intermediate vein range from 158 to 291 °C and ice-melting temperatures correspond to salinities between 0.2 and 1.2 wt. % NaCl (Figure 3.63). Primary liquid-rich FIAs in rhombic calcite show a T_h range from 189 to 203 °C and salinity from 0.2 to 0.5 wt. % NaCl. Secondary liquid-rich FIAs in rhombic calcite show a T_h range from 158 to 160 °C and salinity from 0.7 to 0.9 wt. % NaCl. Secondary FIAs in rhombic calcite containing liquid-rich inclusions with trapped illite show T_h ranging from 193 to 203 °C and salinity from 0.4 to 0.5 wt. % NaCl. Secondary FIAs in quartz consisting of liquid-rich inclusions with trapped illite show a T_h range from 280 to 291 °C and salinity from 0.7 to 1.2 wt. % NaCl.

3.8.4 Nombre de Dios

The Nombre de Dios vein samples show T_h ranging from 161 to 335 °C and ice-melting temperatures correspond to salinities between 0 and 4.6 wt. % NaCl (Figure 3.64). Primary FIAs in quartz consist of coexisting liquid-rich and vapor-rich fluid inclusions and show a T_h range from 206 to 215 °C and salinities from 0.2 to 0.7 wt. % NaCl. Secondary FIAs in quartz consist of coexisting liquid-rich and vapor-rich fluid inclusions and show a T_h range from 180 to 335 °C and salinities from 0.4 to 4.6 wt. % NaCl. Secondary FIAs in quartz consisting of liquid-rich inclusions with trapped illite show a T_h range from 213 to 224 °C and salinity from 2.9 to 3.2 wt. % NaCl.

3.8.5. Bolañitos vein.

Homogenization temperatures of FI from samples collected on the Bolañitos vein range from 185 to 263 °C and salinity ranges from 0 to 1.1 wt. % NaCl (Figure 3.65). Secondary FIAs in rhombic calcite show a T_h range from 185 to 249 °C and salinity from 0 to 0.9 wt. % NaCl. Secondary FIAs in rhombic calcite consisting of liquid-rich inclusions with trapped illite show a T_h range from 185 to 190 °C and salinity from 0.9 to 1.1 wt. % NaCl. Secondary FIAs in jigsaw texture quartz consisting of coexisting liquid-rich and vapor-rich fluid inclusions show a T_h range from 261 to 263 °C and salinity from 0 to 0.2 wt. % NaCl.

3.8.6 San José vein

The San José vein contains FIAs consisting of only vapor-rich FI and FIAs consisting of liquid-rich FI in jigsaw texture quartz that show T_h ranging from 296 to 297 °C and salinity from 0.2 to 0.4 wt. % NaCl.

3.8.7 Lucero vein

The homogenization temperature of FI from the Lucero vein range from 171 to 247 °C and ice-melting temperatures correspond to salinities between 0 and 2.1 wt. % NaCl

(Figure 3.66). Primary liquid-rich FIAs in rhombic calcite show T_h ranging from 199 to 200 °C and salinity from 0.5 to 0.7 wt. %. Secondary FIAs in rhombic calcite consisting of liquid-rich FI show a T_h range from 171 to 247 °C and salinity from 0 to 0.7 wt. %. Secondary FIAs consisting of coexisting liquid-rich and vapor-rich FI hosted in rhombic calcite show a T_h range from 193 to 247 °C and salinity from 0 to 0.7 wt. % NaCl. Secondary FIAs in rhombic calcite contain liquid-rich inclusions with trapped illite and show a T_h range from 183 to 204 °C and salinity from 0.4 to 1.2 wt. % NaCl. Primary liquid-rich FIAs in quartz show a T_h range from 189 to 192 °C and salinity from 1.4 to 1.6 wt. %. Secondary liquid-rich FIAs in quartz show a T_h range from 190 to 224 °C and salinity from 0.9 to 1.4 wt. %. Secondary FIAs in jigsaw texture quartz consisting of coexisting liquid-rich and vapor-rich FI show a T_h range from 193 to 289 °C and salinity from 0.5 to 1.9 wt. % NaCl. Secondary liquid-rich FIAs in adularia show a T_h range from 220 to 221 °C and salinity from 0.4 to 0.5 wt. % NaCl. Note that, based on petrographic examination, fragments of rounded rhombic calcite surrounded by jigsaw texture quartz were observed. The quartz contained secondary liquid-rich FIAs that show T_h ranging from 171 to 210 °C and salinity from 0.4 to 0.7 wt. % NaCl. One sample with fragments of rounded rhombic calcite surrounded by jigsaw texture quartz contained secondary FIAs with coexisting liquid-rich and vapor-rich inclusions with a broad range in liquid-to-vapor ratios and T_h range from 149 to 152 °C and salinity from 0.4 to 0.7 wt. % NaCl.

3.8.8 Karina vein

Homogenization temperatures of FI in samples from the Karina vein range from 146 to 299 °C and salinity ranges from 0.2 to 7.6 wt. % (Figure 3.67). Secondary liquid-rich FIAs in rhombic calcite show a T_h range from 146 to 148 °C and salinity from 0.4 to 0.5 wt. %. Secondary liquid-rich FIAs in jigsaw texture quartz show a T_h range from 189 to 202 °C and salinity from 0.5 to 5.6 wt. % NaCl. Secondary FIAs consisting of coexisting liquid-rich and vapor-rich FI in jigsaw texture quartz show a T_h range from 204 to 205 °C and salinity from 6.3 to 7.6 wt. % NaCl. Note that, fragments of rounded rhombic calcite surrounded by jigsaw texture quartz were identified during petrography. The calcite

contains secondary liquid-rich FIAs with T_h ranging from 168 to 299 °C and salinity from 0.2 to 1.4 wt. % NaCl.

3.8.9 Daniela vein

The Daniela vein shows a T_h range from 177 to 245 °C and salinity from 0.2 to 3.7 wt. % (Figure 3.68). Secondary liquid-rich FIAs in rhombic calcite show a T_h range from 180 to 196 °C and salinity from 0.5 to 1.9 wt. %. Secondary FIAs consisting of coexisting liquid-rich and vapor-rich fluid inclusions in rhombic calcite show a T_h range from 181 to 222 °C and salinities from 0.7 to 3.7 wt. % NaCl. Secondary FIAs with liquid-rich inclusions with trapped illite in rhombic calcite show a T_h range from 218 to 220 °C and salinity from 1.1 to 1.2 wt. % NaCl. Secondary liquid-rich FIAs in jigsaw texture quartz show a T_h range from 223 to 227 °C and salinity from 1.2 to 1.6 wt. % NaCl. Secondary FIAs consisting of coexisting liquid-rich and vapor-rich FI in jigsaw texture quartz show a T_h range from 177 to 245 °C and salinity from 0.2 to 3.4 wt. % NaCl.

3.8.10 Elevation versus homogenization temperature

Along a 3.5 km strike length on the Melladito vein at the surface, there is approximately 100 vertical meters of elevation change. Samples were collected from surface and abandoned underground workings, and evidence of boiling from fluid inclusions and precious metals were recognized. Below of the vertical interval where only underground work and drill core samples were available show evidence of boiling from fluid inclusions at the deepest sample. In general evidence of boiling from fluid inclusions shows decreasing in T_h (230-160 °C) from the surface to underground work and increase T_h (160-250 °C) in deep samples with exception of one sample that shows liquid-rich inclusions with trapped illite crystals (Figure 3.69). Boiling below the deepest levels explored in the Melladito vein is likely, suggesting that the bottom of the boiling horizon has not yet been reached. The oscillation on T_h from coexisting liquid-rich and vapor-rich inclusions with a broad range in liquid-to-vapor ratios as a function of elevation may suggest fluctuation on the hydrothermal events and difference on

porosity, surface tension, and permeability and such fluctuation can see on figure 3.79 that shows the isotherms from 250 to 300 °C.

Homogenization temperatures were obtained from FI in calcite surrounded by jigsaw texture quartz, and no trends in temperature were observed as a function of elevation or location along the structure. Lucero vein samples show an increase in T_h (150 to 285 °C) as a function of elevation. The maximum T_h (285 °C) in the mineralized area was obtained from samples containing coexisting liquid-rich and vapor-rich inclusions with a broad range in liquid-to-vapor ratios. Homogenization temperatures were obtained from FI with trapped illite in quartz, and no trends in temperature were observed as a function of elevation or location along the structure (Figure 3.70). Surface samples from Nombre de Dios vein show strong evidence of boiling based on fluid inclusions in FIAs cutting jigsaw texture quartz, including, evidence of coexisting liquid-rich and vapor-rich inclusions with a broad range in liquid-to-vapor ratios, and liquid-rich inclusions with trapped illite crystals. The homogenization temperature increases from 210 °C to 330 °C as a function of MASL in samples showing FIAs with evidence of intergrown sulfides and coexisting liquid-rich and vapor-rich inclusions with a broad range in liquid-to-vapor ratios(Figure 3.71).

3.8.11 Fluid salinity versus depth

In the Melladito vein FIAs consisting of coexisting liquid-rich and vapor-rich inclusions, and secondary FIAs cutting jigsaw texture quartz show a decrease in salinity in going from 2,170 to 2,370 MASL (Figure 3.72). No trend in salinity as a function of depth is observed in liquid-rich inclusions with trapped illite crystals and in secondary FIAs in calcite cemented by jigsaw texture quartz from surface samples and abandoned underground workings and drill core.

Samples from the Lucero vein show no trend in salinity as a function of elevation. Samples from the upper levels (2,210 MASL) show a larger variation in T_m (-0.2 to -1.2 °C) compared with the deepest sample (2,115 MASL) T_m (-0.5 to -0.6 °C), and both samples show evidence of coexisting liquid-rich and vapor-rich inclusions with a broad range in liquid-to-vapor ratios (Figure 3.73).

The salinity as a function of elevation of samples from the Nombre de Dios vein decrease with decreasing elevation from 2,390 to 2,150 MASL on coexisting liquid-rich and vapor-rich inclusions with a broad range in liquid-to-vapor ratios (Figure 3.74).

3.8.12 Fluid inclusions and paragenesis

The following interpretation is based on detailed observations, including examination of hand samples collected on the surface, from underground workings, drill core and historical mines, structural mapping, and most importantly, petrography. In some samples we were able to collect the complete vein from wall-rock to wall-rock and prepare petrographic thin sections of the entire vein. The paragenetic sequence is divided in five stages (Figure 3.75). The first stage is represented by a compressional tectonic event in the Cretaceous that generated structures that were oriented at 240 azimuth. The T_h for primary FIA in calcite from these veins is 298 °C with average ice-melting temperature of -0.5 °C. Quartz from this stage has a T_h of 236 °C for primary FIA with an average of ice-melting temperature of -0.3 °C. Secondary FIA hosted in quartz from this stage shows a range in T_h from 196 to 287 °C and ice-melting temperatures ranging from -0.1 to -1.2 °C. Stages II and III were produced during extension in the Eocene prior to mineralization. Late in stage III pyrite with traces of gold and silver is present in stockwork.

Stage II shows primary FIAs in quartz with a range in T_h from 180 to 199 °C and ice-melting temperatures ranging from -0.2 to -0.6 °C. Primary FIA in calcite show T_h ranges from 180 to 183 °C and ice-melting temperatures ranging from -0.5 to -0.6 °C. Secondary FIA hosted in quartz show a range in T_h from 178 to 223 °C and ice-melting temperatures ranging from -0.1 to -3.4 °C. Secondary FIAs in calcite show a T_h range from 160 to 247 °C and ice-melting temperatures ranging from -0.2 to -1.3 °C.

Stage III shows primary FIAs in quartz with ranges in T_h from 189 to 192 °C and ice-melting temperatures ranging from -0.8 to -1 °C. Secondary FIA hosted in quartz show a range in T_h from 163 to 221 °C and ice-melting temperatures ranging from 0 to -1.5 °C. Secondary FIAs in calcite show a T_h range from 180 to 219 °C and ice-melting temperatures ranging from -0.2 to -1.1 °C. Secondary FIAs in calcite contain liquid-rich

fluid inclusions with trapped solids (illite) and show a T_h range from 155 to 200 °C and ice-melting temperatures ranging from 0 to -0.6 °C.

Stage IV contains primary FIAs in quartz consisting of coexisting liquid-rich and vapor-rich inclusions with a broad range in liquid-to-vapor ratios and ranges in T_h from 205 to 217 °C and ice-melting temperatures ranging from -0.1 to -0.4 °C. Primary FIAs in quartz consisting of liquid-rich inclusions with trapped illite crystals show ranges in T_h of from 250 to 290 °C and ice-melting temperatures ranging from 0 to -0.3 °C. Primary FIAs in calcite show T_h ranging from 199 to 200 °C and ice-melting temperatures range from -0.3 to -0.4 °C. Bladed calcite contains secondary FIA consisting of coexisting liquid-rich and vapor-rich inclusions with a broad range in liquid-to-vapor ratios and ranges in T_h from 184 to 192 °C and ice-melting temperatures ranging from -0.3 to -0.4 °C. Bladed calcite contains secondary FIAs consisting of liquid-rich inclusions with ranges in T_h from 159 to 192 °C and ice-melting temperatures ranging from -0.4 to -0.5 °C. Adularia contains secondary FIAs consisting of liquid-rich inclusions with ranges in T_h from 220 to 289 °C and ice-melting temperatures ranging from -0.2 to -4.3 °C. Secondary FIAs consisting of coexisting liquid-rich and vapor-rich inclusions with a broad range in liquid-to-vapor ratios show ranges in T_h from 184 to 332 °C and ice-melting temperatures ranging from 0 to -4.8 °C. Secondary FIA in quartz contain only vapor-rich inclusions the T_h range from 252 to 263 °C and ice-melting point ranging from -0.8 to -0.9 °C. Secondary FIAs in quartz consist of liquid-rich inclusions with a T_h range from 182 to 262 °C and ice-melting temperatures ranging from 0 to -2.4 °C. Secondary FIAs consisting of liquid-rich inclusions in calcite have a T_h range of from 181 to 188 °C and ice-melting temperatures ranging from -0.2 to -0.4 °C. Secondary FIAs in quartz consisting of liquid-rich inclusions with trapped illite crystals show ranges in T_h from 219 to 287 °C and ice-melting temperatures ranging from -0.5 to -1.9 °C. Secondary FIAs in calcite consisting of liquid-rich inclusions with trapped illite crystals show ranges in T_h from 184 to 201 °C and ice-melting temperatures ranging from -0.2 to -0.6 °C. Calcite that has been broken and cemented by jigsaw texture silica shows secondary FIAs consisting of liquid-rich inclusions with ranges in T_h from 170 to 299 °C and ice-melting temperatures ranging from -0.2 to -0.6 °C. Note that only one sample contains broken pieces of calcite that have been cemented by jigsaw texture silica and has secondary

FIAs with coexisting liquid-rich and vapor-rich inclusions with a broad range in liquid-to-vapor ratios. These FI show ranges in T_h from 149 to 152 °C and ice-melting point ranging from -0.2 to -0.4 °C. Several samples containing broken calcite cemented by jigsaw texture silica show secondary FIAs with liquid-rich inclusions and ranges in T_h from 168 to 289 °C and ice-melting point ranging from -0.1 to -0.8 °C. Quartz that have been bookend and cemented by jigsaw texture silica show secondary FIAs with liquid-rich inclusions ranges in T_h from 163 to 225 °C and ice-melting point ranging from -0.1 to -0.7 °C. Quartz that have been bookend and cemented by jigsaw texture silica show secondary FIAs with coexisting liquid-rich and vapor-rich inclusions with a broad range in liquid-to-vapor ratios ranges in T_h from 219 to 257 °C and ice-melting point ranging from 0 to -0.6 °C. Euhedral quartz overgrown by plumose texture quartz has trails of secondary liquid-rich inclusions that extend from the euhedral quartz into the plumose quartz. These FI may have been produced during precipitation of the plumose texture quartz. These FIA show T_h from 250 to 257 °C and ice-melting point ranging from -0.2 to -0.3 °C.

Stage V the primary FIAs in calcite shows T_h from 188 to 200 °C and ice-melting point ranging from -0.1 to -0.3 °C. Secondary FIAs in calcite show T_h from 138 to 249 °C and ice-melting point ranging from 0 to -0.8 °C

The primary FIAs in the stages show trend for stage I with high temperature in calcite with T_h form 298 °C and quartz 236 °C. The stage II and stage III calcite and quartz show T_h ranges from 180 to 199 °C. Stage IV shows increasing in T_h in quartz from 205 to 290 °C, and calcite from 199 to 200 °C. Stage V calcite shows T_h from 188 to 200 °C. The ice-melting point in stage I and stage II ranges from -0.3 to -0.6 °C. Stage III it ranges from -0.8 to -1 °C. Stage IV it decrease from 0 to -0.4 °C. Stage V it range from -0.1 to -0.3 °C.

3.8.13 Metal budget in veins from La Luz system

The metal budget shows much variability between veins, from gold-rich to silver-rich, with minor base metal veins. The Nombre de Dios and Karina veins show the highest

gold grades when the chloride concentration is low (1 wt. % NaCl). This suggests that gold and silver are not transported as chloride complexes. The base metal content of samples collected perpendicular (240 azimuth) to the Bolañitos, Daniela and Intermediate veins have low copper, zinc and lead grades. Note that Daniela and Lucero veins show no trace of base metals associated with fluids with 5 wt. % NaCl (Figure 3.76).

Arsenic and antimony have been used as pathfinder elements in epithermal deposits (Rose et al. 1979) In oxidizing environments and at low to moderate pH (pH <4-8), Ag and Arsenic can be moderately mobile whereas gold is immobile, and in reducing environments antimony is immobile (Rose et al. 1979). In the La Luz area, the arsenic content of veins that are parallel (330 azimuth) and perpendicular to (240 azimuth) are the same, except for the Intermediate vein (Figure 3.76). The content of antimony in parallel veins, partially overlap whit Melladito, Nombre de Dios and complete in Plateros vein. The presence of antimony at Bolañitos, Intermediate, Karina, Lucero, and Nombre de Dios veins suggest that maybe sulfosalts are present (Figure 3.76). This has been confirmed based on petrography and hand specimen examination that sulfosalts and sulfides are present.

A clear correlation between fluid salinity and the metal budget of Mexican epithermal deposits has been documented (Albinson et al. 2001). Fluids in gold-rich deposits generally have salinities <8 wt. % NaCl, whereas fluid salinities in Ag-rich deposits range up to about 12 wt. %, and Ag-base metal epithermal deposits have salinities that extend up to about 23 wt. % NaCl. In this study, the average of all of the fluid inclusion salinities is ~1 wt. %. NaCl. Some Ag-rich samples have salinities up to 8 wt. % NaCl. The metal distribution for samples from the Daniela, Lucero, San José, Bolañitos, Intermediate, Melladito, and Plateros veins fall along the Au-Ag binary (Figure 3.77). The Karina and Nombre de Dios veins show an increase in base metals that is consistent with the decrease in precious metal grades (0.0050 ppm Au and 1 ppm Ag). The base metal content in all of the veins is low (6 ppm Cu, 5 ppm Pb, and 10 ppm Zn). The dashed line in all of the ternary diagrams represents the metal budget for samples collected in veins with an orientation of 240 azimuth (Figure 3.77). The generally low salinity of all fluid inclusions in this study is consistent with previous studies that suggest

that gold and silver are not transported as chloride complexes in the epithermal environment, but rather are transported as sulfide and/or hydroxyl complexes (Helgeson 1969, Shenberger and Barnes 1989, Albinson et al. 2001, Stefánsson and Seward 2003, Stefánsson and Seward 2004)

3.9 Denudation rate in La Luz

The depth at which the La Luz veins were formed can be inferred from fluid inclusion data. Samples collected on the surface show FIAs consisting of coexisting liquid-rich and vapor-rich fluid inclusions and hence, do not require a pressure correction. The pressure recorded by samples collected from the surface ranges from 15 to 66 bars and salinity ranges from 0 to 7 wt. % NaCl using data from Khaibullin and Borisov (1966), Haas (1976), Bodnar (1983). Under hydrostatic conditions the pressures would be equivalent to depths of 164 to 900 m below the paleosurface. This suggests that between 164 and 900 m of overlying rock could have been eroded from the La Luz area in the time since the veins formed. If the rocks were eroded continuously over the ~30 my period since they formed (Gross, 1975), the erosion rate would have been between 6 to 31 m/my which compare cited rates <5 to 100 m/m.y (Menard 1961, Wilkinson and McElroy 2007).

3.10 Productive ore zones

In many epithermal precious metal systems, the most productive ore zones were formed at temperatures between 250 to 330 °C. Reconnaissance microthermometric analyses have been conducted on samples from the study area. These data allow us to predict the depth beneath the surface to the 250 °C and 300 °C isotherms for Plateros, Melladito, Nombre de Dios, and Lucero veins, assuming that the temperature with depth follows the boiling point curve. Note that hydrothermal systems associated with the formation of epithermal deposits are dynamic systems, and the boiling horizon likely shifts upward and downward over time as the fluid temperature, flow rate, fracture apertures, etc., vary through time.

3.10.1 Plateros vein.

Two samples collected from the vein at different locations on the surface show FIAs consisting of coexisting liquid-rich and vapor-rich fluid inclusions with T_h ranges from 260 to 269 °C. Our results suggest that the 300 °C isotherm has not yet been reached where the samples were collected in the Plateros vein, and exploration of the deeper parts of the system may identify additional resources (Figure 3.78).

3.10.2 Melladito vein

Evidence of boiling consisting of coexisting liquid-rich and vapor-rich fluid inclusions and assemblages of only vapor-rich fluid inclusions is present in the deep part of the Melladito vein. The homogenization temperatures range from 159 to 263 °C and salinity from 0 to 1.6 wt. % NaCl. Assuming that the temperature with depth follows the boiling point curve and in many epithermal precious metal systems, the most productive ore zones were formed at temperatures between 250-300 °C. These results suggest precious metal mineralization maybe beneath of the deep part where samples were collected (Figure 3.79).

3.10.3 Nombre de Dios

Two samples collected from the surface at different locations along the vein show FIAs consisting of coexisting liquid-rich and vapor-rich fluid inclusions with homogenization temperatures averaging 211 and 235 °C. If the fluid follows the liquid vapor curve the range of temperature where most precious metal mineralization occurred (250-300 °C) in precious metal deposits. This suggests that the range of temperature have no reached jet and possibility of precious metal mineralization may occur underneath where those samples were collected (Figure 3.80).

3.10.4 Lucero vein

Six samples collected from drill core and underground areas on the Lucero vein show FIAs consisting of coexisting liquid-rich and vapor-rich fluid inclusions with

homogenization temperature range from 193 °C and 289 °C. This suggests that the range of temperature have no reached jet and possibility of precious metal mineralization may occur underneath where those samples were collected (Figure 3.81).

3.11 Targets for exploration in the La Luz area and Discussion

Many of the features that indicate boiling, especially colloform texture quartz and bladed calcite, can easily be observed in hand samples and field geologists and drill rig operators can be trained to look for and record these features in drill cuttings. If evidence of boiling is still present at the “stop point” for drilling, the geologist on site might decide to continue drilling as the bottom of the boiling horizon has not yet been reached and there is therefore a probability that a deeper ore zone might be located. The mineral textures can thus help to determine in “real time” if the bottom of the boiling zone (which should also represent the bottom of the precious metal zone) has been reached. Other indicators of boiling, such as the presence of adularia or sericite/illite, can also sometimes be recognized in drill cores and cuttings.

When approaching a mineralized vein along a traverse perpendicular to the vein trend, evidence of boiling is often observed in small fractures and veins that are several tens of meters away from the main mineralized vein, providing a vector that may be used in exploration (Figure 3.28).

On a longitudinal plot boiling intensity appears to be highly variable along strike, suggesting that zones with strong evidence of boiling may represent upflow zones in the hydrothermal system. These areas should be given higher priority compared to zones with no evidence of boiling. Evidence of boiling obtained from mineral textures and fluid inclusions should be integrated with information from field mapping to determine if there are structural controls on when/where boiling occurs that may be useful in identifying future targets.

Even if a sample collected at shallow depths shows no gold or silver (or very low grades) but does show good evidence of boiling, this area should be given high priority

because it means that the bottom of the boiling horizon (and the area that is most likely to contain Au and/or Ag) is located beneath the surface.

Figure 3.82 shows various drill hole intersects with the Lucero vein. Also shown are locations along those same drill holes at which other veins with the same orientation as the Lucero vein were intersected. These veins also show good evidence of boiling, even though some of these samples show low metal grades. The orientation of these veins determined from drill hole intersections and surface outcrops (azimuth 300-320 and dip of 41-58 east) are the same as the orientation of the major mineralized veins in the area, making those veins an important target for further exploration. Because the veins vary in thickness and degree of opening with depth, a drill hole might intersect a part of the vein that is narrow and unmineralized, but the vein might be wider and better mineralized a short distance vertically above or below the point of intersection and should be explored further.

For FIAs consisting of coexisting liquid-rich and vapor-rich fluid inclusions indicating that the FI were trapped on the liquid-vapor curve, a pressure correction to the homogenization temperature is not required and the measured homogenization temperature equals the trapping temperature. As such, microthermometry provides a useful tool for exploration because the depth at which fluids would boil at 250-300 °C can be predicted from the liquid-vapor curve and the maximum depth at which fluids with a temperature of 300 °C would occur can be estimated (Figure 3.78, 3.79, 3.80, 3.81). This represents a useful “lower boundary” for mineralization because studies of numerous epithermal precious metal deposits over the past several decades has shown that metal deposition occurs most often at ~250-300 °C. As an example, if an FIA consists of coexisting liquid-rich and vapor-rich fluid inclusions with T_h of 270 °C, the data from Khaibullin and Borisov (1966) gives a pressure of 54 bars, which corresponds to a depth of 723 m at 0 wt. % NaCl, or 52 bars and 661 m if the salinity is 5 wt. % NaCl. The FI in this study did no show evidence of CO_2 which could increase the depth to the boiling curve by several hundred meters (Bodnar et al. 1985).

The epithermal deposits usually form in extensional or trans-tensional fault systems and the abrupt drops in fluid pressure produced by faulting episodes play an important role in gold-quartz deposition (Sibson et al. 1988). Typically, epithermal deposits are

characterized by multiple vein-filling and/or fracturing events associated with extensional opening. Numerous examples have been documented where the hydrothermally cemented wall-rock breccia shows multiple episodes of brecciation and cementation (Spurr 1925, Hulin 1929). Similar breccias have been described from active faults in active geothermal systems and gold precipitation has been linked to hydrothermal eruptions in Waiotapu, New Zealand (Hedenquist and Henley 1985, Pope et al. 2005). The hydrothermal eruptions can transport material from 300 m depth and eruption velocities of 200 to 300 m/s have been recorded for flow paths along which boiling has occurred (Hedenquist and Henley 1985). Historical earthquakes on the Cerro Prieto, Mexico fault appear to have repeatedly triggered major boiling or flashing episodes within the geothermal field (Sibson 1987). In this area, columns of mud and hot water that reached 200 to 300 m heights and continued for several months after the main earthquake were observed associated with an earthquake in 1852, and continued to intensifying after major aftershocks (Sibson 1987, Bureau of Reclamation 1976). The overpressure in fluids can lead to super-saturation of silica after the fluid depressurizes and the fluid boils thus precipitating amorphous silica (Fournier 1985) and producing the characteristic colloform texture quartz observed in epithermal precious metal deposits. Intense boiling or flashing events in geothermal fields have been documented to produce precious metals mineralization at the Broadlands and Kawerau geothermal fields in New Zealand (4.4 wt. % Au and 15.5 wt. % Ag) and at Cerro Prieto in Mexico (up to 22.9 wt. % Ag and 0.25 wt. % Au) (Brown 1986, Clark and Williams-Jones 1990)

The extensional structures and the vein textures observed in the La Luz system suggest that the fractures hosting mineralization were repeatedly over-pressured and fractured. This interpretation is supported by pressures estimated from fluid inclusions, which vary widely, from 135 to 6 bars (Figure 3.83). Moreover, the presence of abundant FIAs containing only vapor-rich inclusions suggests sudden and catastrophic pressure release, causing the liquid-only (or liquid-dominated) fluid to instantly vaporize. The multiple episodes of boiling distributed over a significant strike distance and depth in the La Luz area increase the likelihood that additional resources will be discovered as exploration continues.

The potential for additional resources in the La Luz area has been documented for veins that extend to the south and north of the main area (Figure 3.2). Veins showing evidence of multiple episodes of boiling in hand specimen and under the microscope, such as the Chayita and San Francisco de Asis veins, represent potential targets. Samples collected from mine dumps close to the El Sauz and the La Joya veins show multiple episodes of boiling in hand specimens. Samples from the eastern part of the Belén vein show evidence of boiling in hand specimen and under the microscope. Detailed geologic mapping and fluid inclusion petrography of samples from this area might identify additional targets.

3.12. Reference

Adams, S. F. (1920). A microscopic study of vein quartz. Economic Geology 15(8): 623-664.

Albinson, T., D. I. Norman, D. Cole and B. Chomiak (2001). Controls on formation of low-sulfidation epithermal deposits in Mexico; constraints from fluid inclusion and stable isotope data. Special Publication (Society of Economic Geologists (U. S.)) 8: 1-32.

Baker, D. (2011). Geology and structure report on the San Ignacio project Guanajuato, Mexico. Unpublished report, Great Panther Silver Limted: 23.

Barton, P. B. (1986). Mineral deposit models; preface. U. S. Geological Survey Bulletin: iii-iv.

Blake, W. P. (1902). Notes on the mines and minerals of Guanajuato, Mex. Transactions of the Society of Mining Engineers of American Institute of Mining, Metallurgical and Petroleum Engineers, Incorporated (AIME): 216-223.

Bodnar, R. J. (1983). A method of calculating fluid inclusion volumes based on vapor bubble diameters and P-V-T-X properties of inclusion fluids. Economic Geology 78: 535-542.

Bodnar, R. J. (1993). Revised equation and table for determining the freezing point depression of H_2O-NaCl solutions. Geochimica et Cosmochimica Acta 57(3): 683-684.

Bodnar, R. J., P. Lecumberi-Sanches, D. Moncada and M. Steele-MacInnis (2013). Fluid Inclusions in Hydrothermal Ore Deposits. Treatise on Geochemistry 2nd Edition. H. D. H. Karl K. Turekian. Oxford: Elsevier Ltd

Bodnar, R. J., T. J. Reynolds and C. A. Kuehn (1985). Fluid-inclusion systematics in epithermal systems. Reviews in Economic Geology 2: 73-97.

Botsford, C. W. (1910). Geology of the Guanajuato District. Mexican Mining Journal: 30-33.

Brown, K. L. (1986). Gold deposition from geothermal discharges in New Zealand. Economic Geology 81(4): 979-983.

Browne, P. R. L. (1978). Hydrothermal alteration in active geothermal fields. Annual review of earth and planetary sciences 6: 229-250.

Buchanan, L. J. (1980). Ore controls of vertically stacked deposits, Guanajuato, Mexico. American Institute of Mining Engineers Preprint 80-82: 26.

Bureau of Reclamation (1976). Record of earthquakes in the Yuma area, Yuma County, Arizona; Imperial County, California: U.S. Department of the Interior, Bureau of Reclamation, Special Report. 73.

Carranza, E. and M. Sadeghi (2012). Geochemical characteristics of mineral deposits: implications for ore genesis. Geochemistry: Exploration, Environment, Analysis 12(2): 89-92.

Church, J. A. (1907a). The Mines of La Luz, Guanajuato, Mexico. The engineering and mining journal: 153-155.

Church, J. A. (1907b). The Mines of La Luz, Guanajuato, Mexico II. The engineering and mining journal: 105-110.

Clark, J. R. and A. E. Williams-Jones (1990). Analogues of epithermal gold-silver deposition in geothermal well scales. Nature 346(6285): 644-645.

Dávila, V. M. and J. Martínez-Reyes (1987). Un edad Cretacica para las rocas basales de la Sierra de Guanajuato. Universidad Nacional Autonoma de Mexico. April 28-30(Resumen): 19-20.

Dong, G., G. Morrison and S. Jaireth (1995). Quartz textures in epithermal veins, Queensland; classification, origin and implication. Economic Geology 90(6): 1841-1856.

Dong, G. and G. W. Morrison (1995). Adularia in epithermal veins, Queensland; morphology, structural state and origin. Mineralium Deposita 30(1): 11-19.

E.W. Lemmon, M.O. McLinden and D.G. Friend (2012) Thermophysical Properties of Fluid Systems. NIST Standard Reference Database Number 69, Eds. P.J. Linstrom and W.G. Mallard, National Institute of Standards and Technology, Gaithersburg MD, 20899, http://webbook.nist.gov, .

Echegoyen-Sanchez, J. (1964). Algunos datos sobre la mineralizacion de la Veta Madre de Guanajuato. in I^{er} Seminario sobre Exploracion Geologico-Minera, Mem.: 134-149.

Endeavour Silver Corp (2012). Longitudinal section of Karina, Lucero, and Daniela veins.

Etoh, J., E. Izawa, K. Watanabe, S. Taguchi and R. Sekine (2002). Bladed Quartz and Its Relationship to Gold Mineralization in the Hishikari Low-Sulfidation Epithermal Gold Deposit, Japan. Economic Geology 97(8): 1841-1851.

Fournier, R. O. (1985). Silica minerals as indicators of conditions during gold deposition. U. S. Geological Survey Bulletin: 15-26.

Gómez, d. l. R. E. (1963). Estudio geológico minero de la zona de La Luz, distrito de Guanajuato, Gto.

Great Panther Silver Limited (2012). Longitudinal section of Melladito and Intermediate veins.

Gross, W. H. (1975). New ore discovery and source of silver-gold veins, Guanajuato, Mexico. Economic Geology 70(7): 1175-1189.

Haas, J. J. (1976). Thermodynamic properties of the coexisting phases and thermochemical properties of the NaCl component in boiling NaCl solutions. Preliminary steam tables for NaCl solutions. Geol. Surv. Bull 1421-B: 1-71.

Hedenquist, J. W. (1990). The thermal and geochemical structure of the broadlands-ohaaki geothermal system, New Zealand. Geothermics 19(2): 151-185.

Hedenquist, J. W., A. Arribas R and E. Gonzalez-Urien (2000). Exploration for epithermal gold deposits. Reviews in Economic Geology 13: 245-277.

Hedenquist, J. W. and R. W. Henley (1985). Hydrothermal eruptions in the Waiotapu geothermal system, New Zealand; their origin, associated breccias, and relation to precious metal mineralization. Economic Geology 80(6): 1640-1668.

Helgeson, H. C. (1969). Thermodynamics of hydrothermal systems at elevated emperatures and pressures. American Journal of Science 267(7): 729-804.

Henley, R. W. and G. O. Hughes (2000). Underground Fumaroles: Excess Heat Effects in Vein Formation. Economic Geology 95(3): 453-466.

Hodgson, C. J. (1989). Uses (and abuses) of ore deposit models in mineral exploration. Ontario Geological Survey Special Volume 3: 31-45.

Hulin, C. D. (1929). Structural control of ore deposition Economic Geology 24: 15-49.

Kaldis, E. (1974). Principles of the vapour growth of single crystals. Crystal growth : theory and techniques. C. H. L. Goodman. London; New York, Plenum Press.

Kamilli, R. J. and H. Ohmoto (1977). Paragenesis, zoning, fluid inclusion, and isotopic studies of the Finlandia Vein, Colqui District, central Peru. Economic Geology 72(6): 950-982.

Khaibullin, K. and N. Borisov (1966). Experimental investigation of the thermal properties of aqueous and vapor solutions of sodium and potassium chlorides at phase equilibrium. Teplofizika Vysokikh Temperatur 4: 518-523.

Lewis, W. J., C. Z. Murahwi and R. J. Leader (2011). NI 43-101 Techical report audit of the resource and reserve estimates for the Guanajuato mines project Guanajuato state, Mexico. 172.

Mango, H. N. (1992). Origin of epithermal Ag-Au-Cu-Pb-Zn mineralization on the Veta Madre, Guanajuato, Mexico. PhD.

Martínez-Reyes, J. and A. F. Nieto-Samaniego (1992). Efectos geológicos de la tectónica reciente en la parte central de México. Universidad Nacional Autónoma de México, Instituto de Geología Revista (9): 33–50.

Menard, H. W. (1961). Some rates of regional erosion. The Journal of geology 69(2): 154-161.

Moncada, D. and Bodnar, J. R. (2012a). Fluid inclusions and mineral textures of samples from the San Ignacio project, Guanajuato, Mexico. Unpublished report, Great Panther Silver Limted: 27.

Moncada, D. and Bodnar, J. R. (2012b). Identification of target areas for exploration in the La Luz area, Guanajuato, Mexico, based on fluid inclusions and mineral textures. Unpublished report, Endeavour Silver Corp.: 29.

Moncada, D. and Bodnar, J. R. (2012c). Gangue mineral textures and fluid inclusion characteristics of the Santa Margarita Vein in the Guanajuato Mining District, Mexico. Central European Journal of Geosciences 4(2): 300-309.

Ortiz, H. L. E., P. Calvet, M. Chiodi and M. C. F. Yanez (1989). Afinidad magmatica y procesos metalogeneticos del cortejo Mesozoico magmatico de la Sierra de Guanajuato, Mexico Central. Asociacion de Ingenieros de Minas, Metalurgistas y Geologos de Mexico, Convencion Nacional, 17h.

Percy, F. M. F. R. G. S. (1906). Mexico's Treasure House (Guanajuato): An Illustrated and Descriptive Account of The Mines adn Their Operations in 1906.

Pope, J. G., K. L. Brown and D. M. McConchie (2005). Gold Concentrations in Springs at Waiotapu, New Zealand: Implications for Precious Metal Deposition in Geothermal Systems. Economic Geology 100(4): 677-687.

Prol-Ledesma, R. M. and P. R. L. Browne (1989). Hydrothermal alteration and fluid inclusion geothermometry of los humeros geothermal field, Mexico. Geothermics 18(5-6): 677-690.

Randall, J. A. (1982). Contacto entre el Terciatio y el Mesozoico en el distrito minero de Guanajuato. Sociedad Geologica Mexicana, Mexico City.

Randall, J. A., A. E. Saldana and K. F. Clark (1994). Exploration in a volcano-plutonic center at Guanajuato, Mexico. Economic Geology 89(8): 1722-1751.

Roedder, E. (1984). Fluid inclusions. Reviews in Mineralogy 12: 644.

Rose, A. W., H. E. Hawkes and J. S. Webb (1979). Geochemistry in mineral exploration. London ; New York, Academic Press.

Sander, M. V. and J. E. Black (1988). Crystallization and recrystallization of growth-zoned vein quartz crystals from epithermal systems; implications for fluid inclusion studies. Economic Geology 83(5): 1052-1060.

Schmal, J. P. (2007) Los antepasados indígenas de los Guanajuatenses. 6.

Shenberger, D. M. and H. L. Barnes (1989). Solubility of gold in aqueous sulfide solutions from 150 to 350°C. Geochimica et Cosmochimica Acta 53(2): 269-278.

Sibson, R. H. (1987). Earthquake rupturing as a mineralizing agent in hydrothermal systems. Geology 15(8): 701-704.

Sibson, R. H., F. Robert and K. H. Poulsen (1988). High-angle reverse faults, fluid-pressure cycling, and mesothermal gold-quartz deposits. Geology 16(6): 551-555.

Simmons, S. F. and B. W. Christenson (1994). Origins of calcite in a boiling geothermal system. American Journal of Science 294(3): 361-400.

Simmons, S. F., N. C. White and D. A. John (2005). Geological Characteristics of Epithermal Precious and Base Metal Deposits. Economic Geology 100th Anniversary Volume Economic Geology; One Hundredth Anniversary Volume, 1905-2005: 485-522.

Spurr, J. E. (1925). The Camp Bird compound veindike Economic Geology 20: 115-152.

Starling, T. (2008). Structural Review of the Deposits of the Northern Guanajuato District, Mexico, Field Visit Conclusions 03-08 prepared for Endeavour Silver Corp, Telluris Consulting: 23.

Stefánsson, A. and T. M. Seward (2003). Experimental determination of the stability and stoichiometry of sulphide complexes of silver(I) in hydrothermal solutions to 400°C. Geochimica et Cosmochimica Acta 67(7): 1395-1413.

Stefánsson, A. and T. M. Seward (2004). Gold(I) complexing in aqueous sulphide solutions to 500°C at 500 bar. Geochimica et Cosmochimica Acta 68(20): 4121-4143.

Sterner, S. M. and R. J. Bodnar (1984). Synthetic fluid inclusions in natural quartz; 1, Compositional types synthesized and applications to experimental geochemistry. Geochimica et Cosmochimica Acta 48(12): 2659-2668.

Stewart, M. (2006). Geology of Guanajuato and La Luz Areas, Mexico.

Vasallo, L. F. and M. Reyes-Salas (2007). Selenian Polybasite From the Guanajuato Mining District, México Bole 3(2): 1-16.

Velazquez, P. (1973). A study of the possibility that the Luz Mineral Camp of Guanajuato can be a resurgent producer of silver and gold. Bs, University of Guanajuato.

Vikre, P. G. (1985). Precious metal vein systems in the National District, Humboldt County, Nevada. Economic Geology 80(2): 360-393.

Waldegger, M. F. (2012). Techical report on the San Ignacio project mineral resource Guanajuato state, Mexico 50.

Ward, H. G. (1828). Mexico in 1827. London.

Wilkinson, B. H. and B. J. McElroy (2007). The impact of humans on continental erosion and sedimentation. Geological Society of America Bulletin 119(1-2): 140-156.

3.13 Figure Captions

Figure 3.1 Location of the La Luz area in the Guanajuato Mining District, Mexico.

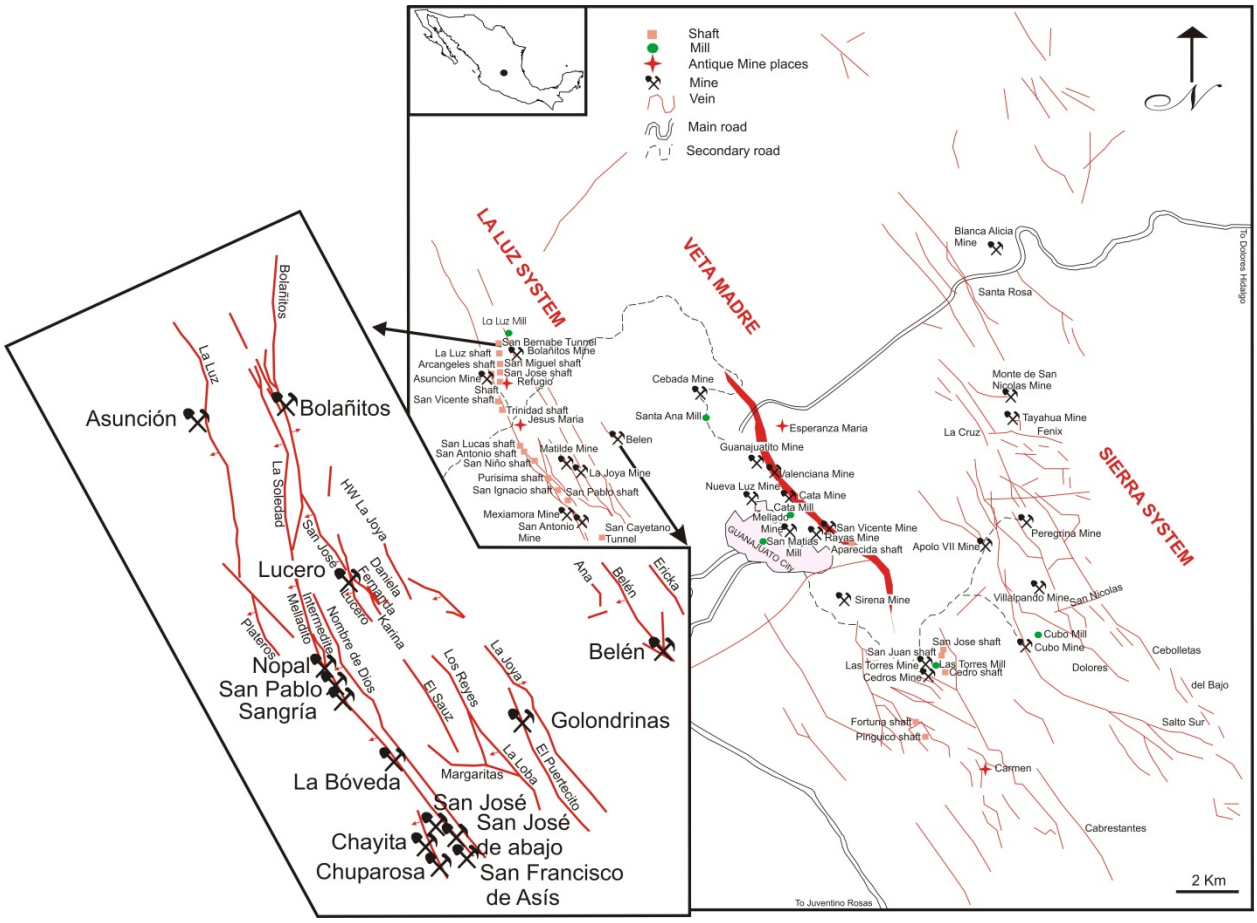

Figure 3.2 Plan view of the La Luz area shoving general geology (modified Church 1907b, Stewart 2006, Baker 2011, Moncada and Bodnar 2012a, Moncada and Bodnar 2012b). Kqfp.- Rhyolite porphyry; Kantf.- Lapilli tuff; Kbas.- Pillow basalt; Kanfl.- Andesite; Ksh.- Mudstone, slate; Jtcp.- Tonalite.

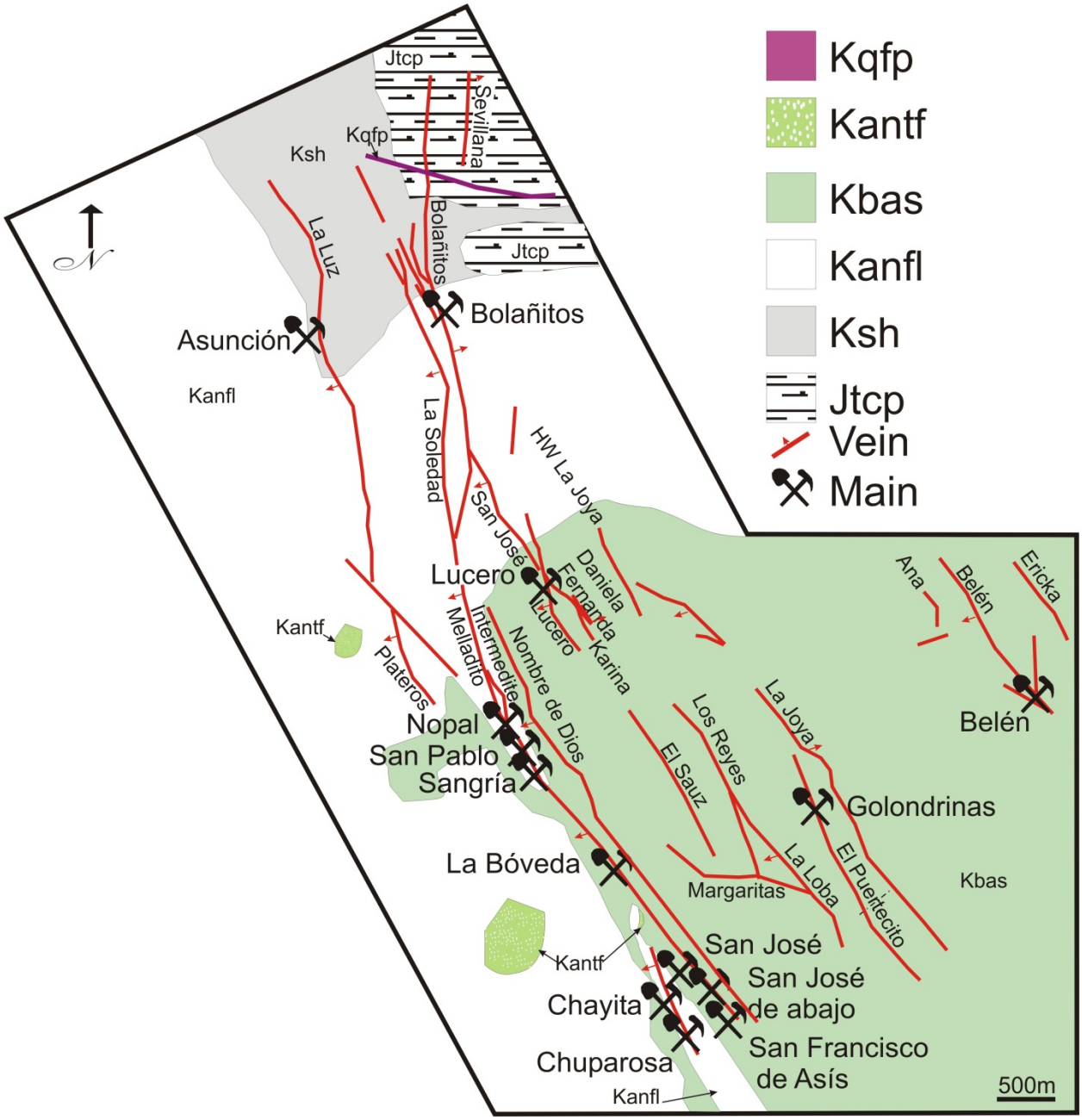

Figure 3.3 Stratigraphic column of the La Luz area adapted from Echegoyen-Sanchez (1964), Stewart (2006), Randall et al. (1994), and Church (1907b).

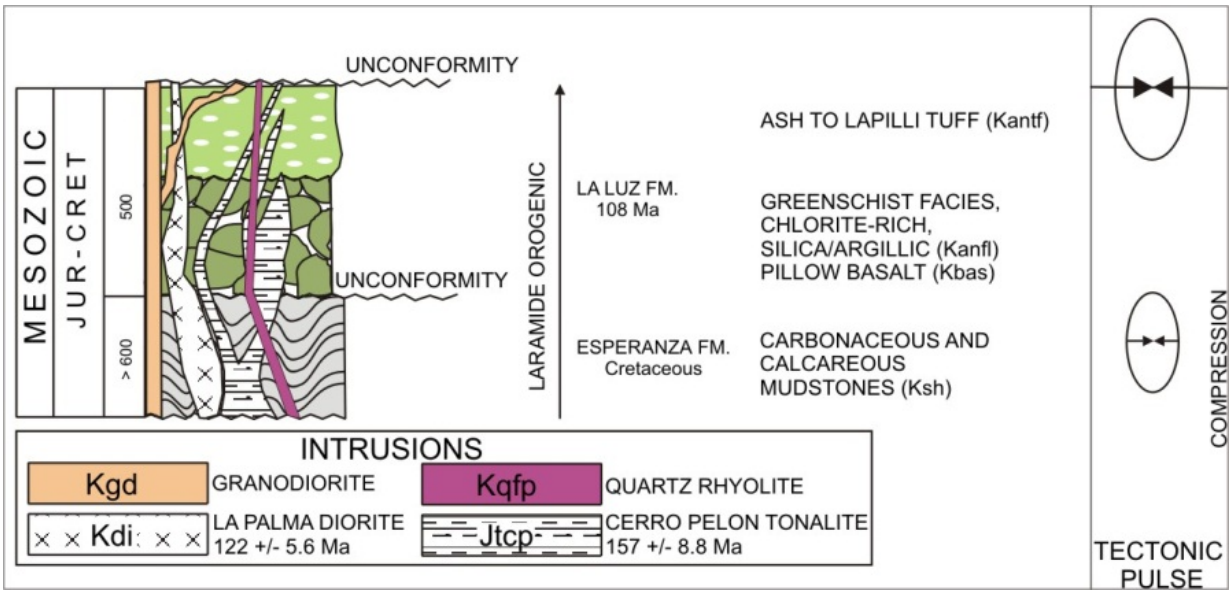

Figure 3.4 Longitudinal section showing the La Luz vein and projection of different veins with 100 ppm Ag Equivalent cut-off. Modified from Gómez (1963), Endeavour Silver Corp (2012), and Great Panther Silver Limited (2012).

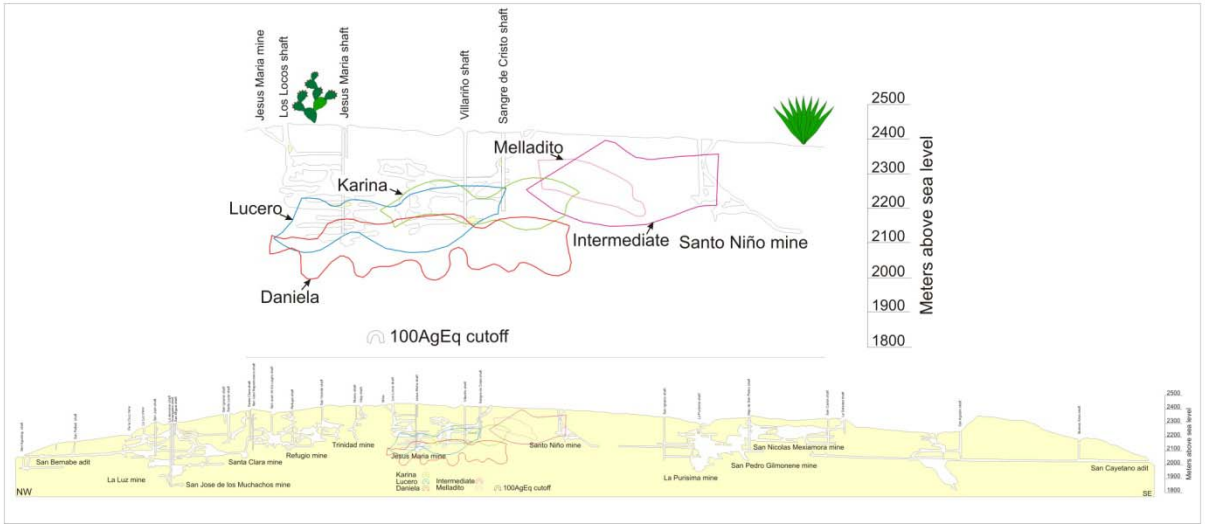

Figure3.5 Relative abundance of the different mineral textures and fluid inclusion characteristics in samples from the La Luz area. The number at the end of each bar represents the number of samples out of the total of 214 samples that contained the feature listed.

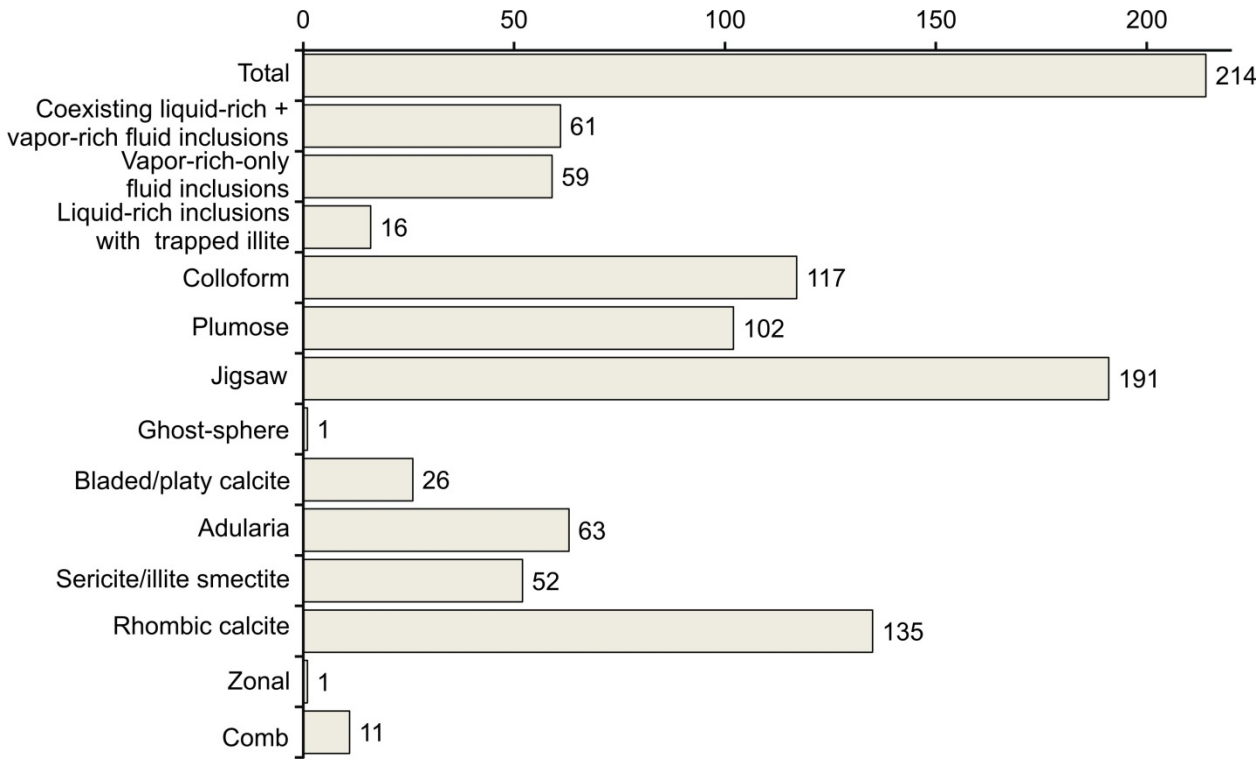

Figure 3.6 Photomicrographs of silica (quartz) and calcite textures resulting from boiling that have been observed in samples from the La Luz area. Jigsaw texture quartz observed in plane polarized light (A) and under crossed nicols (B). Colloform texture silica (now quartz) observed in plane-polarized light (C) and under crossed nicols (D). Plumose texture quartz in plane-polarized light (E) and under crossed nicols (F). Lattice-bladed calcite in plane-polarized light (G) and under crossed nicols (H). Ghost-sphere texture quartz in plane-polarized light (I) and under crossed nicols (J).

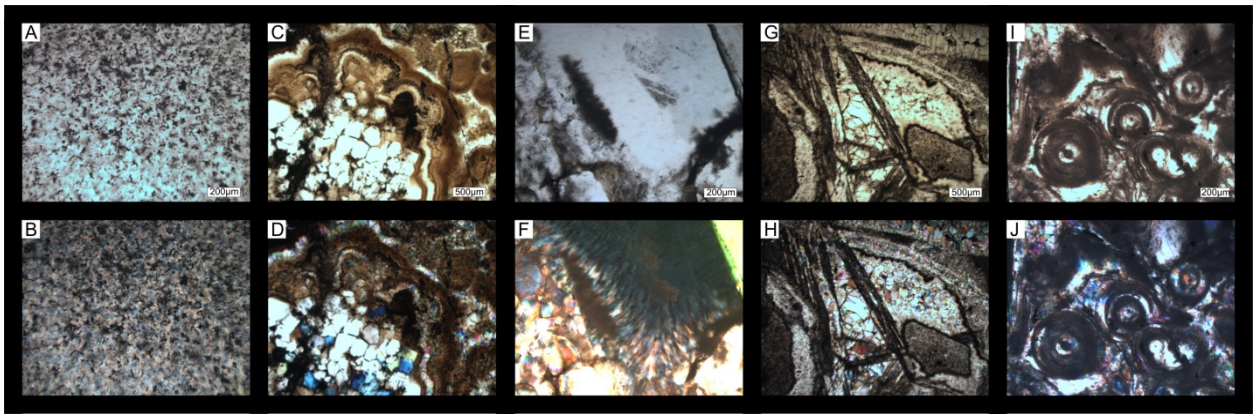

Figure 3.7 Photomicrographs of silica and calcite textures produced when these minerals are precipitated under non-boiling conditions that have been observed in samples from the La Luz area. Zonal texture quartz observed in plane-polarized light (A) and under crossed nicols (B). Comb texture quartz observed in plane-polarized light (C) and under crossed nicols (D). Rhombic calcite observed in plane-polarized light (E) and under crossed nicols (F).

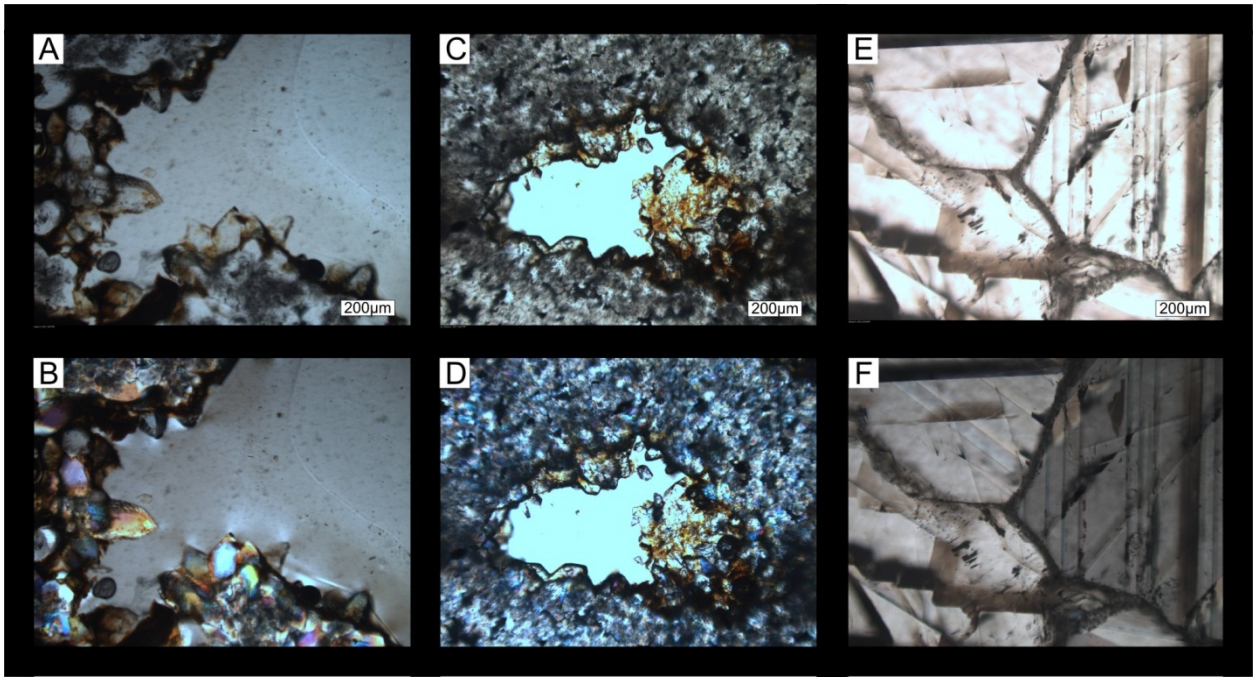

Figure 3.8 Photomicrograph showing quartz under plain transmitted light (A) and under cross polars (B). Part of a fluid inclusion assemblage consisting of coexisting liquid-rich and vapor-rich inclusions, indicative of boiling of the hydrothermal fluid.

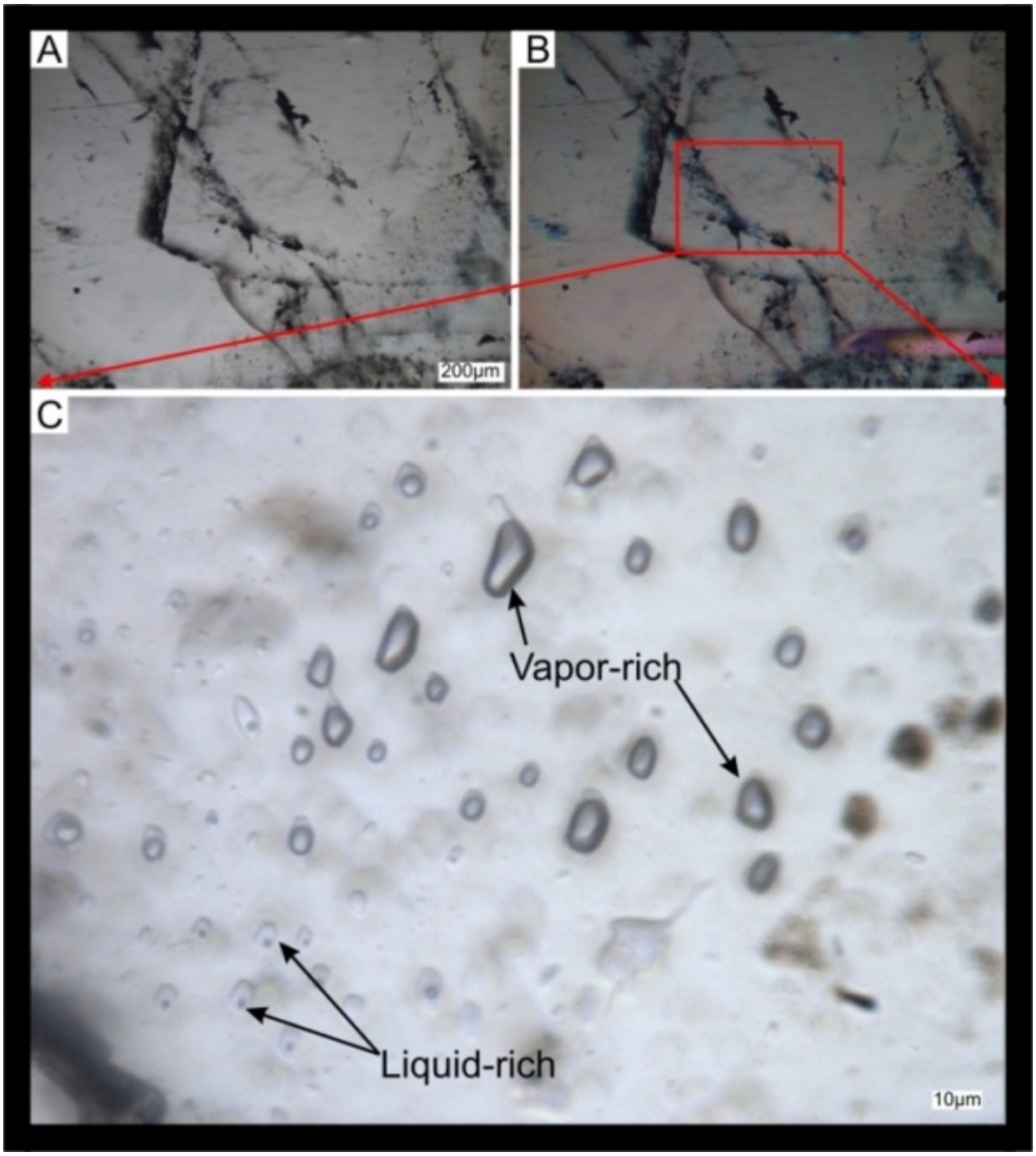

Figure 3.9 Photomicrograph showing bladed calcite under plain transmitted light (A) and under cross polarized light (B). Coexisting liquid-rich and vapor-rich inclusions in calcite that are indicative of trapping from a boiling fluid.

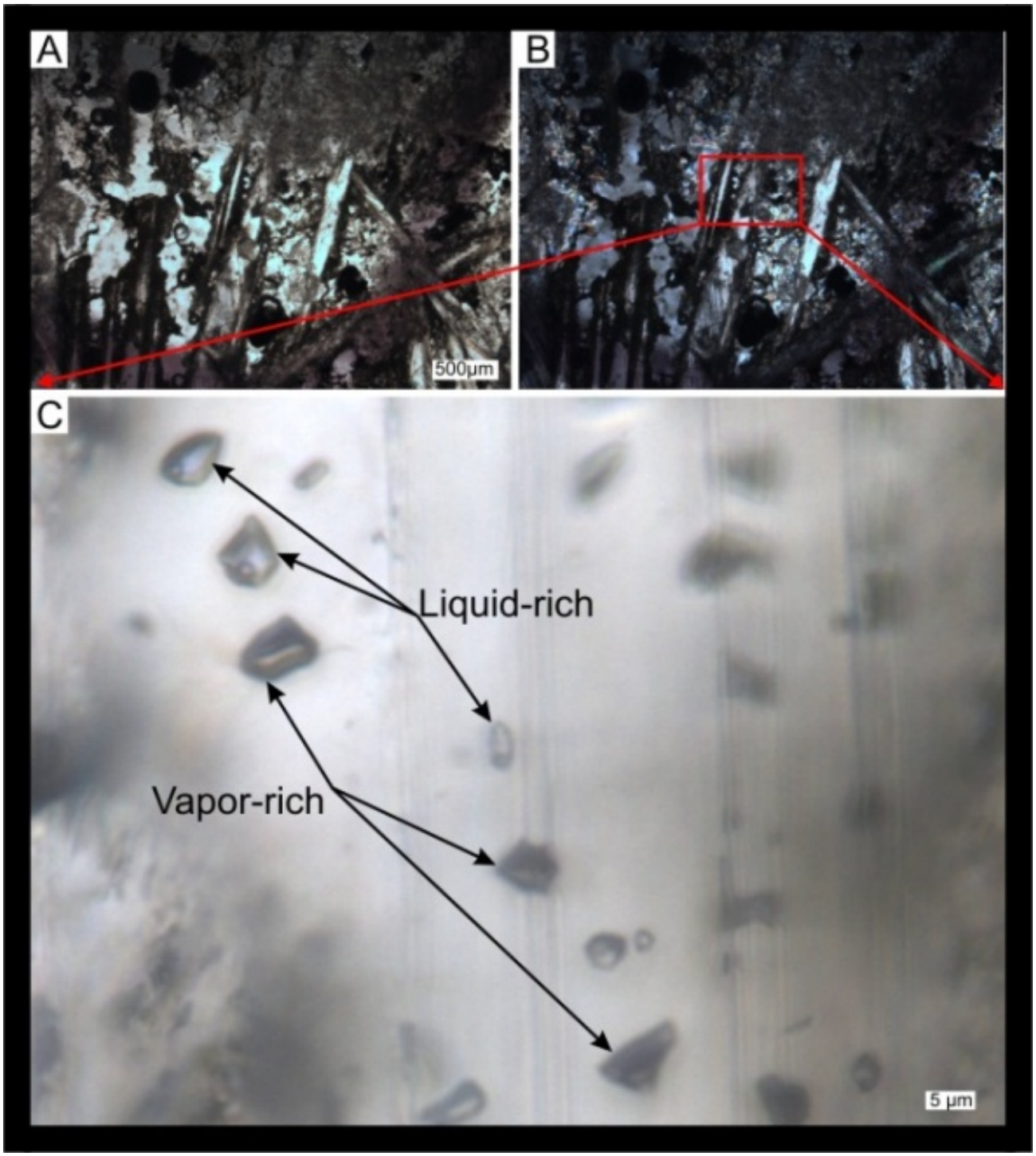

Figure 3.10 Photomicrograph showing quartz under plain transmitted light (A) and under cross polars (B). Part of a fluid inclusion assemblage consisting of only vapor-rich inclusions, indicative of "flashing" or intense boiling of the hydrothermal fluid.

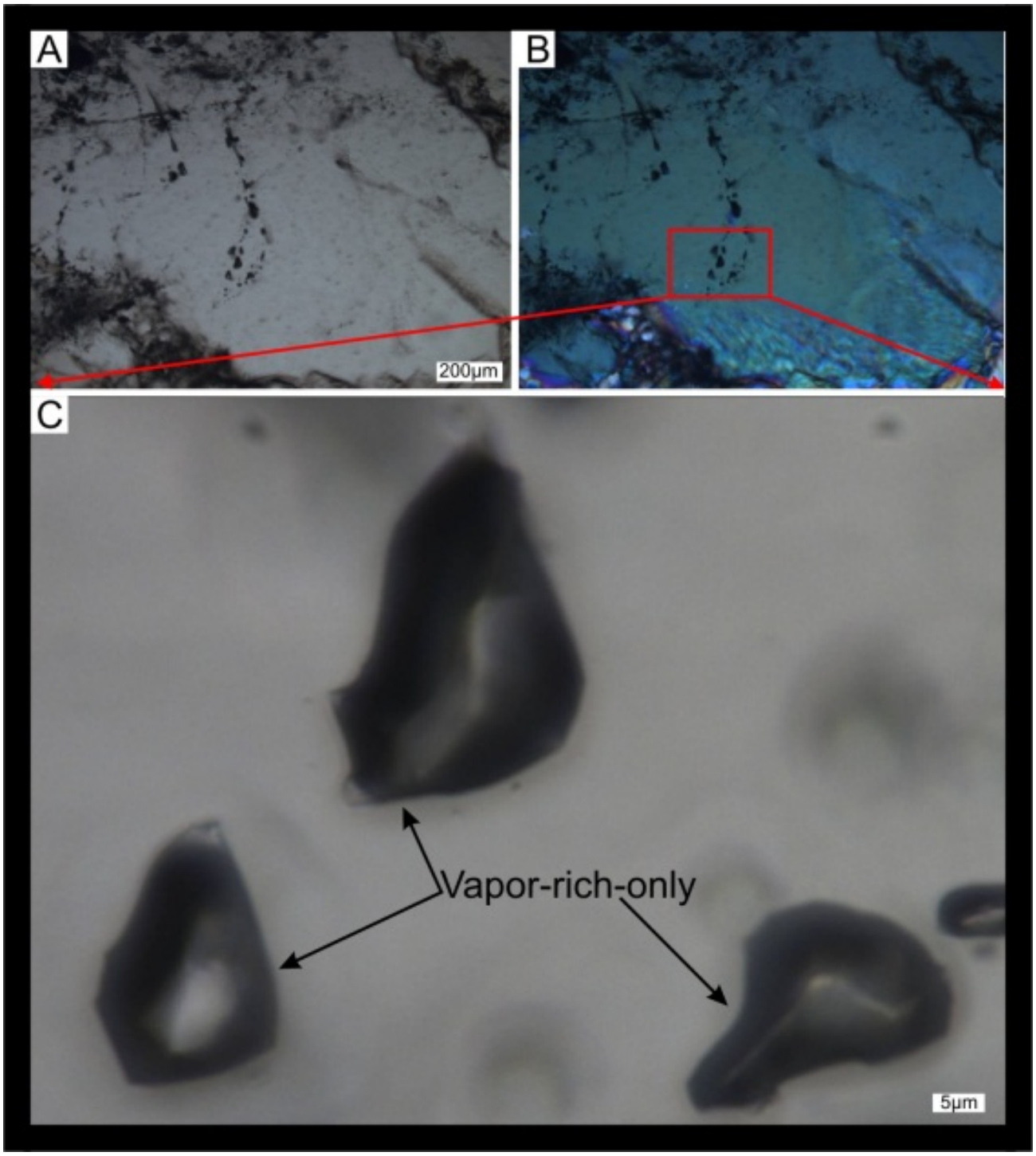

Figure 3.11Photomicrograph showing quartz under plain transmitted light (A) and under cross polarized light (B). Liquid-rich inclusions with trapped illite crystals (C).

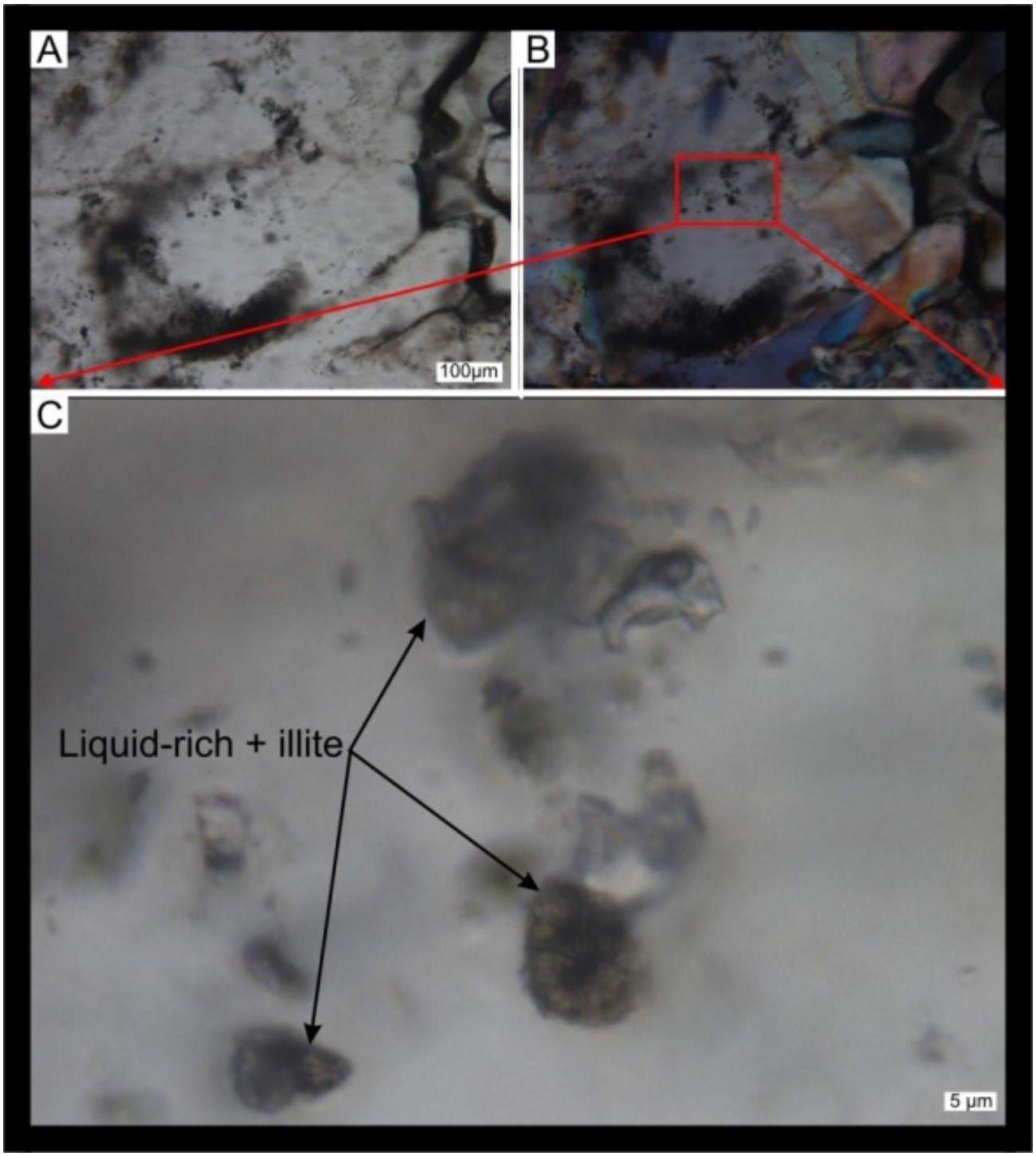

Figure 3.12 Paragenetic sequence of the La Luz system veins.

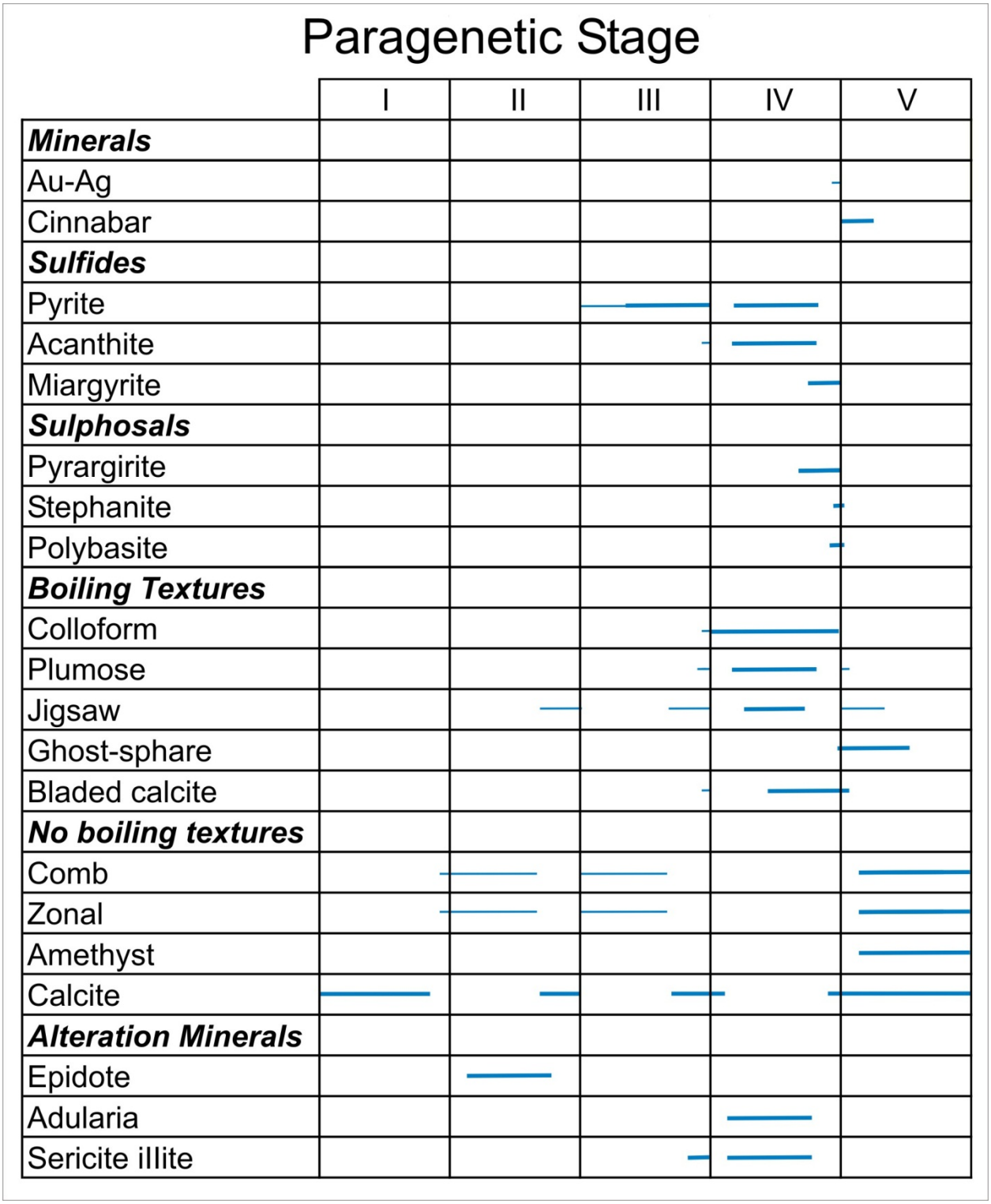

Figure 3.13 Relationship between the average Ag and Au grade and the presence or absence of each mineral or fluid inclusion feature in samples from the La Luz area, collected from veins that have a general azimuth of 330 degrees. Samples were collected from surface outcrops, drill core and underground workings.

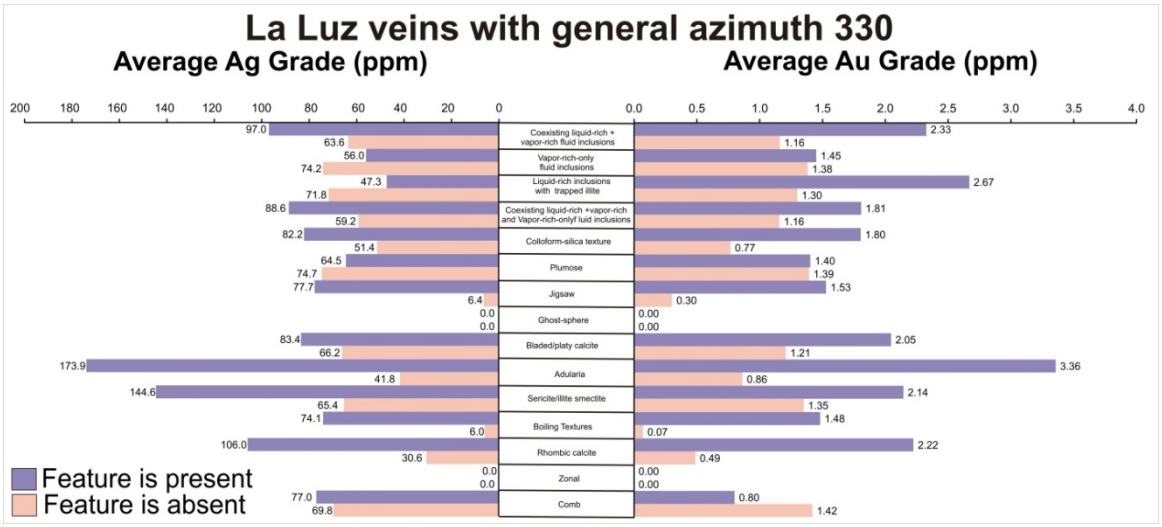

Figure 3.14 Relationship between the average Ag and Au grade and the presence or absence of each mineral or fluid inclusion feature in samples from the La Luz area, collected from veins that have a general azimuth of 240 degrees. Samples were collected from surface outcrops, drill core and underground workings.

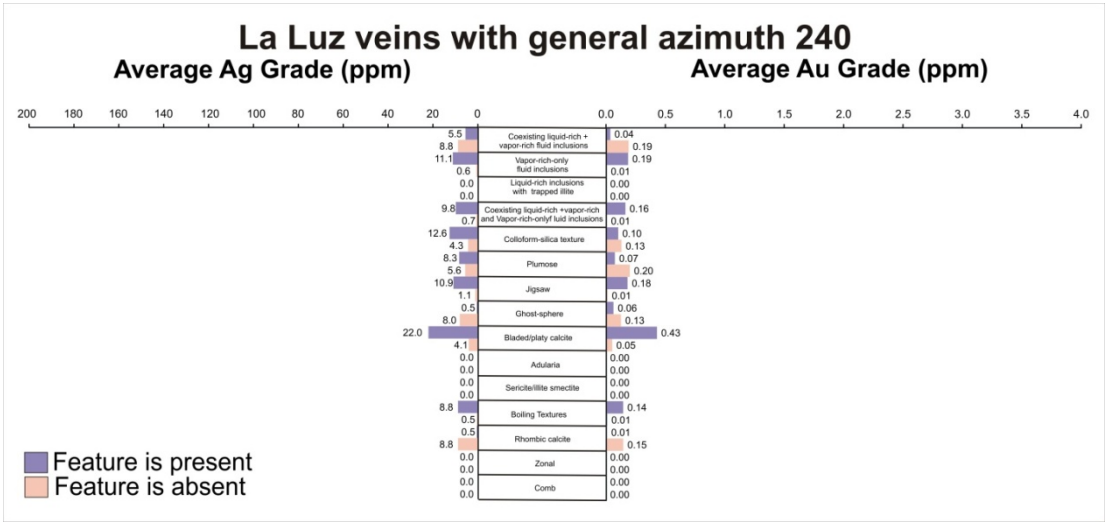

Figure 3.15 Schematic cross section of the different veins in the La Luz area with fluid inclusions, silica, calcite and mineral textures shown as a function of depth.

(CT) Colloform texture quartz, (PT) Plumose texture quartz, (JT) Jigsaw texture quartz, (BC) Bladed calcite replaced by quartz, (Adu) Adularia, (S/I) Sericite/illite.

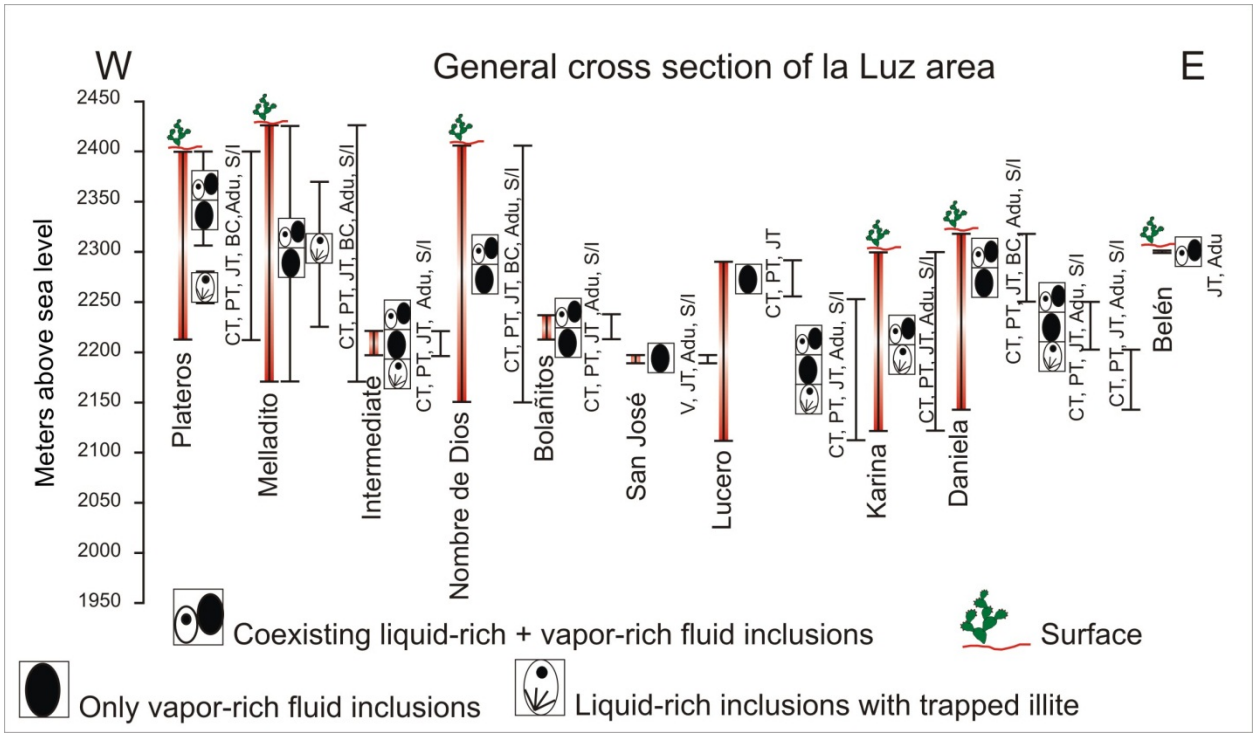

Figure 3.16 (Top) Plan view of the Plateros vein at the La Luz area showing surface sample locations. (Bottom) Longitudinal section showing location of surface sampling and underground samples from the Chayita and Chuparosa mines. No vertical exaggeration.

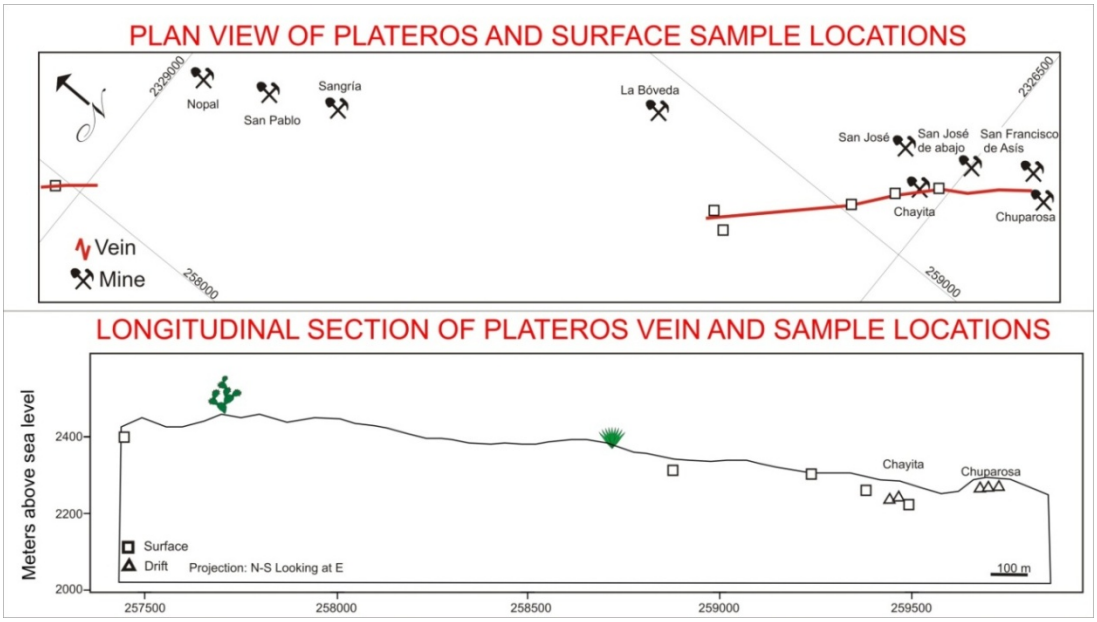

Figure 3.17 Relationship between the average Ag and Au grade and the presence or absence of each mineral or fluid inclusion feature of samples from the Plateros vein, collected from veins that have a general azimuth of 330 degrees. Samples were collected from surface outcrops, drill core and underground workings.

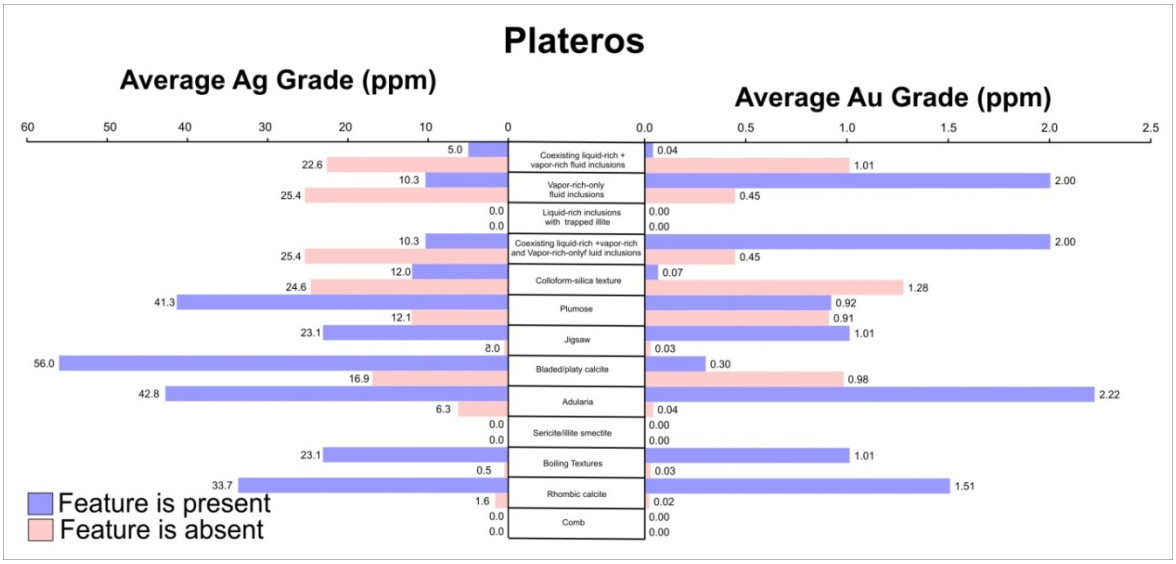

Figure 3.18 Longitudinal section of the Plateros vein showing sample locations and the boiling intensity factor. The boiling intensity factor is defined as the total number of textural and fluid inclusion characteristics that are indicative of boiling that were observed in each sample.

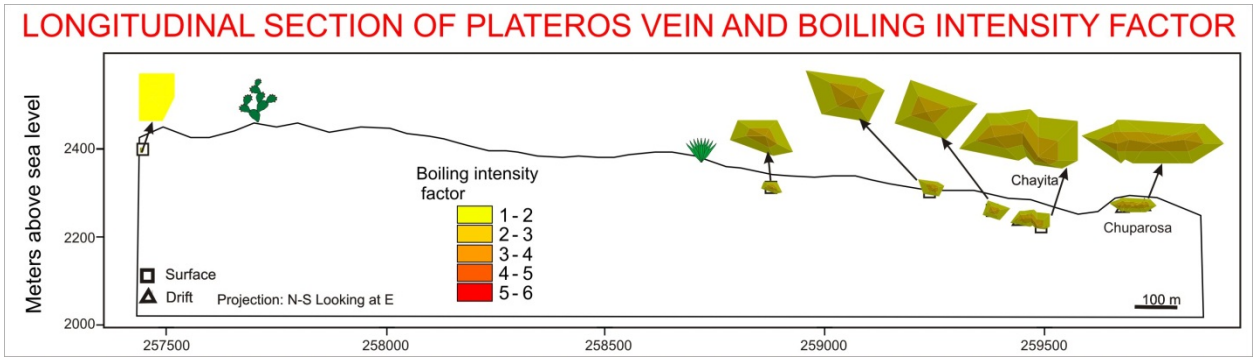

Figure 3.19 Longitudinal section of the Plateros vein showing sample locations, areas that show boiling indicated by the dashed line, and the Au grades in ppm.

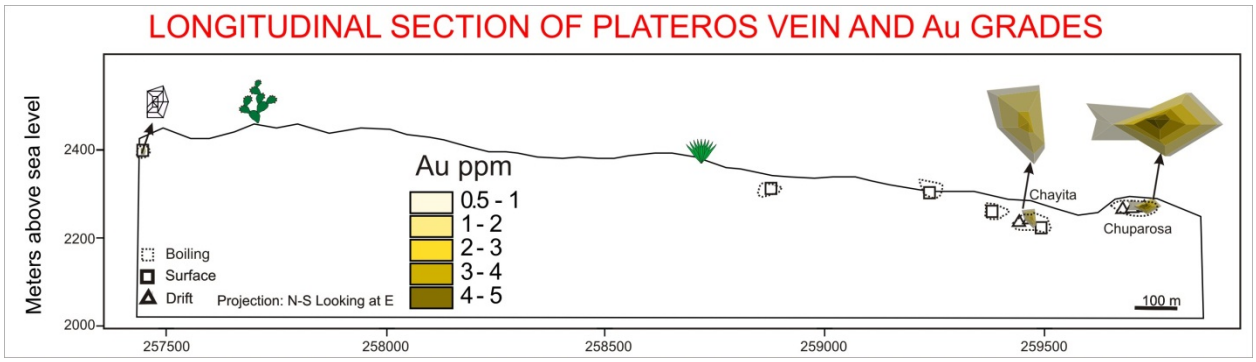

Figure 3.20 Longitudinal section of the Plateros vein showing sample locations, areas that show boiling indicated by the dashed line, and the Ag grades in ppm.

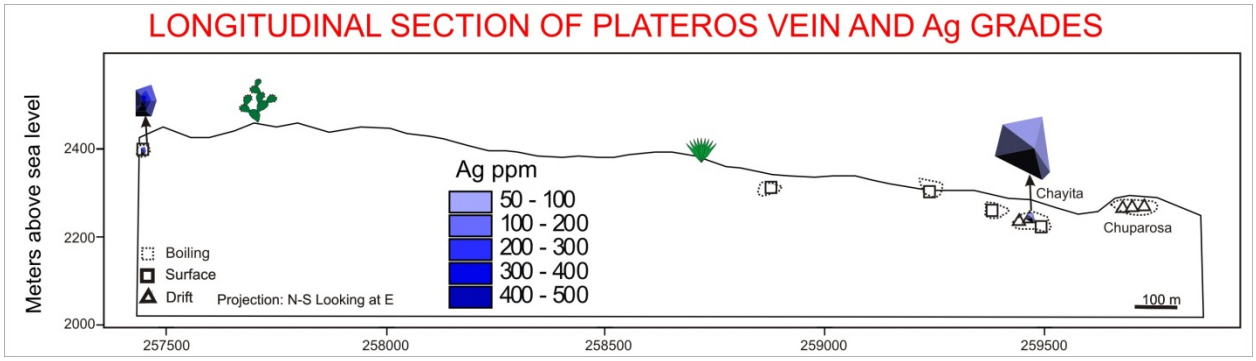

Figure 3.21 (Top) Plan view of the Melladito vein in the La Luz area showing surface sample locations along the vein as well as perpendicular to the vein along traverse A to A'. (Bottom) Longitudinal section of the Melladito vein showing surface, drill core, and underground sampling locations. Also shown is the location of section 750 N. No vertical exaggeration.

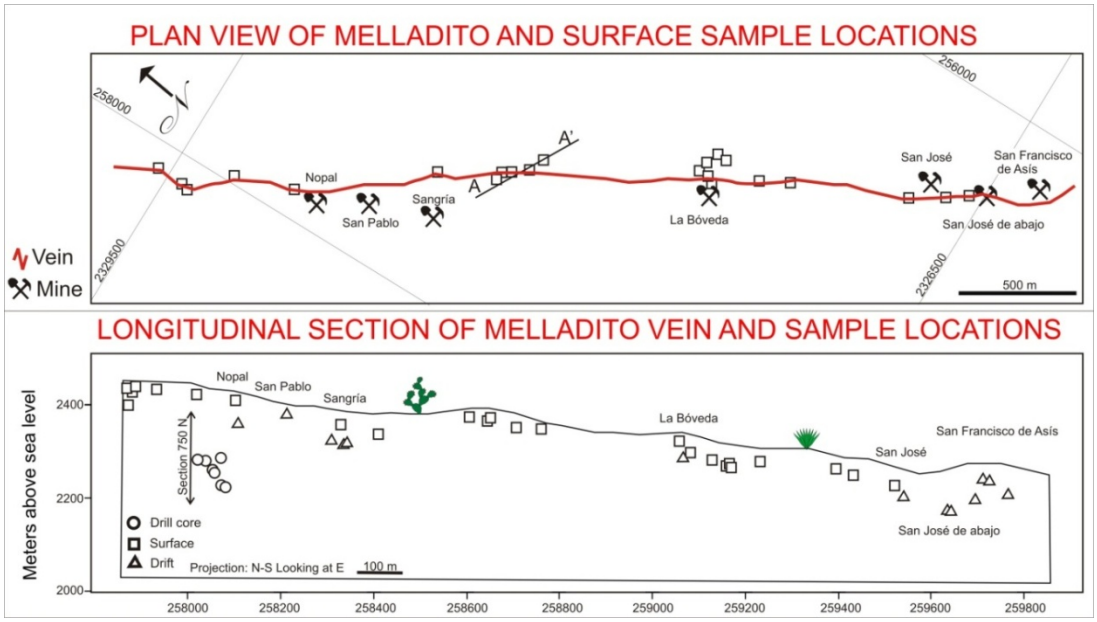

Figure 3.22 Relationship between the average Ag and Au grade and the presence or absence of each mineral or fluid inclusion feature of samples from the Melladito vein, collected from veins that have a general azimuth of 330 degrees. Samples were collected from surface outcrops, drill core and underground workings.

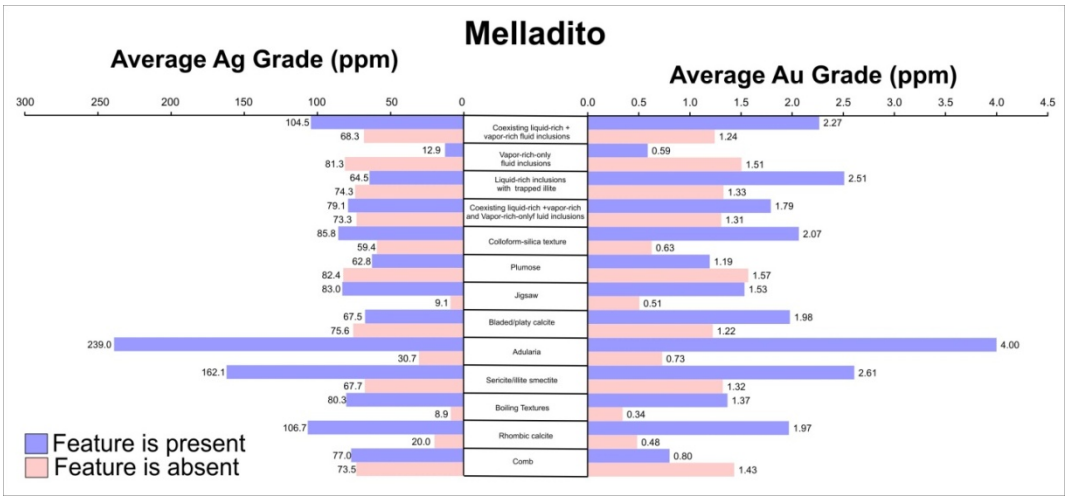

Figure 3.23 Longitudinal section of the Melladito vein showing sample locations and the boiling intensity factor. The boiling intensity factor is defined as the total number of textural and fluid inclusion characteristics that are indicative of boiling that were observed in each sample.

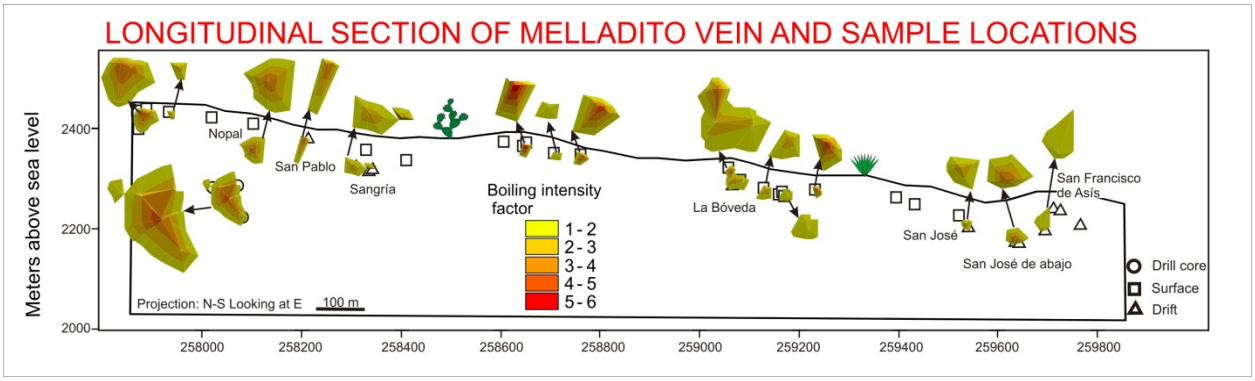

Figure 3.24 Longitudinal section of the Melladito vein showing sample locations, areas that show boiling indicated by the dashed line, and the Au grades in ppm.

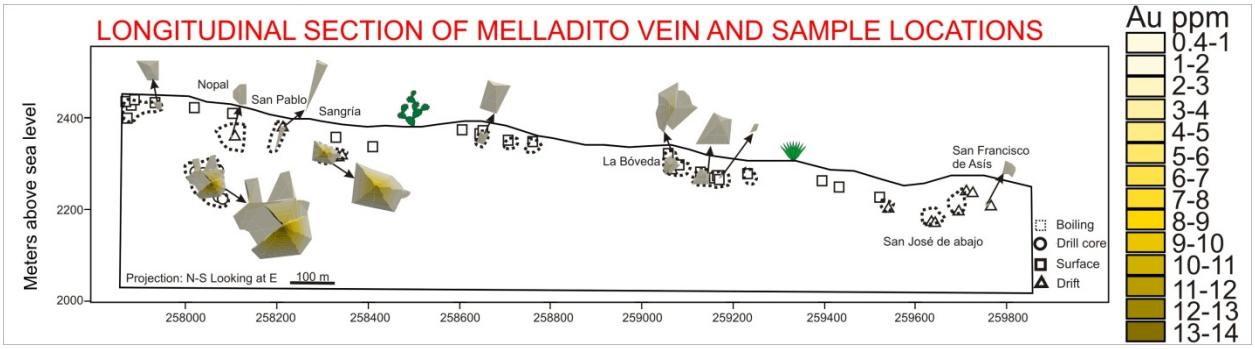

Figure 3.25 Longitudinal section of the Melladito vein showing sample locations, areas that show boiling indicated by the dashed line, and the Ag grades in ppm.

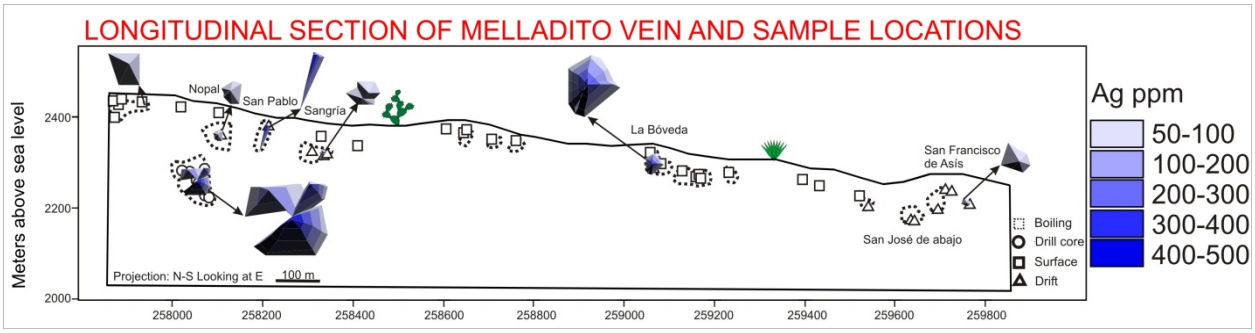

Figure 3.26 Drill hole number 1 from the La Luz area showing the distribution of gold (A), silver (B), and boiling intensity factor (C) as a function of distant from the Melladito vein (vein shown in red on left side of diagram). Note the increase in gold and silver values and the boiling intensity as the vein is approached. CT= colloform texture quartz; JT = jigsaw texture quartz; PT = plumose texture quartz; V = assemblages consisting of only vapor-rich inclusions; LV = assemblages consisting of coexisting liquid-rich and vapor-rich inclusions with a broad range in liquid-to-vapor ratios; Ad= Adularia; BC= bladed calcite or bladed calcite replaced by quartz.

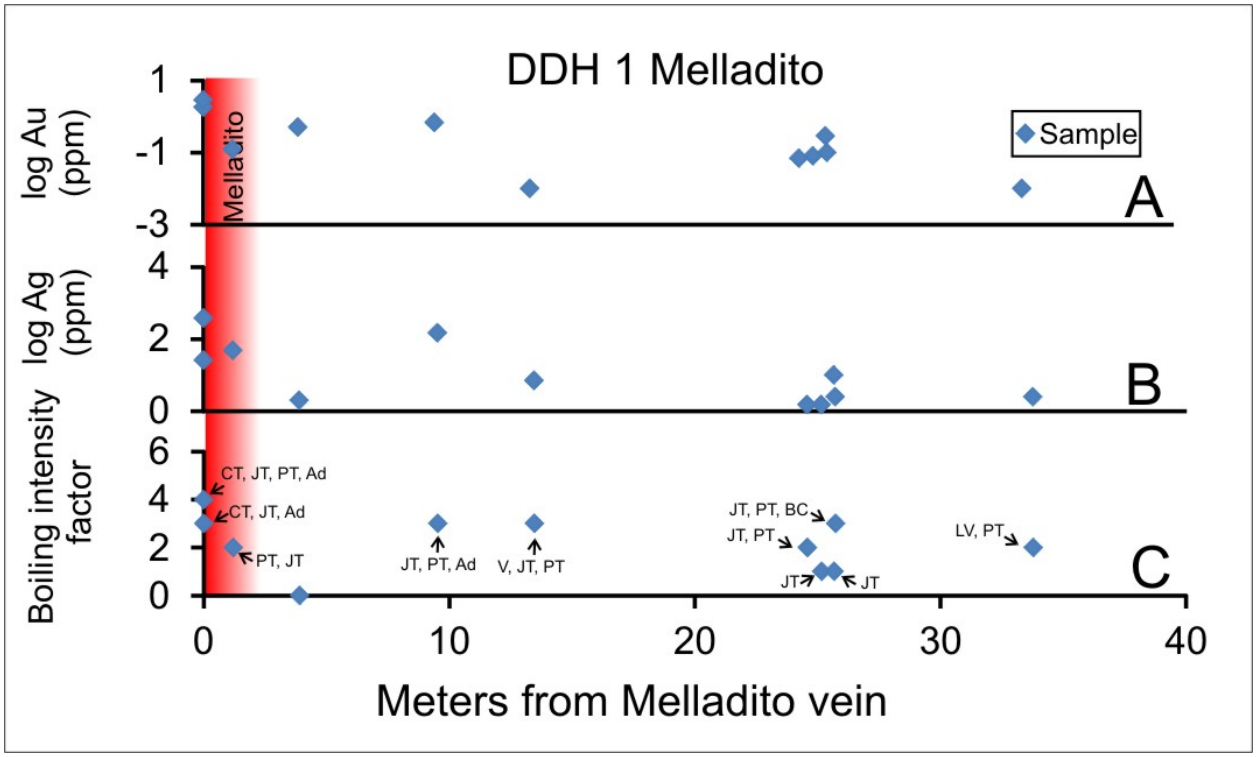

Figure 3.27 Drill hole number 1 from the La Luz area showing the gold and silver grades (top axis) and the percent of samples that show evidence of boiling as a function of elevation or depth in the drill hole. The depth (elevation) where the drill core intersected the Melladito and Intermediate veins is highlighted in red.

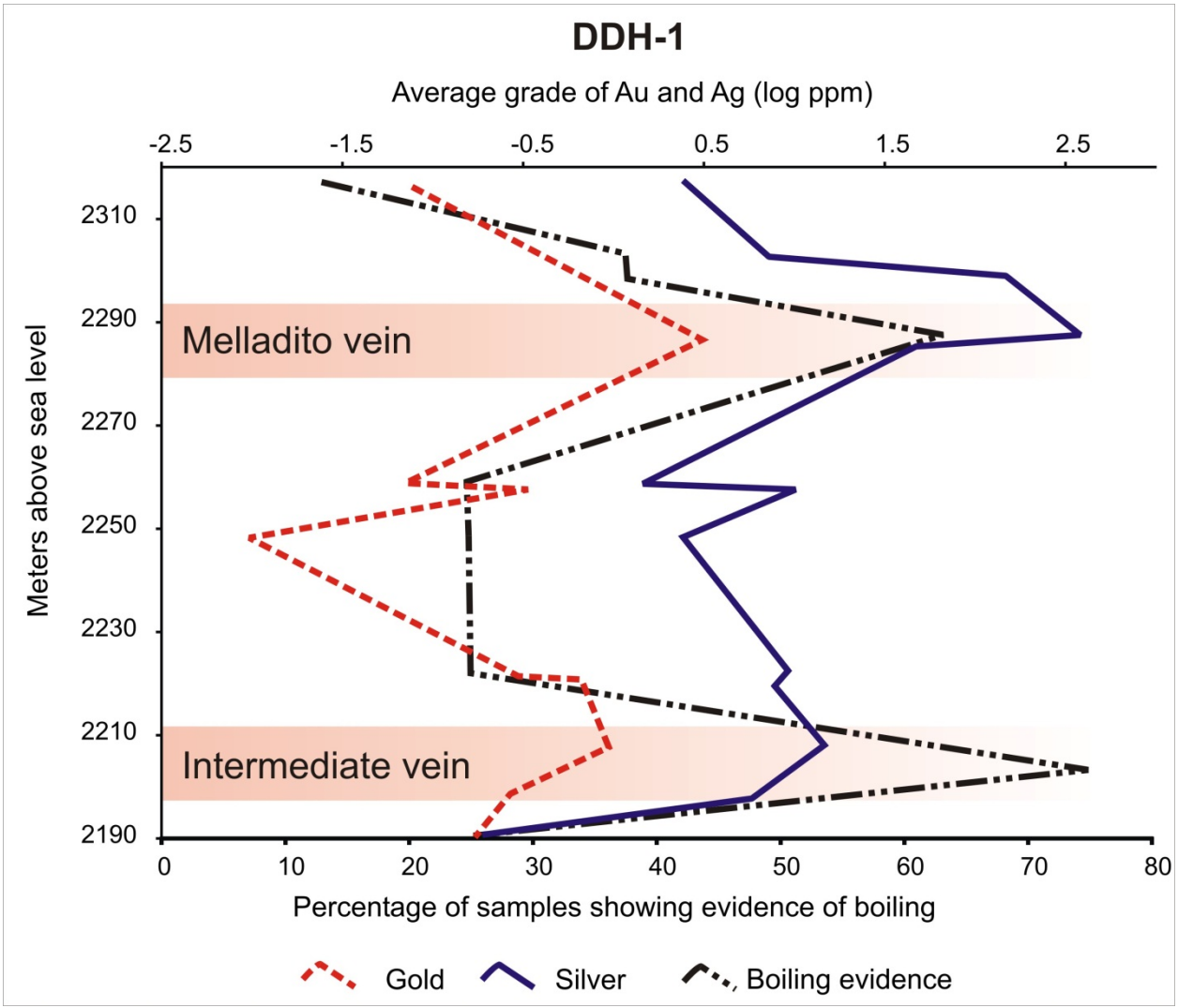

Figure 3.28 Surface traverse perpendicular to the Melladito vein from La Luz area (see Figure 15, top) showing the distribution of gold (A), silver (B) and boiling intensity factor (C) as a function of distant from the Melladito vein (vein shown in red on left side of diagram). Note the increase in gold and silver values and the boiling intensity as the vein is approached. CT= colloform texture quartz; JT = jigsaw texture quartz; PT = plumose texture quartz; V = assemblages consisting of only vapor-rich inclusions; LV = assemblages consisting of coexisting liquid-rich and vapor-rich inclusions with a broad range in liquid-to-vapor ratios; Ad= Adularia; BC= bladed calcite or bladed calcite replaced by quartz; GhSTQ = Ghost-sphere texture quartz.

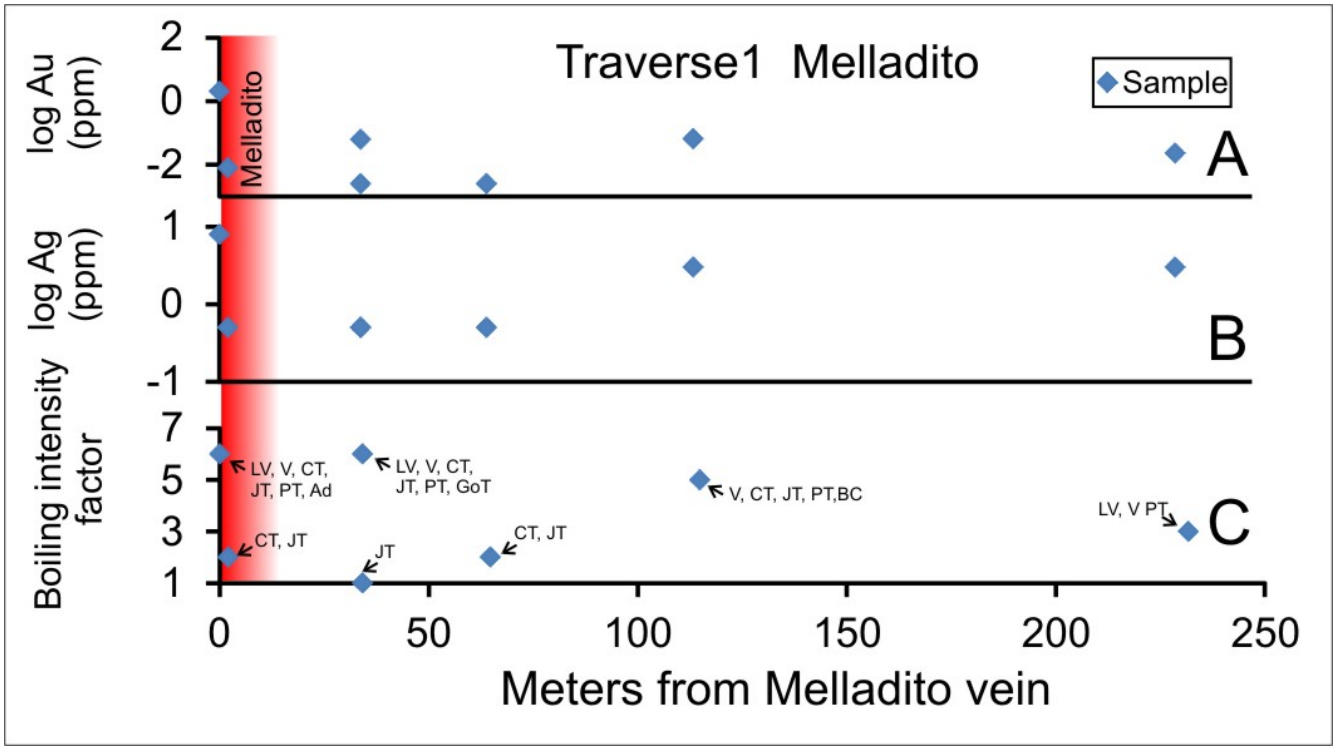

Figure 3.29 Relationship between the average Ag and Au grade of samples from drill core and the presence or absence of each mineral or fluid inclusion feature in samples from the Intermediate vein at the La Luz area with a general azimuth of 330 degrees.

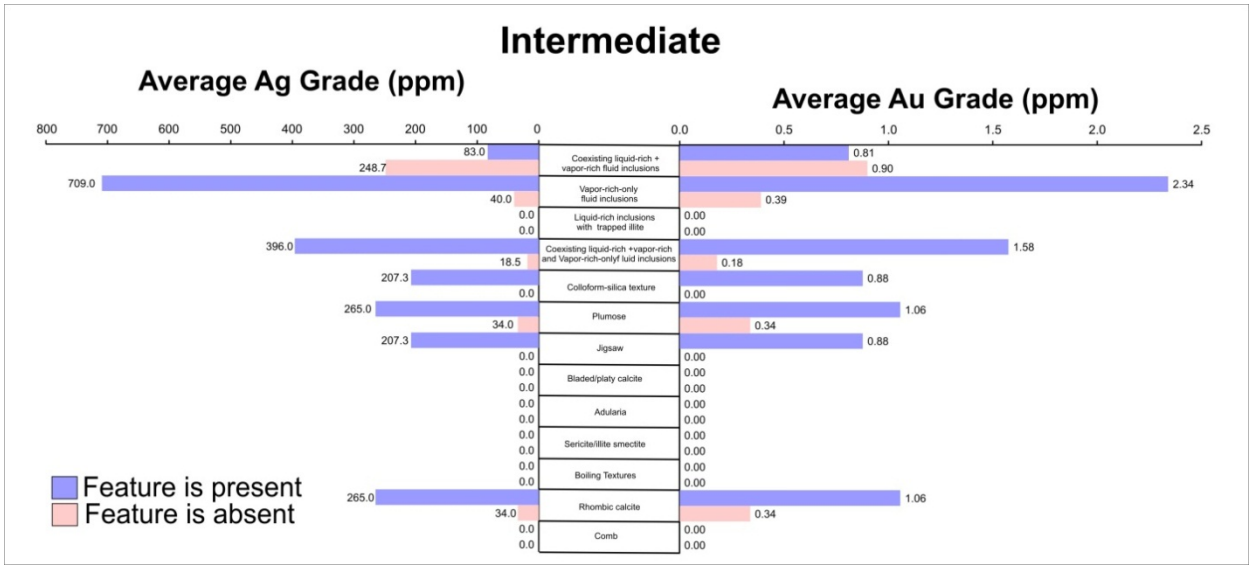

Figure 3.30 Longitudinal section of the Intermediate vein showing sample location and boiling intensity factor.

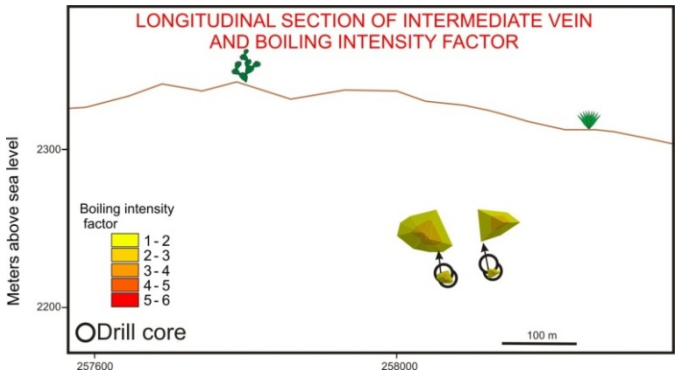

Figure 3.31 Longitudinal section of the Intermediate vein showing sample location, areas that show evidence of boiling (outlined by the dashed line) and Au grades in ppm.

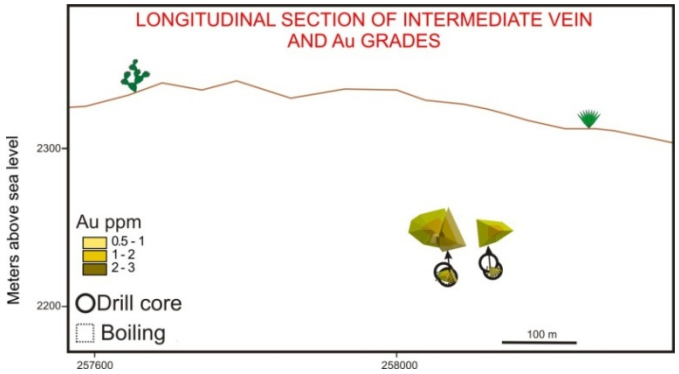

Figure 3.32 Longitudinal section of the Intermediate vein showing sample location, areas that show evidence of boiling (outlined by the dashed line) and Ag grades in ppm.

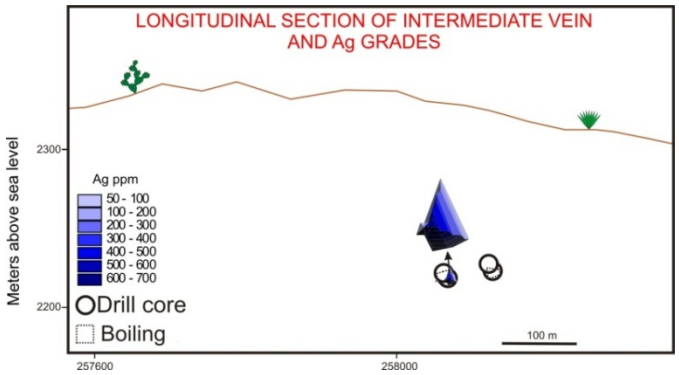

Figure 3.33 (Top) Plan view of the Nombre de Dios vein in the La Luz area showing surface sample locations. (Bottom) Longitudinal section of the Nombre de Dios vein showing surface and drill core sampling locations. No vertical exaggeration.

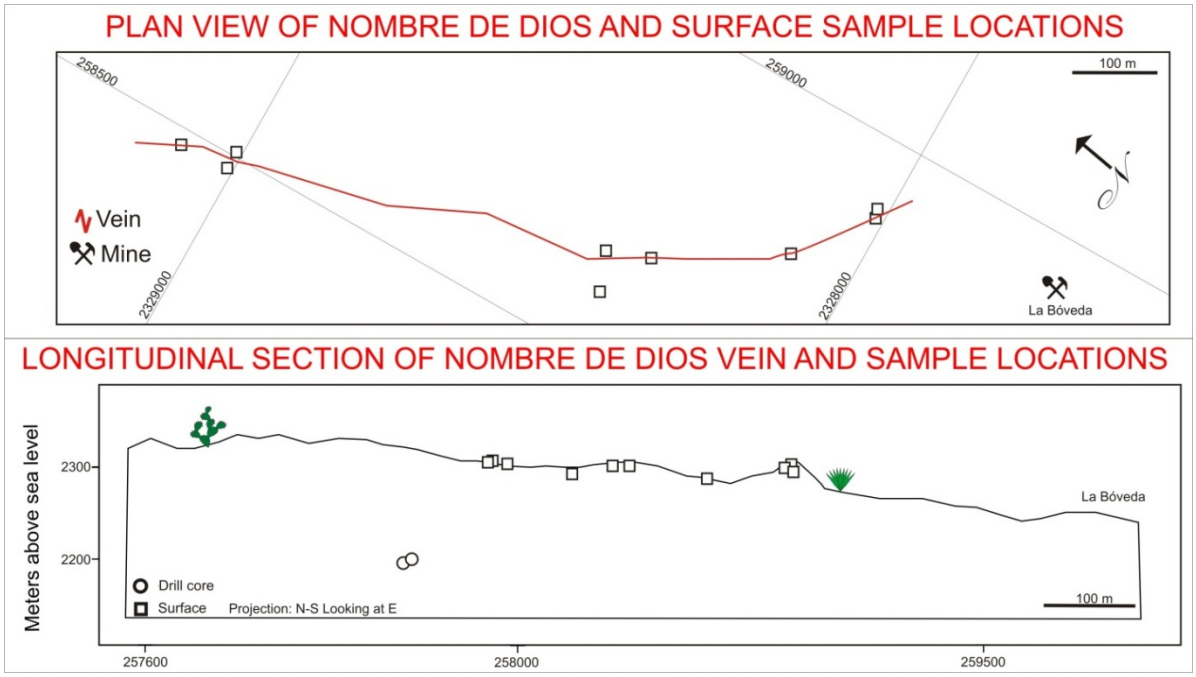

Figure 3.34 Relationship between the average Ag and Au grades of samples from surface and drill core samples, and the presence or absence of each mineral or fluid inclusion feature in samples from the Nombre de Dios vein on the La Luz area, with a general azimuth of 330 degrees.

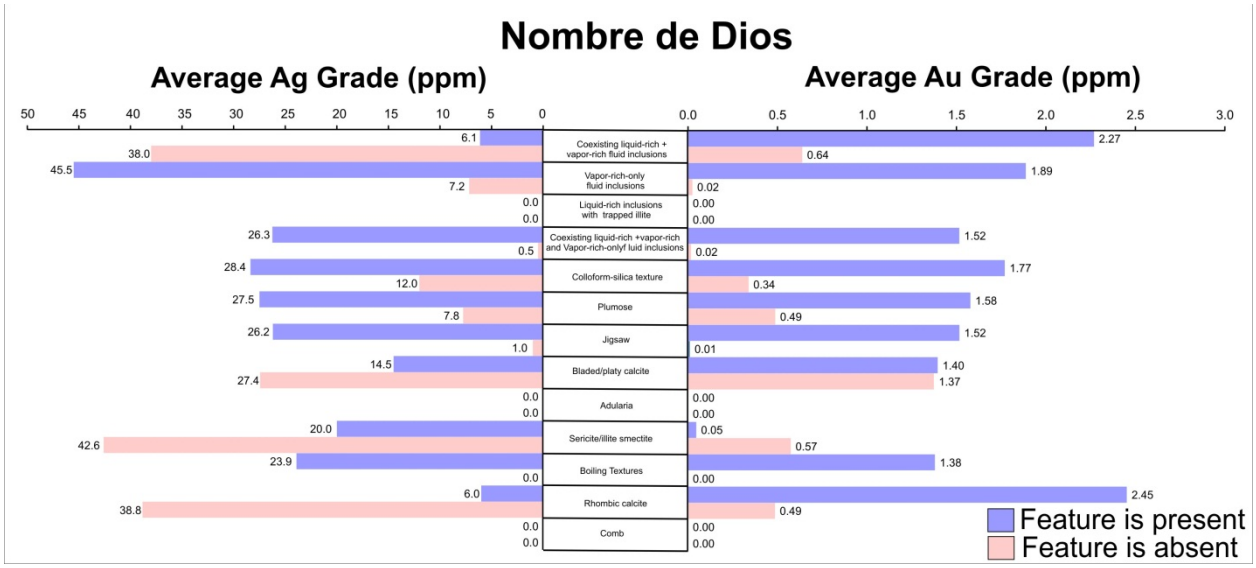

Figure 3.35 Longitudinal section of the Nombre de Dios vein showing sample location and boiling intensity factor.

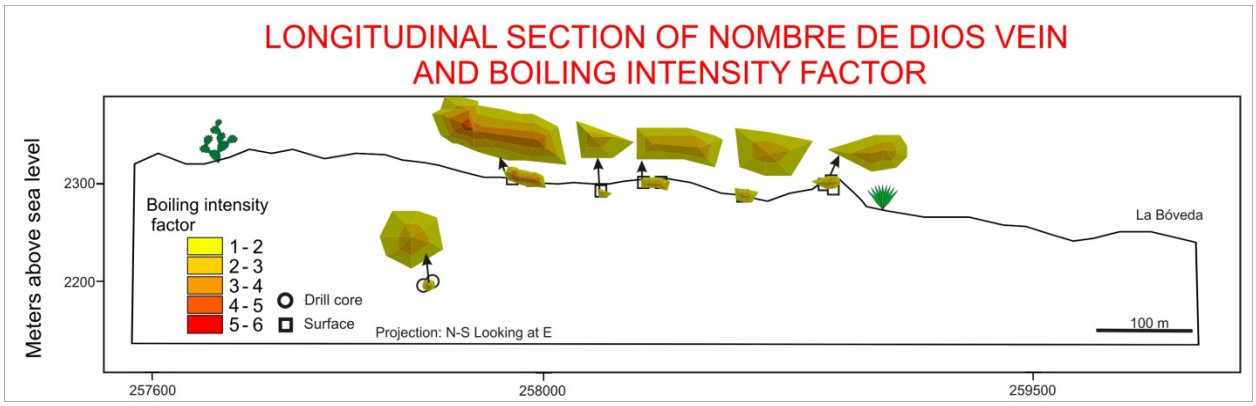

Figure 3.36 Longitudinal section of the Nombre de Dios vein showing sample location and Au grades. Areas where boiling was observed are shown by the dashed lines.

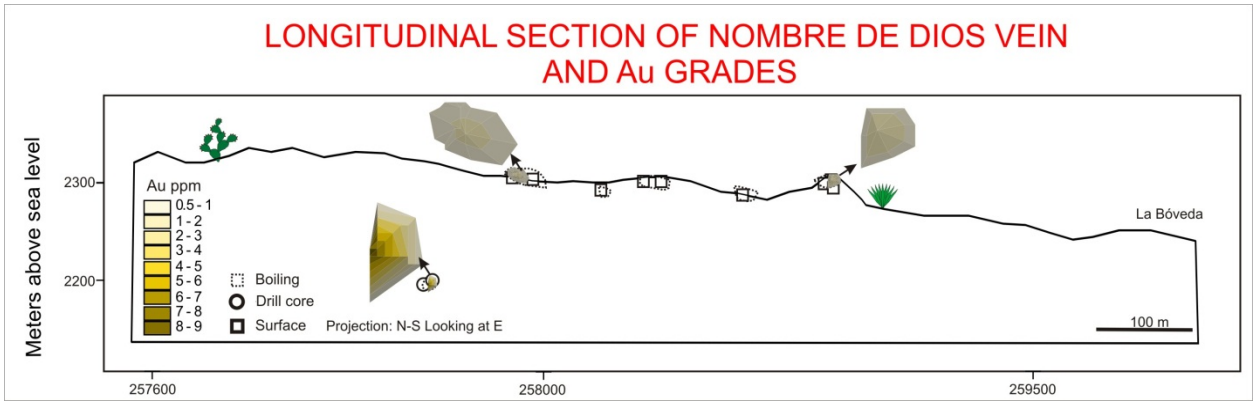

Figure 3.37 Longitudinal section of the Nombre de Dios vein showing sample location and Ag grades. Areas where boiling was observed are shown by the dashed lines.

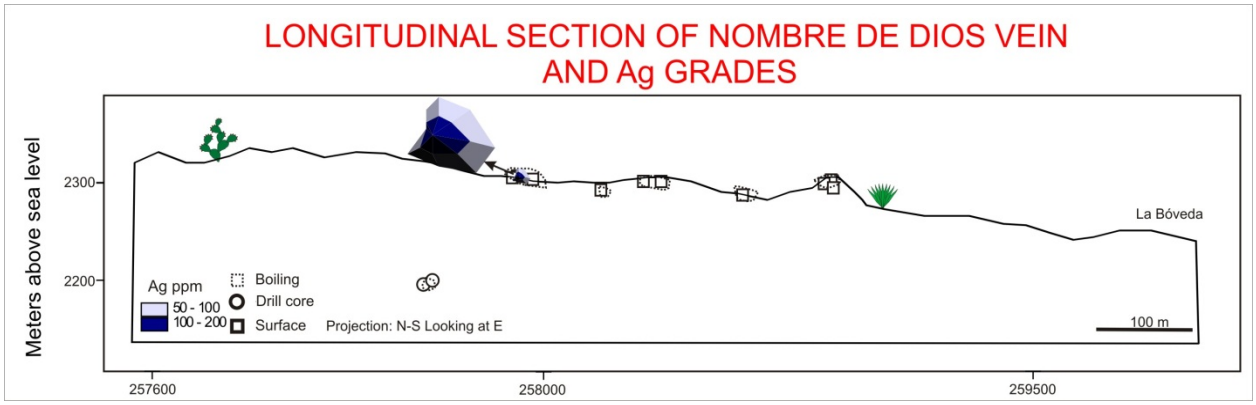

Figure 3.38 Longitudinal section of the Bolañitos vein and underground sample locations, along at N-S projection and looking at east.

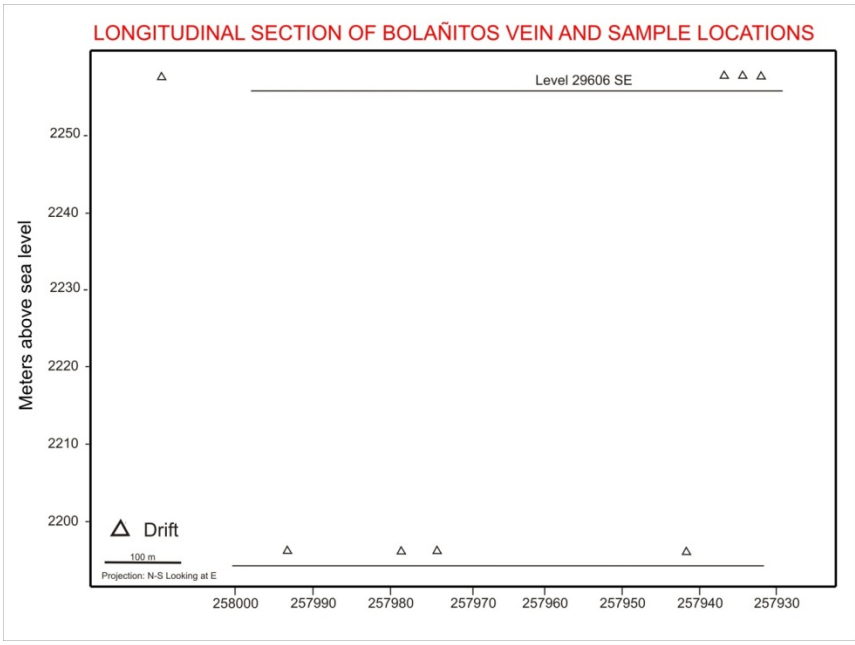

Figure 3.39 Relationship between the average Ag and Au grade of samples and the presence or absence of each mineral or fluid inclusion feature in samples from Bolañitos vein, Guanajuato, Mexico.

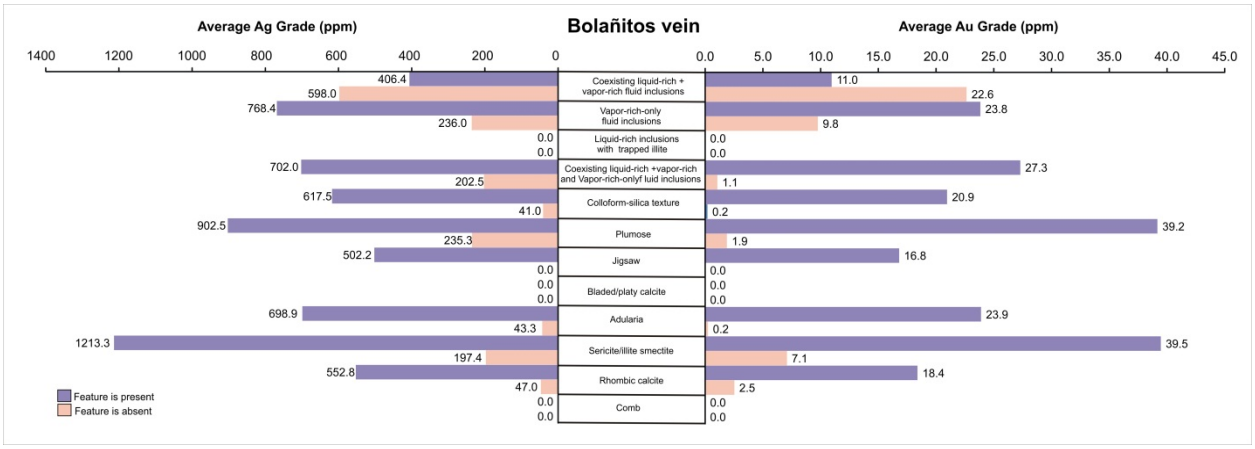

Figure 3.40 Longitudinal section of Bolañitos vein showing sample location and boiling intensity factor.

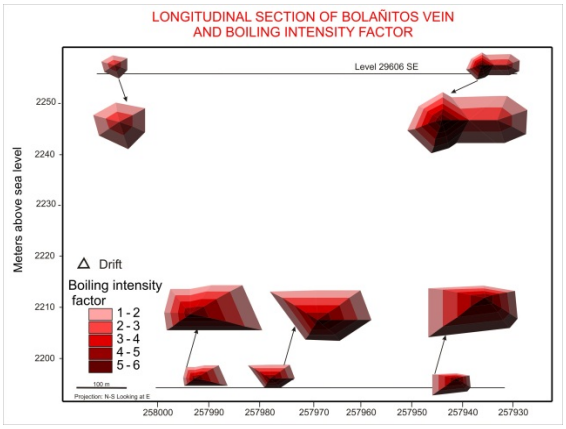

Figure 3.41 Longitudinal section of Bolañitos vein showing Au grades (in ppm).

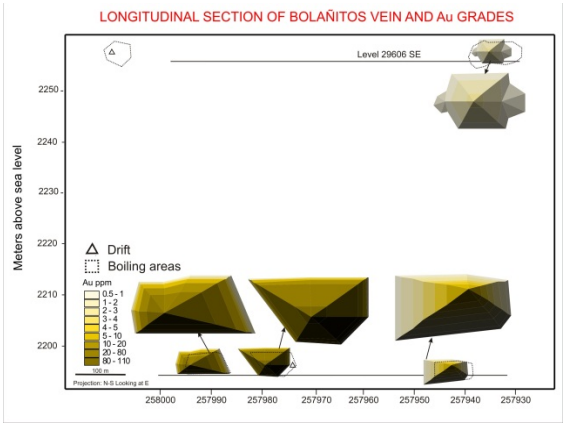

Figure 3.42 Longitudinal section of the Bolañitos vein showing Ag grades (in ppm).

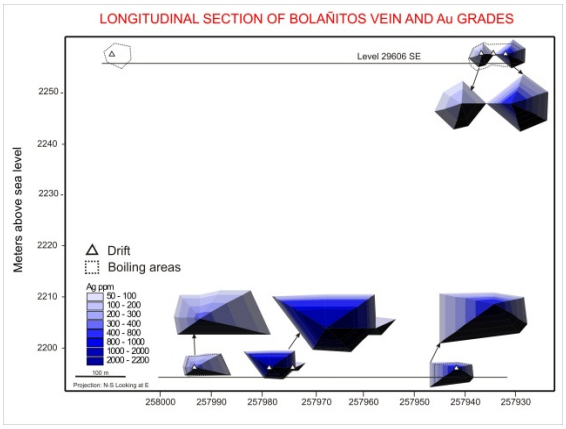

Figure 3.43 Longitudinal section of the Lucero vein, along at N-S projection and looking at east. Open circles correspond to drill core, and open triangles correspond to drift samples.

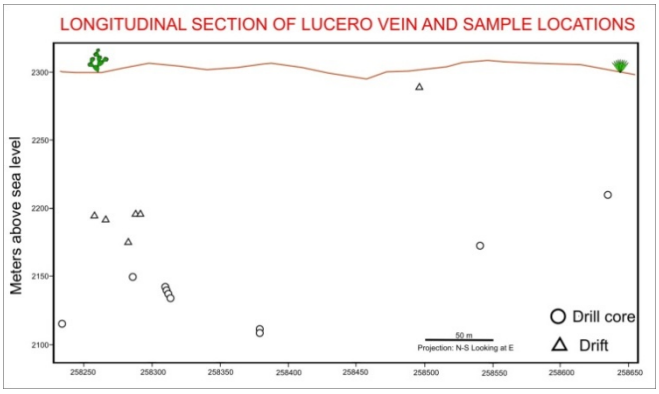

Figure 3.44 Relationship between the average Ag and Au grade of samples and the presence or absence of each mineral or fluid inclusion feature in samples from the Lucero vein.

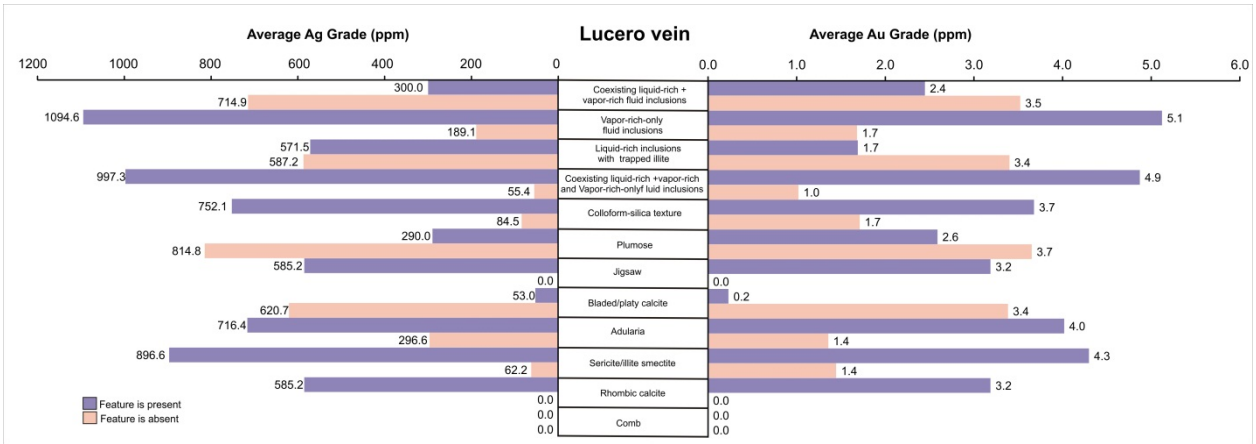

Figure 3.45 Longitudinal section of the Lucero vein and boiling intensity factor for collected samples.

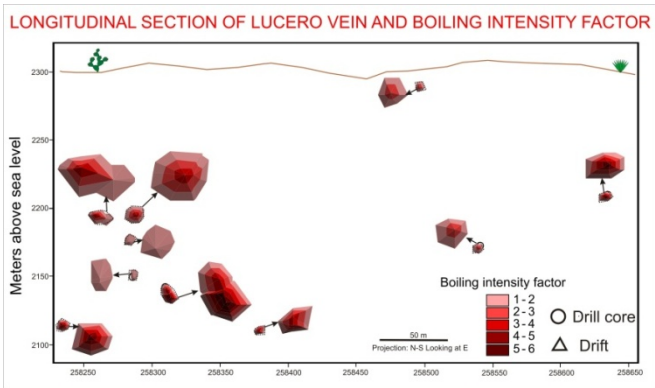

Figure 3.46 Longitudinal section of Lucero vein showing gold grades for samples collected.

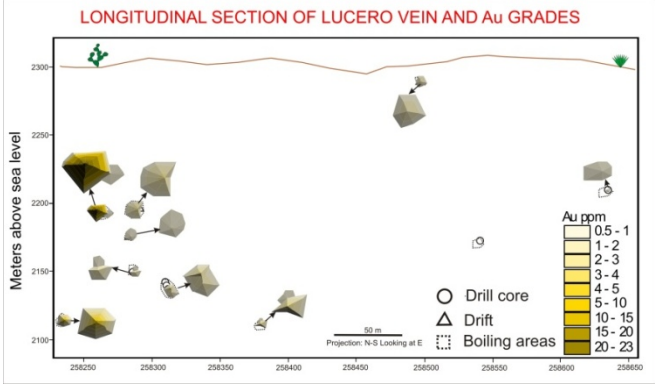

Figure 3.47 Longitudinal section of the Lucero vein showing silver grades for samples collected.

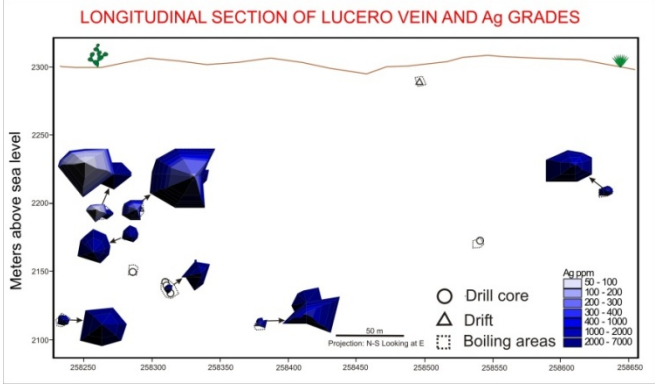

Figure 3.48 Modified longitudinal section of the Lucero vein showing samples collected from drill holes and the different silica, mineral textures and fluid inclusion features observed. Dashed line represents the mineralized horizon reported from (modified Endeavour Silver Corp (2012)).

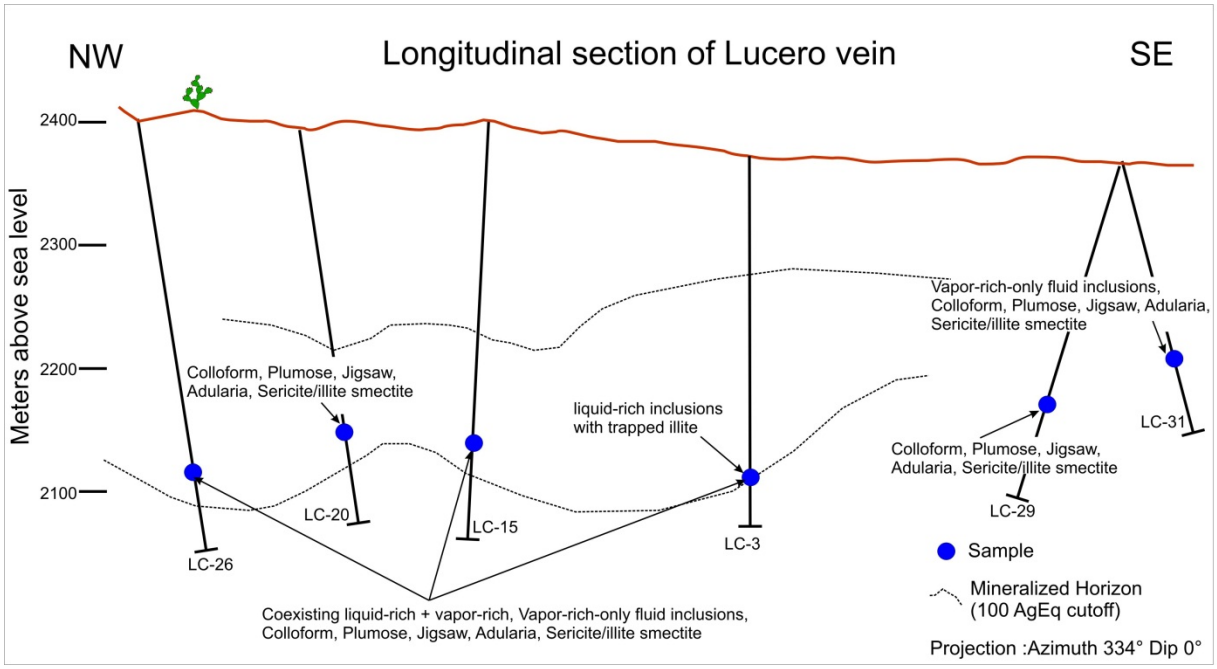

Figure 3.49 Longitudinal section of the Karina vein showing surface, drill core, and underground sampling locations.

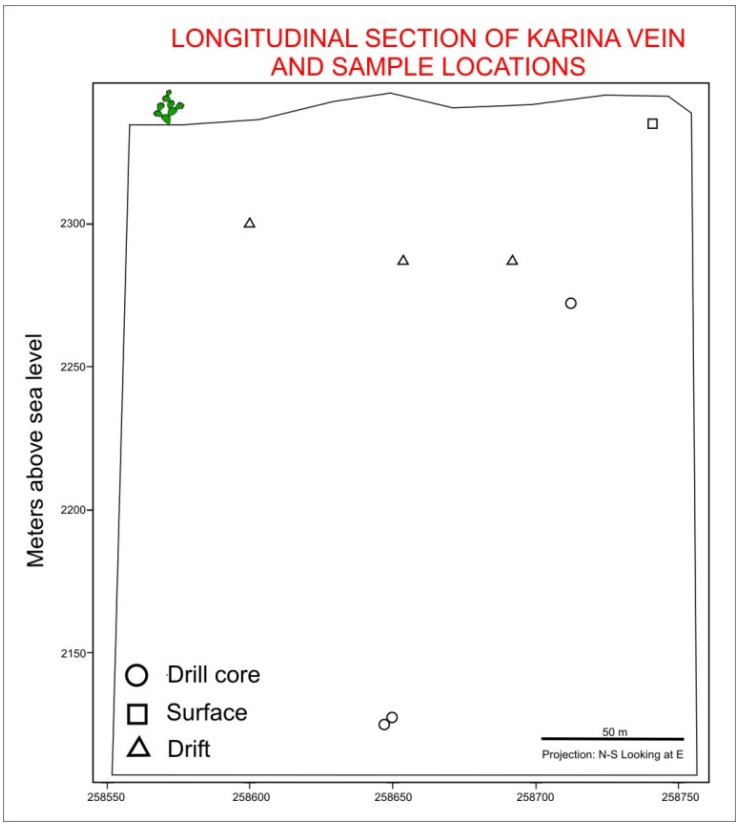

Figure 3.50 Relationship between the average Ag and Au grade of samples and the presence or absence of each mineral or fluid inclusion feature in samples from Karina vein, Guanajuato, Mexico.

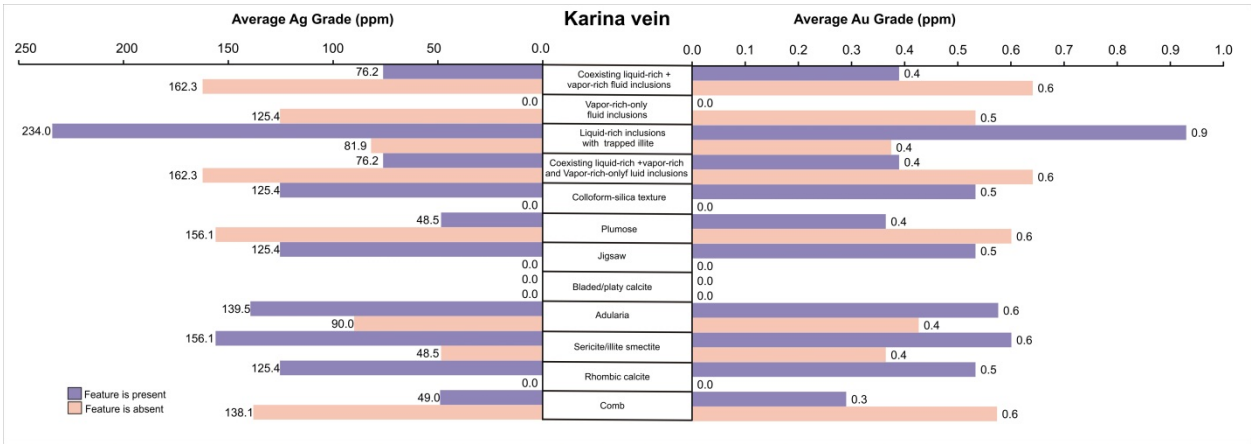

Figure 3.51 Longitudinal section of Karina vein showing sample location and boiling intensity factor.

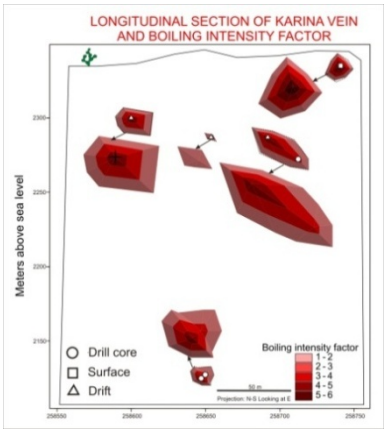

Figure 3.52 Longitudinal section of the Karina vein showing Au grades.

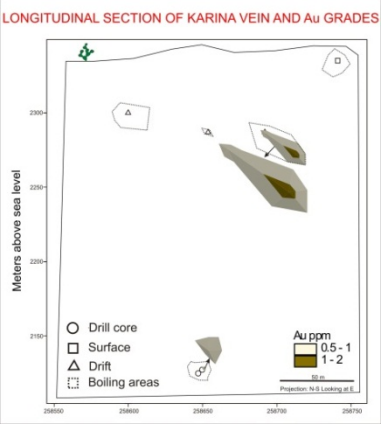

Figure 3.53 Longitudinal section of the Karina vein showing sample location and Ag grades.

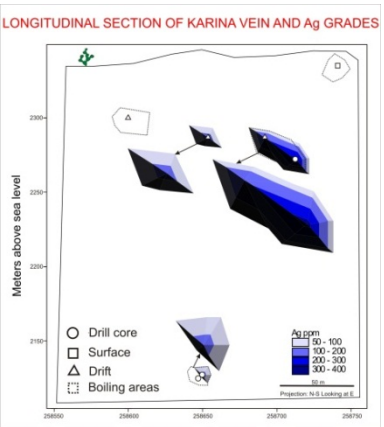

Figure 3.54 Longitudinal section of the Daniela vein and sample locations, along at N-S projection looking east. Open circles correspond to drill core, open squares correspond to surface outcrops and open triangles correspond to drift samples.

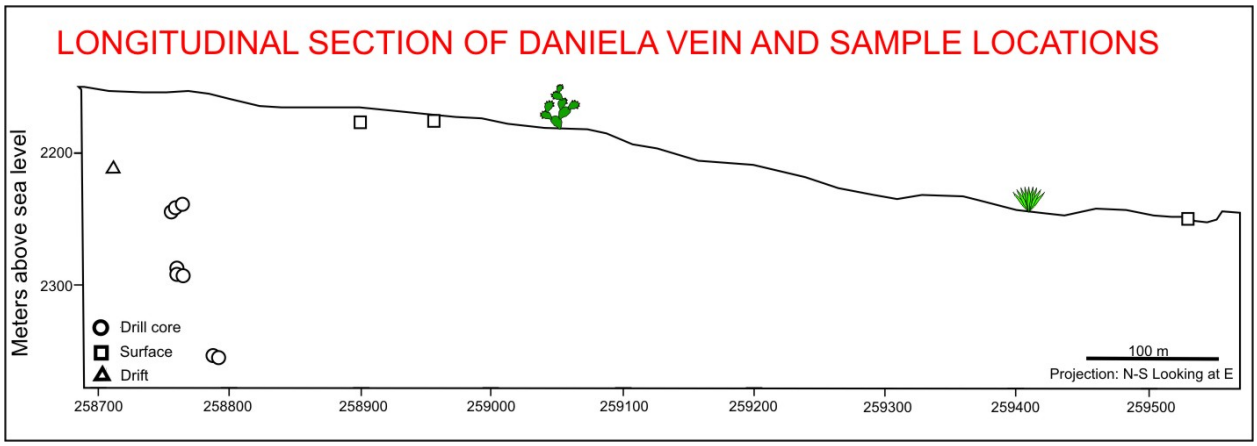

Figure 3.55 Relationship between the average Ag and Au grade of samples and the presence or absence of each mineral or fluid inclusion feature in samples from Daniela vein.

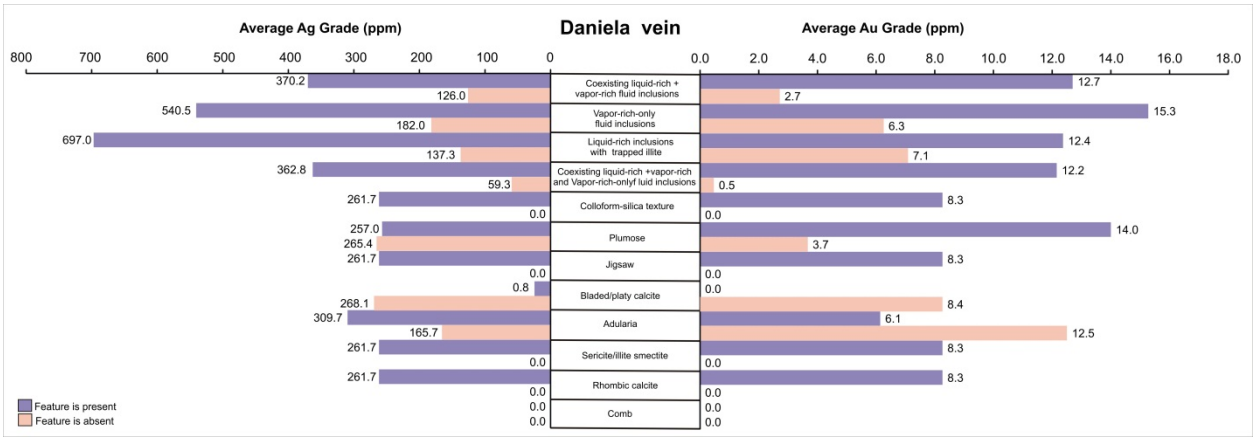

Figure 3.56 Longitudinal section of Daniela vein and boiling intensity factor for samples collected.

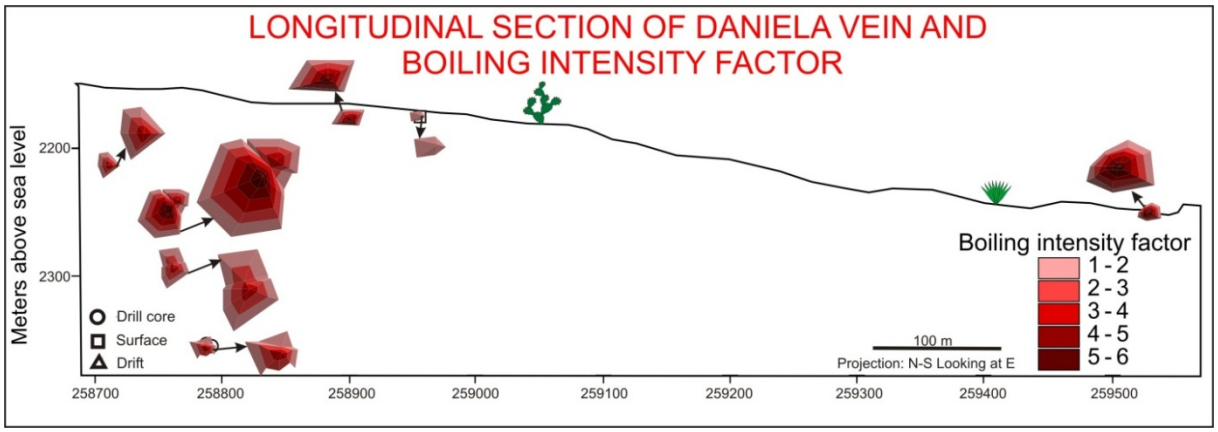

Figure 3.57 Longitudinal section of Daniela vein and gold grades for samples collected.

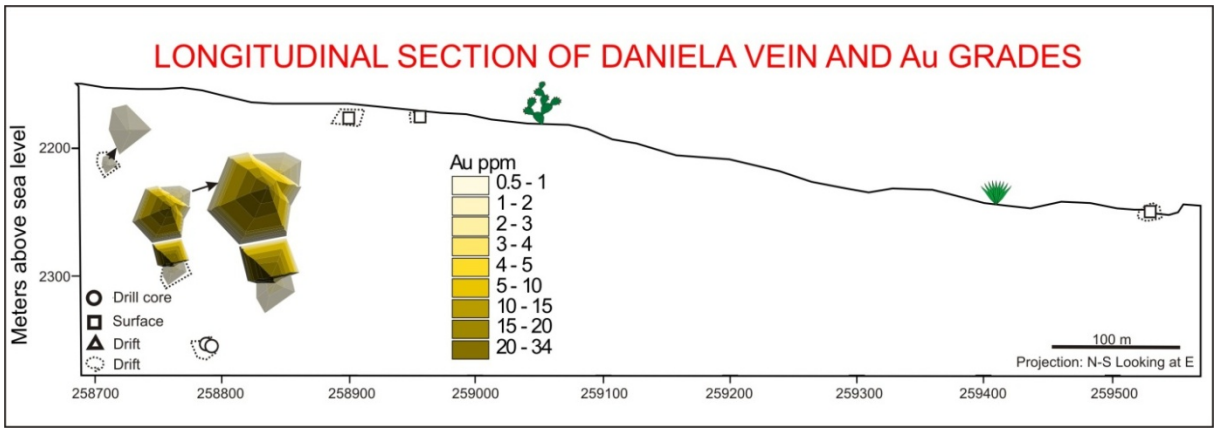

Figure 3.58 Longitudinal section of Daniela vein and silver grades for samples collected.

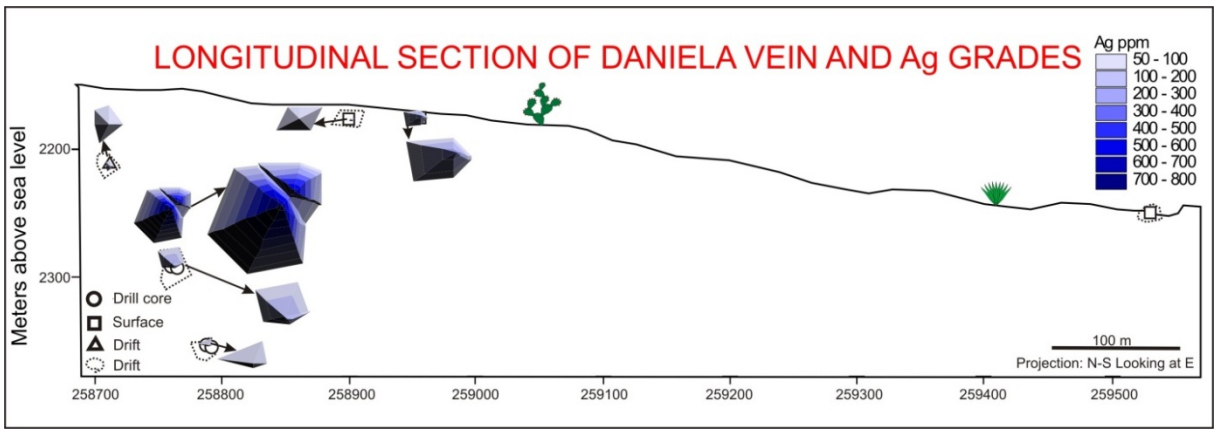

Figure 3.59 Section 28600 showing the Karina and Daniela intersected at different depths by drill holes DN-1, DN-2, and KA-15. At each intersection, the boiling indicators that were observed are listed: (V) Only vapor-rich inclusions, (LS) Liquid-rich with trapped illite (CT) Colloform texture quartz, (PT) Plumose texture quartz, (JT) Jigsaw texture quartz, (BC) Bladed calcite replaced by quartz, (Adu) Adularia, (S/I) Sercite/illite.

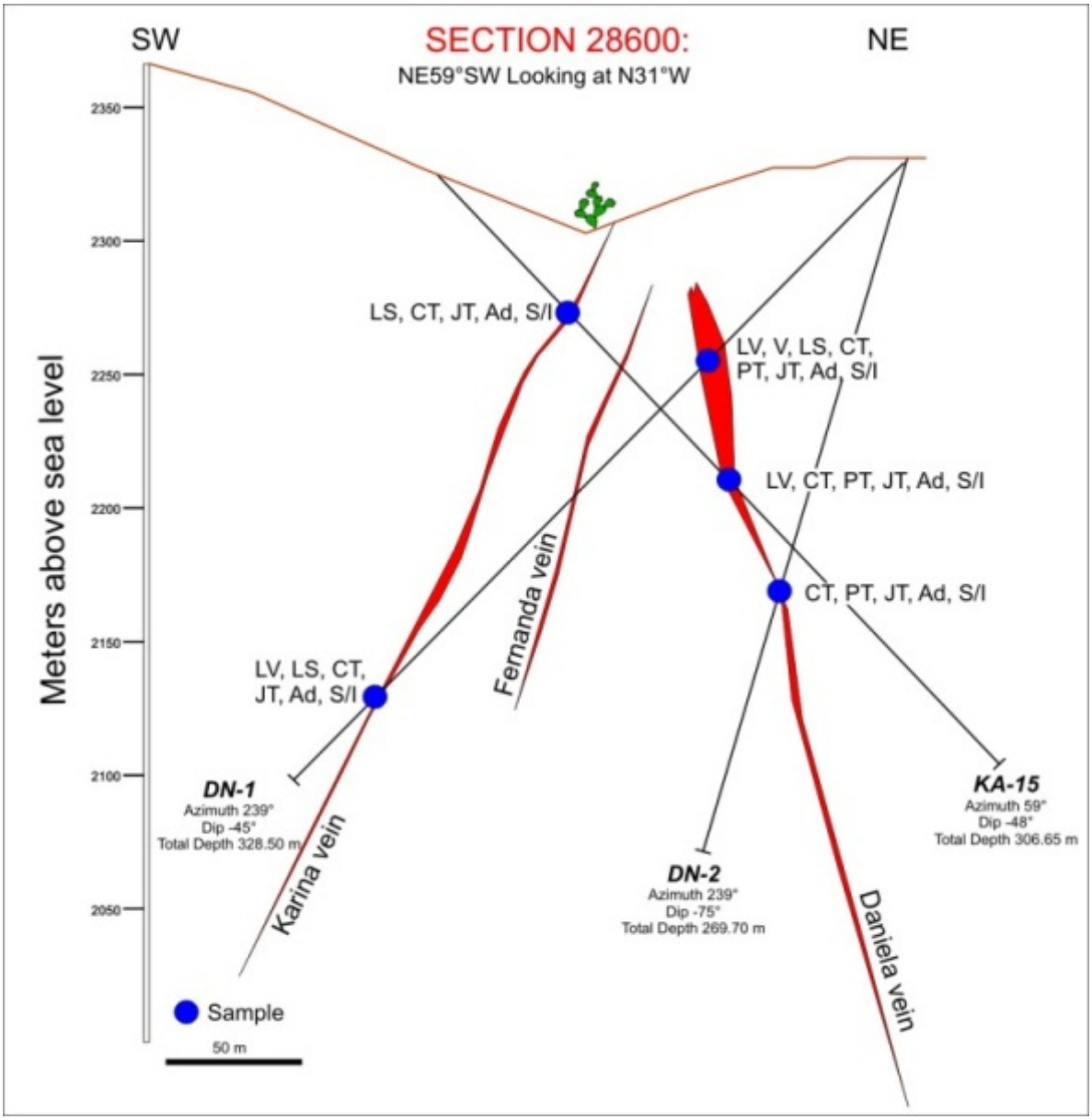

Figure 3.60 Compilation of data from drill holes DN-1, DN-2 and KA-15 that cut the Karina (left) and Daniela (right) veins in section 28600. The top X-axis shows the average gold and silver grades for samples collected as a function of elevation, while the bottom X-axis shows the percentage of samples showing evidence of boiling.

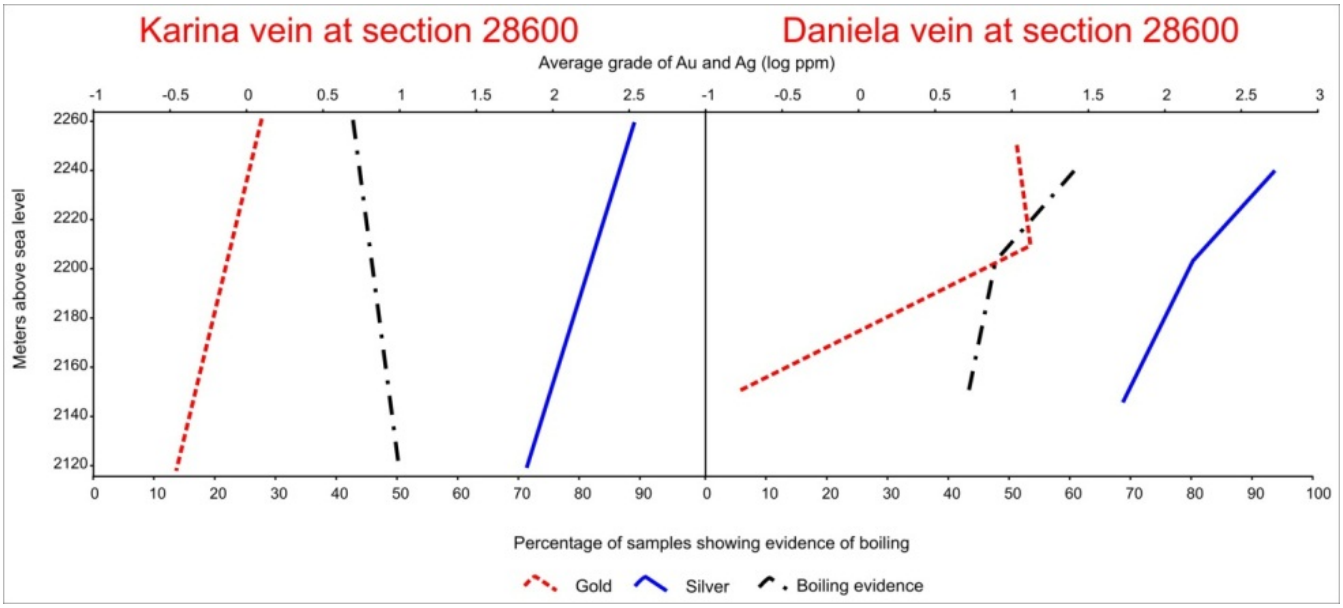

Figure 3.61 Homogenization temperature versus ice-melting temperature for 5 Fluid Inclusion Assemblages (FIAs) from the Plateros vein. Each FIA consists of two or more fluid inclusions with consistent microthermometric behavior. The numbers in each FIA correspond to the notes in the microthermometry table 3.2.

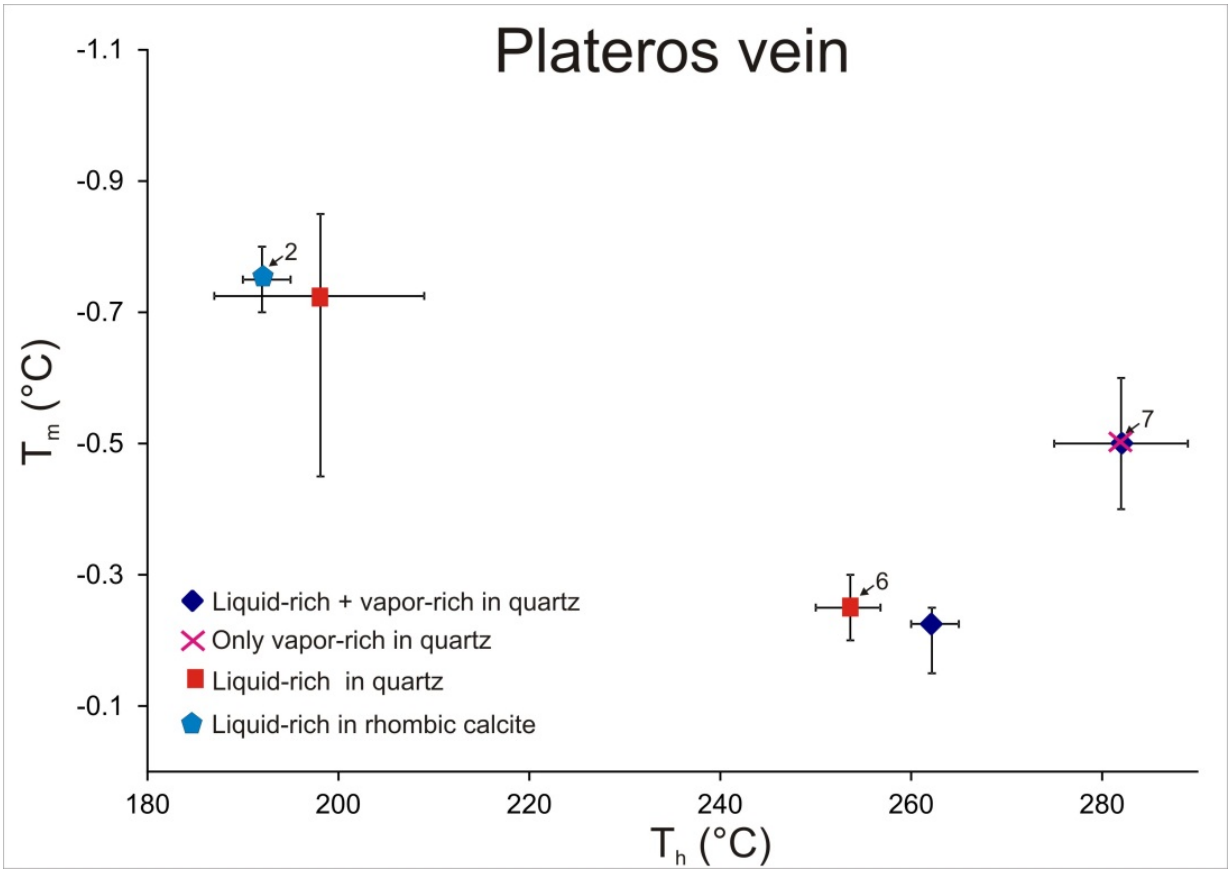

Figure 3.62 Homogenization temperature versus ice-melting temperature for 38 Fluid Inclusion Assemblages (FIAs) from the Melladito vein. Each FIA consists of two or more fluid inclusions with consistent microthermometric behavior. The numbers in each FIA correspond to the notes in the microthermometry table 3.2.

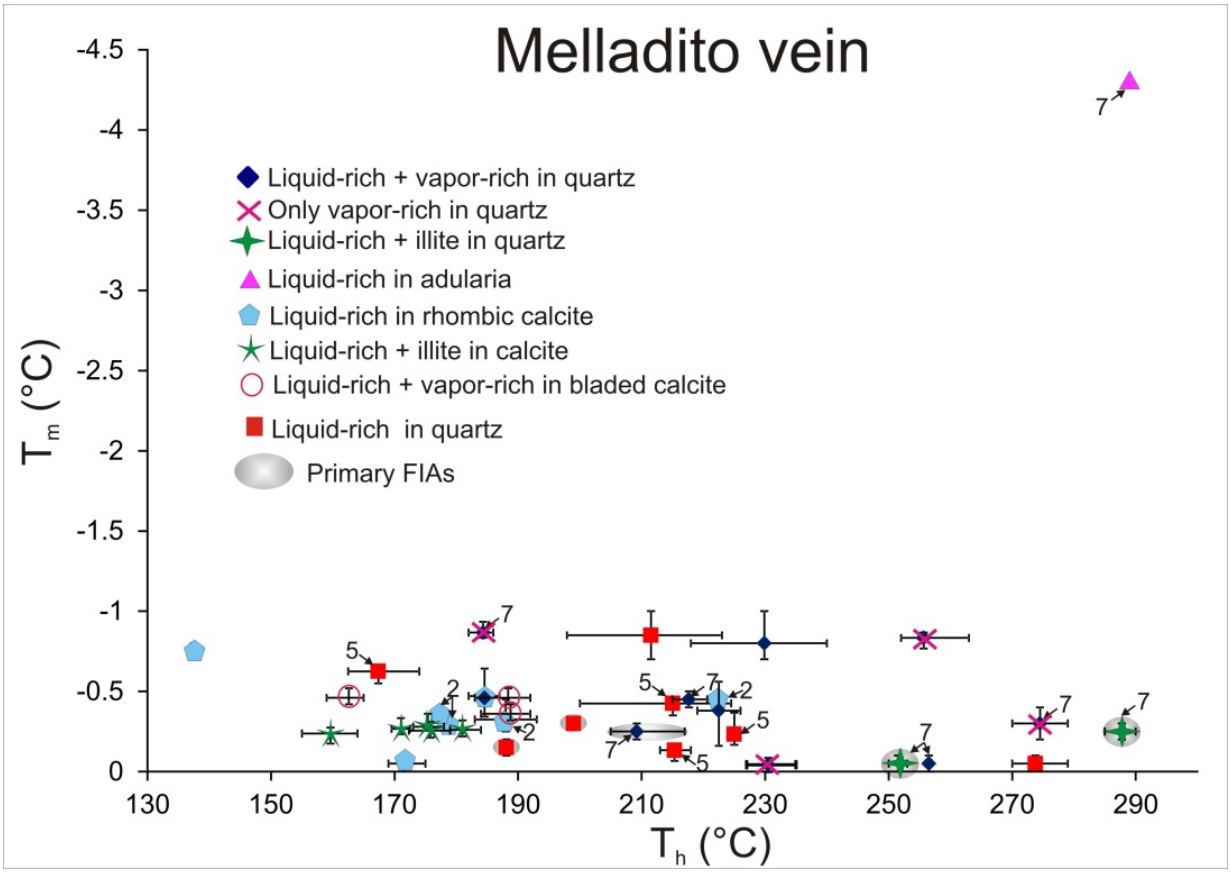

Figure 3.63 Homogenization temperature versus ice-melting temperature for 5 Fluid Inclusion Assemblages (FIAs) from the Intermediate vein. Each FIA consists of two or more fluid inclusions with consistent microthermometric behavior. The numbers in each FIA correspond to the notes in the microthermometry table 3.2.

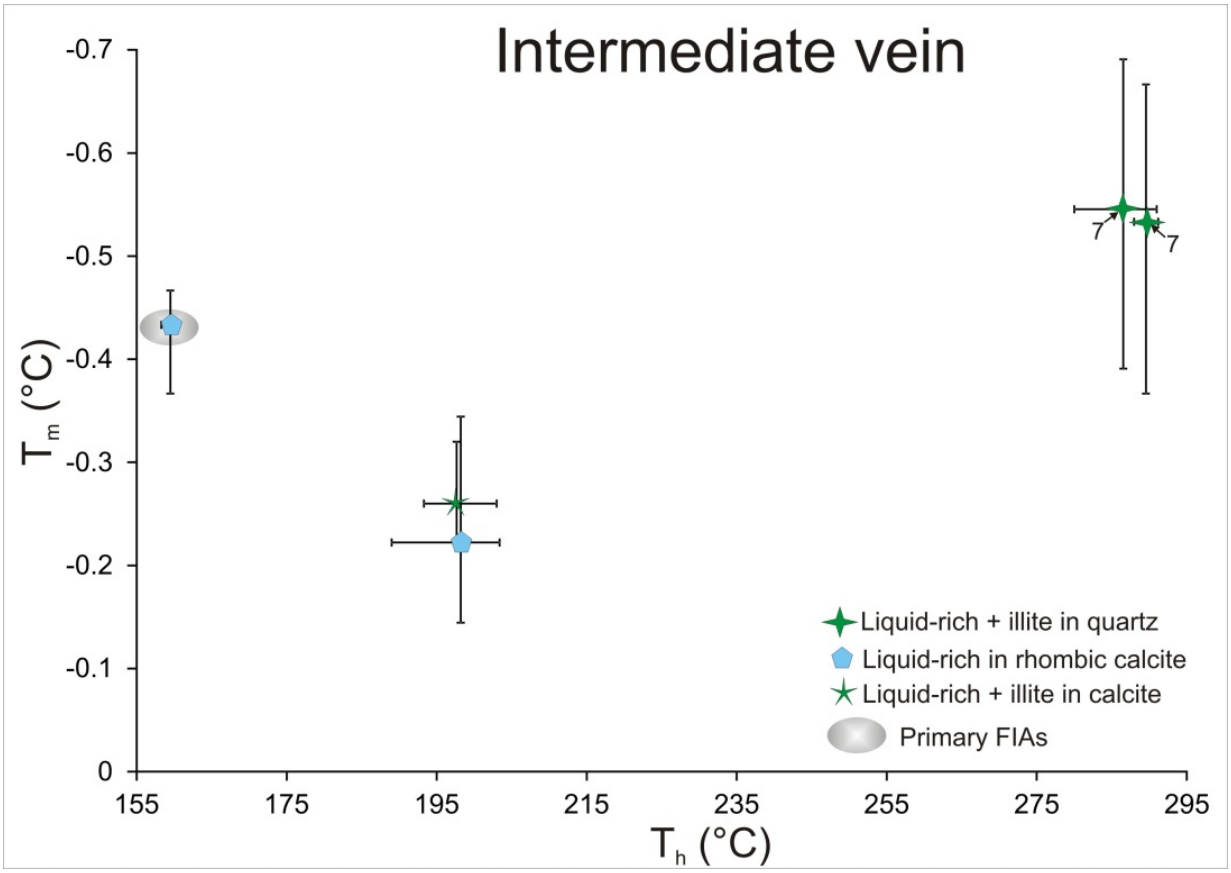

Figure 3.64 Homogenization temperature versus ice-melting temperature for 29 Fluid Inclusion Assemblages (FIAs) from the Nombre de Dios vein. Each FIA consists of two or more fluid inclusions with consistent microthermometric behavior. The numbers in each FIA correspond to the notes in the microthermometry table 3.2.

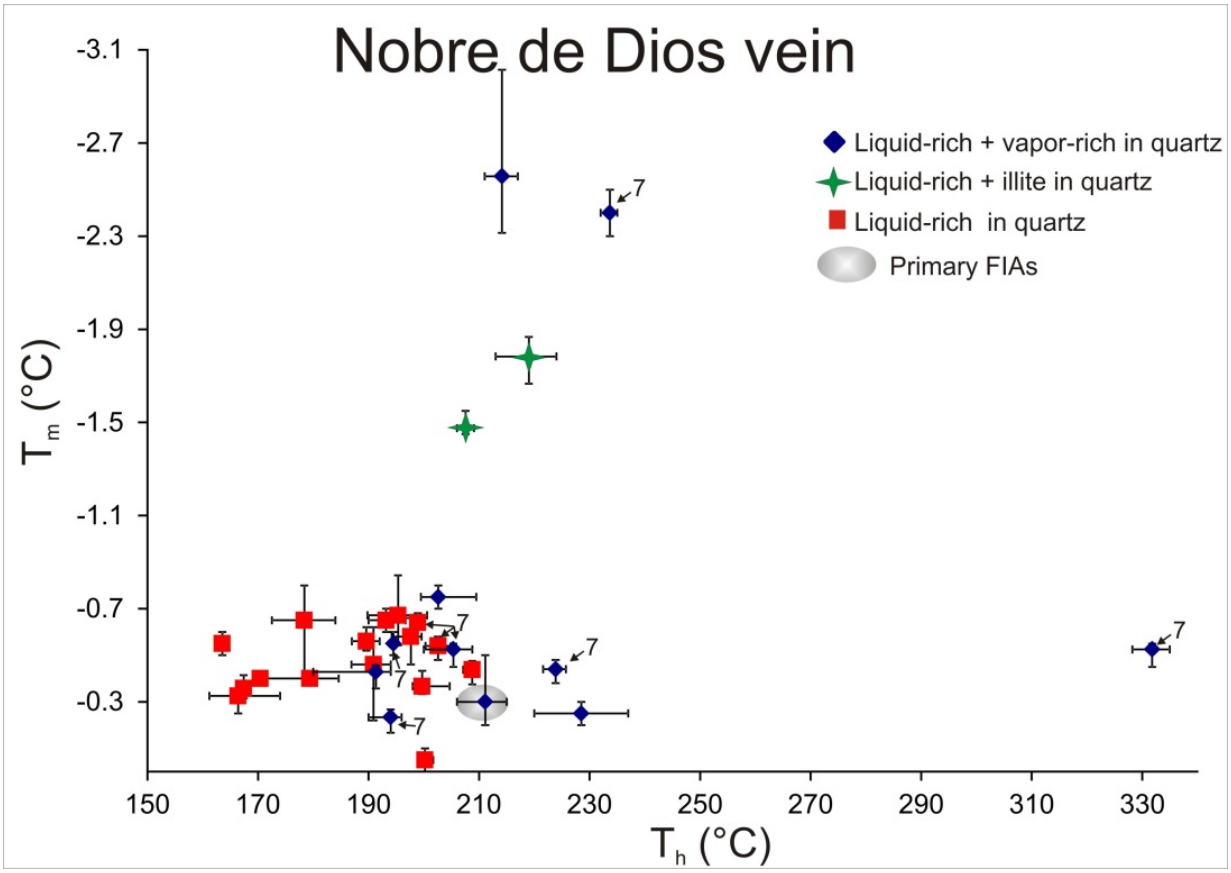

Figure 3.65 Homogenization temperature versus ice-melting temperature for 6 Fluid Inclusion Assemblages (FIAs) from the Bolañitos vein. Each FIA consists of two or more fluid inclusions with consistent microthermometric behavior. The numbers in each FIA correspond to the notes in the microthermometry table 3.2.

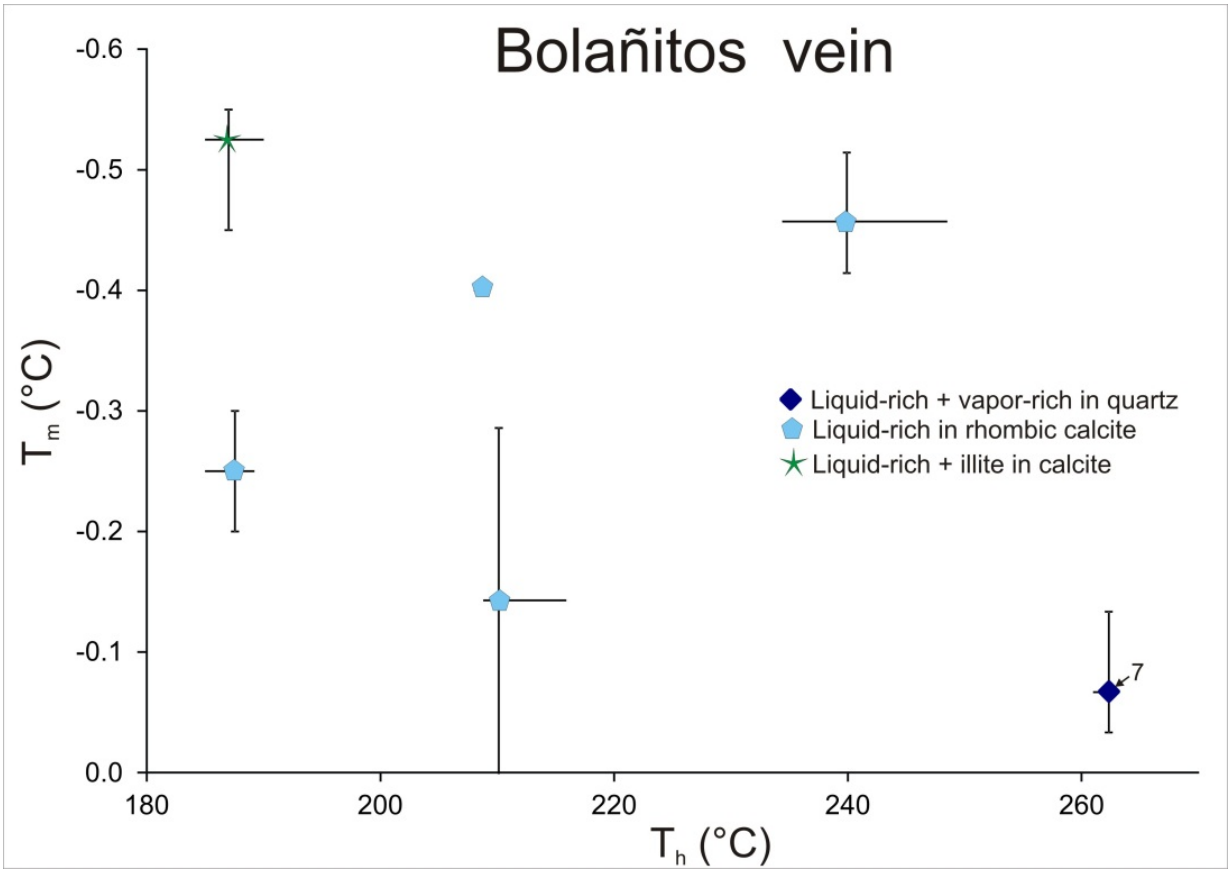

Figure 3.66 Homogenization temperature versus ice-melting temperature for 22 Fluid Inclusion Assemblages (FIAs) from the Lucero vein. Each FIA consists of two or more fluid inclusions with consistent microthermometric behavior. The numbers in each FIA correspond to the notes in the microthermometry table 3.2.

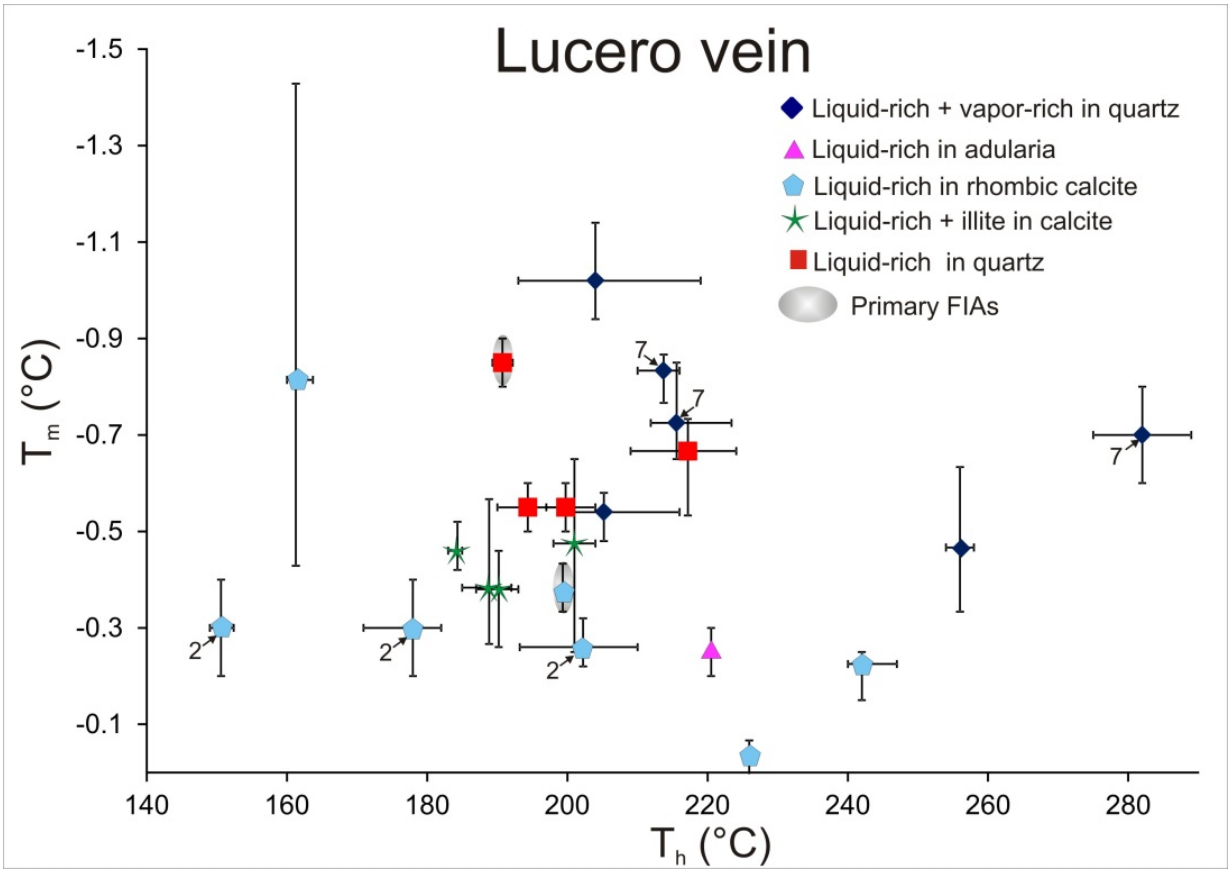

Figure 3.67 Homogenization temperature versus ice-melting temperature for 8 Fluid Inclusion Assemblages (FIAs) from the Karina vein. Each FIA consists of two or more fluid inclusions with consistent microthermometric behavior. The numbers in each FIA correspond to the notes in the microthermometry table 3.2.

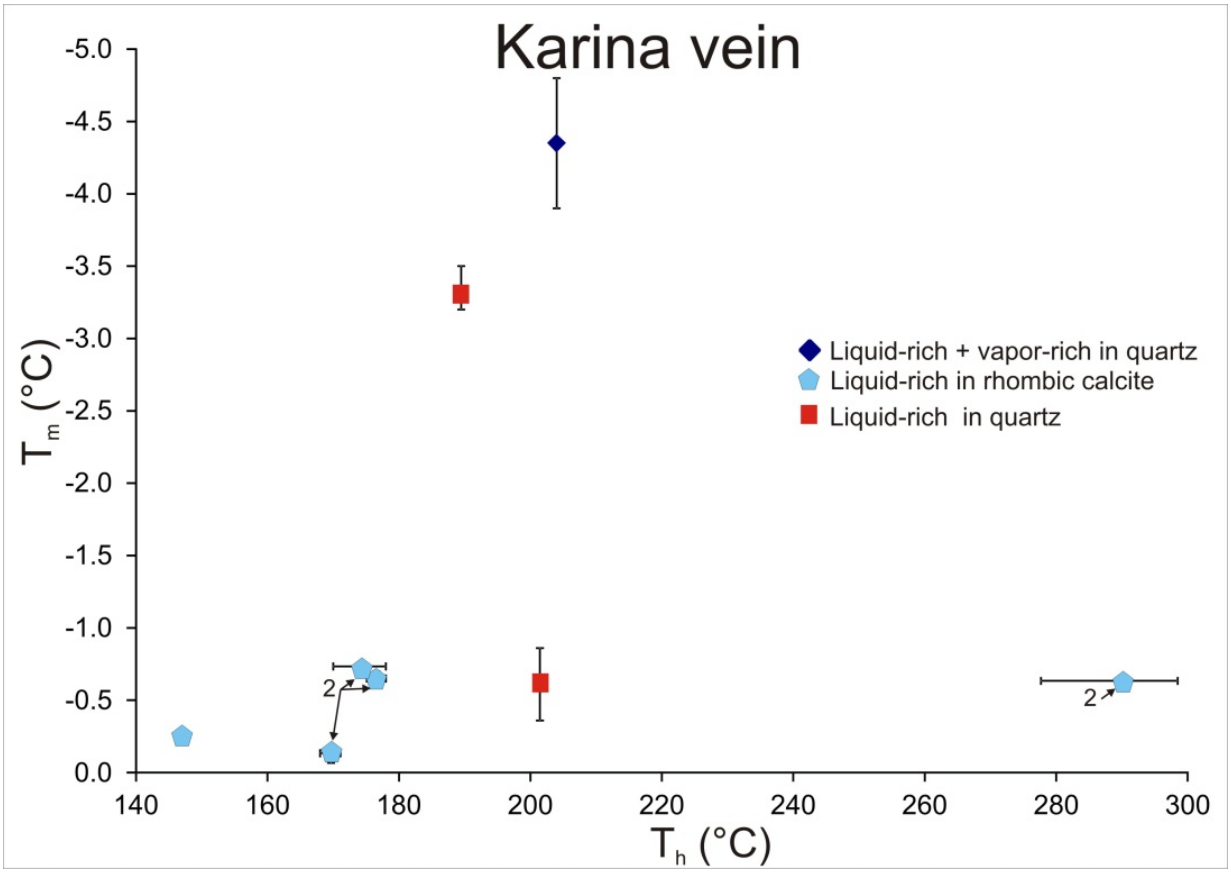

Figure 3.68 Homogenization temperature versus ice-melting temperature for 8 Fluid Inclusion Assemblages (FIAs) from the Daniela vein. Each FIA consists of two or more fluid inclusions with consistent microthermometric behavior. The numbers in each FIA correspond to the notes in the microthermometry table 3.2.

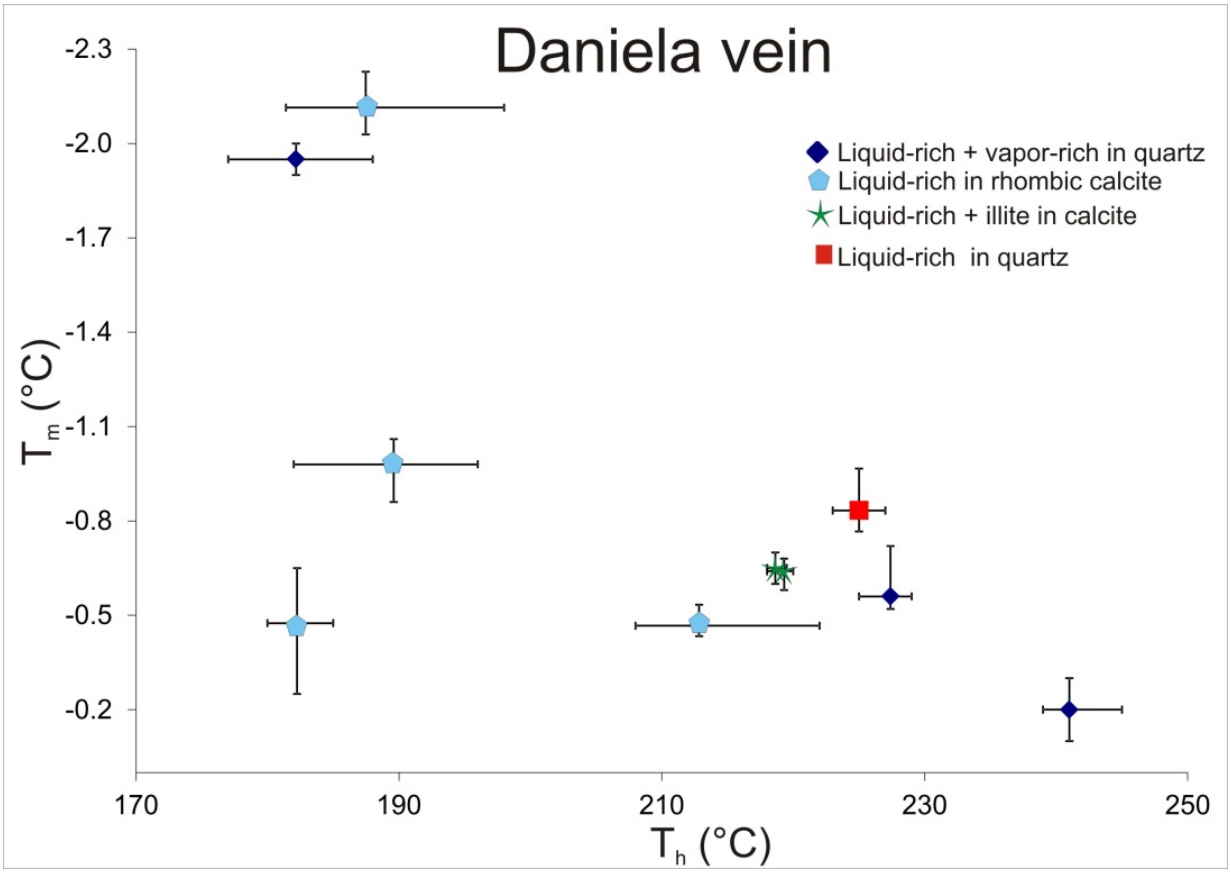

Figure 3.69 Homogenization temperature for individual Fluid inclusions Assemblages (FIAs) as a function of meters above sea level. [2] Calcite with secondary FIAs cemented by jigsaw; [5] FIAs cutting jigsaw texture quartz; IS= [7] Intergrown with sulfides and maybe considered to be ore stage; L+V= coexisting liquid-rich and vapor-rich inclusions with a broad range in liquid-to-vapor ratios; L + illite = Liquid-rich inclusions with trapped illite crystals. FIAs Surface = Liquid-rich fluid inclusions from surface; FIAs (UG/DDH) = Liquid-rich fluid inclusions from underground work and drill core

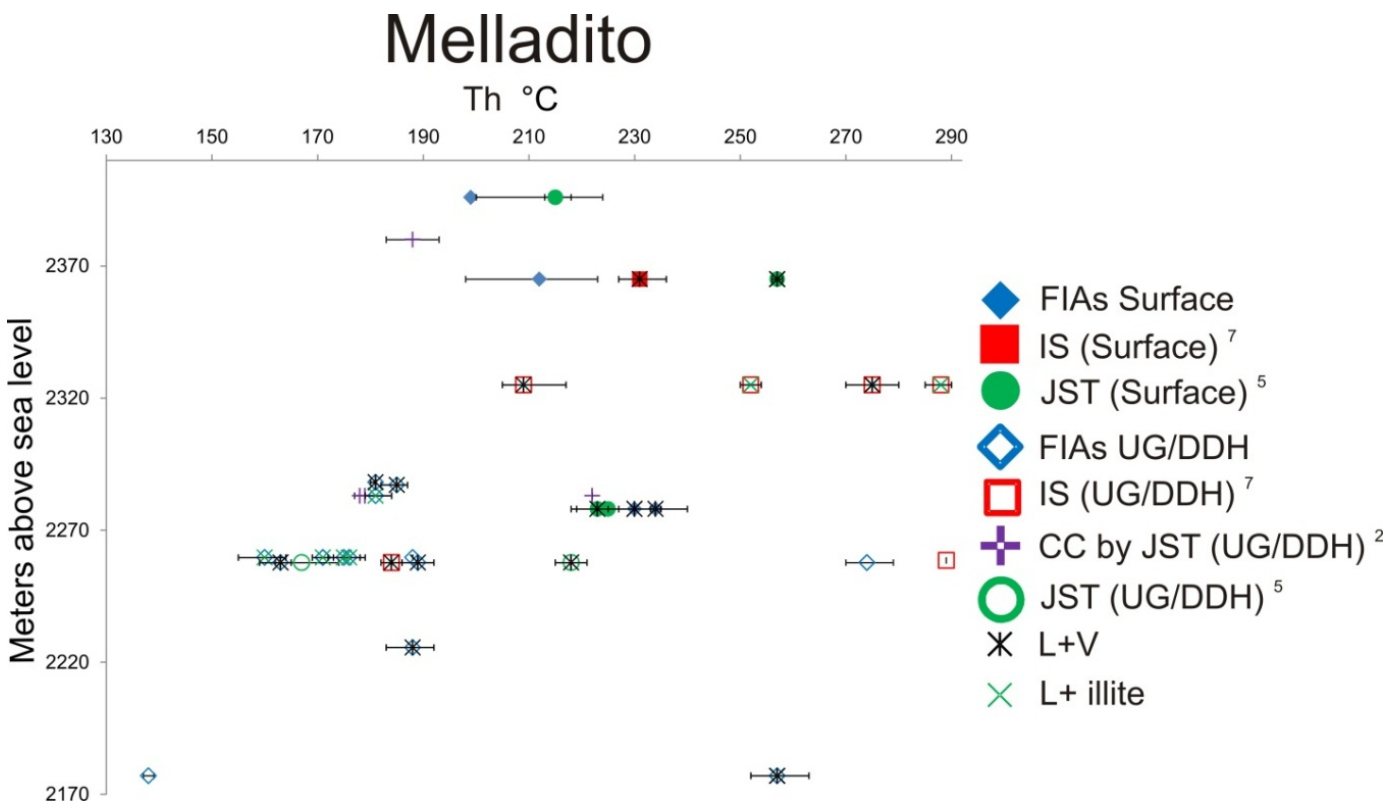

Figure 3.70 Homogenization temperature for individual Fluid inclusions Assemblages (FIAs) as a function of meters above sea level. [2] Calcite with secondary FIAs cemented by jigsaw; IS= [7] Intergrown with sulfides and maybe considered to be ore stage; L+V= coexisting liquid-rich and vapor-rich inclusions with a broad range in liquid-to-vapor ratios; L + illite = Liquid-rich inclusions with trapped illite crystals. FIAs (UG/DDH) = Liquid-rich fluid inclusions from underground work and drill core

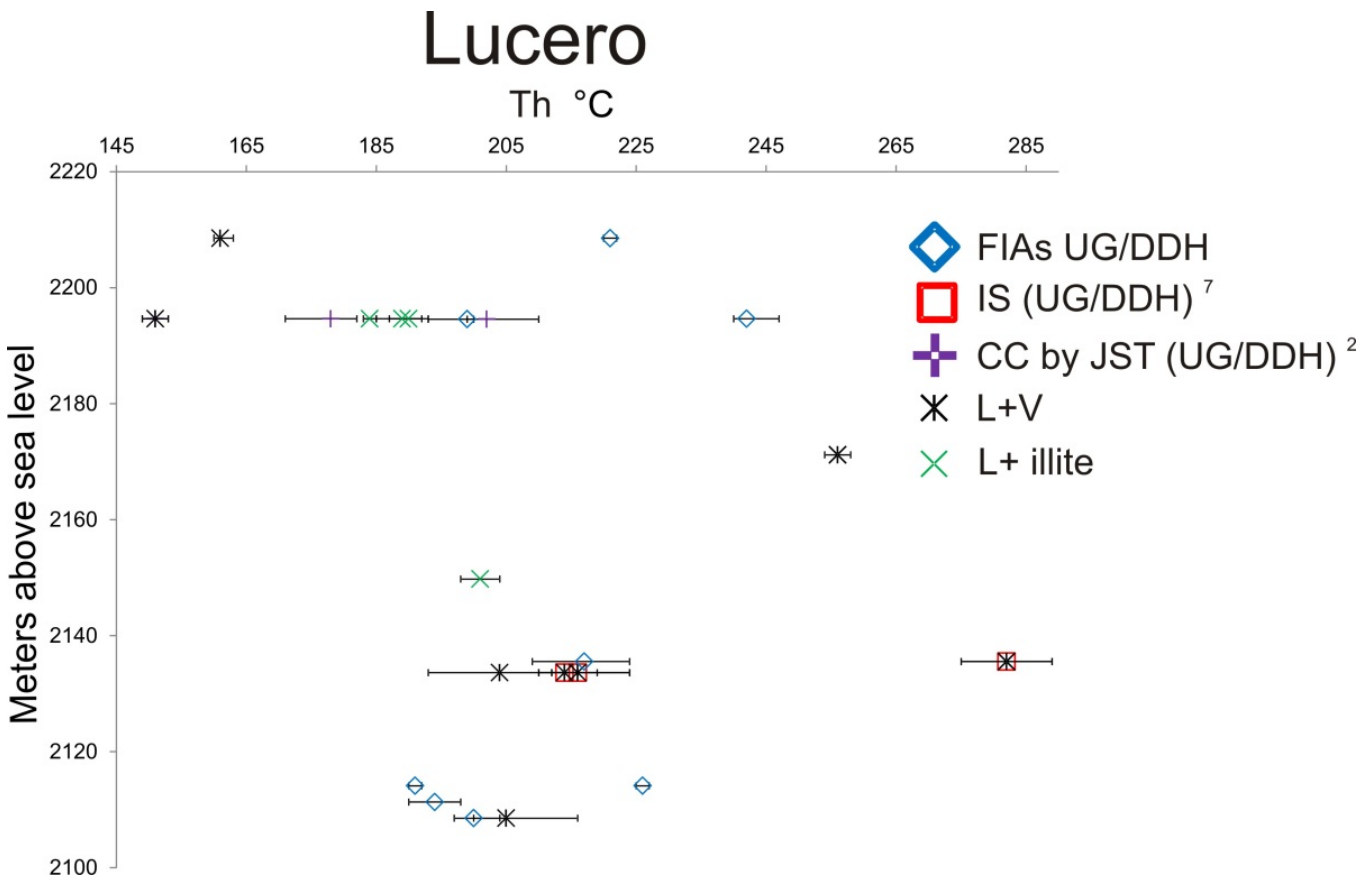

Figure 3.71 Homogenization temperature for individual Fluid inclusions Assemblages (FIAs) as a function of meters above sea level. [5] FIAs cutting jigsaw texture quartz; IS= [7] Intergrown with sulfides and maybe considered to be ore stage; L+V= coexisting liquid-rich and vapor-rich inclusions with a broad range in liquid-to-vapor ratios; L + illite = Liquid-rich inclusions with trapped illite crystals. FIAs Surface = Liquid-rich fluid inclusions from surface; FIAs (UG/DDH) = Liquid-rich fluid inclusions from underground work and drill core

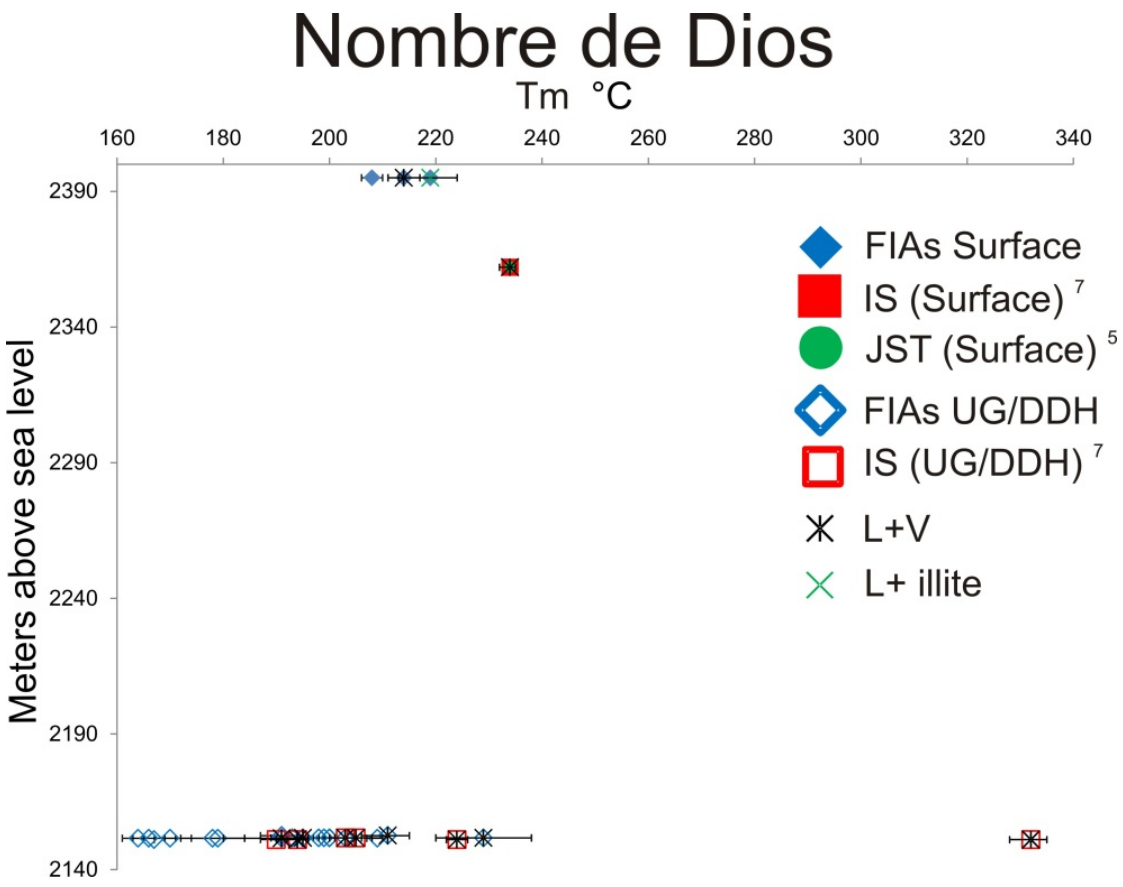

Figure 3.72 Ice-melting temperatures for individual Fluid inclusions Assemblages (FIAs) as a function of meters above sea level. [2] Calcite with secondary FIAs cemented by jigsaw; [5] FIAs cutting jigsaw texture quartz; [7] Intergrown with sulfides and maybe considered to be ore stage; L+V= coexisting liquid-rich and vapor-rich inclusions with a broad range in liquid-to-vapor ratios; L + illite = Liquid-rich inclusions with trapped illite crystals. FIAs Surface = Liquid-rich fluid inclusions from surface; FIAs (UG/DDH) = Liquid-rich fluid inclusions from underground work and drill core

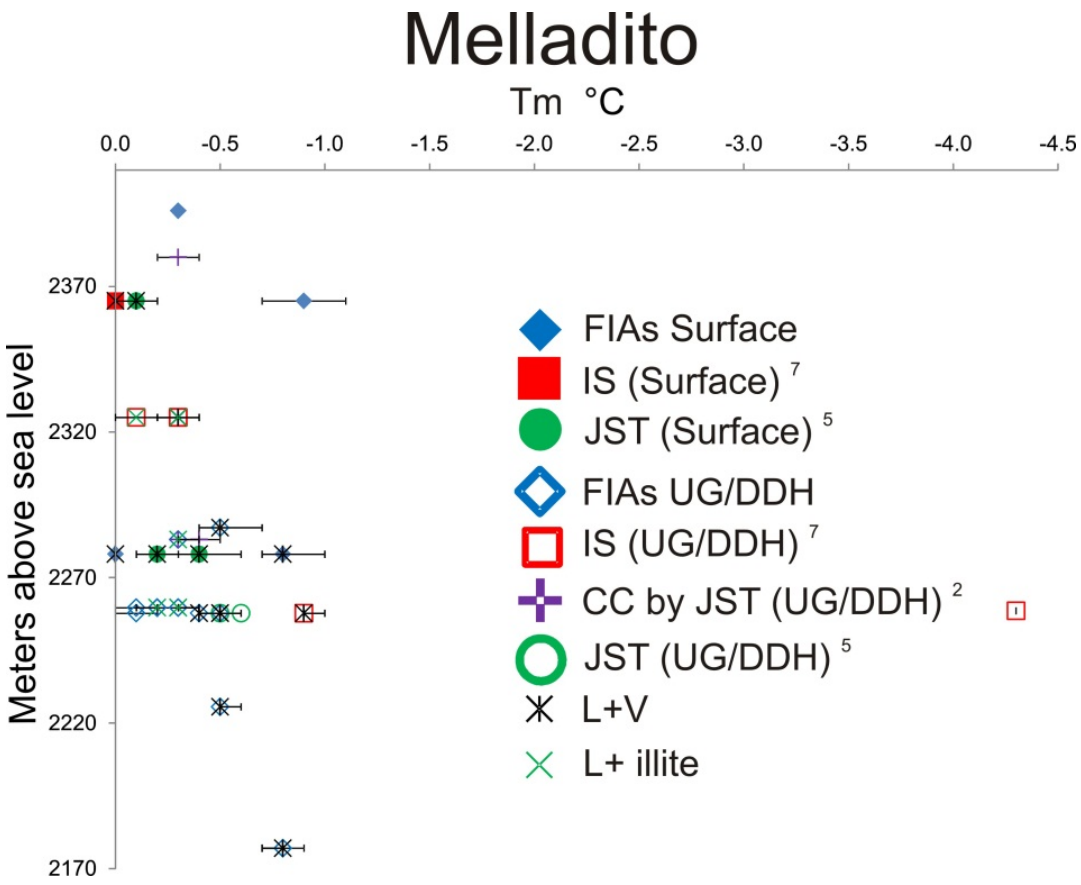

Figure 3.73 Ice-melting temperatures for individual Fluid inclusions Assemblages (FIAs) as a function of meters above sea level. [2] *Calcite with secondary FIAs cemented by jigsaw;* [7] *Intergrown with sulfides and maybe considered to be ore stage; L+V= coexisting liquid-rich and vapor-rich inclusions with a broad range in liquid-to-vapor ratios; L + illite = Liquid-rich inclusions with trapped illite crystals; FIAs (UG/DDH) = Liquid-rich fluid inclusions from underground work and drill core.*

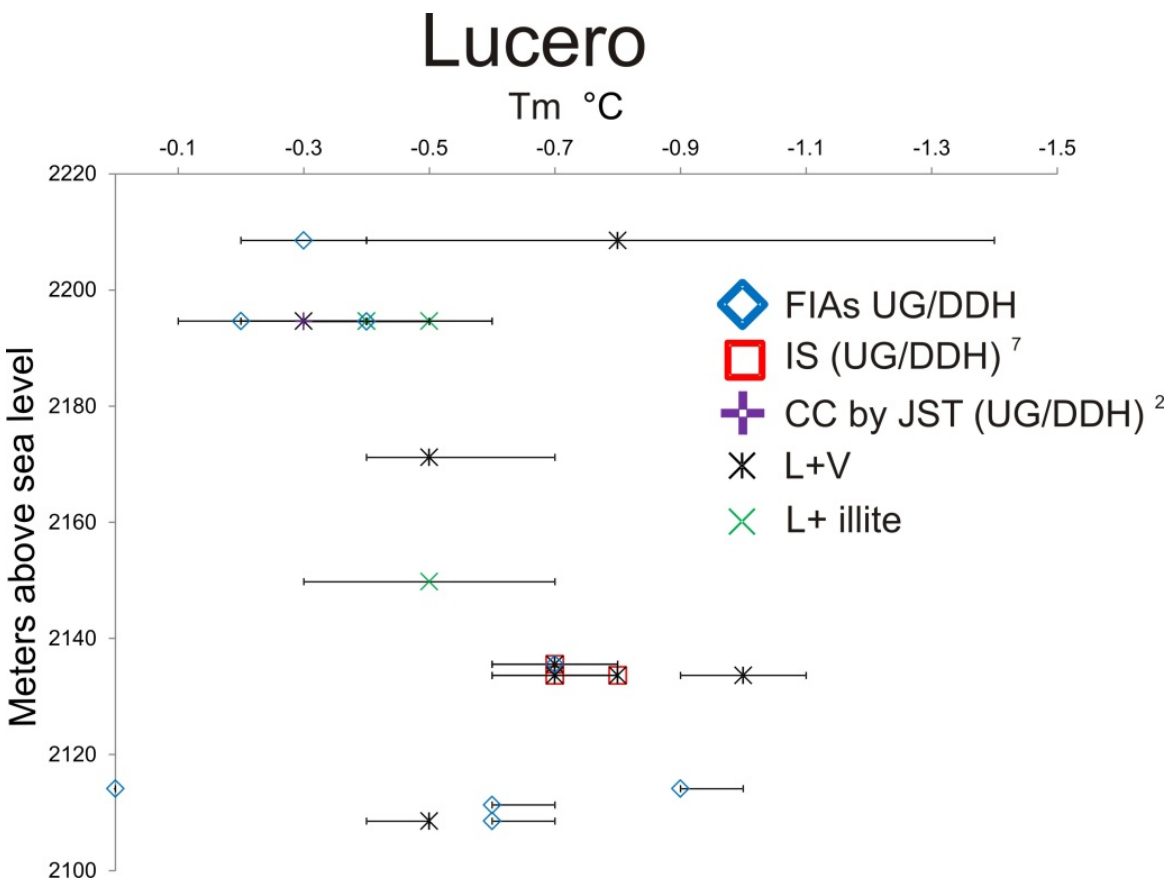

Figure 3.74 Ice-melting temperatures for individual Fluid inclusions Assemblages (FIAs) as a function of meters above sea level from Nombre de Dios vein. [5] FIAs cutting jigsaw texture quartz; [7] Intergrown with sulfides and maybe considered to be ore stage; L+V= coexisting liquid-rich and vapor-rich inclusions with a broad range in liquid-to-vapor ratios; L + illite = Liquid-rich inclusions with trapped illite crystals. FIAs Surface = Liquid-rich fluid inclusions from surface; FIAs (UG/DDH) = Liquid-rich fluid inclusions from underground work and drill core

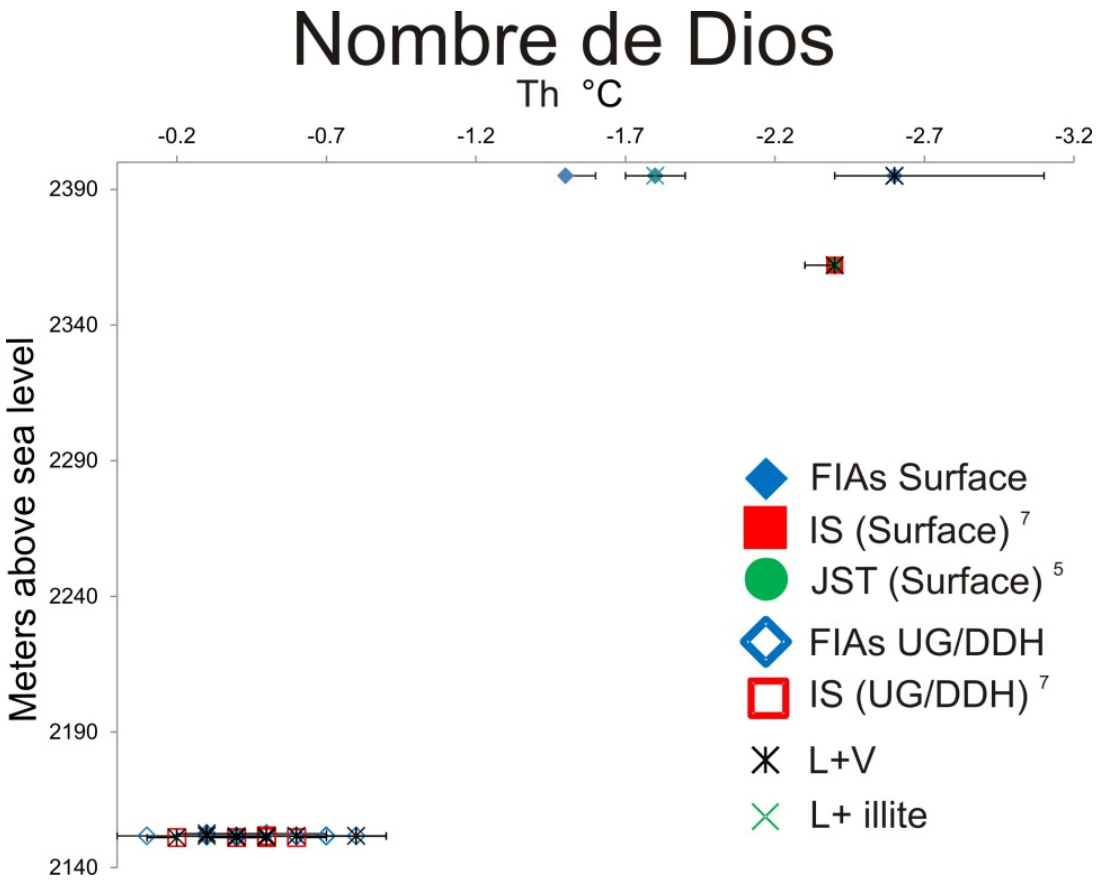

Figure 3.75 Paragenesis and homogenization temperature (above) Ice-melting temperatures (below). S= secondary fluid inclusions; P= primary fluid inclusions; CJ= Calcite with secondary FIAs cemented by jigsaw; JT= FIAs cutting jigsaw texture quartz; PT = FIAs cutting plumose texture quartz.

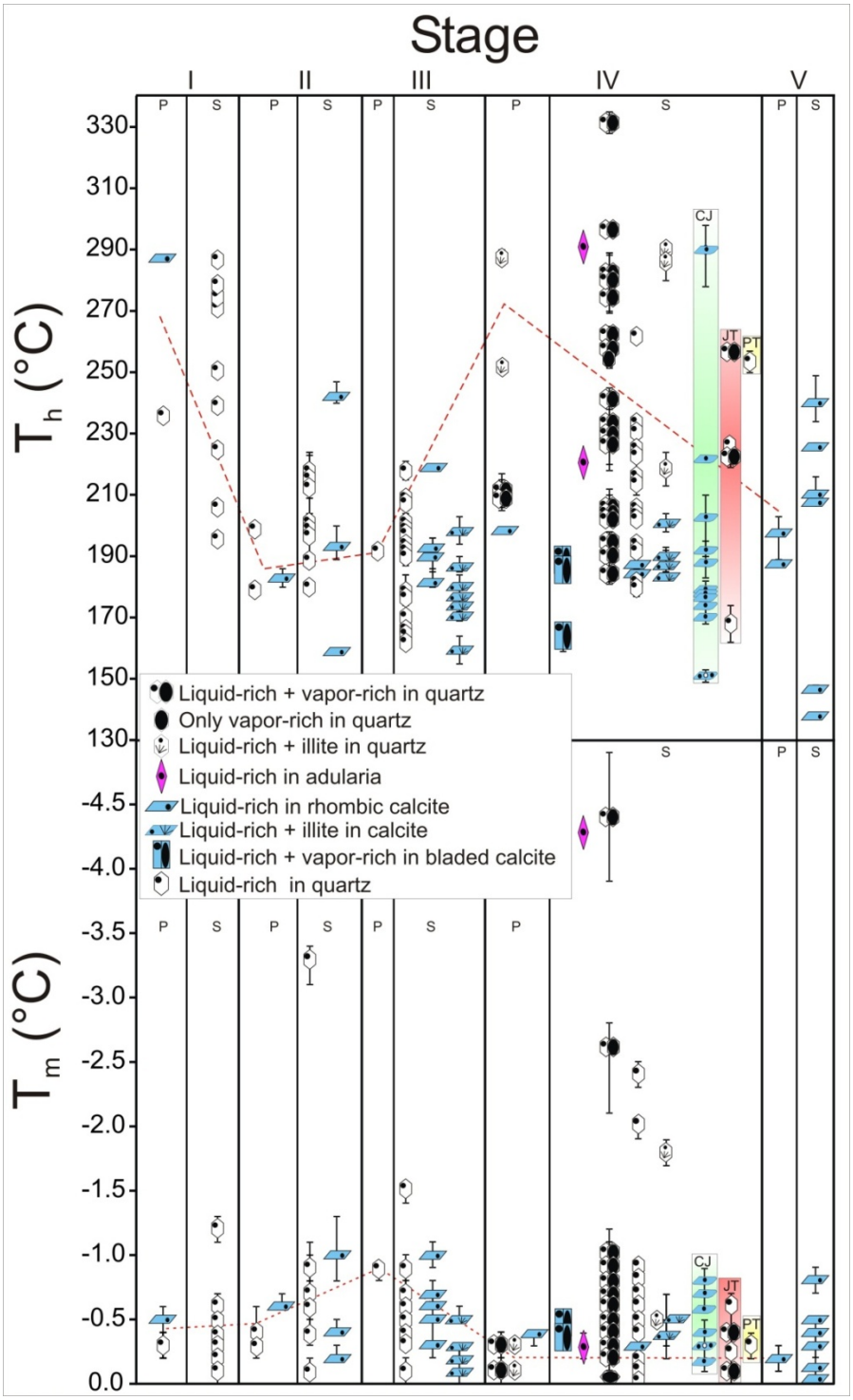

Figure 3.76 Trace elements content of veins from La Luz system and the ice-melting point. The box with pink color represent the range were the samples collected perpendicular 240 azimuth.

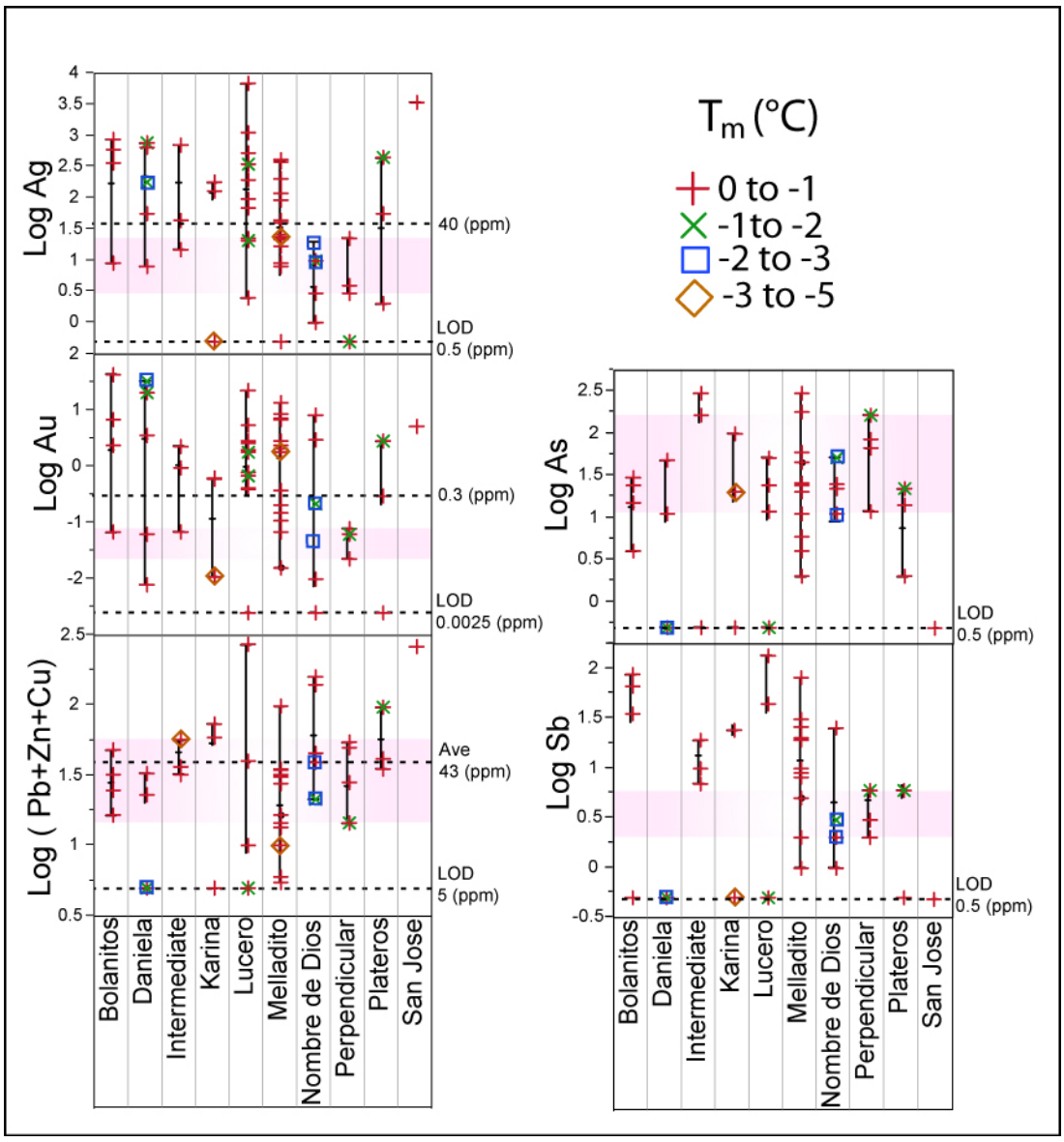

Figure 3.77 Metal budget from La Luz system veins. The dash lines represent the location of samples collected perpendicular 240 azimuth with respect to the ternary diagram.

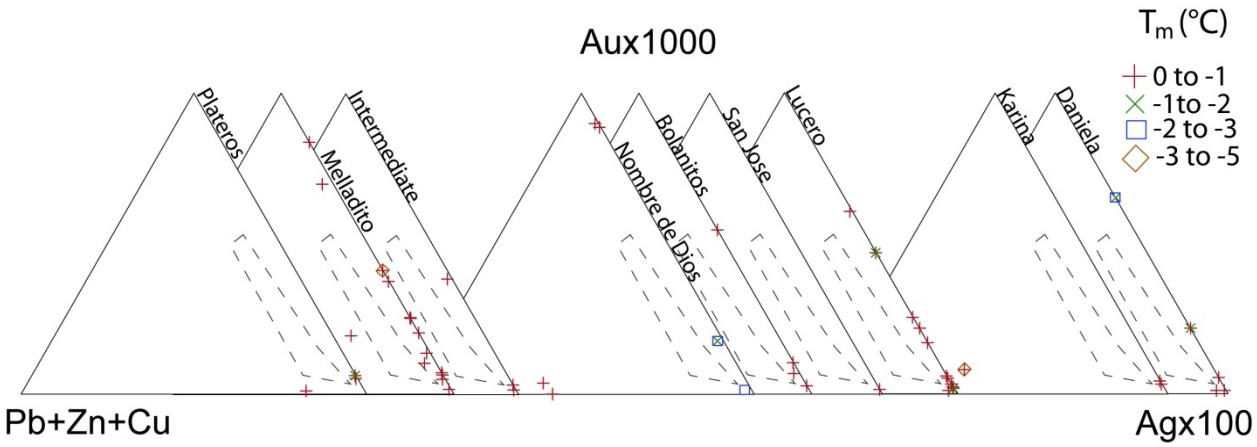

Figure 3.78 Results of reconnaissance microthermometric analyses shown by the blue dots, and the projected 300 °C isotherms from Plateros vein.

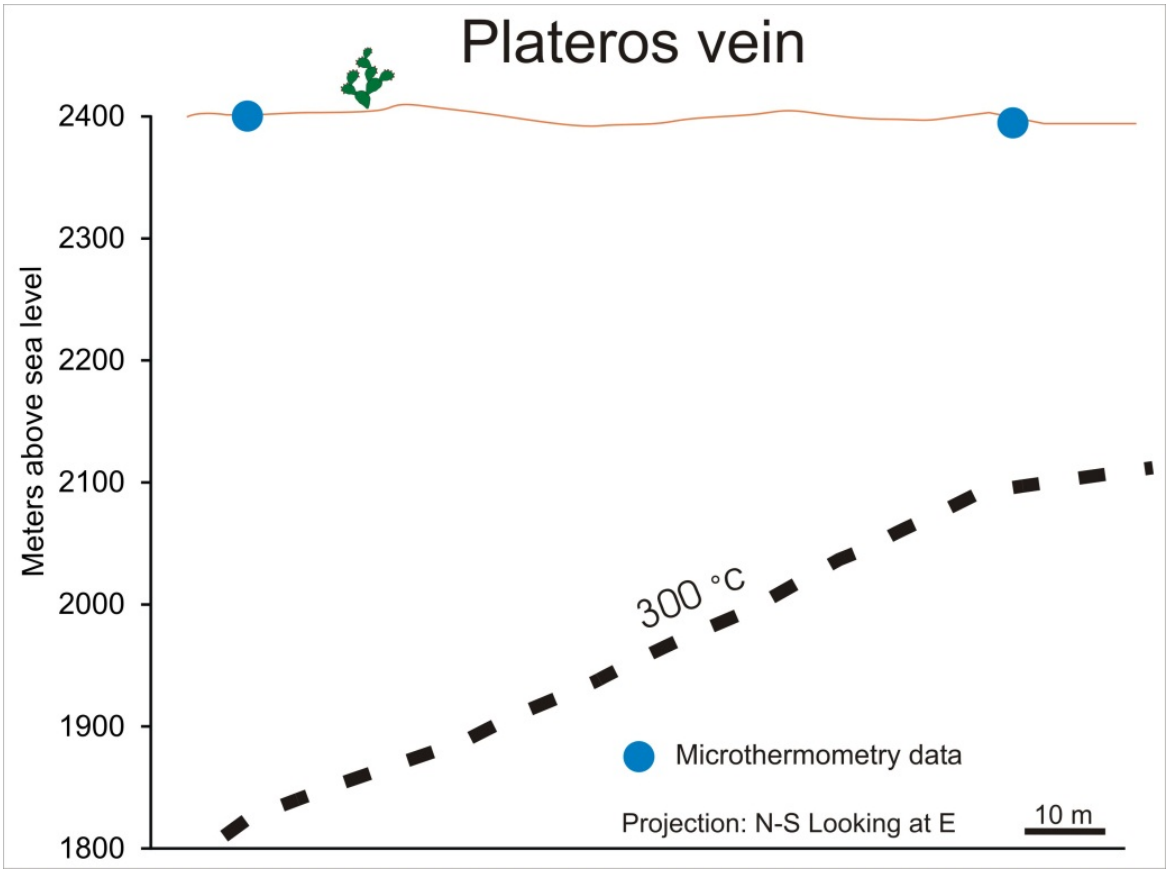

Figure 3.79 Results of reconnaissance microthermometric analyses shown by the blue dots, and the projected depths to the 250 °C and 300 °C isotherms from Melladito vein.

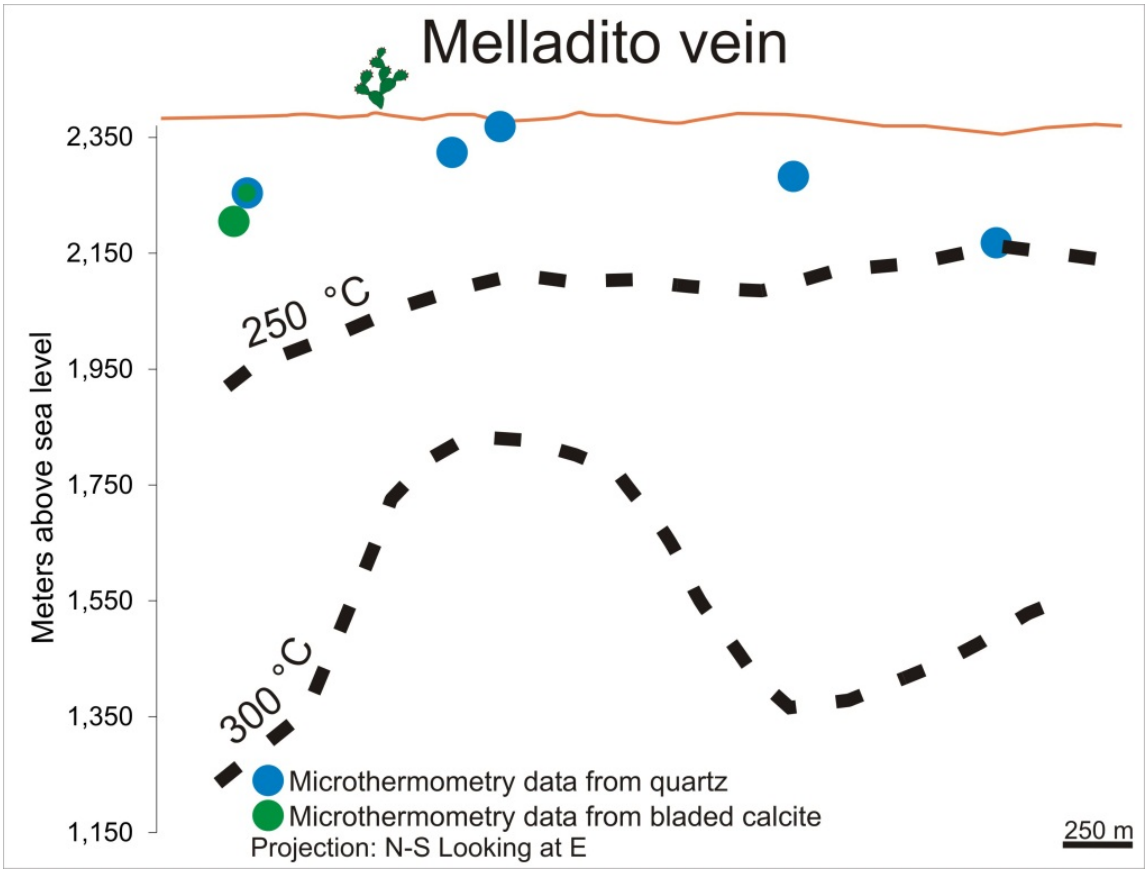

Figure 3.80 Results of reconnaissance microthermometric analyses shown by the blue dots, and the projected depths to the 250 and 300 °C isotherms from Melladito vein.

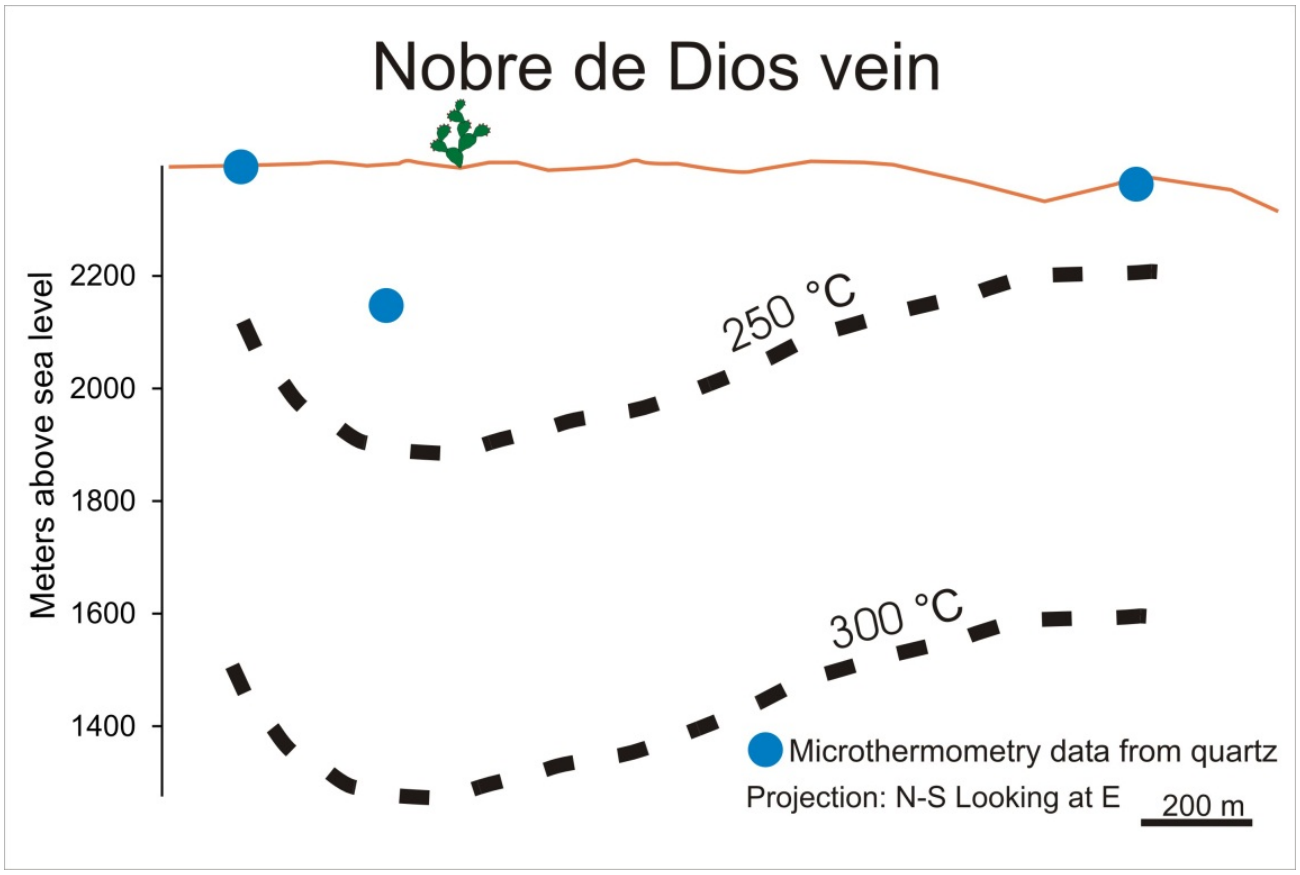

Figure 3.81 Results of reconnaissance microthermometric analyses shown by the blue dots, and the projected depths to the 250 and 300 °C isotherms from Melladito vein.

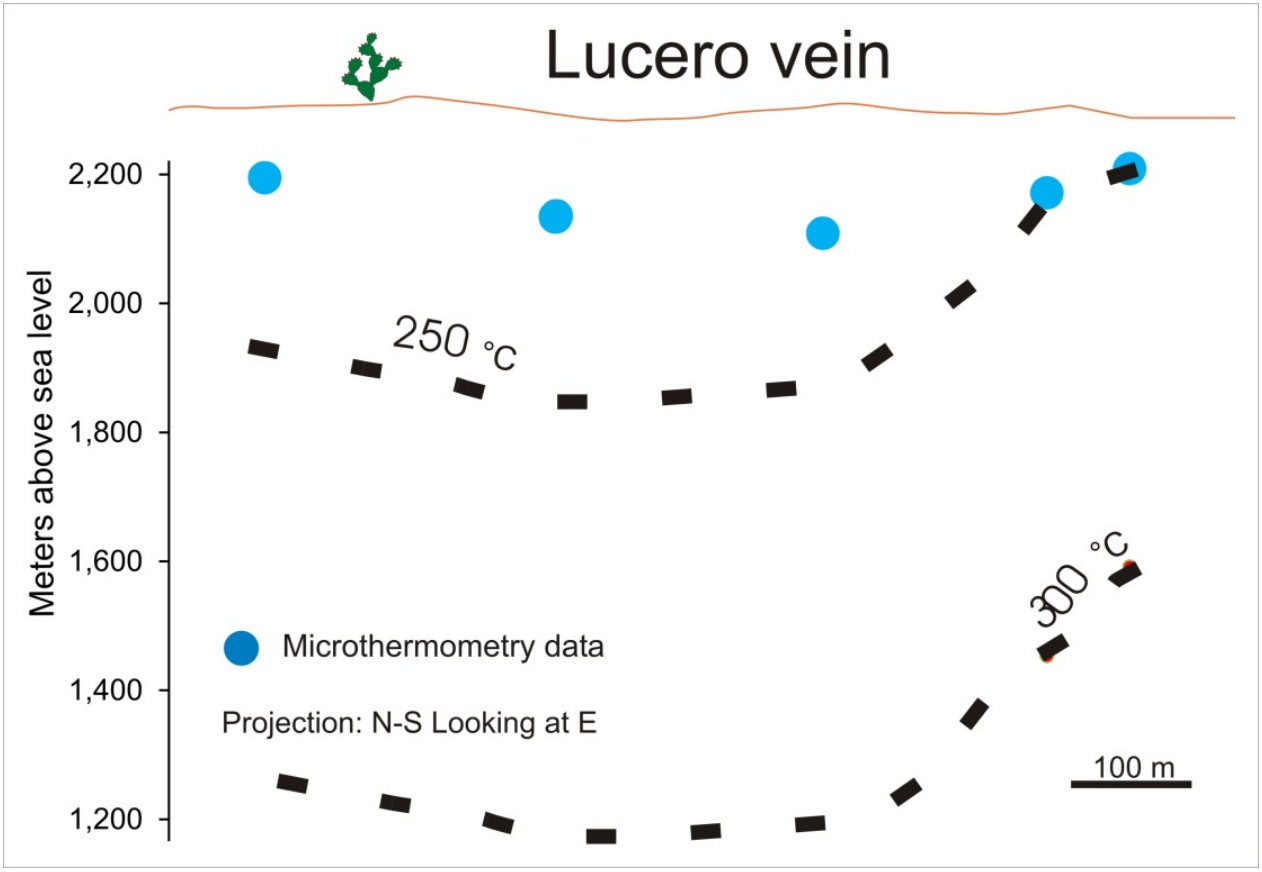

Figure 3.82 Three dimensional view of the Lucero vein with targets for exploration identified by red arrows. Boiling features observed in each sample include: (LV) Coexisting liquid-rich and vapor-rich inclusions, (V) Only vapor-rich inclusions, (LS) Liquid-rich inclusions with trapped illite, (CT) Colloform texture quartz, (PT) Plumose texture quartz, (JT) Jigsaw texture quartz, (Adu) Adularia, (S/I) Sericite/illite.

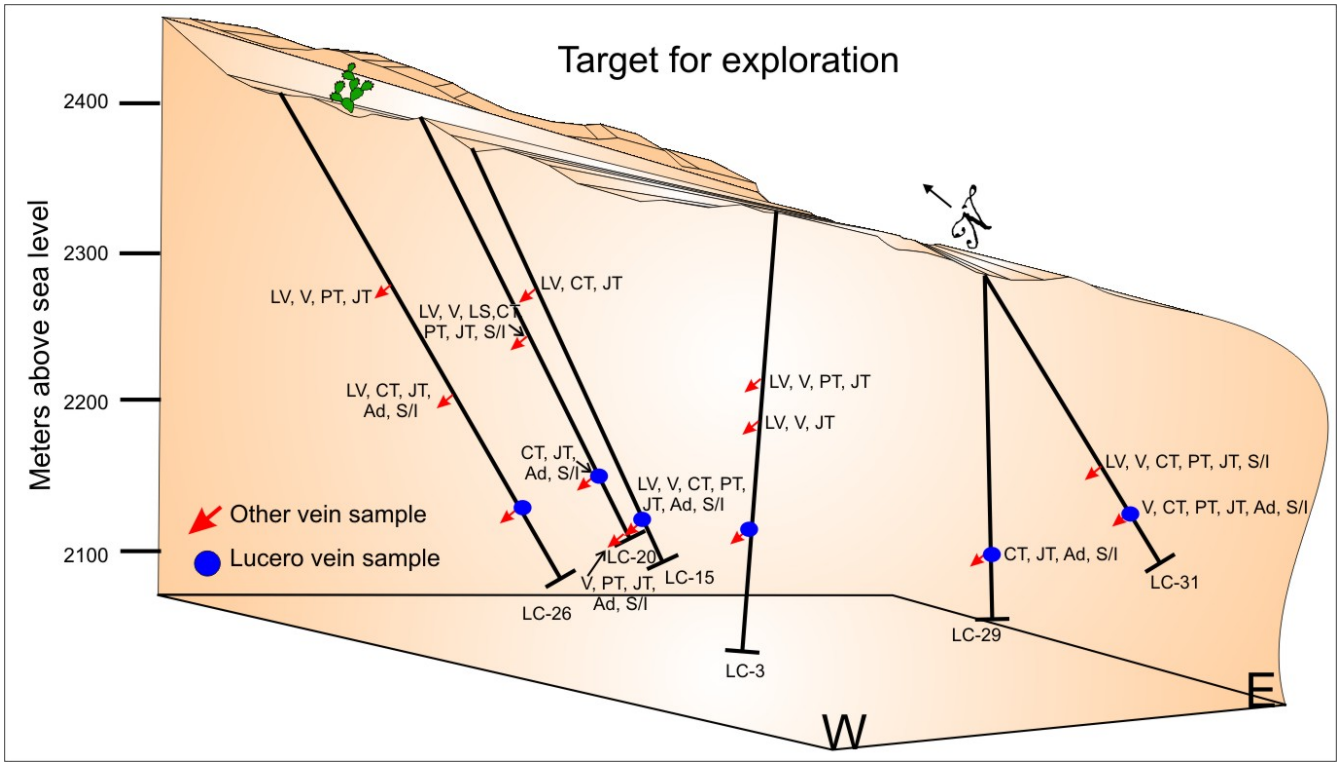

Figure 3.83 Pressure recorded in different veins in la Luz system.

The hydrostatic curves for composition 1 and 7 wt. % NaCl Khaibullin and Borisov (1966) and pure H_2O E.W. Lemmon et al. (2012). P = Primary fluid inclusions. Each point represent single FIAs and maximum and minimum temperature and pressure.

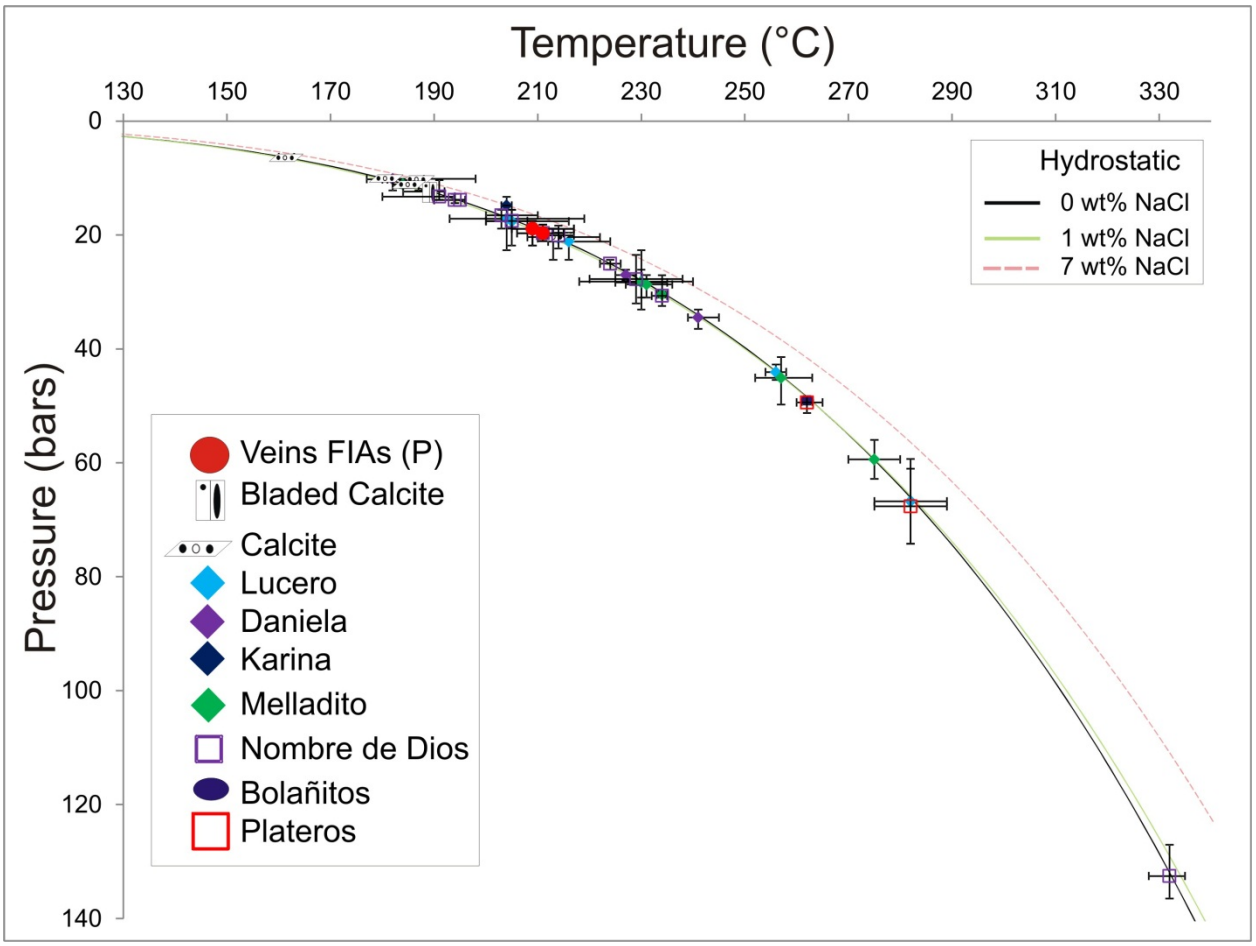

Table 3.1 Samples from drill cores 9 and 14 that cut the Melladito, Intermediate, and Nombre de Dios veins, and textural and fluid inclusion evidence of boiling. 0 = Absent; 1 = Present; LV = Coexisting liquid-rich and vapor-rich inclusions with a broad range in liquid-to-vapor ratios; V = Assemblages consisting of only vapor-rich inclusions; CT= Colloform texture quartz; PT = Plumose texture quartz; JT = Jigsaw texture quartz; BC= Bladed calcite or bladed calcite replaced by quartz; Ad= Adularia; Ca= Rhombic calcite.

Drill Hole	Vein	Sample ID	Au (ppm)	Ag (ppm)	LV	V	CT	PT	JT	BC	Ad	Ca
DDH-9	Melladito	1305-267	3.0	35	0	0	1	0	1	0	1	0
DDH-14	Melladito	1305-268	0.2	6	0	0	1	0	1	0	0	1
DDH-14	Intermediate	1305-269	0.0	3	0	0	1	1	1	0	0	1
DDH-14	Intermediate	1305-270	0.8	83	1	0	1	1	1	0	0	1
DDH-9	Intermediate	1305-263	0.3	34	0	0	1	0	1	0	0	0
DDH-9	Intermediate	1305-264	2.3	709	0	1	1	1	1	0	0	1
DDH-14	Nombre de Dios	1305-271	0.0	1	1	1	0	1	0	0	0	1
DDH-14	Nombre de Dios	1305-272	0.0	1	1	1	1	1	1	0	0	1
DDH-9	Nombre de Dios	1305-265	8.3	10	1	1	1	1	1	0	0	1
DDH-9	Nombre de Dios	1305-266	3.0	3	1	1	1	1	1	1	0	1

Table 3.2 Fluid Inclusion Heating and Freezing Results from the La Luz area S= secondary fluid inclusions; P= primary fluid inclusions; Th= homogenization temperature; Tm= ice melting temperature; n= number of fluid inclusion; L-rich = only liquid-rich inclusions with consistent liquid-to-vapor ratios; LV= coexisting liquid-rich and vapor-rich inclusions with a broad range in liquid-to-vapor ratios; L + illite = Liquid-rich inclusions with trapped illite crystals; V-rich= assemblages consisting of only vapor-rich inclusions; [1]Wt. % NaCl equiv from Bodnar (1993); [2] Calcite with secondary FIAs cemented by jigsaw; [3] FIAs cutting jigsaw texture quartz; [4] FIAs cutting plumose texture quartz; [5] Intergrown with sulfides and maybe considered to be ore stage

Sample	Host	Vein	Type	n	T_h range (°C)	Ave.	T_m range (°C)	Ave.	wt. % NaCl equiv[1]	Ave.	Notes
1401-37	Calcite	Bolañitos	S	7	234-249	240	-0.4 to -0.5	-0.5	0.7 to 0.9	0.8	1401-37I, FIA#5, L-rich, Stage V
1401-38	Calcite	Bolañitos	S	7	209-216	210	0 to -0.4	-0.1	0 to 0.7	0.3	1401-38BII, FIA#7, L-rich, Stage V
1401-38	Calcite	Bolañitos	S	2	208-209	208	-0.4 to -0.4	-0.4	0.7 to 0.7	0.7	1401-38BII, FIA#8, L-rich, Stage V
140-135	Calcite	Bolañitos	S	4	185-190	187	-0.5 to -0.6	-0.5	0.9 to 1.1	0.9	140-35-III, FIA#1, L + illite, Stage III
140-135	Calcite	Bolañitos	S	4	185-189	188	-0.2 to -0.3	-0.3	0.4 to 0.5	0.4	140-35-II, FIA#1, L-rich, Stage IV
1401-41	Quartz	Bolañitos	S	3	261-263	262	0 to -0.1	-0.1	0 to 0.2	0.1	1401-41A, FIA#1, LV, Stage IV5
1401-34	Calcite	Daniela	S	4	180-185	182	-0.3 to -0.7	-0.5	0.5 to 1.2	0.8	1401-34A-III, FIA#8, L-rich, Stage III
1305-260	Calcite	Daniela	S	7	181-198	187	-2 to -2.2	-2.1	3.4 to 3.7	3.6	1305-260B, FIA#1, LV, Stage IV
1305-251	Calcite	Daniela	S	6	218-220	219	-0.6 to -0.7	-0.7	1.1 to 1.2	1.1	1305-251B, FIA#1, L + illite, Stage III
1305-251	Calcite	Daniela	S	5	218-220	219	-0.6 to -0.7	-0.6	1.1 to 1.2	1.1	1305-251B, FIA#2, L + illite, Stage III
1305-254	Calcite	Daniela	S	5	182-196	190	-0.9 to -1.1	-1	1.6 to 1.9	1.7	1305-254B, FIA#1, L-rich, Stage III
1305-254	Quartz	Daniela	S	3	223-227	225	-0.7 to -0.9	-0.8	1.2 to 1.6	1.5	1305-254B, FIA#2, L-rich, Stage IV[5]
1401-32	Quartz	Daniela	S	5	225-229	227	-0.4 to -0.6	-0.6	0.7 to 1.1	1	1401-32B, FIA#2, LV, Stage IV
1401-32	Quartz	Daniela	S	4	239-245	241	-0.1 to -0.3	-0.2	0.2 to 0.5	0.4	1401-32B, FIA#3, LV, Stage IV
1305-260	Quartz	Daniela	S	6	177-188	182	-1.9 to -2	-2	3.2 to 3.4	3.3	1305-260A, FIA#1, LV, Stage IV
1405-270	Calcite	Intermediate	S	6	158-160	159	-0.4 to -0.5	-0.4	0.7 to 0.9	0.8	1405270B-FI, FIA#1, L-rich, Stage II
1105-215	Calcite	Intermediate	P	9	189-203	198	-0.1 to -0.3	-0.2	0.2 to 0.5	0.4	1105215-II-FI, FIA#1, L-rich, Stage V
1405-264	Quartz	Intermediate	S	11	280-291	287	-0.4 to -0.7	-0.5	0.7 to 1.2	1	1405264A-II, FIA#1, L + illite, Stage IV[5]
1405-264	Quartz	Intermediate	S	6	288-291	290	-0.4 to -0.7	-0.5	0.7 to 1.2	0.9	1405264A-II, FIA#2, L + illite, Stage IV[5]
1405-264	Calcite	Intermediate	S	5	193-203	198	-0.2 to -0.3	-0.3	0.4 to 0.5	0.5	1405264A-II, FIA#1, L + illite, Stage III
1401-31	Quartz	Karina	S	5	201-202	201	-0.3 to -0.8	-0.6	0.5 to 1.4	1	14-0131II, FIA#4, L-rich, Stage II
1401-31	Quartz	Karina	S	2	204-205	204	-3.9 to -4.8	-4.4	6.3 to 7.6	6.9	14-0131II, FIA#1, LV, Stage IV
1401-31	Quartz	Karina	S	4	189-190	189	-3.1 to -3.4	-3.3	5.1 to 5.6	5.4	14-0131II, FIA#6, L-rich, Stage II
1305-232	Calcite	Karina	S	6	168-171	170	-0.1 to -0.2	-0.2	0.2 to 0.4	0.2	1305-232B-II, FIA#1, L-rich, Stage IV[2]
1305-232	Calcite	Karina	S	2	175-178	177	-0.6 to -0.7	-0.7	1.1 to 1.2	1.1	1305-232B-II, FIA#2, L-rich, Stage IV[2]
1305-232	Calcite	Karina	S	3	170-178	174	-0.7 to -0.8	-0.7	1.2 to 1.4	1.3	1305-232B-I, FIA#1, L-rich, Stage IV[2]
1305-232	Calcite	Karina	S	3	278-299	290	-0.6 to -0.7	-0.6	1.1 to 1.2	1.1	1305-232B-I, FIA#3, L-rich, Stage IV[2]
1305-255	Calcite	Karina	S	2	146-148	147	-0.2 to -0.3	-0.3	0.4 to 0.5	0.4	1305-255C, FIA#1, L-rich, Stage V
1401-43	Calcite	Lucero	S	5	193-210	202	-0.2 to -0.3	-0.3	0.4 to 0.5	0.5	140143C-I, FIA#1, L-rich, Stage IV[2]
1401-43	Calcite	Lucero	P	3	199-200	199	-0.3 to -0.4	-0.4	0.5 to 0.7	0.6	140143C-I, FIA#2, L-rich, Stage IV
905-168	Quartz	Lucero	S	4	212-223	216	-0.6 to -0.8	-0.7	1.1 to 1.4	1.3	905-168D-I, FIA#1, LV, Stage IV[5]
905-168	Quartz	Lucero	S	3	210-216	214	-0.8 to -0.9	-0.8	1.4 to 1.6	1.5	905-168D-III, FIA#2, LV, Stage IV[5]
1401-44	Calcite	Lucero	S	4	240-247	242	-0.2 to -0.3	-0.2	0.4 to 0.5	0.4	1401-44E, FIA#1, L-rich, Stage II

Sample	Host	Vein	Type	n	T_h range (°C)	Ave.	T_m range (°C)	Ave.	wt. % NaCl equiv[1]	Ave.	Notes
1401-44	Calcite	Lucero	S	3	171-182	178	-0.2 to -0.4	-0.3	0.4 to 0.7	0.5	1401-44E, FIA#2, L-rich, Stage IV[2]
905-167	Quartz	Lucero	S	3	275-289	282	-0.6 to -0.8	-0.7	1.1 to 1.4	1.2	905-167B-I, FIA#1, LV, Stage IV5
905-167	Quartz	Lucero	S	6	209-224	217	-0.6 to -0.8	-0.7	1.1 to 1.4	1.2	905-167B-I, FIA#2, L-rich, Stage II
1401-45	Calcite	Lucero	S	4	149-152	151	-0.2 to -0.4	-0.3	0.4 to 0.7	0.5	1401-45B-I, FIA#1, LV, Stage IV[2]
905-140	Calcite	Lucero	S	3	225-227	226	0 to -0.1	0	0 to 0.2	0.1	905-140C-II, FIA#1, L-rich, Stage V
905-140	Quartz	Lucero	P	2	189-192	191	-0.8 to -0.9	-0.9	1.4 to 1.6	1.5	905-140C-II, FIA#2, L-rich, Stage III
1401-45	Calcite	Lucero	S	5	183-185	184	-0.4 to -0.5	-0.5	0.7 to 0.9	0.8	1401-45B-V, FIA#1, L + illite, Stage IV
1401-45	Calcite	Lucero	S	5	187-193	190	-0.3 to -0.5	-0.4	0.5 to 0.9	0.7	1401-45B-V, FIA#2, L + illite, Stage IV
905-168	Quartz	Lucero	S	5	193-219	204	-0.9 to -1.1	-1	1.6 to 1.9	1.8	905-168D-IV, FIA#1, LV, Stage IV
1401-45	Calcite	Lucero	S	6	185-192	189	-0.2 to -0.5	-0.4	0.4 to 0.9	0.7	1401-45B-IV, FIA#1, L + illite, Stage IV
905-153	Adularia	Lucero	S	2	220-221	221	-0.2 to -0.3	-0.3	0.4 to 0.5	0.4	905-153B, FIA#1, L-rich, Stage IV
905-153	Calcite	Lucero	S	7	160-164	161	-0.2 to -1.2	-0.8	0.4 to 2.1	1.4	905-153B, FIA#2, LV, Stage IV
905-158	Calcite	Lucero	S	4	198-204	201	-0.3 to -0.7	-0.5	0.5 to 1.2	0.8	905-158, FIA#1, L + illite, Stage IV
905-127	Quartz	Lucero	S	5	200-216	205	-0.5 to -0.6	-0.5	0.9 to 1.1	0.9	905-127-I, FIA#1, LV, Stage IV
905-127	Quartz	Lucero	S	4	197-204	200	-0.5 to -0.6	-0.6	0.9 to 1.1	1	905-127-I, FIA#2, L-rich, Stage II
905-148	Quartz	Lucero	S	3	254-258	256	-0.3 to -0.6	-0.5	0.5 to 1.1	0.8	905-148A-I, FIA#2, LV, Stage IV
905-125	Quartz	Lucero	S	2	190-199	194	-0.5 to -0.6	-0.6	0.9 to 1.1	1	905-125A-II, FIA#1, L-rich, Stage III
564	Quartz	Melladito	S	4	200-225	215	-0.4 to -0.5	-0.4	0.7 to 0.9	0.7	564-FI, FIA#1, L-rich, Stage II
564	Quartz	Melladito	S	3	213-218	215	-0.1 to -0.2	-0.1	0.2 to 0.4	0.2	564-FI, FIA#2, L-rich, Stage II
564	Quartz	Melladito	P	4	199-199	199	-0.3 to -0.3	-0.3	0.5 to 0.5	0.5	564-FI, FIA#4, L-rich, Stage II
705-70	Quartz	Melladito	S	7	227-235	231	0 to -0.1	0	0 to 0.2	0.1	70570A-III-FI, FIA#1, LV, Stage IV[5]
578	Calcite	Melladito	S	2	137-138	138	-0.7 to -0.8	-0.8	1.2 to 1.4	1.3	578A-FI, FIA#1, L-rich, Stage V
1105-205	Calcite	Melladito	S	6	180-181	181	-0.2 to -0.4		0.4 to 0.7	0.5	1105205A-I, FIA#1, LV, Stage IV
DM10	Calcite	Melladito	S	2	177-178	178	-0.3 to -0.4	-0.4	0.5 to 0.7	0.6	DM10B-I-FI, FIA#1, L-rich, Stage IV[2]
DM10	Calcite	Melladito	S	2	222-222	222	-0.4 to -0.4	-0.4	0.7 to 0.7	0.7	DM10B-I-FI, FIA#2, L-rich, Stage IV[2]
DM10	Calcite	Melladito	S	2	179-179	179	-0.3 to -0.3	-0.3	0.5 to 0.5	0.5	DM10B-I-FI, FIA#3, L-rich, Stage IV[2]
DM12	Calcite	Melladito	S	5	173-178	175	-0.2 to -0.3	-0.3	0.4 to 0.5	0.5	DM12A-III, FIA#1, L + illite, Stage III
DM12	Calcite	Melladito	S	9	172-179	176	-0.2 to -0.3	-0.3	0.4 to 0.5	0.5	DM12A-III, FIA#2, L + illite, Stage III
DM12	Calcite	Melladito	P	2	188-188	188	-0.1 to -0.2	-0.2	0.2 to 0.4	0.3	DM12A-III, FIA#3, L-rich, Stage V
DM12	Calcite	Melladito	S	6	170-173	171	-0.2 to -0.3	-0.3	0.4 to 0.5	0.5	DM12A-III, FIA#4, L + illite, Stage III
DM12	Calcite	Melladito	S	8	155-164	160	-0.2 to -0.3	-0.2	0.4 to 0.5	0.4	DM12A-I, FIA#1, L + illite, Stage III
DM10	Calcite	Melladito	S	5	179-184	181	-0.2 to -0.3	-0.3	0.4 to 0.5	0.5	DM10B-II-FI, FIA#1, L + illite, Stage III
DM5	Adularia	Melladito	S	2	289-289	289	-4.3 to -4.3	-4.3	6.9 to 6.9	6.9	DM5B, FIA#1, L-rich, Stage IV[5]
DM12	Calcite	Melladito	S	6	169-175	171	0 to -0.1	-0.1	0 to 0.2	0.1	DM12A-II, FIA#2, L-rich, Stage III
DM7	Calcite	Melladito	S	7	182-187	185	-0.3 to -0.6	-0.5	0.5 to 1.1	0.8	DM7-I, FIA#1, LV, Stage IV
DM4	Quartz	Melladito	S	4	270-279	274	0 to -0.1	-0.1	0 to 0.2	0.1	DM4A-II, FIA#1, L-rich ,Stage I
DM4	Bladed calcite	Melladito	S	5	184-192	189	-0.3 to -0.4	-0.4	0.5 to 0.7	0.6	DM4B-I, FIA#1, LV, Stage IV
DM4	Bladed calcite	Melladito	S	5	159-165	163	-0.4 to -0.5	-0.5	0.7 to 0.9	0.8	DM4B-I, FIA#2, L-rich, Stage IV
DM14	Quartz	Melladito	S	4	215-221	218	-0.4 to -0.5	-0.5	0.7 to 0.9	0.8	DM14-II, FIA#1, LV, Stage IV[5]
DM14	Quartz	Melladito	S	4	163-174	167	-0.6 to -0.7	-0.6	1.1 to 1.2	1.1	DM14-II, FIA#2, L-rich, Stage IV[3]
578	Quartz	Melladito	S	3	252-263	257	-0.8 to -0.9	-0.8	1.4 to 1.6	1.5	578C, FIA#1, LV, V-rich (Th), Stage IV
DM14	Quartz	Melladito	S	3	182-186	184	-0.8 to -0.9	-0.9	1.4 to 1.6	1.5	DM14-I, FIA#1, LV, V-rich, Stage IV[5]
705-70	Quartz	Melladito	S	2	256-257	257	0 to -0.1	-0.1	0 to 0.2	0.1	70570B-I, FIA#2, LV, Stage IV[3]
705-70	Quartz	Melladito	S	9	198-223	212	-0.7 to -1	-0.9	0 to 1.7	1.3	70570B-I, FIA#3, L-rich, Stage II
551	Calcite	Melladito	S	2	183-193	188	-0.2 to -0.4	-0.3	0.4 to 0.7	0.6	551B, FIA#1, L-rich, Stage IV[2]
555	Quartz	Melladito	S	2	270-279	275	-0.2 to -0.4	-0.3	0.4 to 0.7	0.5	555-I, FIA#1, LV, V-rich, Stage IV[5]
555	Quartz	Melladito	P	6	205-217	209	-0.2 to -0.3	-0.3	0.4 to 0.5	0.4	555-II, FIA#1, LV, Stage IV
555	Quartz	Melladito	P	2	250-253	252	0 to -0.1	-0.1	0 to 0.2	0.1	555-II, FIA#2, L + illite, Stage IV[5]
555	Quartz	Melladito	P	4	285-290	288	-0.2 to -0.3	-0.3	0.4 to 0.5	0.4	555-II, FIA#3, L + illite, Stage IV[5]
905-83	Quartz	Melladito	S	4	219-226	223	-0.2 to -0.6	-0.4	0.4 to 1.1	0.7	90583, FIA#1, LV, Stage IV[3]

Sample	Host	Vein	Type	n	T_h range (°C)	Ave.	T_m range (°C)	Ave.	wt. % NaCl equiv[1]	Ave.	Notes
905-83	Quartz	Melladito	S	1	225-225	225	-0.1 to -0.3	-0.2	0.2 to 0.5	0.4	90583, FIA#2, L-rich, Stage IV[3]
905-83	Quartz	Melladito	S	2	233-235	234					90583, FIA#4, LV, V-rich, Stage IV
905-83	Quartz	Melladito	S	6	225-235	230	-0.2 to -0.3	-0.2	0.4 to 0.5	0.4	90583, FIA#5, LV, Stage IV
905-83	Quartz	Melladito	S	8	218-240	230	-0.6 to -0.9	-0.8	1.1 to 1.6	1.4	90583, FIA#6, LV, Stage IV
DM3	Bladed calcite	Melladito	S	5	183-192	188	-0.4 to -0.5	-0.5	0.7 to 0.9	0.8	DM3A, FIA#1, L-rich, Stage IV
1405-272	Quartz	Nombre de Dios	S	3	169-185	179	-0.4 to -0.4	-0.4	0.7 to 0.7	0.7	1405272A-I-FI, FIA#1, L-rich, Stage III
1405-272	Quartz	Nombre de Dios	S	4	173-184	178	-0.5 to -0.9	-0.7	0.9 to 1.6	1.1	1405272A-I-FI, FIA#2, L-rich, Stage III
1405-272	Quartz	Nombre de Dios	S	5	170-172	170	-0.4 to -0.4	-0.4	0.7 to 0.7	0.7	1405272A-I-FI, FIA#3, L-rich, Stage III
1405-271	Quartz	Nombre de Dios	S	5	187-194	191	-0.3 to -0.7	-0.5	0.5 to 1.2	0.8	1405271A-II-FI, FIA#2, L-rich, Stage III
1405-272	Quartz	Nombre de Dios	S	6	163-165	164	-0.5 to -0.6	-0.6	0.9 to 1.1	1	1405272A-II-FI, FIA#1, L-rich, Stage III
1405-272	Quartz	Nombre de Dios	S	8	207-210	209	-0.4 to -0.5	-0.4	0.7 to 0.9	0.8	1405272A-II-FI, FIA#2, L-rich, Stage III
1405-272	Quartz	Nombre de Dios	S	7	180-194	191	-0.4 to -0.5	-0.4	0.7 to 0.9	0.8	1405272A-II-FI, FIA#3, LV, Stage IV
1405-272	Quartz	Nombre de Dios	S	8	161-174	166	-0.3 to -0.4	-0.3	0.5 to 0.7	0.6	1405272A-III-FI, FIA#1, L-rich, Stage III
1405-265	Quartz	Nombre de Dios	S	5	194-200	198	-0.5 to -0.7	-0.6	0.9 to 1.2	1	1405265B-III-FI, FIA#1, L-rich, Stage III
1405-265	Quartz	Nombre de Dios	S	2	194-195	195	-0.5 to -0.6	-0.6	0.9 to 1.1	1	1405265B-III-FI, FIA#2, LV, Stage IV[5]
1405-265	Quartz	Nombre de Dios	S	6	198-205	200	-0.3 to -0.4	-0.4	0.5 to 0.7	0.6	1405265B-III-FI, FIA#3, L-rich, Stage III
1405-265	Quartz	Nombre de Dios	S	7	190-201	195	-0.5 to -0.8	-0.7	0.9 to 1.4	1.2	1405265B-III-FI, FIA#4, L-rich, Stage IV[5]
1405-265	Quartz	Nombre de Dios	S	4	200-209	205	-0.5 to -0.6	-0.5	0.9 to 1.1	0.9	1405265B-III-FI, FIA#5, LV, Stage IV[5]
1405-265	Quartz	Nombre de Dios	S	2	220-237	229	-0.2 to -0.3	-0.3	0.4 to 0.5	0.4	1405265B-II-FI, FIA#2, LV, Stage IV
1405-265	Quartz	Nombre de Dios	S	8	199-202	200	0 to -0.1	-0.1	0 to 0.2	0.1	1405265B-II-FI, FIA#4, L-rich, Stage III
1405-265	Quartz	Nombre de Dios	S	10	198-200	199	-0.6 to -0.7	-0.6	1.1 to 1.2	1.1	1405265B-I-FI, FIA#1, L-rich, Stage III
1405-265	Quartz	Nombre de Dios	S	4	200-210	203	-0.7 to -0.8	-0.8	1.2 to 1.4	1.3	1405265B-I-FI, FIA#2, LV, Stage IV
1405-265	Quartz	Nombre de Dios	S	4	190-197	193	-0.6 to -0.7	-0.7	1.1 to 1.2	1.1	1405265B-I-FI, FIA#3, L-rich, Stage III
1405-265	Quartz	Nombre de Dios	S	5	200-205	203	-0.5 to -0.6	-0.5	0.9 to 1.1	0.9	1405265B-I-FI, FIA#4, L-rich, Stage IV
1405-266	Quartz	Nombre de Dios	S	5	187-192	190	-0.5 to -0.6	-0.6	0.9 to 1.1	1	1405266B-I, FIA#1, L-rich, Stage IV[5]
305-05	Quartz	Nombre de Dios	S	4	206-209	208	-1.4 to -1.5	-1.5	2.4 to 2.6	2.5	30505B-I-FI, FIA#1, L + illite, Stage III
1405-266	Quartz	Nombre de Dios	S	5	222-226	224	-0.4 to -0.5	-0.4	0.7 to 0.9	0.8	1405266A-I-FI, FIA#2, LV, Stage IV[5]
1405-266	Quartz	Nombre de Dios	S	7	167-168	167	-0.3 to -0.4	-0.4	0.5 to 0.7	0.6	1405266A-I-FI, FIA#3, L-rich, Stage III
1405-271	Quartz	Nombre de Dios	P	8	206-215	211	-0.1 to -0.4	-0.3	0.2 to 0.7	0.5	1405271A-I-FI, FIA#1, LV, Stage IV
305-05	Quartz	Nombre de Dios	S	7	211-217	214	-2.1 to -2.8	-2.6	3.5 to 4.6	4.3	30505C-II, FIA#1, LV, L + illite, Stage IV
305-05	Quartz	Nombre de Dios	S	6	213-224	219	-1.7 to -1.9	-1.8	2.9 to 3.2	3	30505C-II, FIA#2, L + illite, Stage IV
1405-266	Quartz	Nombre de Dios	S	4	328-335	332	-0.5 to -0.6	-0.5	0.9 to 1.1	0.9	1405266B-II, FIA#1, LV, Stage IV[5]

Sample	Host	Vein	Type	n	T_h range (°C)	Ave.	T_m range (°C)	Ave.	wt. % NaCl equiv[1]	Ave.	Notes
1405-266	Quartz	Nombre de Dios	S	3	190-196	194	-0.2 to -0.3	-0.2	0.4 to 0.5	0.4	1405266B-II, FIA#2, LV, Stage IV[5]
705-64	Quartz	Nombre de Dios	S	3	232-235	234	-2.3 to -2.5	-2.4	3.9 to 4.2	4	70564B-I, FIA#1, LV, Stage IV[5]
905-163	Calcite	Other_vein	S	2	208-211	210	-0.2 to -0.3	-0.3	0.4 to 0.5	0.4	905-163D, FIA#1, LV, Stage IV
905-180	Quartz	Perpendicular	S	6	220-231	225	-0.5 to -0.7	-0.6	0.9 to 1.2	1.1	905180A-I-FI, FIA#2, L-rich, Stage I
705-67	Calcite	Perpendicular	P	2	288-288	288	-0.4 to -0.5	-0.5	0.7 to 0.9	0.8	70567-I-FI, FIA#1, L-rich, Stage I
705-67	Quartz	Perpendicular	S	2	262-280	271	-0.1 to -0.2	-0.2	0.2 to 0.4	0.3	70567-I-FI, FIA#2, L-rich, Stage I
905-180	Quartz	Perpendicular	S	4	275-278	276	-0.2 to -0.3	-0.3	0.4 to 0.5	0.4	905180A-IV-FI, FIA#1, L-rich, Stage I
705-67	Quartz	Perpendicular	S	5	193-199	196	-1.1 to -1.3	-1.2	1.9 to 2.2	2.1	70567-III-FI, FIA#1, L-rich, Stage I
705-67	Quartz	Perpendicular	S	7	247-254	251	-0.5 to -0.7	-0.6	0.9 to 1.2	1	70567-II-FI, FIA#1, L-rich, Stage I
705-67	Quartz	Perpendicular	P	2	236-237	236	-0.2 to -0.3	-0.3	0.4 to 0.5	0.4	70567-II-FI, FIA#2, L-rich, Stage I
705-63	Quartz	Perpendicular	S	2	270-289	279	0 to -0.1	-0.1	0 to 0.2	0.1	70563-I, FIA#1, L-rich, Stage I
705-63	Quartz	Perpendicular	S	3	239-241	240	-0.1 to -0.2	-0.2	0.2 to 0.4	0.3	70563-II, FIA#1, L-rich, Stage I
705-63	Quartz	Perpendicular	S	5	198-213	206	-0.5 to -0.6	-0.5	0.9 to 1.1	0.9	70563-II, FIA#2, L-rich, Stage I
305-07	Quartz	Perpendicular	S	2	285-289	287	-0.3 to -0.4	-0.4	0.5 to 0.7	0.6	30507, FIA#1, L-rich, Stage I
563	Quartz	Plateros	S	8	187-209	198	-0.6 to -1	-0.7	1.1 to 1.7	1.3	563A, FIA#1, L-rich, Stage II
563	Quartz	Plateros	S	2	275-289	282	-0.4 to -0.6	-0.5	0.7 to 1.1	0.9	563A, FIA#2, LV, V-rich, Stage IV[5]
905-178	Calcite	Plateros	P	4	190-195	192	-0.7 to -0.8	-0.8	1.2 to 1.4	1.3	905178B, FIA#1, L-rich, Stage IV[3]
561	Quartz	Plateros	S	6	250-257	254	-0.2 to -0.3	-0.3	0.4 to 0.5	0.4	561-I, FIA#1, L-rich, Stage IV[4]
561	Quartz	Plateros	S	4	260-265	262	-0.2 to -0.3	-0.2	0.4 to 0.5	0.4	561-I, FIA#2, LV, Stage IV
1401-46	Quartz	San José	S	2	296-297	297	-0.1 to -0.2	-0.2	0.2 to 0.4	0.3	140146-II, FIA#1, L-rich, Stage IV[5]
1105-208	Quartz	Traverse Melladito	S	8	200-204	202	-0.8 to -0.9	-0.9	1.4 to 1.6	1.5	1105208A-I-FI, FIA#1, LV, Stage III
1105-211	Calcite	Traverse Melladito	S	6	189-200	193	-0.8 to -1.3	-1	1.4 to 2.2	1.7	1105211A, FIA#1, L-rich, Stage II
1105-210	Calcite	Traverse Melladito	S	5	186-196	192	-0.2 to -0.3	-0.3	0.4 to 0.5	0.5	1105210A, FIA#2, L-rich, Stage III
1105-202	Quartz	Traverse Melladito	P	4	178-182	180	-0.2 to -0.6	-0.4	0.4 to 1.1	0.7	1105202A-III, FIA#1, L-rich, Stage II
1105-202	Quartz	Traverse Melladito	S	6	178-182	180	-0.5 to -0.6	-0.6	0.9 to 1.1	1	1105201A-II, FIA#1, L-rich, Stage II
1105-202	Calcite	Traverse Melladito	P	4	180-185	183	-0.5 to -0.6	-0.6	0.9 to 1.1	1	1105201A-II, FIA#2, L-rich, Stage II

Appendix A. Sample locations and description for Chapter 3

Sample	UTM X	UTM Y	Elevation (m)	Au	Ag	Cu	Pb	Zn	As	Sb	LV	L+illite	V	CT	PT	JT	GhSTQ	BC	S/I	Ad	Ca	ZTQ	CoTQ	Vein	Type	Analysis	Mine
305-02	258303	2329660	2410	0.8	21.0	8.0	0.5	2.5	4.0	3.0	0	0	1	0	0	1	0	1	0	0	0	0	0	Nombre de Dios	Surface	Perpendicular	
305-03	258303	2329660	2400	1.1	40.0	9.0	0.5	7.0	5.0	1.0	0	0	1	1	1	1	0	1	0	0	0	0	0	Nombre de Dios	Surface	Oriented	
305-04	258306	2329514	2396	1.5	162.0	7.0	0.5	5.0	6.0	4.0	0	0	1	1	1	1	0	0	0	0	0	0	0	Nombre de Dios	Surface	Oriented	
305-05	258306	2329514	2395	0.2	10.0	11.0	0.5	10.0	52.0	3.0	0	0	1	1	1	1	0	0	0	0	0	0	0	Nombre de Dios	Surface	Oriented	
305-06	258340	2329519	2350	0.3	26.0	32.0	0.5	22.0	146.0	3.0	0	0	1	1	1	1	0	0	0	0	0	0	0	Melladito	Surface	Perpendicular	
305-07	258340	2329519	2350	0.1	4.0	17.0	0.5	11.0	86.0	2.0	0	0	1	0	1	1	0	0	0	0	0	0	0	Melladito	Surface	Perpendicular	
305-08	258351	2329510	2389	0.0	0.5	7.0	0.5	2.5	11.0	1.0	0	0	1	1	0	1	0	1	0	0	0	0	0	Nombre de Dios	Surface	Oriented	
705-63	258420	2328425	2333	0.0	3.0	49.0	0.5	5.0	12.0	3.0	1	0	1	0	1	0	0	0	0	0	0	0	0	Melladito	Surface	Perpendicular	
705-64	258498	2328533	2362	0.0	20.0	35.0	0.5	6.0	9.0	2.0	1	0	0	0	1	1	0	0	1	0	0	0	0	Nombre de Dios	Surface	Oriented	
705-65	258600	2328565	2385	0.0	0.5	14.0	0.5	7.0	63.0	4.0	0	0	0	1	1	1	0	0	0	0	0	0	0	Nombre de Dios	Surface	Oriented	
705-66	258637	2328464	2382	0.0	0.5	40.0	0.5	46.0	2.0	0.5	1	0	0	0	0	1	0	0	0	0	0	0	0	Nombre de Dios	Surface	Perpendicular	
705-67	258617	2328300	2373	0.1	0.5	8.0	0.5	6.0	166.0	6.0	1	0	1	1	1	1	1	0	0	0	0	0	0	Melladito	Surface	Perpendicular	
705-68	258617	2328300	2373	0.0	0.5	13.0	0.5	9.0	6.0	0.5	0	0	0	0	0	1	0	0	0	0	0	0	0	Melladito	Surface	Oriented	
705-69	258654	2328293	2368	0.0	0.5	53.0	0.5	44.0	13.0	0.5	0	0	0	1	0	1	0	0	0	0	0	0	0	Melladito	Surface	Oriented	
705-70	258652	2328270	2365	2.1	8.0	80.0	0.5	18.0	300.0	9.0	1	0	1	1	1	1	0	0	0	1	0	0	0	Melladito	Surface	Oriented	
705-71	258716	2328194	2348	0.0	0.5	61.0	0.5	20.0	3.0	0.5	0	0	0	1	0	1	0	0	0	0	0	0	0	Melladito	Surface	Oriented	
705-72	258766	2328184	2345	0.1	3.0	15.0	0.5	14.0	47.0	3.0	0	0	1	1	1	1	0	1	0	0	0	0	0	Melladito	Surface	Oriented	
705-73	258825	2328163	2355	0.0	0.5	46.0	0.5	12.0	3.0	0.5	0	0	0	1	0	1	0	0	0	0	0	0	0	Nombre de Dios	Surface	Oriented	
705-74	259012	2328009	2384	0.2	8.0	2.5	0.5	2.5	10.0	0.5	0	0	0	0	0	1	0	0	0	0	0	0	0	Nombre de Dios	Surface	Oriented	
705-75	259024	2328023	2386	2.0	39.0	9.0	0.5	2.5	9.0	6.0	1	0	0	1	1	1	0	1	0	0	0	0	0	Nombre de Dios	Surface	Oriented	
905-76	259067	2327509	2320	0.1	50.0	9.0	0.5	6.0	6.0	12.0	0	0	0	1	1	1	0	1	0	0	0	0	0	Melladito	Surface	Oriented	
905-77	259088	2327559	2300	0.0	1.0	33.0	0.5	18.0	65.0	4.0	0	0	0	0	1	1	0	0	0	0	0	0	0	Melladito	Surface	Oriented	
905-78	259090	2327579	2295	0.2	41.0	27.0	0.5	7.0	300.0	20.0	0	0	0	0	1	1	0	0	0	0	0	0	0	Melladito	Surface	Oriented	
905-79	259137	2327575	2278	1.9	2.0	13.0	0.5	2.5	53.0	3.0	1	0	0	1	0	0	0	1	0	0	0	0	0	Melladito	Surface	Oriented	
905-80	259178	2327534	2265	0.2	9.0	39.0	0.5	6.0	102.0	3.0	0	0	0	0	1	1	0	0	0	0	0	0	0	Melladito	Surface	Oriented	
905-81	259173	2327528	2268	0.1	0.5	26.0	0.5	12.0	127.0	0.5	1	0	0	0	1	0	0	0	0	0	0	0	0	Melladito	Surface		
905-82	259175	2327345	2273	0.6	2.0	54.0	0.5	25.0	179.0	9.0	0	0	0	0	1	1	0	0	0	0	0	0	0	Melladito	Surface		
905-83	259238	2327224	2278	0.0	0.5	6.0	0.5	10.0	45.0	5.0	1	0	1	1	1	1	0	0	0	0	0	0	0	Melladito	Surface	Oriented	
1005-175	259533	2326627	2228	0.0	0.5	91.0	0.5	67.0	17.0	2.0	0	0	1	0	0	1	0	0	0	0	0	0	0	Melladito	Surface		
1005-176	259380	2326645	2258	0.0	0.5	30.0	30.0	37.0	19.0	1.0	0	0	0	0	0	1	0	0	0	0	0	0	0	Plateros	Surface	Oriented	
1005-177	259481	2326548	2225	0.0	0.5	22.0	0.5	23.0	26.0	0.5	0	0	0	0	0	1	0	0	0	0	0	0	0	Plateros	Surface	Oriented	
1005-178	259481	2326548	2225	0.3	56.0	8.0	0.5	27.0	14.0	6.0	0	0	0	0	0	1	0	1	1	1	1	0	0	Plateros	Surface	Oriented	
1005-179	259438	2326761	2250	0.0	0.5	7.0	0.5	15.0	15.0	2.0	0	0	0	0	0	1	0	0	0	0	0	0	0	Melladito	Surface		
1005-180	259401	2326760	2265	0.1	23.0	35.0	0.5	15.0	67.0	6.0	1	0	1	1	1	1	0	1	0	0	0	0	0	Melladito	Surface	Perpendicular	
1005-181	259245	2326745	2309	0.0	5.0	34.0	0.5	29.0	63.0	3.0	1	0	1	1	1	1	0	0	0	0	0	0	0	Plateros	Surface	Oriented	
0905186A	259407	2326014	2208								1	0	1	1	1	1	0	0	0	0	0	0	0	Other_Vein	Surface		
1105-187	259442	2326034	2235	0.0	0.5	13.0	0.5	7.0		4.0	0	0	0	0	0	0	0	0	0	0	0	0	0	Other_Vein	Surface	Oriented	
1105-187	259443	2326034	2235	0.0	2.0	11.0	0.5	19.0	41.0	3.0	0	0	0	0	1	1	0	0	0	0	1	0	0	Other_Vein	Surface	Oriented	
1105-188	259537	2326144	2211	0.0	0.5	10.0	0.5	8.0		1.0	0	0	1	1	1	1	0	0	0	0	1	0	0	Plateros	Surface	Oriented	
1105-189	259560	2326179	2200	0.0	0.5	48.0	0.5	20.0	108.0	2.0	0	0	0	0	1	0	0	0	0	1	1	0	0	Plateros	Surface	Perpendicular	
1105-190	259667	2326316	2178	0.2	0.5	19.0	0.5	10.0		10.0	0	0	0	1	0	1	0	0	0	1	1	0	0	Plateros	Surface	Oriented	
1105-191	259667	2326316	2178	0.0	1.0	15.0	0.5	12.0		8.0	0	0	0	0	1	0	0	0	0	1	0	0	0	Plateros	Surface	Oriented	
1105-192	258976	2326982	2320	0.0	0.5	2.5	0.5	20.0	6.0	1.0	0	0	0	0	0	0	0	0	0	0	1	0	0	Plateros	Surface	Perpendicular	
1105-193	258879	2327066	2311	0.0	0.5	7.0	0.5	15.0	5.0	0.5	0	0	1	0	1	0	0	0	0	0	0	0	0	Plateros	Surface		
1105-196	258904	2327138	2320	0.0	0.5	10.0	0.5	6.0	3.0	0.5	0	0	1	0	0	1	0	0	0	0	0	0	0	Plateros	Surface	Oriented	
1105-197	258953	2327192	2320	0.0	0.5	2.5	0.5	2.5	10.0	1.0	0	0	0	0	0	1	0	0	0	1	0	0	0	Plateros	Surface		
1105-201	258045	2329117	2318	0.1	2.5						1	0	0	1	1	1	0	1	0	0	0	0	0	Melladito	DDH-1		
1105-202	258045	2329117	2317	0.1	1.5						0	0	0	0	0	1	0	0	0	0	1	0	0	Melladito	DDH-1		
1105-203	258061	2329131	2299	0.7	149.0	6.0	0.5	13.0	120.0	14.0	0	0	0	0	1	1	0	0	0	1	1	0	0	Melladito	DDH-1		
1105-204	258066	2329135	2293	0.5	2.0	23.0	0.5	22.0	400.0	3.0	0	0	0	0	0	0	0	0	0	0	1	0	0	Melladito	DDH-1		
1105-205	258070	2329139	2288	1.8	26.0	2.5	0.5	2.5			0	0	0	1	0	1	0	0	0	1	1	0	0	Melladito	DDH-1	Oriented	
1105-206	258071	2329139	2287	2.9	385.0	8.0	0.5	15.0	2.0	19.0	0	0	0	0	0	1	0	0	1	1	1	0	0	Melladito	DDH-1	Oriented	
1105-207	258072	2329140	2286	0.1	49.0	27.0	0.5	53.0	84.0	5.0	0	0	0	0	1	1	0	0	0	0	1	0	0	Melladito	DDH-1		
1105-208	258096	2329160	2259	0.1	1.5						0	0	0	0	1	1	0	0	0	0	1	0	0	Melladito	DDH-1		
1105-209	258097	2329161	2258	0.3	10.0	27.0	0.5	28.0	189.0	4.0	0	0	0	0	0	1	0	0	0	0	0	0	0	Melladito	DDH-1		
1105-210	258105	2329168	2248	0.0	2.5						1	0	0	0	1	0	0	0	0	0	1	0	0	Melladito	DDH-1		
1105-211	258058	2329128	2303	0.0	7.0						0	0	1	0	1	1	0	0	0	0	1	0	0	Melladito	DDH-1		
1105-212	258128	2329187	2222	0.3	9.0	35.0	0.5	38.0	500.0	6.0	0	0	0	0	1	1	0	0	0	0	1	0	0	Melladito	DDH-1		
1105-213	258130	2329188	2220	0.7	8.0	36.0	0.5	36.0	2.0	3.0	0	0	0	0	0	0	0	0	0	0	1	1	0	Melladito	DDH-1		
1105-214	258144	2329201	2203	0.1	1.5						0	0	1	1	1	1	0	1	1	0	1	0	0	Melladito	DDH-1		
1105-215	258140	2329197	2208	1.0	15.0	17.0	0.5	19.0	0.5	7.0	0	0	0	1	0	0	1	0	0	0	1	0	0	Intermediate	DDH-1	Oriented	
1105-216	258143	2329200	2204	0.1	3.0						0	0	0	0	0	1	0	0	0	0	1	0	0	Melladito	DDH-1		
1105-217	258149	2329204	2198	0.3	6.0						0	0	0	0	0	0	0	0	0	0	0	0	0	Melladito	DDH-1		

Sample	UTM X	UTM Y	Elevation (m)	Au	Ag	Cu	Pb	Zn	As	Sb	LV	L+illite	V	CT	PT	JT	GhSTQ	BC	S/I	Ad	Ca	ZTQ	CoTQ	Vein	Type	Analysis	Mine
1305-263	258075	2329322	2200	0.3	34.0	51.0	0.5	57.0	0.5	0.5	0	0	0	1	0	1	0	0	0	0	0	0	0	Intermediate	DDH-9	Compare 2A	
1305-264	258076	2329322	2199	2.3	709.0	17.0	0.5	39.0	164.0	19.0	0	0	1	1	1	1	0	0	0	0	1	0	0	Intermediate	DDH-9	Compare 3A	
1305-265	258107	2329348	2152	8.3	10.0	18.0	0.5	27.0	22.0	2.0	1	0	1	1	1	1	0	0	0	0	1	0	0	Nombre de Dios	DDH-9	Compare 4A	
1305-266	258107	2329349	2151	3.0	3.0	13.0	0.5	26.0	11.0	1.0	1	0	1	1	1	1	0	1	0	0	1	0	0	Nombre de Dios	DDH-9	Compare 5A	
1305-267	258020	2329276	2285	3.0	35.0	2.5	20.0	20.0	12.0	6.0	0	0	0	1	0	1	0	0	0	1	0	0	0	Melladito	DDH-9	Compare 1A	
1305-268	258018	2329277	2285	0.2	6.0	60.0	10.0	90.0	270.0	25.0	0	0	0	1	0	1	0	0	0	0	1	0	0	Melladito	DDH-14	Compare 1A	
1305-269	258073	2329326	2201	0.0	3.0	60.0	10.0	150.0	170.0	25.0	0	0	0	1	1	1	0	0	0	0	1	0	0	Intermediate	DDH-14	Compare 2A	
1305-270	258074	2329326	2199	0.8	83.0	10.0	10.0	20.0	140.0	25.0	1	0	0	1	1	1	0	0	0	0	1	0	0	Intermediate	DDH-14	Compare 3A	
1305-271	258105	2329353	2153	0.0	1.0	70.0	10.0	80.0	25.0	25.0	1	0	1	0	1	0	0	0	0	0	1	0	0	Nombre de Dios	DDH-14	Compare 4A	
1305-272	258105	2329354	2152	0.0	1.0	50.0	10.0	80.0	25.0	25.0	1	0	1	1	1	1	0	0	0	0	1	0	0	Nombre de Dios	DDH-14	Compare 5A	
Oct_2011_1056551	258207	2328688	2380	0.1	22.0	2.5	0.5	2.5	4.0	2.0	1	1	0	1	1	1	0	0	0	0	1	0	0	Melladito	Underground	Oriented	San Pablo
Oct_2011_1056552	258208	2328691	2380	2.0	465.0	24.0	0.5	22.0	11.0	42.0	1	0	0	1	0	1	0	0	0	1	1	0	0	Melladito	Underground	Oriented	San Pablo
Oct_2011_1056553	258334	2328444	2320	0.6	61.0	7.0	0.5	12.0	37.0	15.0	0	0	0	0	0	1	0	0	1	0	0	0	0	Melladito	Underground	Oriented	Sangria
Oct_2011_1056554	258335	2328441	2322	0.2	75.0	9.0	0.5	8.0	33.0	6.0	0	0	0	1	1	1	0	0	0	0	1	0	0	Melladito	Underground	Oriented	Sangria
Oct_2011_1056555	258304	2328439	2325	8.7	17.0	7.0	0.5	2.5	6.0	1.0	1	0	0	1	1	1	0	0	0	0	1	0	0	Melladito	Underground	Oriented	Sangria
Oct_2011_1056556	258101	2328902	2360	0.4	75.0	6.0	0.5	8.0	36.0	8.0	0	0	0	1	1	1	0	1	0	0	0	0	1	Melladito	Underground	Oriented	Nopal
Oct_2011_1056557	258027	2329267	2420	0.0	0.5	17.0	0.5	21.0	4.0	0.5	0	0	0	0	0	0	0	0	0	0	0	0	0	Melladito	Surface	Oriented	
Oct_2011_1056558	258112	2329012	2405	0.0	1.0	7.0	0.5	7.0	8.0	0.5	0	0	0	1	1	1	0	0	0	0	0	0	0	Melladito	Surface	Perpendicular	
Oct_2011_1056559	257842	2329083	2400	0.0	0.5	59.0	0.5	26.0	1.0	0.5	0	0	0	0	0	0	0	0	0	0	0	0	0	Between Plateros and Melladito	Surface	Oriented	
Oct_2011_1056560	257788	2329191	2421	0.0	0.5	61.0	0.5	19.0	0.5	0.5	1	0	1	0	0	0	0	0	0	0	0	0	0	Between Plateros and Melladito	Surface	Perpendicular	
Oct_2011_1056561	257568	2329012	2400	0.0	2.0	15.0	0.5	26.0	2.0	0.5	1	0	0	1	1	1	0	0	0	0	0	0	0	Plateros	Surface		
Oct_2011_1056562	257537	2329136	2398	0.0	0.5	7.0	0.5	9.0	0.5	8.0	0	0	0	0	0	1	0	0	0	0	0	0	0	Plateros	Surface		
Oct_2011_1056563	257444	2329106	2395	2.9	439.0	28.0	10.0	59.0	22.0	6.0	1	0	0	1	0	1	0	1	0	0	0	0	0	Plateros	Surface	Oriented	
Oct_2011_1056564	257878	2329414	2396	0.1	9.0	10.0	0.5	25.0	59.0	8.0	0	0	0	1	0	1	0	0	0	0	1	0	0	Melladito	Surface	Oriented	
Oct_2011_1056565	257880	2329423	2435	0.2	47.0	26.0	0.5	31.0	139.0	6.0	0	0	0	1	1	1	0	1	0	0	0	0	0	Melladito	Surface	Oriented	
Oct_2011_1056566	257940	2329360	2431	1.4	72.0	12.0	0.5	10.0	16.0	10.0	0	0	0	1	0	1	0	1	0	0	0	0	1	Melladito	Surface	Oriented	
Oct_2011_1056567	257893	2329562	2435	0.0	0.5	15.0	0.5	44.0	9.0	1.0	0	0	0	1	0	1	0	0	0	0	0	0	0	Melladito	Surface	Oriented	
Oct_2011_1056568	257890	2329570	2430	0.0	3.0	11.0	0.5	8.0	41.0	11.0	0	0	0	1	1	1	0	1	0	0	0	0	0	Melladito	Surface	Oriented	
Oct_2011_1056569	259691	2326270	2200	0.0	1.0	19.0	0.5	11.0	28.0	6.0	0	0	0	1	0	1	0	0	0	0	1	0	0	Melladito	Underground	Oriented	
Oct_2011_1056570	259706	2326342	2245	0.0	3.0	64.0	0.5	21.0	49.0	7.0	0	0	0	0	0	1	0	0	0	0	1	0	0	Melladito	Underground	Oriented	
Oct_2011_1056571	259720	2326356	2240	0.0	0.5	15.0	0.5	16.0	16.0	0.5	0	0	0	0	0	1	0	0	0	0	1	0	0	Melladito	Underground	Oriented	
Oct_2011_1056572	259671	2326186	2270	0.0	0.5	17.0	0.5	7.0	34.0	0.5	0	0	0	0	0	0	0	0	0	0	0	0	0	Plateros	Underground	Oriented	La chuparosa
Oct_2011_1056573	259680	2326192	2273	0.1	1.0	16.0	0.5	32.0	50.0	3.0	0	0	0	1	0	1	0	0	0	0	1	0	0	Plateros	Underground	Oriented	La chuparosa
Oct_2011_1056574	259699	2326198	2271	1.0	11.0	2.5	0.5	5.0	21.0	3.0	0	1	1	0	0	1	0	0	0	1	1	0	0	Plateros	Underground	Oriented	La chuparosa
Oct_2011_1056575	259724	2326207	2272	5.0	15.0	18.0	0.5	17.0	37.0	3.0	0	1	1	0	0	1	0	0	0	1	1	0	0	Plateros	Underground	Oriented	La chuparosa
Oct_2011_1056576	259447	2326576	2240	0.1	30.0	37.0	10.0	32.0	15.0	3.0	0	0	0	1	1	1	0	0	0	0	1	0	0	Plateros	Underground	Oriented	Chayita
Oct_2011_1056577	259467	2326565	2242	2.6	89.0	19.0	0.5	19.0	30.0	6.0	0	0	0	0	1	1	0	0	0	1	1	0	0	Plateros	Underground	Oriented	Chayita
Oct_2011_1056578	259637	2326495	2177	0.1	44.0	6.0	0.5	26.0	300.0	10.0	1	0	1	0	1	1	0	0	0	0	1	0	0	Melladito	Underground	Oriented	San Jose de abajo
Oct_2011_1056579	259635	2326494	2177	0.0	5.0	34.0	0.5	16.0	79.0	3.0	0	0	0	1	1	1	0	0	0	1	1	0	0	Melladito	Underground	Oriented	San Jose de abajo
Oct_2011_1056580	259905	2326628	2267	0.2	26.0	6.0	0.5	11.0	55.0	8.0	0	0	0	0	0	1	0	0	0	0	1	0	0	Other_Vein	Surface	Float	
Oct_2011_1056581	259537	2326719	2210	0.0	23.0	7.0	0.5	14.0	68.0	8.0	0	0	0	0	1	1	0	1	0	0	1	0	0	Melladito	Underground	Oriented	San Jose
Oct_2011_1056582	259759	2326290	2210	0.5	84.0	7.0	0.5	15.0	38.0	19.0	0	0	0	0	0	1	0	0	0	0	1	0	1	Melladito	Underground	Oriented	San Francisco de Asis
Oct_2011_1056583	259063	2327519	2297	3.9	350.0	7.0	0.5	19.0	50.0	23.0	0	0	0	0	0	1	0	0	0	1	1	0	0	Melladito	Underground	Oriented	La Boveda
Oct_2011_1056584	259064	2327519	2297	1.0	293.0	2.5	0.5	13.0	22.0	28.0	0	0	0	1	0	1	0	0	0	1	1	0	0	Melladito	Underground	Oriented	La Boveda
Oct_2011_1056584A	259064	2327519	2297	1.0	293.0	2.5	0.5	13.0	22.0	28.0	0	0	0	1	1	1	0	0	0	0	1	0	0	Melladito	Underground	Float	
DM3	258077	2329214	2226	0.4	24.0	14.0	5.0	13.0	182.0	8.0	0	1	0	1	0	1	0	1	0	0	1	0	0	Melladito	ESI11-004	Melladito	
DM4	258057	2329171	2258	13.7	408.0	2.5	5.0	7.0	11.0	26.0	0	0	0	1	0	1	0	1	0	1	1	0	0	Melladito	ESI11-021	Melladito	
DM5	258056	2329171	2259	1.8	26.0	2.5	5.0	2.5			0	0	1	1	1	1	0	1	0	0	1	0	0	Melladito	ESI10-001	Melladito	
DM6	258071	2329139	2288	0.2	28.0	13.0	5.0	27.0			0	0	0	0	0	0	0	0	0	0	0	0	0	Melladito	ESI10-001	Melladito	
DM7	258071	2329139	2287	2.9	385.0	8.0	5.0	15.0	2.0	19.0	1	0	0	0	1	1	0	0	0	1	1	0	0	Melladito	ESI10-001	Melladito	
DM8	258077	2329214	2225	0.4	24.0	14.0	5.0	13.0	182.0	8.0	0	0	0	0	0	0	0	0	0	1	0	0	0	Melladito	ESI10-004	Melladito	
DM9	258035	2329176	2284	0.2	4.2	3.0	1.0	3.0	86.0	38.0	0	0	0	1	0	1	0	0	0	0	1	0	0	Melladito	ESI11-017	Melladito	
DM10	258036	2329177	2283	2.4	93.0	2.0	1.0	3.0	24.0	81.0	0	1	0	1	0	1	0	0	0	0	1	0	0	Melladito	ESI11-017	Melladito	
DM11	258037	2329178	2282	2.2	156.0	9.0	1.0	3.0	18.0	77.0	0	0	0	1	0	1	0	1	0	0	1	0	0	Melladito	ESI11-017	Melladito	
DM12	258056	2329170	2260	7.2	119.0	19.0	5.0	7.0	20.0	31.0	0	1	0	1	0	1	0	1	0	0	1	0	0	Melladito	ESI11-021	Melladito	
DM13	258056	2329171	2259	13.7	408.0	2.5	5.0	7.0	11.0	26.0	0	0	0	1	1	1	0	0	0	1	1	0	0	Melladito	ESI11-021	Melladito	
DM14	258057	2329171	2258	6.9	201.0	2.5	5.0	6.0	26.0	10.0	1	0	0	1	0	1	0	0	1	1	1	0	0	Melladito	ESI11-021	Melladito	
1301-31	NA	NA	NA	0	0.5	17	5	52	20	0.5	1	0	1	1	1	1	0	0	0	0	1	0	0	Karina	Surface	NA	NA
1301-32	NA	NA	NA	0.1	57	13	5	15	11	0.5	1	0	1	1	1	1	0	0	0	0	0	0	0	Daniela	Surface	NA	NA
1301-33	NA	NA	NA	0.6	254	8	5	25	5	0.5	0	0	0	1	0	1	0	0	0	0	0	0	0	Daniela	Surface	NA	NA
1301-34	NA	NA	NA	0	8	5	5	13	48	0.5	1	0	1	1	1	1	0	1	0	0	1	0	0	Daniela	Surface	NA	NA
1401-35	NA	NA	NA	0.1	9	2.5	5	9	4	0.5	1	0	1	0	0	1	0	0	0	0	1	0	0	Bolañitos	MINE	NA	NA
1401-36	NA	NA	NA	0.7	193	7	5	19	179	46	1	0	1	1	1	1	0	0	0	1	1	0	0	Bolañitos	MINE	NA	NA

Sample	UTM X	UTM Y	Elevation (m)	Au	Ag	Cu	Pb	Zn	As	Sb	LV	L+illite	V	CT	PT	JT	GhSTQ	BC	S/I	Ad	Ca	ZTQ	CoTQ	Vein	Type	Analysis	Mine
1401-36-2	NA	NA	NA	1	642	2.5	5	20	28	112	0	0	0	1	0	1	0	0	0	1	1	0	0	Bolañitos	MINE	NA	NA
1401-36-3	NA	NA	NA	2.5	47	6	5	17	60	62	0	0	0	1	0	1	0	0	0	1	0	0	0	Bolañitos	MINE	NA	NA
1401-36-4	NA	NA	NA	0.3	48	2.5	5	9	7	14	0	0	0	1	0	1	0	0	0	0	1	0	0	Bolañitos	MINE	NA	NA
1401-37	NA	NA	NA	45	370	6	5	14	15	67	1	0	0	1	1	1	0	0	0	1	1	0	0	Bolañitos	MINE	NA	NA
1401-38	NA	NA	NA	2.4	867	6	5	37	30	35	1	0	1	1	1	1	0	0	1	1	1	0	0	Bolañitos	MINE	NA	NA
1401-39	NA	NA	NA	109	2180	98	5	19	23		0	0	1	1	1	1	0	0	1	1	1	0	0	Bolañitos	MINE	NA	NA
1401-40	NA	NA	NA	0.3	73	32	5	14	186	34	0	0	0	0	0	1	0	0	0	0	1	0	0	Bolañitos	MINE	NA	NA
1401-41	NA	NA	NA	7	593	6	5	21	24	87	1	0	1	1	0	1	0	0	1	1	1	0	0	Bolañitos	MINE	NA	NA
1401-42	NA	NA	NA	0.8	87	2.5	5	9	32	43	0	0	0	1	0	1	0	0	0	0	1	0	0	Lucerito	MINE	NA	NA
1401-42A	NA	NA	NA								0	0	0	0	0	1	0	0	0	1	1	0	0	Lucerito	MINE	NA	NA
1401-43	NA	NA	NA	23	6780	140	30	101	24		0	0	1	1	0	1	0	0	0	1	1	0	0	Lucerito	MINE	NA	NA
1401-44	NA	NA	NA	0.4	68	2.5	5	2.5	52	44	1	0	1	0	0	1	0	0	0	0	1	0	0	Lucerito	MINE	NA	NA
1401-45	NA	NA	NA	2.6	1120	2.5	10	28	12	136	1	1	0	1	1	1	0	0	1	0	1	0	0	Lucerito	MINE	NA	NA
1401-46	NA	NA	NA	5.2	3430	138	30	94			0	0	1	0	0	1	0	0	1	1	0	0	0	San Jose	MINE	NA	NA
1401-47	NA	NA	NA	1.1	181	8	5	14	45		0	0	0	1	0	1	0	0	0	0	1	0	0	Lucerito	MINE	NA	NA
905-118	NA	NA	NA	0.9	2.5						0	0	0	0	1	1	0	0	0	0	1	0	0		DDH-LC-03	NA	NA
905-119	NA	NA	NA	0.2	8						1	0	0	0	1	1	0	0	0	0	1	0	0		DDH-LC-03	NA	NA
905-120	NA	NA	NA	0	0.5	44	5	65	15	3	0	0	1	0	0	1	0	0	0	0	1	0	0		DDH-LC-03	NA	NA
905-121	NA	NA	NA	1.1	6	155	5	51	22	2	1	0	1	0	0	0	0	0	0	0	1	0	0		DDH-LC-03	NA	NA
905-122	NA	NA	NA	0	11						0	0	0	0	1	1	0	0	0	0	1	0	0		DDH-LC-03	NA	NA
905-123	NA	NA	NA	0	2.5						0	0	0	1	1	1	0	0	0	0	1	0	0		DDH-LC-03	NA	NA
905-124	NA	NA	NA	0.8	85						0	0	0	0	0	1	0	0	1	0	1	0	0	Lucerito	DDH-LC-03	NA	NA
905-125	NA	NA	NA	2.9	525						0	1	0	1	1	1	0	0	1	1	1	0	0	Lucerito	DDH-LC-03	NA	NA
905-127	NA	NA	NA	0	2.5						1	0	1	0	1	1	0	0	0	0	0	0	1	Lucerito	DDH-LC-03	NA	NA
905-128	NA	NA	NA	0.7	6						0	0	0	0	1	1	0	0	0	0	1	0	0		DDH-LC-03	NA	NA
905-129	NA	NA	NA	0.2	7	51	5	45	70	2	0	0	1	0	0	1	0	0	0	0	1	0	0		DDH-LC-26	NA	NA
905-130	NA	NA	NA	0.1	17						1	0	1	0	1	1	0	0	0	0	1	0	0		DDH-LC-26	NA	NA
905-131	NA	NA	NA	0	0.5	51	5	54	4	1	0	0	0	0	1	1	0	0	0	0	1	0	0		DDH-LC-26	NA	NA
905-132	NA	NA	NA	0.1	0.5	6	5	50	200	2	1	1	1	0	1	1	0	0	0	0	1	0	1		DDH-LC-26	NA	NA
905-133	NA	NA	NA	1	54						0	0	0	0	0	1	0	0	0	0	1	0	0		DDH-LC-26	NA	NA
905-134	NA	NA	NA	0.6	111	13	5	17	27	0.5	1	0	1	1	1	1	0	0	1	0	1	0	1		DDH-LC-26	NA	NA
905-135	NA	NA	NA	1.5	189						1	0	0	1	0	1	0	0	1	1	0	0	0		DDH-LC-26	NA	NA
905-136	NA	NA	NA	0.1	7	6	5	66	82	0.5	0	0	0	0	0	1	0	0	0	0	1	0	0		DDH-LC-26	NA	NA
905-137	NA	NA	NA	3.8	65						0	0	0	0	0	1	0	0	1	0	0	0	0		DDH-LC-26	NA	NA
905-138	NA	NA	NA	0.4	3	26	5	45	200	0.5	0	0	0	1	1	1	0	0	0	0	1	0	0		DDH-LC-26	NA	NA
905-139	NA	NA	NA	5.4	194						0	0	1	1	1	1	0	0	1	1	1	0	0	Lucerito	DDH-LC-26	NA	NA
905-140	NA	NA	NA	5.4	194						1	0	0	0	1	1	0	0	1	1	1	0	0	Lucerito	DDH-LC-26	NA	NA
905-141	NA	NA	NA	3.9	34						1	0	0	1	0	1	0	0	1	1	1	0	0		DDH-LC-26	NA	NA
905-142	NA	NA	NA	5.5	19						0	0	0	1	1	1	0	0	1	0	0	0	0		DDH-LC-26	NA	NA
905-143	NA	NA	NA	0.1	1	30	5	18	100	0.5	0	0	0	0	1	1	0	0	0	0	1	0	0		DDH-LC-26	NA	NA
905-144	NA	NA	NA	0.2	2.5						0	0	0	1	0	1	0	0	1	0	1	0	0		DDH-LC-29	NA	NA
905-145	NA	NA	NA	0	14						0	0	0	0	0	1	0	0	1	0	0	0	1		DDH-LC-29	NA	NA
905-146	NA	NA	NA	3.5	452						0	0	0	1	1	1	0	1	1	1	0	0	1		DDH-LC-29	NA	NA
905-147	NA	NA	NA	0.1	0.5	27	5	71	161	0.5	0	0	0	0	0	1	0	0	0	0	1	0	0		DDH-LC-29	NA	NA
905-148	NA	NA	NA	0.4	2.5						0	0	0	1	0	1	0	0	1	1	1	0	0	Lucerito	DDH-LC-29	NA	NA
905-149	NA	NA	NA	0.1	2	2.5	5	14	0.5	1	0	0	0	0	0	0	0	0	0	0	1	0	0		DDH-LC-31	NA	NA
905-150	NA	NA	NA	0	0.5	10	5	30	47	0.5	0	0	0	0	0	1	0	0	0	0	1	0	0		DDH-LC-31	NA	NA
905-151	NA	NA	NA	0	2.5						1	0	1	1	1	1	0	0	1	0	0	0	0		DDH-LC-31	NA	NA
905-152	NA	NA	NA	0	0.5	10	5	58	90	0.5	0	0	0	0	0	0	0	0	0	0	0	0	0		DDH-LC-31	NA	NA
905-153	NA	NA	NA	0.7	351						0	0	1	1	1	1	0	0	1	1	1	0	0	Lucerito	DDH-LC-31	NA	NA
905-154	NA	NA	NA	0.2	78	27	5	41	199	2	0	0	0	0	0	1	0	0	1	0	0	0	0		DDH-LC-20	NA	NA
905-155	NA	NA	NA	0.7	275						1	1	1	1	1	1	0	0	1	0	1	0	0		DDH-LC-20	NA	NA
905-156	NA	NA	NA	0.8	215						0	0	0	1	0	0	0	0	0	0	1	0	0		DDH-LC-20	NA	NA
905-157	NA	NA	NA	1.9	27						0	0	0	1	0	1	0	0	0	0	1	0	0	Lucerito	DDH-LC-20	NA	NA

Sample	UTM X	UTM Y	Elevation (m)	Au	Ag	Cu	Pb	Zn	As	Sb	LV	L+illite	V	CT	PT	JT	GhSTQ	BC	S/I	Ad	Ca	ZTQ	CoTQ	Vein	Type	Analysis	Mine
905-158	NA	NA	NA	0.8	23						0	1	0	0	0	1	0	0	1	1	1	0	0	Lucerito	DDH-LC-20	NA	NA
905-159	NA	NA	NA	6.4	501						0	0	0	1	1	1	0	0	1	1	0	0	0		DDH-LC-20	NA	NA
905-160	NA	NA	NA	1.1	2.5						0	1	1	0	1	1	0	0	0	0	0	0	0		DDH-LC-20	NA	NA
905-161	NA	NA	NA	0	2.5						0	0	0	0	1	1	0	0	1	1	1	0	0		DDH-LC-20	NA	NA
905-162	NA	NA	NA	0	2.5						0	0	0	1	0	1	0	0	1	1	1	0	0		DDH-LC-15	NA	NA
905-163	NA	NA	NA	0.8	42						1	0	0	1	1	1	0	0	1	0	1	0	0		DDH-LC-15	NA	NA
905-164	NA	NA	NA	0	10						0	0	0	0	1	1	0	0	0	0	1	0	0		DDH-LC-15	NA	NA
905-165	NA	NA	NA	0.2	53						0	0	0	0	1	1	0	1	1	1	1	0	0	Lucerito	DDH-LC-15	NA	NA
905-166	NA	NA	NA	2.7	151						0	0	1	1	0	1	0	0	1	1	1	0	0	Lucerito	DDH-LC-15	NA	NA
905-167	NA	NA	NA	2	97						1	0	1	1	1	1	0	0	1	1	1	0	0	Lucerito	DDH-LC-15	NA	NA
905-168	NA	NA	NA	1.9	21						1	0	1	1	1	1	0	0	0	1	1	0	0	Lucerito	DDH-LC-15	NA	NA
905-169	NA	NA	NA	0.4	2.5						0	0	0	1	1	1	0	0	1	0	1	0	0		DDH-LC-15	NA	NA
1305-230	NA	NA	NA	0.3	49	8	5	6	60	16	0	0	0	1	1	1	0	0	0	1	1	0	1	Karina	MINE	NA	NA
1305-230A	NA	NA	NA	0.4	48	13	210	8	174	17	1	0	0	1	1	1	0	0	0	0	1	0	0	Karina	MINE	NA	NA
1305-231	NA	NA	NA	1.1	71	5	70	2.5	14	9	0	0	0	1	1	1	0	0	1	1	1	0	0	Daniela	MINE	NA	NA
1305-232	NA	NA	NA	0.6	178	36	5	18	100	24	1	0	0	1	0	1	0	0	1	1	1	0	0	Karina	MINE	NA	NA
1305-233	NA	NA	NA	0.4	132	2.5	20	6	63	28	0	0	0	1	0	1	0	0	1	0	1	0	0	Karina	MINE	NA	NA
1305-234	NA	NA	NA	0.5	28	2.5	50	23	60	54	0	0	0	1	0	1	0	0	0	0	0	0	0		MINE	NA	NA
1305-235	NA	NA	NA	0.2	36	5	5	26	220	14	0	0	1	0	0	1	0	0	1	1	1	0	0		MINE	NA	NA
1305-236	NA	NA	NA	2	14	2.5	30	2.5	15	3	0	0	0	1	0	1	0	0	0	1	1	0	0	Lucerito	MINE	NA	NA
1305-251	NA	NA	NA	3.6	639						1	1	0	1	0	1	0	0	0	1	1	0	0	Daniela	DN-1	NA	NA
1305-252	NA	NA	NA	9.5	326						0	0	0	1	0	1	0	0	1	1	1	0	0	Daniela	DN-1	NA	NA
1305-253	NA	NA	NA	9.5	326						0	0	1	1	0	1	0	0	1	1	1	0	0	Daniela	DN-1	NA	NA
1305-254	NA	NA	NA	21	755						1	1	1	1	1	1	0	0	1	1	1	0	0	Daniela	DN-1	NA	NA
1305-255	NA	NA	NA	0.6	131						0	1	0	1	0	1	0	0	1	1	1	0	0	Karina	DN-1	NA	NA
1305-256	NA	NA	NA	0.1	2.5						1	0	0	1	0	1	0	0	1	1	1	0	0	Karina	DN-1	NA	NA
1305-257	NA	NA	NA	0.2	85						0	0	0	1	0	1	0	0	1	0	1	0	0	Daniela	DN-2	NA	NA
1305-258	NA	NA	NA	0.1	22						0	0	0	1	1	1	0	0	1	1	1	0	0	Daniela	DN-2	NA	NA
1305-259	NA	NA	NA	1.3	337						0	1	0	1	0	1	0	0	1	1	1	0	0	Karina	KA-15	NA	NA
1305-260	NA	NA	NA	34	180						1	0	0	0	1	1	0	0	1	0	1	0	0	Daniela	KA-15	NA	NA
1305-261	NA	NA	NA	3.6	232						1	0	0	1	0	1	0	0	1	0	1	0	0	Daniela	KA-15	NA	NA
1305-262	NA	NA	NA	1.5	45						1	0	0	1	0	1	0	0	1	1	1	0	0	Daniela	KA-15	NA	NA
1105-198	NA	NA	NA	1.8	232	37	1	26	160	62	1	0	0	1	0	1	0	0	0	1	0	0	0	Belen	Mine	NA	NA
405-12	NA	NA	NA	0.3	14		1		11	3	0	0	0	0	0	1	0	0	0	0	0	0	0	Belen	Surface	NA	NA

Concentration of metals in ppm

V = assemblages consisting of only vapor-rich inclusions
LV = coexisting liquid-rich and vapor-rich inclusions with a broad range in liquid-to-vapor ratios
L+illite= liquid-rich inclusions with trapped illite
CT= colloform texture
JT = jigsaw texture
PT = plumose texture
GhSTQ = ghost-sphere texture quartz
S/I= Sericite/Illite smectite
BC= Bladed calcite or bladed
Ad= Adularia
CoTQ = comb texture quartz
ZTQ = zonal texture quartz